McGill University

CONTACT METAMORPHISM, WALLROCK ALTERATION, AND MINERALIZATION AT THE TROUT LAKE STOCKWORK MOLYBDENUM DEPOSIT, SOUTHEASTERN BRITISH COLUMBIA

by

Robert Linnen

.

A thesis submitted to the Faculty of Graduate Studies and Research in partial fulfillment of the requirements for the degree of Master of Science in the department of Geological Sciences

Montreal, Quebec

Canada

© 1985

ABSTRACT

The Trout Lake stockwork molybdenum deposit is associated with a small Late Cretaceous granodiorite-quartz diorite stock which intruded Lower Paleozoic metasediments. The mineralization is hosted by both the Trout Lake Stock and surrounding quartz-biotite schists. The following sequence of thermal events has been determined: contact metamorphism, followed by skarn, biotite-calcite, late potassic, silicic, and phyllic alteration. Molybdenum mineralization is largely associated with silicic alteration. Textural relationships suggest that molybdenite precipitation is linked to sericite-carbonate replacement of alkali feldspar. Interpretations using phase equilibria, mineral chemistry, and fluid inclusion data, indicate that the earliest hydrothermal fluids were H_2O-rich, of low salinity, and had a temperature of approximately 400 ^{O}C. During the emplacement of the deposit the temperature decreased and XCO_2 increased, either synchronously or independently. The increase of XCO_2 is interpreted to be the result of mixing between two fluids. Molybdenite precipitated in response to decreasing temperature, pH, and K/Na activity ratio. It is proposed that the Trout Lake deposit represents part of a large metallogenic episode which also produced tungsten skarn, and vein-type base and precious metal deposits within the Kootenay Arc in British Columbia.

SOMMAIRE

Trout Lake, un gisement de molybdene de type "stockwerk", est associé à un petit stock granodioritique à quartzo-dioritique d'âge Crétacé, emplacé dans des métasédiments d'âge Paléozoïque Inférieur. La minéralisation a été mise en place dans le stock de Trout Lake ainsi que dans les schistes à quartz-biotite encaissants. La séquence suivante d'évènements thermiques a été determinée: métamorphisme de contact, suivi par les stades d'altération suivants: skarn, biotite-calcite, potassique, siliceuse, et phylliteuse. La minéralisation en molybdene est surtout associée a l'altération siliceuse. Les relations texturales indiquent que la précipitation de la molybdénite est reliée au remplacement des feldspaths alcalins par l'assemblage sericite-calcite. En Utilisant les équilibres de phases, la chimie des minéraux et les données d'inclusions fluides, nous suggérons ici que les fluides précoces étaient riches en H_2O, de faible salinité et à une temperature de 400°C. Durant l'emplacement du gisement, la température a décrut et le XCO_2 a augmenté, soit de façon synchrone ou indépendamment. L'augmentation du XCO_2 est interprétée comme etant le resultat d'un melange de deux fluides. La molybdenite a précipite dû a la baisse de la température, du pH et du rapport K/Na dans le fluide. Nous suggérons ici que le gisement de Trout Lake ne représente qu'une partie d'un grand épisode métallogénique qui a aussi produit des skarns à tungstène et des gisements filoniens de métaux usuels et précieux, à l'intérieur de l'Arc Kootenay en Colombie-Britannique.

AKNOWLEDGEMENTS

TABLE OF CONTENTS

LIST OF FIGURES

LIST OF TABLES

LIST OF PLATES

1.1   INTRODUCTION

The Trout Lake stockwork molybdenum deposit is located in the Selkirk mountains, 50 kilometers southeast of Revelstoke British Columbia, at 50 38' N, 117 36' W (Fig. 1-1).   The deposit is associated with a Late Cretaceous granodiorite-quartz diorite stock, with the molybdenum mineralization hosted by both the stock and surrounding.   A contact metamorphic aureole surrounding the Trout Lake Stock can be distinguished using calc-silicate mineral assemblages in the metasedimentary rocks.   The purpose of this study is: to characterize the metamorphic, alteration, and mineralization events; determine the sequence of these events; and model the evolution of the deposit.   Phase equilibria, mineral chemistry, and fluid inclusion data are utilised to constrain the physical and chemical conditions of each event. Structural studies were undertaken to determine the controls on mineralized and barren quartz vein emplacement.

1.2   PREVIOUS WORK

The earliest descriptions of the geology of the Trout Lake area were provided by Dawson (1889) and Brock (1903), but it was not until 1929 that a geological map of the area was published (Walker and Bancroft, 1929).   Areas studied by Fyles and Eastwood (1962), Read (1973), Reesor (1973), Read (1976), and by Read and Wheeler (1976) are all within 100 kilometers of Trout Lake (Fig. 1-1), and collectively provide

a good understanding of the regional geology. Detailed geological studies of the Trout Lake stockwork molybdenum deposit and the immediately surrounding area have been made by Boyle and Leitch (1983), and Psutka et al. (1982) respectively.

1.3 REGIONAL GEOLOGY

The Trout Lake molybdenum deposit is located within a tectonic terrain known as the Kootenay Arc. This terrain is underlain by a succession of Precambrian to Mesozoic metasediments and metavolcanics, and Mesozoic plutonic rocks, which lie between the Purcell Anticlinorium to the east and the Shushwap metamorphic complex to the west. The stratigraphic column, as originally defined by Walker and Bancroft (1929), is from oldest to youngest, the Hamill Group, the Badshot Formation, the Lardeau Group, the Milford Group, and the Kaslo Group.

In the area surrounding the Trout Lake deposit only the Lardeau, Milford, and Kaslo Groups are present (Fig. 1-2). Elsewhere the Lardeau Group is underlain by the Badshot Formation, which from paleontological evidence, has been assigned a Lower Cambrian age (Reesor, 1973). Fossils from the base of the Milford Group indicate an Upper Mississippian age (Fyles and Eastwood, 1962). Therefore the age of the Lardeau Group, which hosts the Trout Lake deposit, is post-Late Cambrian to pre-Upper Mississippian.

A detailed geological map of the area immediately surrounding the Trout Lake deposit is based on field work that

Figure 1-1 Previous Work

       1) Walker and Bancroft (1929)

       2) Fyles and Eastwood (1962)

       3) Reesor (1973)

       4) Read (1973)

       5) Read and Wheeler (1976)

       6) Read (1976)

       7) Psutka et al. (1982)

       Solid square represents this study

REVELSTOKE

N

6

2

2

7

TROUT
LAKE

4

6

4

1

UPPER ARROW LAKE

KOOTENAY LAKE

5 — 3 — 51°N

5 — 3 — 50°N

118°W

117°W

REVELSTOKE

VANCOUVER

0   10   20   30 Km
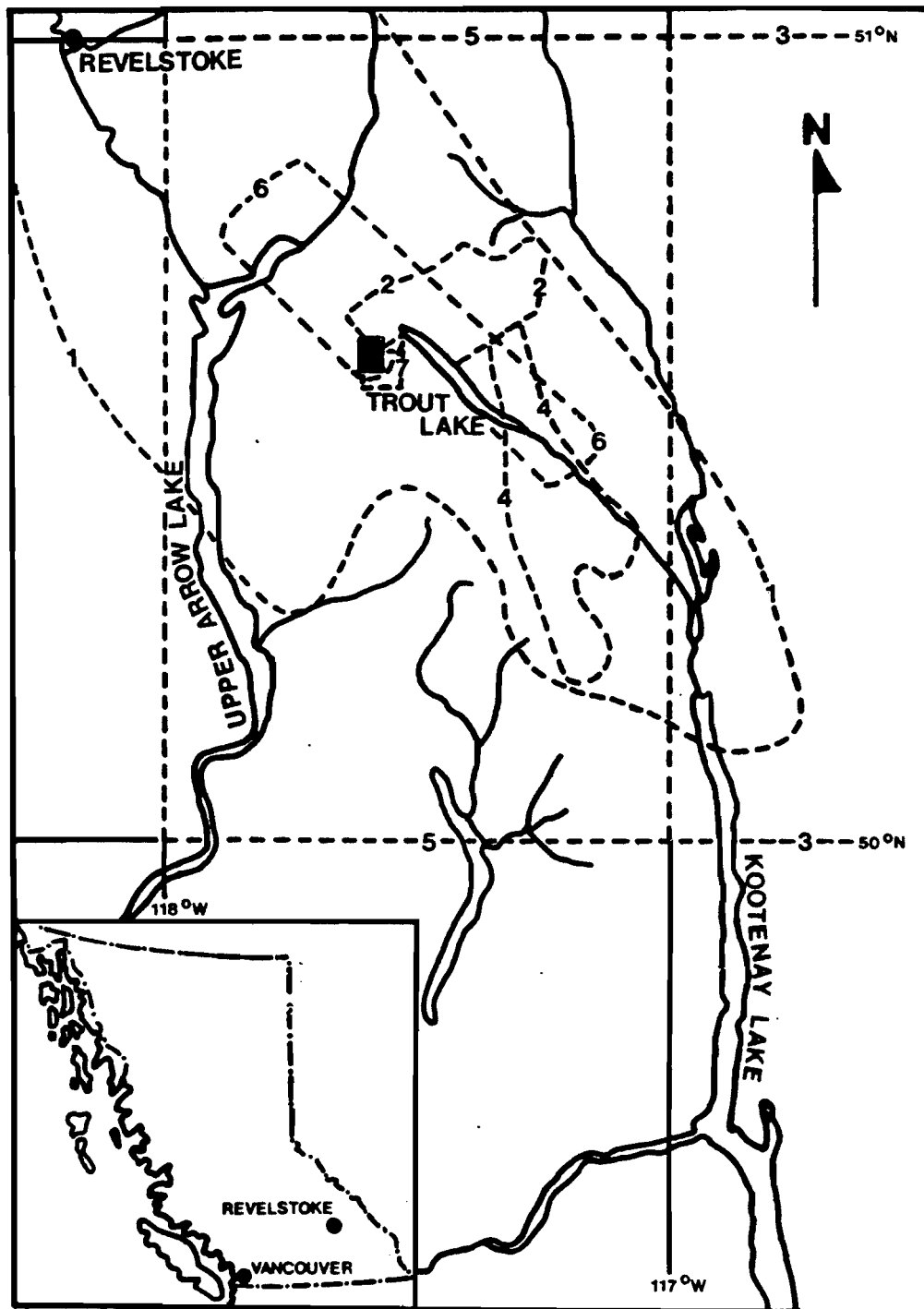
was completed during the summer of 1982 (Fig. 1-3 ; for location see Fig. 1-2). Nine litholgical units were distinguished; the first five are metasedimentary and comprise part of the Lardeau Group, and the last four are either plutonic or related to the molybdenum deposit. All units are defined on the basis of lithology, and the same lithological unit may occur at different stratigraphic horizons.

1.3.1   LITHOLOGY

Unit 1 consists of phyllites, pelitic quartzites, and quartz-biotite schists. These are light grey to green and characteristically are well foliated with alternating phyllitic and quartz-rich layers of less than one, to five millimeters in thickness. The phyllitic layers consist of biotite, muscovite, chlorite, and plagioclase. The quartz layers are composed almost entirely of quartz with minor amounts of plagioclase, K-feldspar, biotite, muscovite, chlorite, and accessory zircon. Generally the sulphide content in this unit is low, but pyrite has been observed in some samples. Graphitic horizons are rarely observed.

Unit 2 consists of carbonate rocks. There are two distinct types: a banded black and white or massive white recrystallized calcareous limestone, and a massive buff recrystallized dolomite. Mineralogically these rocks are nearly pure carbonate, but may also contain minor quartz, plagioclase, muscovite, or biotite.

Unit 3 is a light to dark brown or grey layered

Figure 1-2 Regional Geology

Structure and lithology after Read (1976).
Regional metamorphism after Read and Brown
(1981).
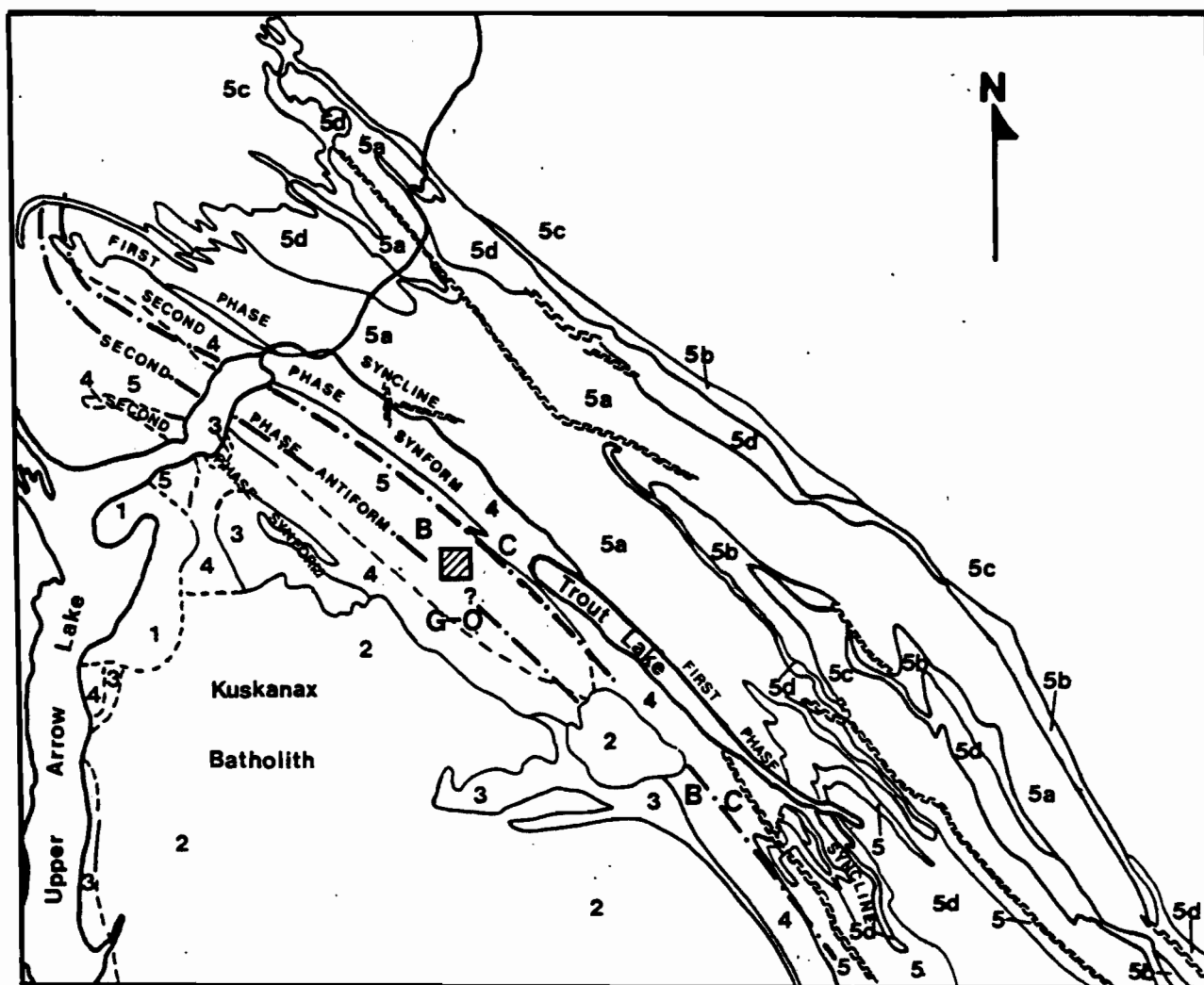
Legend

CRETACEOUS TO JURASSIC

| 1 | Granodiorite |

JURASSIC

| 2 | Monzonite, Syenite |

PERMIAN TO TRIASSIC

| 3 | Kaslo Group — Metavolcanics |

UPPER PALAEOZOIC

| 4 | Milford Group — marble, metaconglomerate, metasandstone |

LOWER PALAEOZOIC

| 5 | Lardeau Group — undivided |

a— Broadview Formation limestone, phyllite

b— Sharon Creek Formation siliceous phyllite

c— Index Formation phyllite, metavolcanics

d— metavolcanics

SYMBOLS

Contact mapped, assumed

Fault

Thesis Area

Division Between Metamorphic Zones

C Chlorite Zone

B Biotite Zone

G–O Garnet-Oligoclase Zone

calcareous phyllite or calc-silicate schist. This unit is similar in appearance to unit 1, except that it is calcareous. The mineralogy is also similar to that of unit 1 but, depending of metamorphic grade, calcite, K-feldspar, tremolite, and clinozoisite are also present. The biotite and K-feldspar contents are characteristically much higher in this unit than in unit 1, and disseminated pyrrhotite is also common.

Unit 4 is a dark brown, calcareous quartzite which is gradational from unit 3, but is distinguishable by its massive texture. Minor carbonate and calc-silicate minerals and disseminated pyrrhotite are generally present, making it mineralogically very similar to unit 3. However, the modal quartz content is higher.

Unit 5 consists of a sequence of dark green metavolcanic rocks that probably have basaltic to andesitic compositions. They are generally massive and are commonly intercalated with massive dolomite. Chlorite and tremolite are the dominant minerals, and impart a dark green colour to the rock.

These five units comprise the Lardeau Group in the area surrounding the Trout Lake deposit. Fyles and Eastwood (1962) subdivided the Lardeau Group into six formations including the two uppermost Jowett and Broadview Formations, and the basal Index Formation. Psutka et al. (1982) concluded that the metavolcanics (unit 5) are part of the Jowett Formation, and that the metasediments (units 1 to 4) correlate either with the Broadview or Index Formations. It is more probable that

Units (1) to (4) correlate with the Broadview Formation since the Milford Group lies to the northeast in the core of a synform (Fig. 1-2) and the stratigraphically lower Jowett Formation lies to the southwest. However, correlation is difficult as the stratigraphic column can locally be incomplete (Read, 1973) and several of the formations which comprise the Lardeau Group have similar lithologies.

Units 7 and 8 are granodiorite and quartz diorite respectively and comprise the Trout Lake Stock. The granodiorite is light grey and equigranular, whereas the quartz diorite is dark grey, more porphyritic and can contain xenoliths of quartz-biotite schist. Granodiorite comprises the bulk of the Trout Lake Stock and, except for one small outcrop in the southern part of the thesis area, is restricted to the Trout Lake Stock. The quartz diorite occurs as thin dykes generally less than one meter thick both within and peripheral to the Trout Lake Stock. However, all quartz diorite dykes are probably co-magmatic owing to their textural and mineralogical similarities.

Unit 9 is quartz stockwork, and was formed by massive quartz replacement of metasedimentary and plutonic rocks, and by open-space filling. It is hydrothermal in origin and its distribution is restricted to within the limits of the deposit.

Unit 6, skarn, also has a hydrothermal origin. Its distribution is controlled by the intersection of faults with carbonate horizons (unit 2) in the vicinity of the Trout Lake Stock. It is dark green owing to the presence of pyroxene,

and is massive. The latter characteristic distinguishes it from the calc-silicate schist which is banded and has a metamorphic origin. Garnet, tremolite, clinozoisite, carbonate, and pyrrhotite are other minerals commonly found in the skarn unit.

Molybdenum mineralization is restricted on surface to an area within 100 meters of the Trout Lake Stock and is hosted almost entirely by units 1,7,8, and 9. Only trace amounts have been found in the calc-silicate and carbonate units. In addition, there are several base metal, silver and tungsten showings within the area of Figure 1-3 including two former producers, the Lucky Boy and Copper Chief deposits.

1.3.2 REGIONAL PLUTONISM AND METAMORPHISM

The Paleozoic stratigraphic succession in the Kootenay Arc was intruded during the Mesozoic Era by plutons of intermediate to felsic composition. The oldest intrusions are mid-Jurassic, e.g. the Kuskanax Batholith (150-164 Ma.),and generally have monzonitic or syenitic compositions (Read and Brown, 1981). A second major plutonic event occurred in the mid-Cretaceous Period, e.g. the Battlerange Batholith (91-120 Ma.), and these rocks have granodiorite or quartz monzonite compositions (Read and Brown, 1981).

The youngest regional thermal event (evidenced by the resetting of K-Ar isotopes in muscovite and biotite) is believed to have occurred in the Early Tertiary (Mathews, 1983), but this event is poorly documented near the thesis area. Furthur south in the Kootenay arc, in northern

FIGURE 1-3 SURFACE GEOLOGY

Legend below

LEGEND

LITHOLOGICAL UNITS

Pelitic Quartzite

Carbonate

Calcareous Phyllite

Calcareous Quartzite

Metavolcanics

Skarn

Granodiorite

Quartz Diorite

Quartz Stockwork

SYMBOLS

Fault observed and approximate, inferred

Anticline

Syncline

Geological Contact observed and approximate, inferred

Abandoned Mine

Lost Trail Fault

Copper Chief Fault

Lucky
Boy

Adit Fault

Adit

Wilke Creek

Copper
Chief

Three Man Fault

Z Fault

not
mapped

N

0   250   500 m
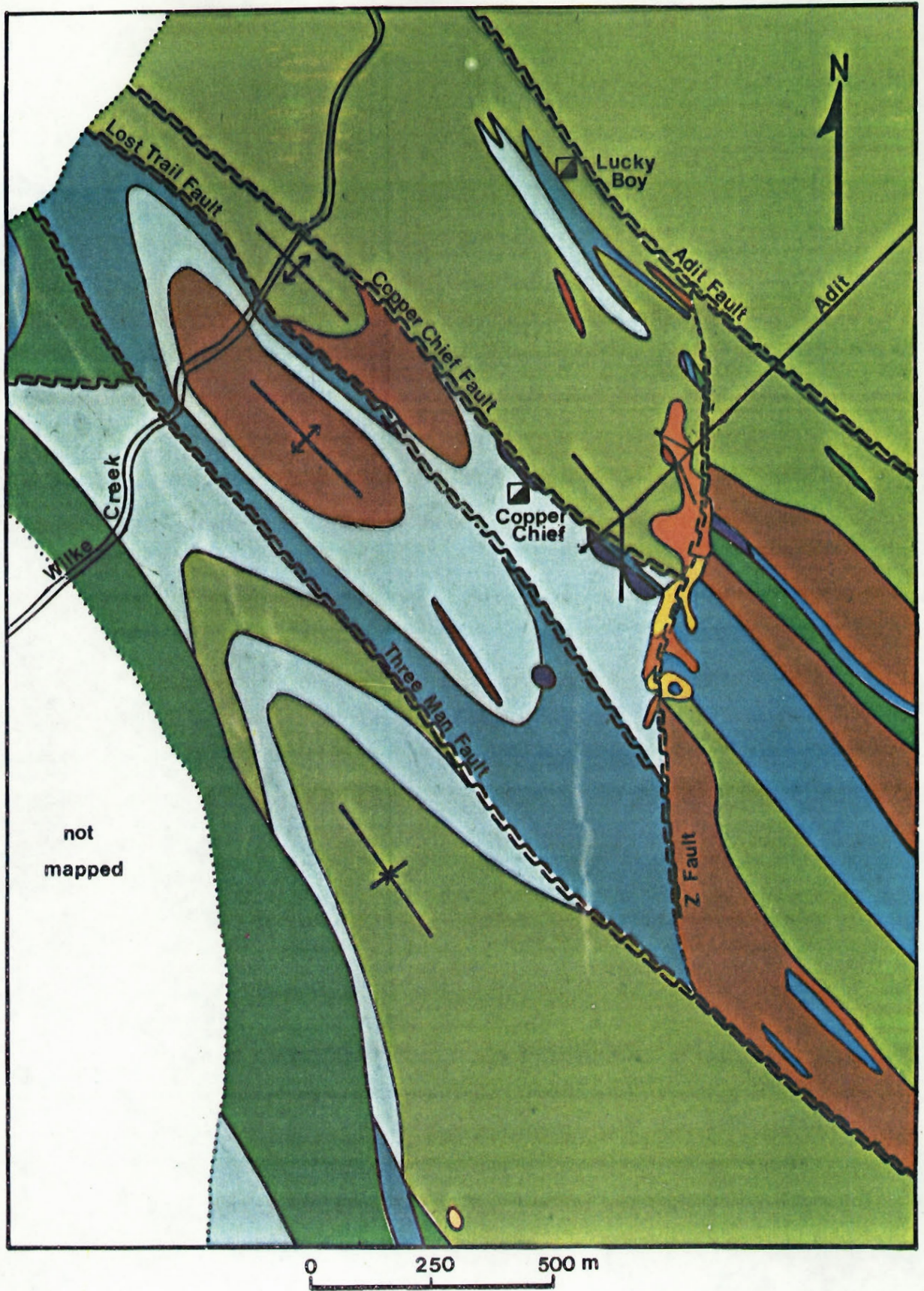
Washington and Idaho, Miller and Engels (1975) have documented the occurrence of Early Teriary granites which are largely of the "two-mica" suite. Archibald et al. (1983) report an Eocene (50 Ma.) syenite which represents this event near the United States border, approximately 200 kilometers southeast of Trout Lake.

The youngest intrusion currently known in the region immediately surrounding the thesis area is the Trout Lake Stock which has been dated at 76 Ma. by the K-Ar method applied to biotite (Boyle and Leitch, 1983). The Trout Lake Stock may have been potentially affected by Early Tertiary fluids and therefore the actual age of the Trout Lake Stock could be Early Tertiary to Mid Cretaceous. Additional dating of hydrothermal biotite or muscovite could conceivably resolve this problem since the molybdenum mineralization both pre- and post-dates the emplacement of the Trout Lake Stock.

Regional metamorphic grade increases from chorite to garnet-oligoclase facies toward the mid-Jurassic plutons, which, in the Trout Lake area, is the Kuskanax Batholith (Read and Brown, 1981) (Fig. 1-2). The Trout Lake molybdenum deposit is approximately 5 kilometers northwest of the Kuskanax Batholith and lies near the garnet-oligoclase regional metamorphic isograd. A contact metamorphic aureole surrounds the Trout Lake Stock and overprints the regional metamorphism.

1.3.3 STRUCTURAL SETTING

The region has undergone up to four phases of deformation (Read, 1973) but generally only 2 phases are recognizable in any given area. The first phase of deformation occurred during the Devonian to Mississippian Periods, and was followed by two phases of deformation which were associated with the emplacement of the mid-Jurassic batholiths (Read, 1973). Older portions of these batholiths are foliated, whereas younger portions are not, indicating that the intrusions are both syn- and post-kinematic. The fourth phase of deformation is only developed locally and most likely is also associated with the Jurassic plutonism (Read, 1973). The Trout Lake Stock is not foliated, which supports the post-Jurassic age date.

The core of a phase-two synform is defined by the Milford Group, trends northwest, and forms the depression filled by Trout Lake (Read, 1976) (Fig. 1-2). To the southwest, a phase-two antiform is defined by the Lardeau Group (Read, 1976) (Fig. 1-2). The Milford Group defines another synform which lies to the southwest of the antiform defined by the Lardeau Group (Fig. 1-2).

The area mapped in this study is a portion of a phase-two antiform (Fig. 1-2). Several synclinal and anticlinal structures are interpreted within this portion of the antiform (Fig. 1-3). Folds are interpreted to be plunging to the northwest at a low angle. This is supported by field measurements of lineations which plunge between 0 and 45 degrees to the northwest. Generally only a single steeply

dipping northwest-southeast trending axial plane foliation is recognisable. Owing to the lack of visible bedding, or the preservation of previous foliations, structures are interpreted largely on the basis of lithological distribution. The carbonate unit is the best structural marker, and defines several folds and structural discontinuities (Fig. 1-3).

Four faults are interpreted in the thesis area on the basis of structural discontinuities and observed fault breccias (Fig. 1-3). The Three Man, Lost Trail, Adit, and Copper Chief faults are all parallel to the regional structural fabric. The latter two faults were also intersected by diamond drill holes. The linearity of these faults over changing topography indicates that they are vertical or steeply dipping. The location of the Z fault has been established by surface outcrop of fault breccias, and intersections by diamond drill holes. The Z fault has a northerly trend and is steeply dipping to vertical. The relationships of the Three Man and Adit faults to the Z fault are not known. However, the Trout Lake Stock intruded along, and is cut by the Z fault. Therefore the Z fault was active after the emplacement of the Trout Lake Stock, and possibly extends north of the Adit fault, and south of the Three Man fault.

1.4 GENERAL GEOLOGY OF THE DEPOSIT

The geology of the Trout Lake deposit has been interpreted on the basis of information from diamond drill holes and adit exposure. Section and plan views though the

Figure 1-4   Cross section through the Trout Lake deposit

Legend is the same as Figure 1-3.

SW

NE

Lost Trail Fault

Copper Chief Fault

Z Fault

Adit Fault

0.1% MoS2

Adit

0   100   200 m
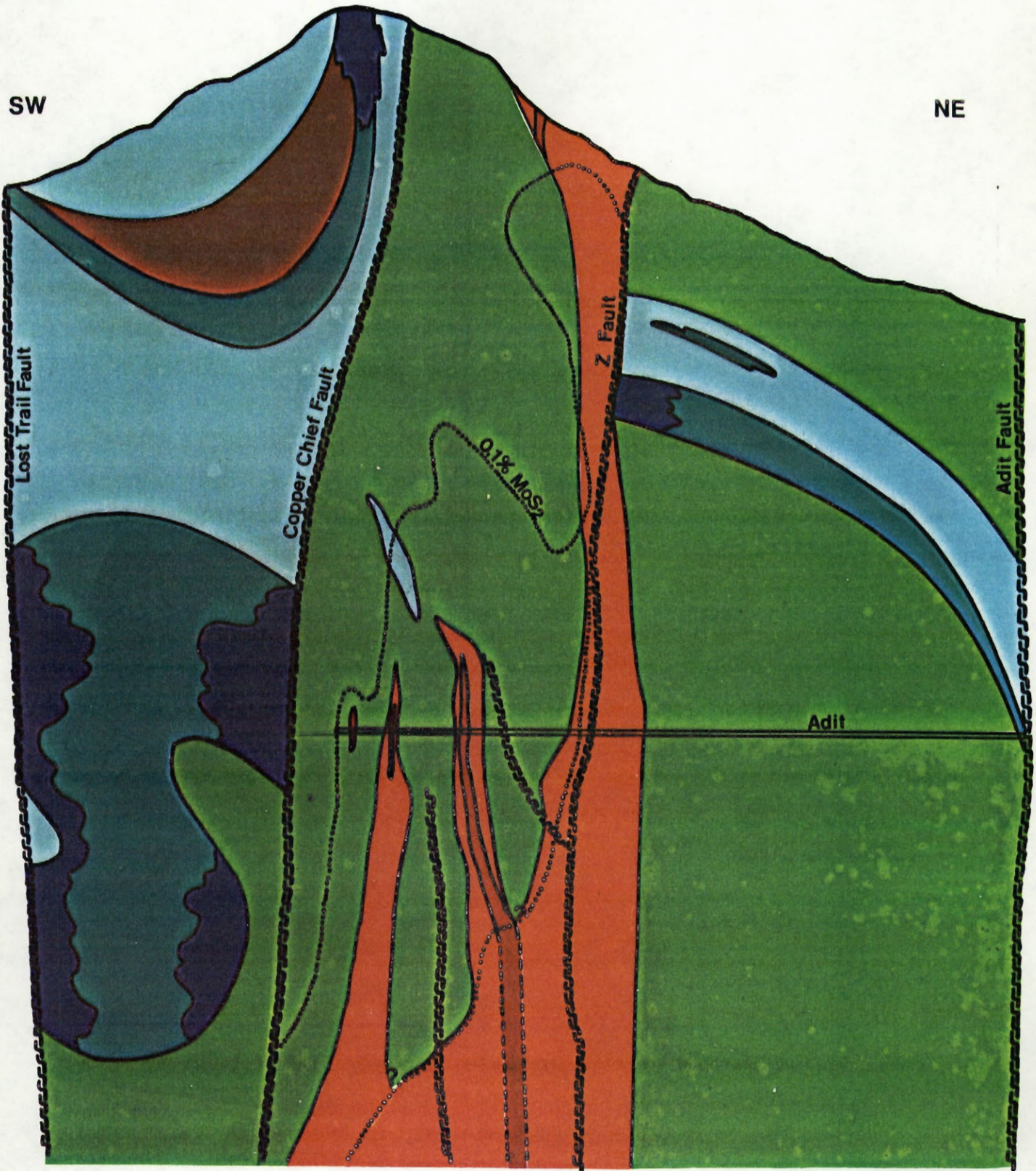
centre of the deposit are represented by Figures 1-4 and 1-5 respectively. The zone of molybdenum mineralization as defined by a 0.1 % MoS_2 contour is also represented in Figures 1-4 and 1-5.

From Figures 1-4 and 1-5 it is apparent that molybdenum mineralization is associated with neck-like stocks which are lenticular in plan-view. Three subvertical faults: the Adit, Z,and Copper Chief, divide the host rock into three distinct blocks. The northeasterly block is virtually devoid of molybdenum mineralization and is composed largely of quartz-biotite schist with subordinate carbonate and calcareous schist horizons. The central block, which contains almost all the molybdenum mineralization, is dominantly quartz-biotite schist, with a few scattered horizons of calcareous schist. The southwesterly block, which hosts tungsten skarns and minor molybdenum mineralization, is comprised of the carbonate, calcareous schist, and calcareous quartzite units.

1.4.1 DESCRIPTION OF THE METASEDIMENTS

The zone of mineralization lies almost entirely within the central block (Fig. 1-4), which, as discussed above, is composed largely of unit 1. The quartz-biotite schist is texturally and mineralogically similar to its regional equivalent (unit 1), but the modal abundance of biotite and K-feldspar is greater. In the northeasterly block, the modal abundance of K-feldspar and biotite decreases outward from the deposit to regional levels. Biotite, quartz and feldspar are typically less than 0.5 mm in diameter in the metamorphic

Figure 1-5   Plan view of the Trout Lake deposit at the adit
level.   Legend is the same as in Figure 1-3.

0.1 % MoS₂

Z Fault

Adit

N

Copper Chief Fault
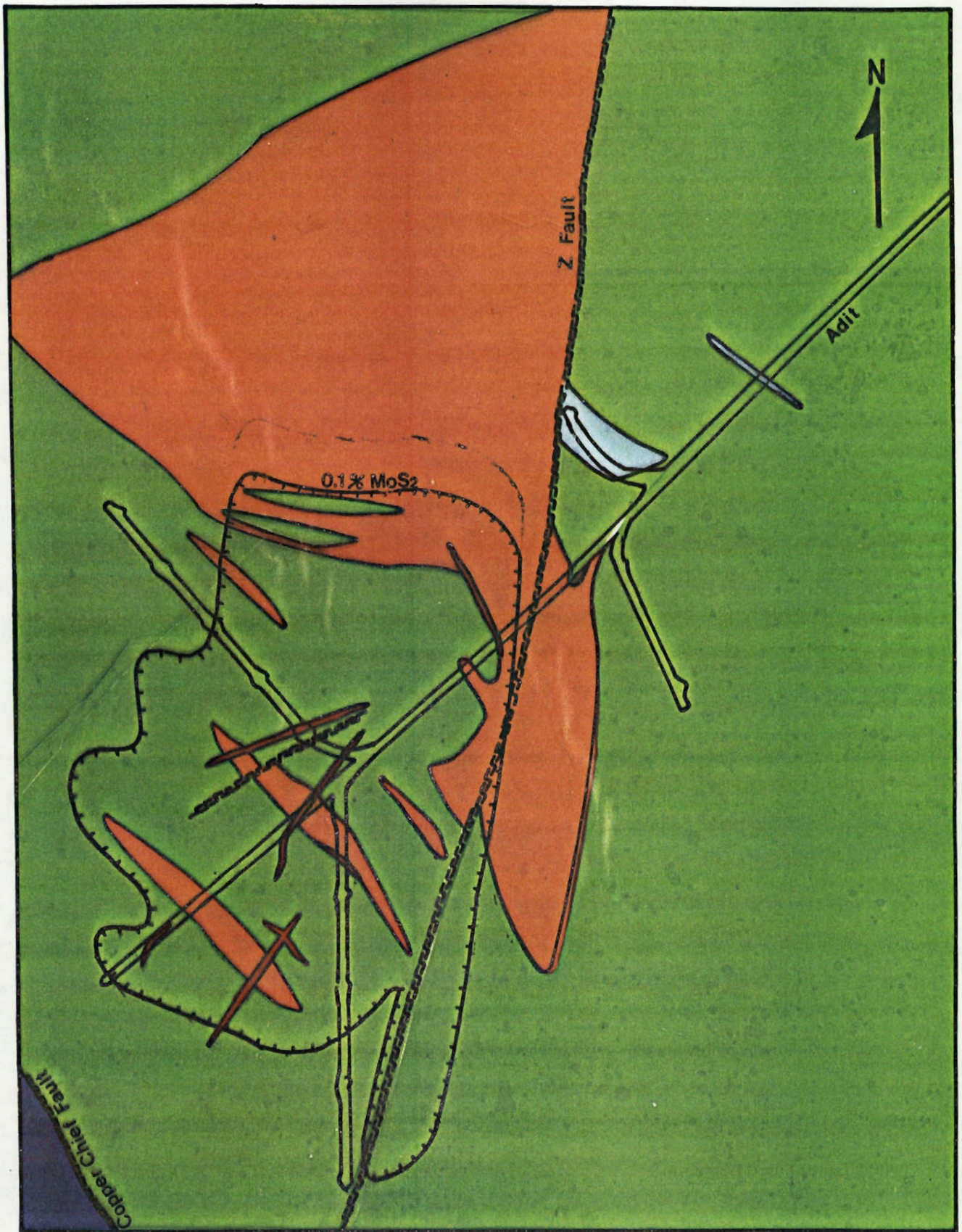
0   50   100m

units, but are coarser grained in zones of alteration with grain sizes ranging up to 2.0 mm in diameter. Unit 3 in the central block is a biotite-tremolite schist which, mineralogically, is distinguished from its regional metamorphic equivalent by the lack of K-feldspar and clinozoisite.

1.4.2 DESCRIPTION OF THE INTRUSIVE ROCKS

The deposit is centered around two small (10-20 meters thick) lenticular pipes (Figs. 1-4, 1-5). These pipes have a vertical extent of over 300 meters and consist of at least three intrusive phases. Through cross cutting relations the following sequence has been established: 1) early granodiorite, 2) quartz diorite, 3) late granodiorite. Collectively the pipes are adjacent to the main granodioritic body, intersecting and probably cross cutting it at depth.

The main and early granodiorites are identical in appearance. Characteristically they are light grey, equigranular, and medium grained (0.5-2.0 mm). Rarely, rounded quartz grains greater than 2mm in diameter are present. Both are comprised largely of interlocking zoned plagioclase crystals, with interstitial quartz and K-feldspar. Biotite is the dominant mafic mineral and generally is disseminated. Zoned hornblende crystals also occur but are less common. No rock sample examined in this study was completely unaltered. Biotite is altered to chlorite +/- sphene and calcite. Plagioclase grains are generally altered to sericite + calcite, but K-feldpathization and albitization

of plagioclase are also common. Stock boundaries display little evidence of chilled margins. Foliations defined by biotite layers are a common feature of the stock margins. These foliations are parallel to the intrusive contacts and are interpreted to reflect flow banding.

The quartz diorite is dark grey, has a more porphyrytic texture and commonly contains xenoliths of quartz-biotite schistor, less commonly, vein quartz. Quartz and plagioclase phenocrysts 2.0 to 3.0 mm in diameter (rarely up to 1.0 cm) are set in a plagioclase-quartz-biotite matrix with an average grain size of 0.5 mm. Cross-cutting relationships show that the quartz diorite is generally younger than quartz veins, and that it cuts the early granodiorite. Therefore the quartz diorite is placed relatively late in the sequence of geological events. However, the quartz diorite is cut by the quartz stockwork which contains a significant proportion of molybdenum mineralization. Mineralogically, the quartz diorite is quite similar to the granodiorite, but has less K-feldspar. The differences in modal abundance of K-feldspar warrants the classification by Boyle and Leitch (1983) of two seperate rock types. However, the origin of much of the K-feldspar is ambiguous, being late magmatic to hydrothermal. Bulk compositions from X-ray fluorescence analysis, discussed below, confirm that there are compositional differences in these rock types.

The youngest igneous unit is the late granodiorite. It is medium grey, contains abundant xenoliths of quartz-biotite schist, and generally has quartz envelopes along the

contacts. Volumetrically this unit is insignificant because the dykes are all less than 0.5 meters thick and typically are only 10 to 20 cm thick. However, this unit is important in the intrusive sequence since it crosscuts the quartz diorite unit and is the youngest igneous phase yet identified.

Boyle and Leitch (1983) describe an additional aplite dyke phase. Mineralogically the "aplite" is comprised of plagioclase, K-feldspar, muscovite, and carbonate. However, grey patches are commonly observed in this unit, and these most likely represent remnant granodiorite surrounded by strong sericitc alteration. Therefore the "aplite" is probably hydrothermally altered granodiorite, not an additional igneous phase.

Major element analyses of representative igneous rock samples are listed in Table 1-1. Analyses were determined by X-ray fluorescence at the University of Montreal. Sample 1291 is from the main granodiorite, samples 1444 and 1446 are early granodiorite, and samples 1454 and 4DrS 32 are quartz diorite. In comparison to quartz diorite, the granodiorite has a higher SiO_2 and K_2O content, but lower CaO, Fe_2O_3, and P_2O_5. The S/I index (Al/Ca+Na+K) has been calculated for each analysis and varies from 1.09 to 1.19. This suite is therefore slightly peraluminous but does not contain primary muscovite, cordierite, garnet, or sillimanite. Pyrrhotite and pyrite are the dominant opaque phases, and are probably secondary.

TABLE 1-1

Sample	1291(gnd)	1444(gnd)	1446(gnd)	1454(qzd)	4DrS32(qzd)
SiO_2	72.49	74.77	69.35	67.72	67.30
Al_2O_3	14.41	13.66	14.47	15.20	15.94
Fe_2O_3	1.93	2.90	4.60	4.70	4.42
MgO	0.45	0.20	0.77	1.23	0.94
CaO	2.13	3.08	4.00	4.02	4.25
Na_2O	2.59	2.95	2.58	2.51	3.33
K_2O	3.67	1.32	1.16	1.43	1.26
TiO_2	0.18	0.26	0.40	0.43	0.45
P_2O_5	0.07	0.10	0.22	0.27	0.23
MnO	0.05	0.04	0.09	0.09	0.07
H_2O+	0.48	0.22	0.94	0.87	0.84
CO_2	0.73	0.22	0.66	0.52	0.21
TOTAL	99.18	99.72	99.51	98.99	99.24
S/I	1.19	1.15	1.15	1.17	1.09

1.5 SUMMARY

The Trout Lake stockwork molybdenum deposit is associated with a multi-stage granodiorite-quartz diorite complex of Early Tertiary to Cretaceous age. The stock post-dates pervasive deformation, and intrudes the Lardeau Group of metasediments. The metasediments had previously been affected by Jurassic deformation and metamorphism. Phyllites, pelitic quartzites, and calc-silicate schists occur in the area immediately surrounding the deposit and these probably correlate to the Broadview Formation. These metasediments have been tightly folded along northwest-trending axes and subsequently faulted. The deposit is hosted largely by the quartz-biotite schist (unit 1), and by the Trout Lake Stock (units 7 and 8).

CHAPTER 2: METAMORPHISM

The Lardeau Group of metasediments surrounding the Trout Lake Stock has been affected by three thermal events: regional metamorphism associated with the emplacement of the Mid Jurassic Kuskanax Batholith; contact metamorphism; and hydrothermal alteration. The latter two are associated with the Trout Lake Stock. The differentiation of these processes is important in understanding the conditions of contact metamorphism and hydrothermal alteration at the deposit.

2.1 METAMORPHIC ASSEMBLAGES

The mineralogical compositions of over one hundred samples were determined by microscopic examination of thin sections, supplemented by microprobe analyses of minerals in selected samples. Figure 2-1 shows the locations and mineralogy of samples which were selected for microscopic examination. At the outset it is important to note that several faults cut the thesis area (Fig. 1-3) and that the timing of these faults is unclear. There is no indisputable evidence which suggests that regionally metamorphosed, contact metamorphosed, or hydrothermally altered rocks were significantly displaced by these faults. However, the apparent discontinuity of contact metamorphic isograds across the Z fault (Fig. 2-2) may indicate post-contact metamorphic displacement. Slickensides observed on molybdenite along the Z fault indicate that at least minor fault movement occurred after the emplacement of mineralization.

Figure 2-1 Metamorphic mineral assemblages

LEGEND

sample location:
X
Minerals Present:

▽ biotite
△ chlorite
▼ k feldspar
▲ actinolite
□ muscovite
■ clinozoisite
○ calcite
● sphene
◐ rutile

all samples contain
quartz & plagioclase

N

Adit

0   25o   5oo m
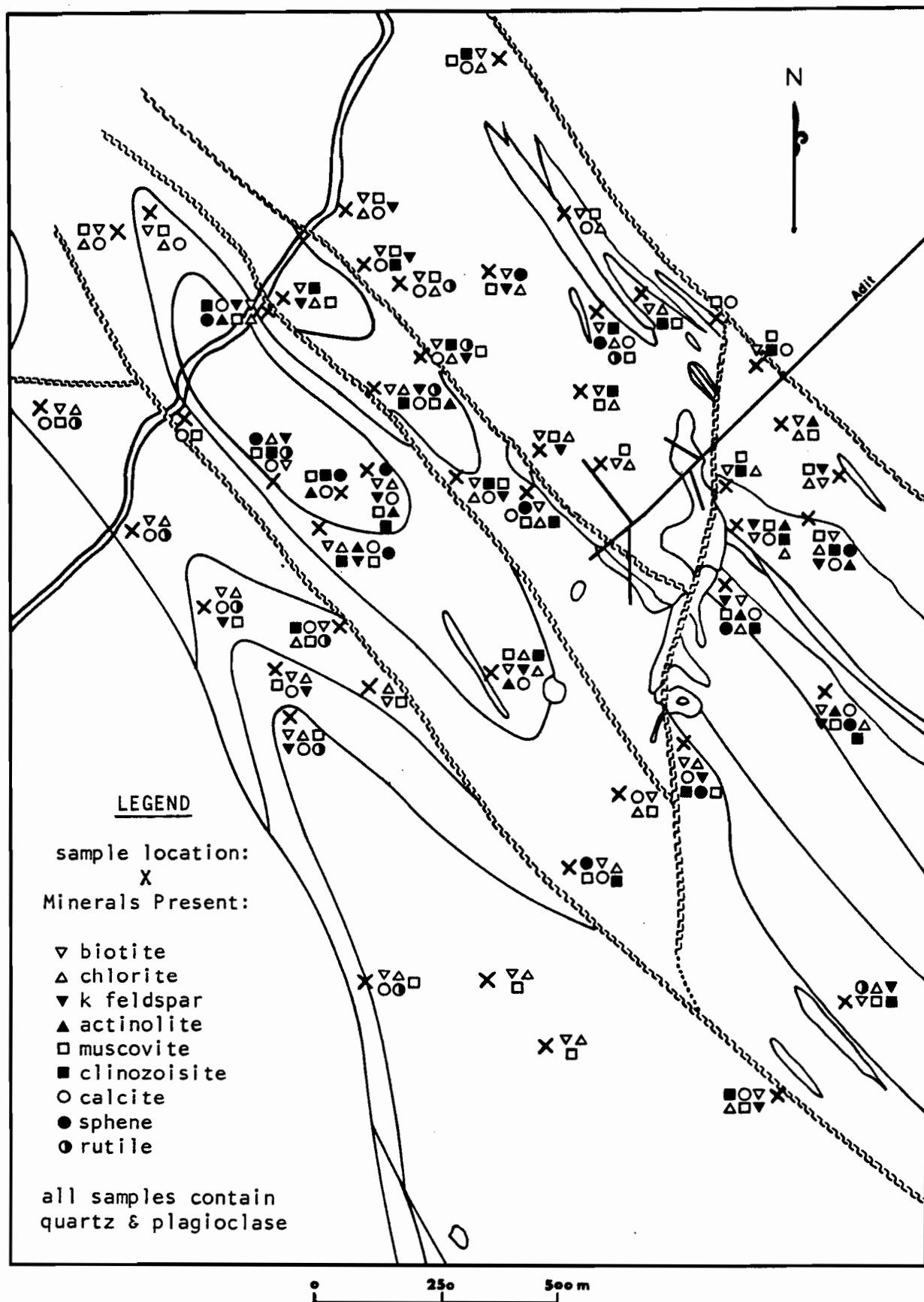
Northeastof the Adit Fault, the dominant lithologic unit is the pelitic quartzite (unit 1), which also contains a few calcareous schist layers (unit 3). These rocks contain muscovite, chlorite, biotite, quartz, and albite, with accessory K-feldspar, calcite, and anatase. In this area biotite is present only in trace amounts but is absent 500 meters further to the northeast (beyond the confines of Fig. 2-1). The abundance of biotite in the rock increases southwest of the Adit fault. Biotite replaces chlorite along cleavage planes parallel to foliation, which defines the transition from chlorite to biotite regional metamorphic zones. Along the outer margins of the thesis area, northwest of Wilkie Creek and southwest of the Three-Man Fault similar mineralogical assemblages are encountered in calcareous and non-calcareous schists. The only mineralogical difference between the calcareous and non-calcareous schists is the calcite content.

Mineralogical changes, particularly in the calcareous schists between the Adit and Three Man faults, define contact metamorphic aureoles around the Trout Lake Stock and a small quartz diorite dyke located 500 meters southwest of the stock. Within these aureoles, mineral orientation (including biotite) is random and the rocks are more coarse grained than outside the aureoles. Plagioclase grains are generally twinned outside the aureoles but not twinned within the aureoles. There are no textural or mineralogical differences between metasedimentary rocks directly in contact with intrusions, and those found elsewhere in the aureoles.

Figure 2-2 Contact metamorphic isograds

ISOGRADS

● TREMOLITE
   ANORTHITE

○ TREMOLITE
   K-FELDSPAR

■ ANORTHITE
   K-FELDSPAR

□ SPHENE

▲ ANORTHITE
   CALCITE

N

Adit

0   250   500 m
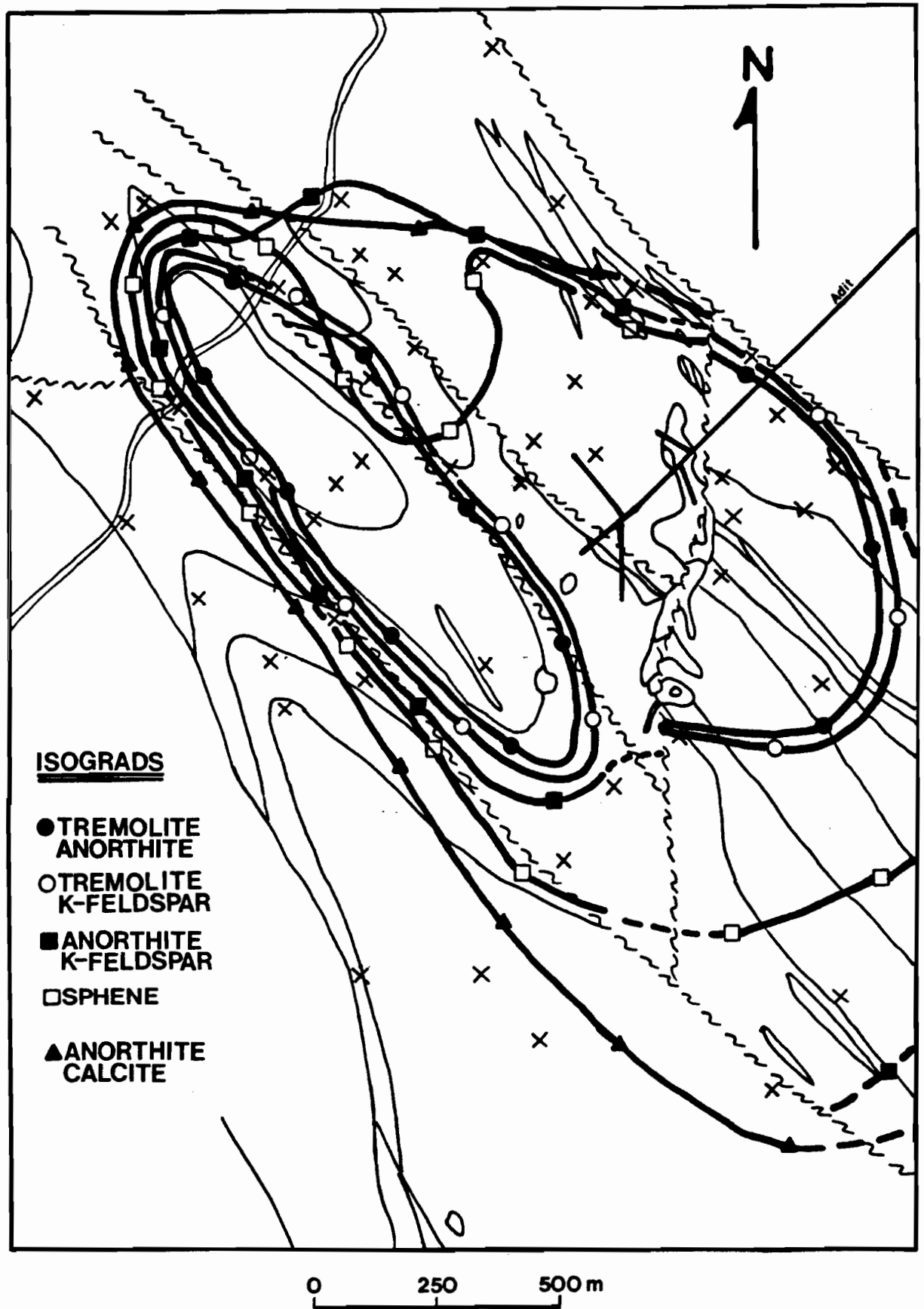
A typical calcareous schist (unit 3) or calcareous quartzite (unit 4) within the contact aureoles consists of muscovite, chlorite, biotite, tremolite, K-feldspar, plagioclase, quartz, calcite, clinozoisite, and sphene. Marbles (unit 2) are nearly pure calcite with accessory quartz, plagioclase, clinozoisite, tremolite, chlorite, biotite, muscovite, and sphene. The pelitic quartzite (unit 1) has been relatively unaffected by the contact metamorphism. However, a modal increase of biotite and a random orientation of minerals is observed, and clinozoisite may be present. Sericitizedporphyroblasts are common in the pelitic quartzite within the contact aureoles, and may rarely contain remnant andalusite. To date, no andalusite has been identified outside the contact aureoles. Rare poikioblastic garnet porphyroblasts are also present in pelitic quartzites within the aureoles. These range up to 1 mm in diameter and are surrounded by foliated sheet silicates. They are therefore interpreted as having a regional metamorphic origin. Microprobe analyses (Table 2-1) indicate that the garnets are almandine-spessartine in composition with a grossular component of less than 10 percent. Table 2-1 also lists representative microprobe analyses of minerals present in the calcareous schist and pelitic quartzite units within the aureoles.

2.2 REGIONAL METAMORPHISM

Regional metamorphic zones, based on the data of Read and Brown (1981) are: a garnet-oligoclase zone and isograd adjacent to the Kuskanax Batholith with biotite and chlorite zones developed successively outward (Fig. 1-2). More detailed mapping by Psutka et al. (1982) places the Trout Lake Stock within the garnet-oligoclase zone of regional metamorphism. The chlorite zone lies to the northeast of the adit fault and therefore the thesis area lies within the biotite zone. However, the thesis area is possibly not within the garnet-oligoclase zone. The regional metamorphic garnets in the pelitic quartzite unit coexist with albitic plagioclase, as determined by microprobe analyses (Table 2-1). In addition, all plagioclase compositions determined by microprobe analysis from outside the aureole are albitic (including those from the southwestern corner, closest to the Kuskanax Batholith) (Fig. 2-3). This contradicts the interpretation by Psutka et al.(1982) that the deposit lies within the garnet-oligoclase isograd, and suggests rather that the deposit is within the biotite regional metamorphic zone

Sericitization of porphyroblasts, which rarely contain remnant andalusite, probably represents retrograde contact metamorphism of regional metamorphic andalusite. Because no andalusite porphyroblasts have been observed outside the contact aureole the possibility that andalusite is a result of contact metamorphism, can not be ruled out.

2.3 DESCRIPTION OF CONTACT METAMORPHIC ISOGRADS

Mineral assemblages identified by thin section inspection were used to interpret contact metamorphic isograds. Figure 2-1 shows the mineralogy and location of selected samples, and Fig. 2-2 shows the interpreted isograds. Reactions using calc-silicate minerals were found to be the most useful in defining contact metamorphic isograds, but block faulting may complicate interpretation since some or all of the faults have had post-contact metamorphic movement. No reactions in the pelitic quartzite were found useful in characterizing contact metamorphism although, in some samples, the presence of clinozoisite was used to define the anorthite-calcite isograd. Isograds representing the surface traces of five reactions are shown on Fig. 2-2. The isograds on Fig. 2-2 are lines which separate the following product and reactant assemblages:

1) $2Zo + CO_2 = 3An + Cc + H_2O$

2) $Ru + Cc + Q = Sp + CO_2$

3) $5Ph + 6\ Cc + 24\ Q = 3Tr + 5Kf + 6CO_2 + 2H_2O$

4) $3Ch + 3Cc + 7Q = Tr + An + 3CO_2 + 3H_2O$

5) $Mu + Cc + 2Q = Kf + An + CO_2 + H_2O$

Table 2-2 lists the mineral abbreviations used in the above reactions, and others introduced later in this chapter. The isograds are interpreted from observed mineral assemblages where the minerals represent product, reactant, or isobarically univariant assemblages, and isograds are named on the basis of product assemblages. These isograds are developed concentrically around the Trout Lake Stock, and a

Figure 2-3   Distribution and composition of plagioclase and
             clinozoisite. Circles represent the locations
             of clinozoisite-bearing samples. Squares
             represent the locations of clinozoisite-absent
             samples. The lower numbers are the range of
             plagioclase compositions observed in that
             sample. The upper number is the median
             plagioclase composition of the observed range.

● 26
3-60

N

● 10
0-24

■

■

■

● 22
10-26

■ 47
33-47

● 10
5-13

● 23
10-28

■ 47
1-55

■

● 10
0-26

■ 23
7-41

● 0
0-0

■

Adit

● 1
0-1

■ 47
4-55

● 4
0-15

● 1
0-1

■

| 0 | 250 | 500 m |
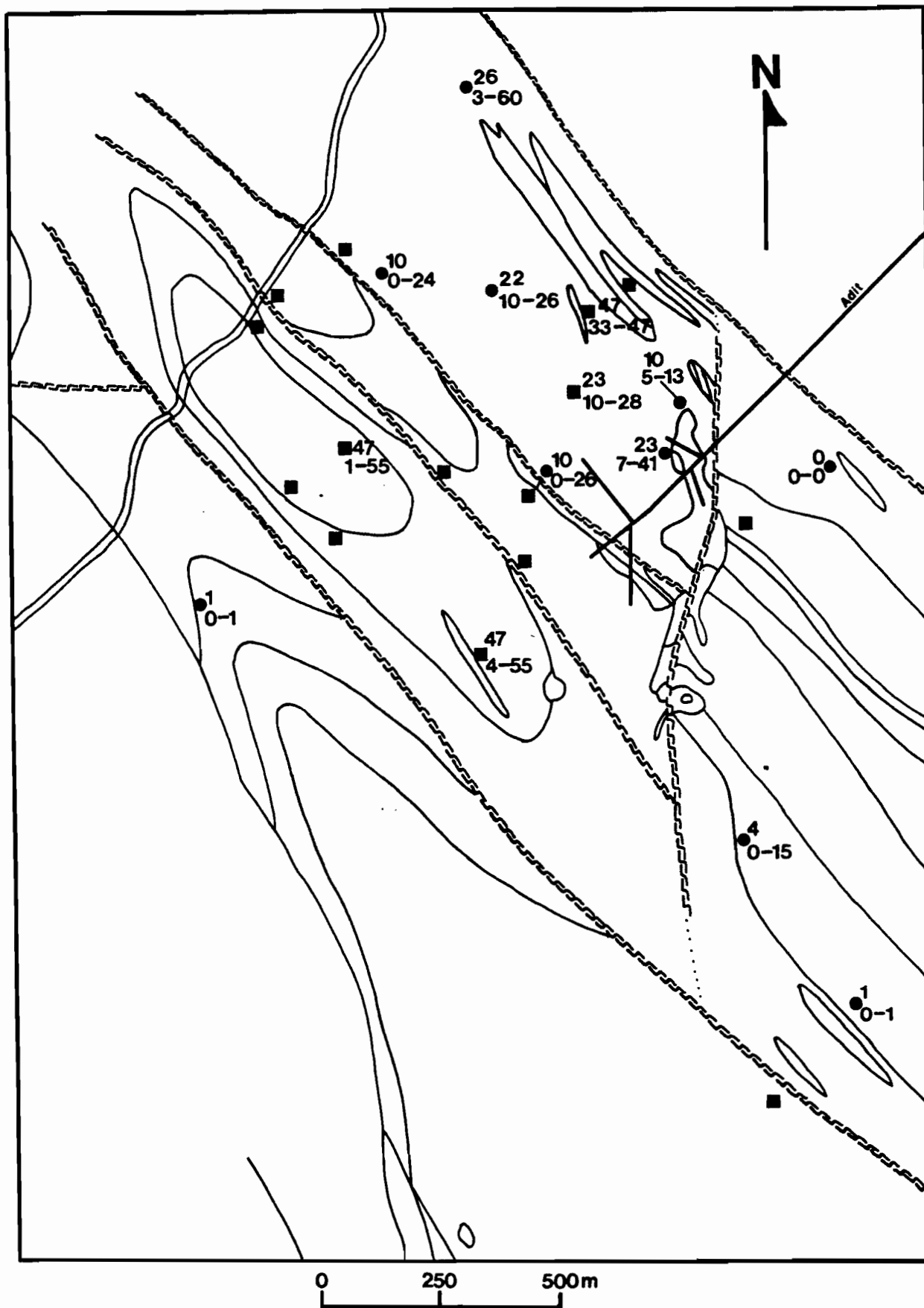
quartz diorite dyke 500 meters southwest of the Trout Lake Stock. This pattern suggests that the mineral assemblages originated as a result of the same Late Cretaceous intrusive event. Owing to the lack of calcareous units northwest of the Z fault, and overprinting of hydrothermal alteration around the deposit, the aureole around the quartz diorite dyke provides more useful data for the interpretation of contact metamorphism.

The anorthite-calcite and sphene isograds (Reactions 1 and 2) occur furthest out with tremolite-K feldspar, tremolite-anorthite, and anorthite-K feldspar isograds (Reactions 3-5) closer to the intrusions. Two contact aureoles can be distinguished using the innermost isograds. One is around the Trout Lake Stock and the other around the quartz diorite dyke to the southwest. The inner isograds are not deve.loped northwest of the Trout Lake Stock as no calcareous horizons are present in that area.

The isograds around the quartz diorite dyke have an oval shape, with the long axis parallel to the regional structure (Fig. 2-2). This may be a result of the change in topography, the presence of a northwesterly plunging pluton at depth, or a combination of both. Isograds are closely spaced at a distance from the intrusions, telescoping outward with no mineralogical changes adjacent to the intrusions. Isograds east of the Trout Lake Stock are not as well constrained, cut a flatter topography and do not have an oval shape. The intersection of granodiorite at depth by a diamond drill hole west of Wilke Creek (H.C. Boyle, pers. comm., 1981) supports

the hypothesis of a northwesterly plunging pluton. Neither intrusion observed on surface is large enough (in particular the quartz diorite dyke which is only 1 meter thick) to cause the observed contact metamorphic aureole. Therefore it follows that the contact metamorphic aureole must have been caused by a pluton at depth. This pluton is assumed to be the parent magma for both the Trout Lake Stock and the peripheral quartz diorite dykes. The latter are similar in texture and mineralogy to the quartz diorite in the Trout Lake Stock. The textural and mineralogical consistency of the quartz diorite dykes combined with the similarity between the two contact aureoles suggests that both the Trout Lake Stock and the peripheral quartz diorite dykes were coeval with the intrusion of the deep-seated pluton.

There are a few cases of crosscutting isograds in the contact aureole. The sphene isograd crosscuts the tremolite-K feldspar, tremolite-anorthite, and K feldspar-anorthite isograds near the Copper Chief and Lost Creek faults (Fig. 2-2). The K feldspar-anorthite isograd lies between the tremolite-Kfeldspar and sphene isograds around the quartz diorite dyke, but between the sphene and anorthite-calcite isograds around the Trout Lake Stock. The significance of crosscutting isograds will be discussed later in this chapter.

Finally, a cerium-bearing zoisite (probably allanite) has been observed as cores in clinozoisite grains. Its distribution, (Fig. 2-3) like that of clinozoisite, is restricted to within the contact metamorphic aureole.

TABLE 2-1

TYPICAL COMPOSITIONS OF CONTACT METAMORPHIC MINERALS

Minerals From The Calcareous Schist

	Bi	Ch	Mu	Tr	Zo	Plag
SiO_2	38.53	28.86	46.03	55.20	39.38	55.40
TiO_2	1.52	0.00	0.35	0.02	0.11	N.A.
Al_2O_3	16.79	20.83	35.66	2.19	28.94	27.57
MgO	16.98	22.95	0.71	19.05	0.06	N.A.
FeO	10.83	14.98	1.03	7.83	4.43	0.59
MnO	0.54	0.57	0.02	0.49	0.08	N.A.
CaO	0.03	0.03	0.00	12.50	23.70	9.87
Na_2O	0.02	0.07	0.50	0.27	0.01	5.65
K_2O	10.69	0.01	9.25	0.11	0.02	0.47
Tot.	96.92	88.47	93.62	98.21	96.85	99.46

Minerals From The Pelitic Quartzite

	Bi	Ch	Mu	Plag	Gar
SiO_2	34.80	25.76	49.72	68.89	35.63
TiO_2	2.80	0.13	0.00	N.A.	0.11
Al_2O_3	17.69	20.26	34.83	19.86	21.53
MgO	8.48	12.77	1.60	N.A.	1.26
FeO	20.82	26.78	1.40	0.11	24.93
MnO	0.38	0.47	0.11	N.A.	15.22
CaO	0.02	0.09	0.01	0.06	0.74
Na_2O	0.33	0.03	0.14	10.60	0.16
K_2O	10.37	0.02	9.88	0.09	0.01
Tot.	96.30	86.86	97.78	99.61	99.60

Compositions are in weight percent as determined by elctron microprobe analysis. Bi represents biotite, Ch chlorite, Mu muscovite, Tr tremolite, Plag plagioclase, Gar garnet, and N.A. not analysed.

2.4 CONSTRUCTION OF T-XCO2 DIAGRAMS

The contact metamorphic condition for each isograd was evaluated using temperature versus mole fraction of carbon dioxide ($T-XCO_2$) diagrams. It was assumed that, for the corresponding equilibria, the metamorphic fluid was a carbon dioxide-water mixture, and that the partial pressure of water

plus the partial pressure of carbon dioxide is equivalent to the total fluid pressure. Reactions that involve the minerals observed in thin section are used to interpret the temperature and XCO_2 conditions of the fluid with which they equilibrated.

The effect of adding methane to the CO_2-H_2O system is to shift reaction curves to to lower temperatures (Kerrick, 1974). Addition of sodium chloride or other salts shifts reaction curves to to higher temperatures (Jacobs and Kerrick, 1981). Fluids inclusions from this deposit contain both methane and salts (discussed in Chapter 7). Because the effects of complex fluids on mineral equilibria are poorly understood it will be assumed that any changes in reaction space caused by the presence of methane and salt in contact metamorphic fluids cancelled each other and that the fluid composition can be represented in the CO_2-H_2O system.

Each of the reactions used can be represented by the system $SiO_2-Al_2O_3-TiO_2-MgO-CaO-K_2O-CO_2-H_2O$. Individual reactions are characterized by the equation $K = A/T + B + C(P-1)/T$ where K is the reaction constant, A, B, and C are constants related to the changes of enthalpy, entropy and volume for the reaction, T is absolute temperature, and P is pressure in bars.

Minerals are assumed to have unit activity, and therefore the reaction constant is related solely to the activities of CO_2 and H_2O. Plagioclase is the only mineral which is not assumed to have unit activity. Many of the reactions involve anorthite, whereas microprobe analyses indicate that plagioclase from tremolite-bearing metasediments are

dominantly An_{40} to An_{60} (Fig 2-3), where An_X is the mole fraction of anorthite in plagioclase. Therefore an equilibrium composition of An_{50} is assumed for contact metamorphism. In all reactions involving anorthite the An_{50} activity has been included in the reaction constant using activity coefficients from Saxena and Ribbe (1972).

The last assumption concerns the use of the iron-free end-members of various minerals. For the reactions involving ferromagnesian minerals the Fe/Mg ratios will remain relatively constant (i.e. partitioning of Fe and Mg between these minerals is small) therefore most of the changes in thermodynamic properties cancel, leaving the positions of the curves virtually unchanged in $T-XCO_2$ space (Rice, 1977; Williams-Jones, 1982). Furthurmore, the compositions of the ferromagnesian minerals involved are Mg-rich (Table 2-1), meaning that any effect of iron partitioning will be small.

Table 2-2 presents a complete list of the reactions calculated for the T-XCO2 diagram with the appropriate reaction constants. Changes of reaction constants due to anorthite activity in plagioclase are omitted from this table. Water fugacity data is from Burnham et al. (1969), and carbon dioxide fugacity from Burnham and Wall (unpublished data). The effect of non-ideal mixing is to shift calculated reactions to higher temperatures at low XCO_2 conditions (Jacobs and Kerrick, 1981). However, unless all major fluid species can be included in an equation of state, which at present is not possible for the $H_2O-CO_2-NaCl-CH_4$ system, any model will be in error. Therefore the simplest model, ideal

mixing of H_2O and CO_2 is assumed.

TABLE 2-2 CONTACT METAMORPHIC REACTIONS

	A	B	C
(1) 2Zo+CO_2 = 3An+Cc+H_2O	-2718	5.13	-0.353
(2) Ru+Cc+Q = Sp+CO_2	-3551	7.60	0.119
(3) 5Ph+6Cc+24Q=3Tr+5Kf+6CO_2+2H_2O	-31211	64.32	0.799
(4) Ch+3Cc+7Q= Tr+An+3CO_2+3H_2O	-29752	56.82	0.538
(5) Mu+Cc+2Q= Kf+An+CO_2+H_2O	-9515	18.34	0.070
(6) Ch+6Zo+7Q= Tr+10An+6H_2O	-37906	72.21	-0.521
(7) Mu+2Zo+2Q= Kf+4An+2H_2O	-12233	23.47	-0.283
(8) Tr+6Zo+2Q = 5Di+9An+4H_2O	-29129	53.17	-0.544
(9) Tr+3Cc+2Q= 5Di+3CO_2+H_2O	-20975	37.78	0.515

Reaction (1) is derived from Hunt and Kerrick (1977), reaction (2) from Hewitt (1975), reaction (3) from Best (1978), reaction (12) from Hewitt (1973), rection (13) from Slaughter et al. (1975), and reaction 14 from Storre and Nitsch (1972). All other reactions are linear combinations of the above. An represents anorthite, Cc calcite, Ch chlorite, Di diopside, Kf K-feldspar, Mu muscovite, Ph phlogopite, Q quartz, Ru rutile, Sp sphene, Tr tremolite, and Zo zoisite.

2.4.1 PRESSURE ESTIMATE

In order to construct a $T-XCO_2$ diagram, the pressure must first be determined or assumed. Owing to the lack of a geobarometer or estimates of the amount of erosion in the immediate area, confining pressure must be assumed. Climax-Henderson type molybdenum deposits form at depths of 0.6 to greater than 4.5 kilometers (Westra and Keith, 1981). However, Climax-type deposits are high-level volcanic related deposits, and as the bulk of the Trout Lake Stock has a granitic texture, with the "porhyrytic" quartz diorite unit still having a plutonic texture, and the lack of any extrusive equivalent to the Trout Lake Stock, it is likely that this deposit formed in a slightly deeper environment.

Approximately 100 kilometers to the south, but still in

the Kootenay Arc, the Bluebell Pb-Zn-Ag deposit of similar age is estimated from fluid inclusion, sulphide stability, and clay stability data, to have formed under hydrostatic conditions at a depth of approximately 6 kilometers (Ohmoto and Rye, 1970). In the same area, Archibald et al. (1983) estimate, from aluminosilicate assemblages, that the metasediments presently exposed were at a depth of 7 kilometers during the Mid to Late Cretaceous. It is therefore probable that the Trout Lake Stock and contact aureole also formed at a depth of 6 to 7 kilometers. Given the above depth of formation the total fluid pressure would therefore have been between 500 and 2000 bars, depending on whether it was dominantly hydrostatic or lithostatic. Lithostatic conditions will be assumed for the contact metamorphism.

2.5 INTERPRETATION

The reactions listed in Table 2-2 have been determined in $T-XCO_2$ space (Fig. 2-4) at a fluid pressure of 2000 bars using the assumptions discussed above. Two types of relativelyflat-shaped reaction curves areplotted,calcite consuming at higher XCO_2, or zoisite consuming at lower XCO_2 conditions. The isobarically univariant zoisite reactions terminate in isobaric invariant points at the intersection with the near-vertical $2Zo + CO_2 = 3An + Cc + H_2O$ curve (Reaction 1). Three of the invariant points correspond to assemblages observed in the rocks: the Mu + Cc + Q + An + Kf + Zo; Ph + Cc + Q + Tr + Kf + Zo + An; and Ch + Cc + Q + Tr + An + Zo isobarically invariant assemblages. These invariant

Figure 2-4   Contact metamorphic reactions in T-XCO$_2$ space

TOTAL PRESSURE 2000 BARS
AN_{50} PLAGIOCLASE ASSUMED
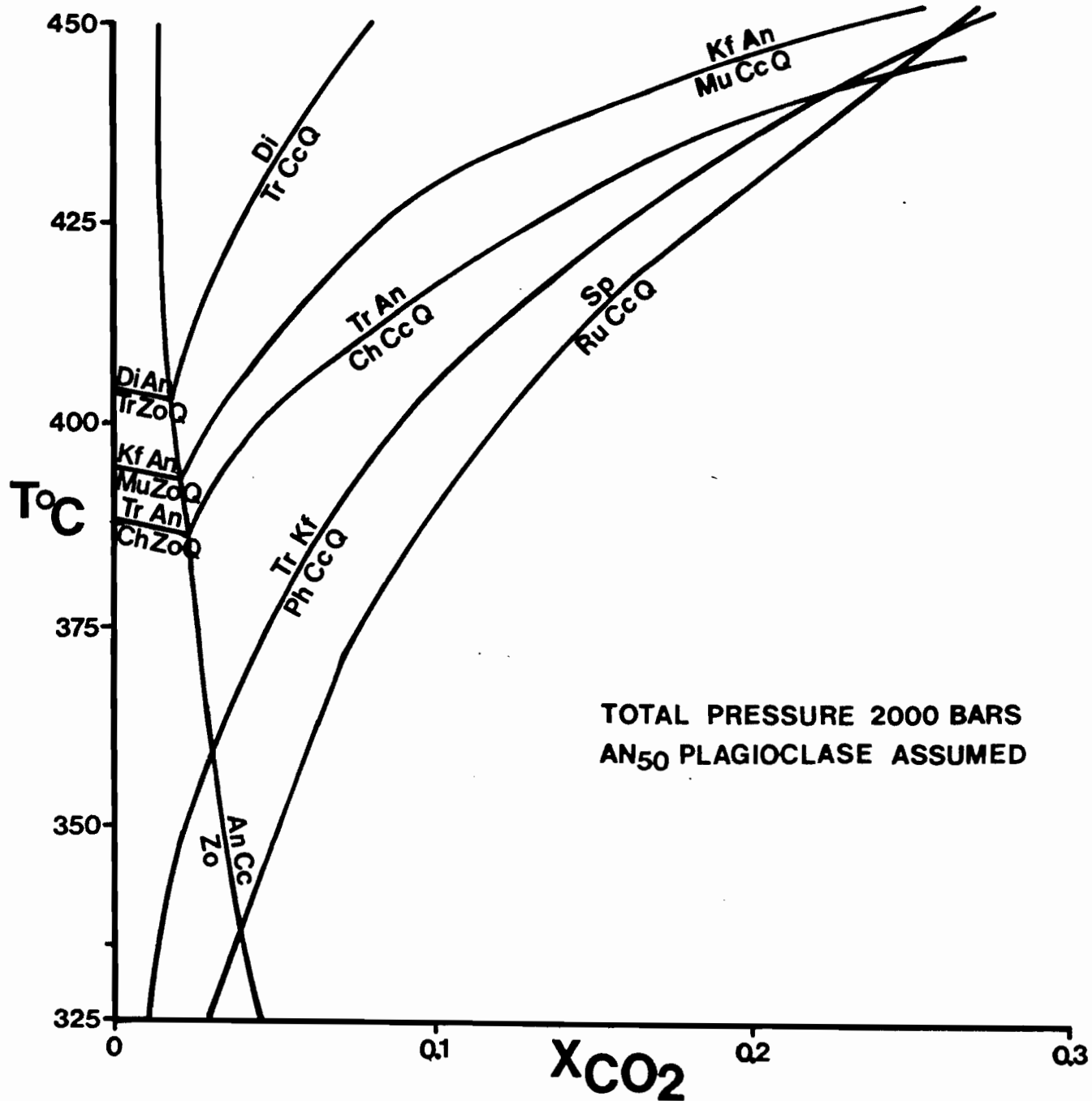
points fall in the narrow temperature range of 360 to 390 ^{o}C, and at an XCO_2 of less than 0.05.

Greenwood (1975) suggested that invariant assemblages may be the result of internal buffering of fluid compositions by mineral reactions. For CO_2-generating reactions (positive slopes in $T-XCO_2$ space), the case for most reactions in this study, internal buffering along a given reaction will result in increasingly CO_2-rich fluid compositions at higher temperatures until isobarically invariant or temperature maxima conditions are reached. At the isobarically invariant conditions, reactions proceed until one or more reactants is consumed, then the fluid composition is buffered along a new reaction until isobarically invariant or temperature maxima conditions are reached. Conversely, if fluid compositions are externally buffered, the fluid composition remains constant over a range of temperatures, which restricts the possible mineral assemblages. Reactions such as tremolite-K feldspar produce more CO_2 than H_2O, therefore internal fluid buffering would result in the formation of isobarically invariant assemblages at high XCO_2. The low and constant XCO_2 interpreted in this study suggests that the fluid was externally buffered, or at least externally controlled. Similar arguments for external fluid buffering have been proposed by Williams-Jones (1982), and Ferry (1983).

Inspection of mineral assemblages present in individual samples (Fig. 2-1) shows that the apparent isobarically invariant assemblages are generally either collectively present or absent. Two explanations for this are possible.

Either some minerals existed metastably over small temperature or XCO_2 intervals, or the number of components used is too small to represent the real reaction space of the minerals in equilibrium. Independent of the explanation, the water-rich nature of the fluid and the consistency of fluid composition suggests that the fluid was externally buffered.

2.5.1 EVIDENCE FOR EQUILIBRIUM

Figure 2-5 is a plot of the iron mole fraction (Fe/Fe+Mg) in biotite compared to coexisting chlorite, tremolite, and phengitic muscovite. In each case an increase in the iron content of biotite is accompanied by higher iron in the coexisting silicate. If a linear or parabolic function describes the iron and magnesium distribution, a partitioning coefficient can be calculated, implying an equilibration of phases. The distribution of iron and magnesium between biotite and chlorite is linear, which implies equilibrium. The correlation of X_{Fe} in biotite with that of muscovite and tremolite is similar, but with a higher degree of scatter. The ferromagnesian minerals within the contact aureole all have random orientations and share grain boundaries with little visible replacement. This textural and chemical evidence suggests that all these minerals formed coevally and equilibrated with the same contact metamorphic fluid. Plagioclase compositions within the aureole are fairly constant (Fig. 2-3). Calcareous units generally contain An_{50} to An_{55} plagioclase, with An_{25} to An_{30} plagioclase present in pelitic quartzites. The consistency of plagioclase chemistry

Figure 2-5   Distribution of iron and magnesium between

biotite and   a) chlorite

b) tremolite

c) muscovite

The mole fraction of iron X_{Fe} is (Fe/Fe +Mg).
Bars represent the compositional range
observed in each sample.   Solid circles
represent median values of the compositional
range.
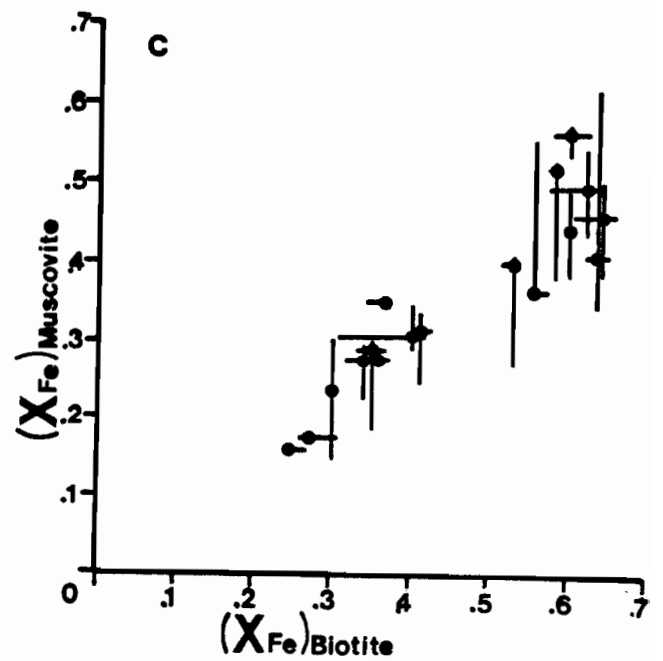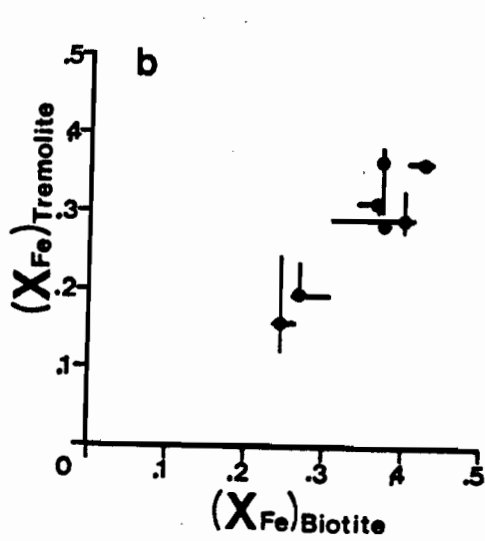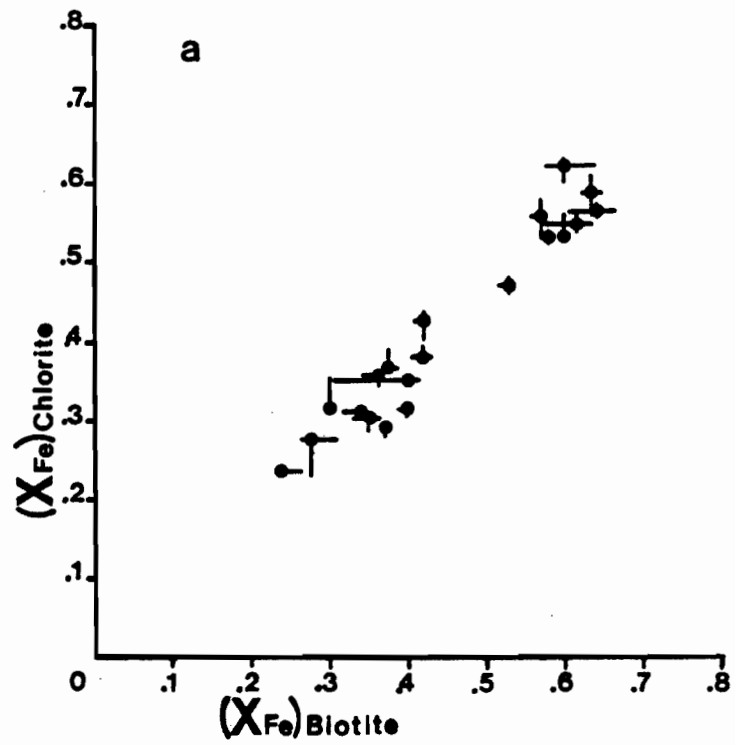
also suggests equilibration with the contact metamorphic fluid.

Possible evidence of disequilibrium is that chlorite grains commonly contain inclusions of calcite and sphene, and that sphene can have rutile inclusions. The inclusions in chlorite may have resulted from the complete replacement of tremolite, although no remnant tremolite is observed in chlorite, nor is chlorite observed to replace tremolite. The largest amount of scatter on the Fe-Mg partition plots (Fig. 2-5) is between biotite and tremolite, which again could indicate disequilibrium. However, the confinement of tremolite to within the contact aureole strongly suggests a contact metamorphic origin. It is possible that tremolite equilibrated in the early stages of contact metamorphism and that as the contact metamorphic fluid evolved it cooled and/or increased in XCO_2, with biotite and chlorite equilibrating at a later stage. A temperature of 360 to 390 °C and XCO_2 of less than 0.05 are reasonable estimates of contact metamorphic conditions in spite of possible disequilibrium.

The crosscutting nature of the sphene isograd, as previously mentioned, suggests possible disequilibrium. Rutile inclusions in sphene suggest that rutile is slow to react and therefore may be metastable in some samples. The fact that the sphene isograd crosscuts the tremolite-anorthite, tremolite-K feldspar, and anorthite-K feldspar isograds near the Copper Chief and Lost Creek faults is probably due to rutile metastability. Around the quartz diorite dyke the anorthite-K feldspar isograd lies between the

tremolite-K feldspar and sphene isograds, but around the Trout Lake Stock it lies outside the sphene isograd. This is probably due to the occurrence of hydrothermal K-feldspar in apparently unaltered samples, causing a misinterpretation of the mineral assemblage data. Alternatively, the activity of K-feldspar may deviate from unity in some samples and the isograd, as defined, fails to account for solid solutions in minerals. The aureole around the quartz diorite dyke has no crosscutting isograds and therefore data from this area is used to estimate the conditions of contact metamorphism.

2.5.2 DISCUSSION

Several observations imply that heat transfer during contact metamorphism was advective rather than conductive. Conductive heat transfer results in high temperature mineral assemblages in the rocks at the contact with the intrusion, and a concave-shaped maximum temperature profile outward from the intrusion. Advective heat transfer results in a convex-shaped maximum temperature profile, with lower temperature mineral assemblages concentrated at a distance away from the intrusion (Norton and Knight, 1977; Williams-Jones, 1981).

The close spacing between inner and outer isograds at Trout Lake suggests that the maximum temperature heat profile away from the intrusion was relatively flat and then declined sharply, a profile characteristic of advective heat transfer. The lack of high temperature mineral assemblages adjacent to intrusions supports this hypothesis. Conductive metamorphism results in the minerals buffering the metamorphic fluid, and

because calc-silicate reactions produce more carbon dioxide than water, the XCO_2 of the fluid increases with temperature (Greenwood, 1975; Rice, 1977; Williams-Jones, 1981). The widespread occurrence of clinozoisite in the aureole implies low XCO_2 fluid conditions. This is also consistent with advective-type metamorphism, and suggests, as was previously discussed, that the fluid composition was externally controlled.

The occurrence of cerium-bearing zoisite, which in some instances comprises up to 5% of the rock, may also support a model of advective heat transfer. Cerium and other incompatible elements are concentrated in late-stage magmatic fluids. These fluids, when exsolved, could form a component of the contact metamorphic fluid. The rare earths transported by that fluid would concentrate in minerals such as zoisite or sphene. The lack of cerium-bearing zoisite or any other minerals which could concentrate rare earths outside the aureole may imply rare earth metasomatism and, by inference, fluid transport of heat. However, without support of whole rock rare earth geochemical analyses it cannot be conclusively demonstrated that the rare earths were not derived from the metasediments and concentrated in the zoisite during contact metamorphism.

Clinopyroxene has been identified in some samples, but it has a limited distribution, and occurs in veins or as massive replacements of marble (unit 2). The restricted rather than pervasive distribution of clinopyroxene indicates that it was formed as hydrothermal alteration rather than during contact

metamorphism. The lack of contact metamorphic clinopyroxene in equilibrium with clinozoisite restricts the temperature of contact metamorphism to less than 405 ^{o}C (Fig. 2-4).

As interpreted from the isobaric invarient assemblages, the three innermost isograds enclose an area over which the contact metamorphic fluid stayed at relatively constant composition and temperature. The two outermost isograds represent a lower temperature and possibly higher XCO_2 fluid. The fluid composition and temperature cannot be as well constrained for these isograds owing to the lack of invariant assemblages. However, if the fluid was still externally buffered or controlled, these isograds represent lower temperatures.

2.6 SUMMARY

Contact metamorphic isograds around the Trout Lake molybdenum deposit are poorly defined owing to overprinting by hydrothermal alteration and the lack of any distinctive reactions in the pelitic quartzite lithology. To the southwest a well defined contact aureole is centred around a one meter thick quartz diorite dyke. This dyke is similar in appearance to the quartz diorite of the Trout Lake Stock and is assumed to be an apophyses of a parent pluton at depth which caused the contact metamorphism. An advective model for heat transport is required to explain the distribution of the isograds. If the total pressure during metamorphism was 2000 bars then, within the aureole the fluid was at 360 to 400 ^{o}C and had an XCO_2 of less than 0.05. Outside the aureole, the

isograds representing reactions (1) and (2) were produced by a rapid drop in temperature and/or increase in XCO_2. The isograds and plutonic rocks around the deposit are similar to those around the quartz diorite dyke, therefore it is highly probable that a contemperaneous contact metamorphic fluid of similar chemistry affected the rocks surrounding the Trout Lake Stock and the quartz diorite dyke prior to mineralization.

CHAPTER 3: ALTERATION

3.1 ALTERATION TYPES

Skarn, potassic, silicic, and phyllic, are the four major types of alteration associated with the Trout Lake deposit. Figure 3-1 shows the extent of surface alteration. Although phyllic alteration has the widest distribution, individual zones of pervasive phyllic alteration are small, irregular, and generally associated with faults. The field of this alteration (Fig. 3-1) is thus simply an area in which phyllic alteration may be found. The limit of pervasive potassic alteration is somewhat arbitrary. There is a continuum between pervasive potassic alteration and contact metamorphism. This problem will be discussed at length later in this chapter. Both silicic and skarn alteration occur as massive replacement, and Fig. 3-1 shows the respective zones of pervasive alteration. Silicic alteration forms the core of alteration at surface, and is associated with the bulk of the surface molybdenum mineralization. Skarn alteration occurs at the intersection of faults with limestone (unit 2) near the Trout Lake Stock, and locally contains tungsten mineralization.

3.1.1 SKARN ALTERATION

The skarn unit was developed around faults in limestone by massive replacement by calc-silicate minerals (Figs. 1-3, 1-4, 1-5). An occurrence of skarn replacing marble is shown in Plate 3-1. Replacement textures indicate that two skarn

events, prograde and retrograde, occurred. The prograde mineral assemblage consists of clinopyroxene, garnet, calcite, quartz, and rare wollastonite. The retrograde skarn is composed of tremolite, clinozoisite, calcite, quartz, and rare idocrase. Plagioclase is rarely preserved, and is assumed to be metastable when present, owing to its limited occurrence and the stability of clinozoisite + calcite. Biotite replacement of tremolite is common, which indicates that both the retrograde and prograde skarn events occurred before potassic alteration. The mineral assemblages present in skarn and other alteration types are summarized in Table 3-1.

3.1.2 POTASSIC ALTERATION

Potassic alteration is difficult to recognise because biotite or K-feldspar haloes around veins or fractures are not extensively developed, and these two minerals are present in unaltered metasedimentary and igneous rock samples. Minerals from the area surrounding the deposit have four potential origins: detrital, regional metamorphic, contact metamorphic, or hydrothermal. In the case of biotite a detrital origin can be discarded as biotite would have been altered to clay during sedimentary processes. The regional metamorphic phase is easily recognised as the grains define foliation(s), that distinguishes them from the contact metamorphic and hydrothermal biotites which are coarser grained and have a random orientation.

In an effort to distinguish between the texturally similar contact metamorphic and hydrothermal types, biotite

Figure 3-1   Surface alteration

Biotite as a Percentage
of Total Sheet Silicates
□ <25   ▤ 50-75
▨ 25-50   ■ >75

Percentage of K-Feldspar
O <2
◑ 2-5
● >5

▤ Silicic Alteration

▨ Skarn

Limit of Potassic Alteration

Limit of Phyllic Alteration

Contact Metamorphic Aureole

Geological Contact

Fault

0   250   500m
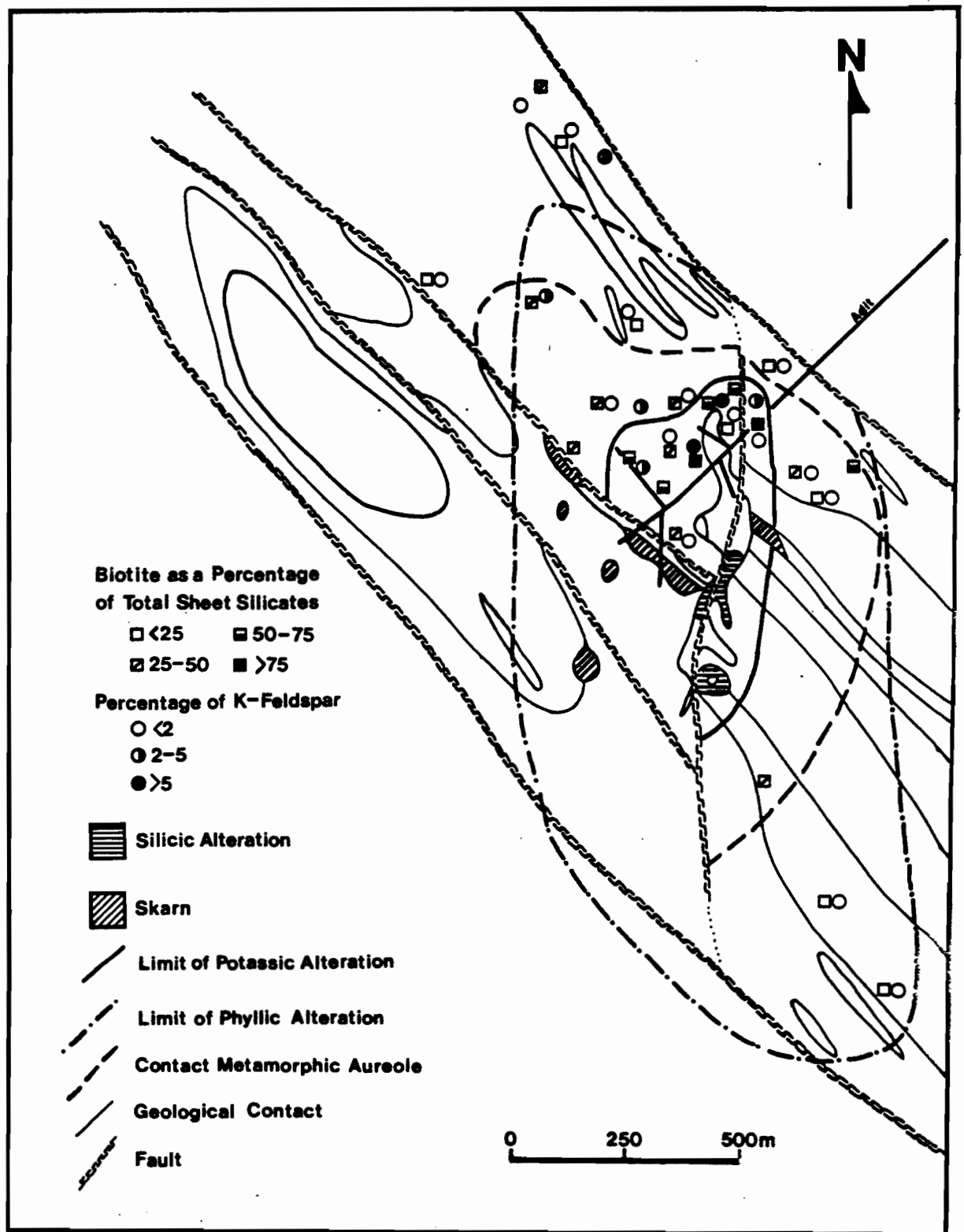
abundances were determined by thin section inspection as a modal percent versus the total modal percentage of sheet silicates observed in thin sections. It is apparent, by using the biotite content of quartz-biotite schists (unit 1), that a zone of intense biotization (greater than 50 % biotite) may be defined which is associated with the deposit at surface (Fig. 3-1). Within this zone of alteration, biotite rarely occurs as veins or haloes around veins crosscutting quartz-biotite and calc-silicate schists (units 1 and 3). In addition, clinozoisite is absent within the zone of intense biotization.

Surrounding the zone of intense biotization is a zone of moderate biotization (25 to 50 % biotite), which contains plagioclase with an approximate composition of An_{25} (Fig.2-3) and cerium-bearing zoisite. The lack of cerium-bearing zoisite and the occurrence of albitic plagioclase outside the zone of moderate biotization coincides with the occurrence of biotite at regional metamorphic abundance levels (less than 25 %). In a sample from northwest of the deposit, in the moderately biotizedzone, randomly oriented biotite occurs along fractures accompanied by cerium-bearing zoisite, which illustrates their coincidence in time and space. It is also noteworthythat in this sample, the randomly oriented biotite in the pelitic layers appear to be coeval with the fracture-filling biotite. Biotite apparently formed continuously from the contact metamorphic to the potassic alteration stages. The fluids which caused contact metamorphism probably also resulted in the formation of cerium-bearing zoisite, changed the plagioclase compositions, and increased the modal

abundance of biotite. The zone of moderate biotization is probably largely the result of contact metamorphism as it lies between the zones of low biotite abundance (regional metamorphic), and intense biotization (potassic alteration). However, the division between intense and moderate biotization is somewhat arbitrary. The limit of intense biotization does not necessarily correspond to the limit of biotite alteration sensu stricto. Therefore the zones of intense and moderate biotization merely represent the approximate location of the areas affected by potassic alteration and contact metamorphism respectively.

Similarly, in the plane of the adit, at the core of the deposit, the pelitic layers in the quartz-biotite schist are generally comprised of biotite, or biotite + muscovite. Outside the zone of mineralization, the chlorite content increases and biotite content decreases with increasing distance from the deposit as was the case with surface alteration. The number of thin sections from this plane unfortunately is insufficient to quantitatively characterize biotization.

The surface distribution of K-feldspar mimics that of biotite (Fig. 3-1). Intense K-feldspathization (greater than 5 % K-feldspar) has a sporadic distribution,but is associated solely with the deposit and therefore constitutes potassic alteration. With increasing distance from the deposit, the K-feldspar content decreases sharply. The high K-feldspar contents near the deposit are hydrothermal in origin, occurring dominantly within quartz segregations in the quartz-

biotite schists. The lower K-feldspar contents peripheral to the deposit could be of hydrothermal, metamorphic, or detrital origin. In the plane of the adit (Fig. 3-2) potassic alteration is prominent at the core of the deposit. However, a large proportion of the host rock has undergone both potassic and phyllic alteration, which has been termed mixed alteration in Figure 3-2. Plate 3-2 shows potassically altered quartz-biotite schist from the core of the deposit.

Potassic alteration can be subdivided into biotite-calcite, and late potassic alteration stages. The formation of biotite and K-feldspar in intensely biotized rocks occurred largely during biotite-calcite alteration. During late potassic alteration, biotite-calcite alteration was overprinted by quartz-albite veins with biotite haloes. These haloes have a distinct mineral assemblage of biotite, muscovite, quartz, calcite, albitic plagioclase, and sphene. Some sphene grains contain inclusions of rutile.

The mineral assemblages observed in biotite-calcite alteration are dependant on the original lithology. Calcareous rocks (tremolite-biotite schists) are composed of tremolite, biotite, chlorite, muscovite, plagioclase (An_{30}), quartz, calcite, and sphene. They differ from the contact metamorphic equivalent lithology by the lack of K-feldspar and clinozoisite, and by having a more sodic plagioclase. Pelitic rocks (quartz-biotite schists) are composed of quartz, biotite, K-feldspar, plagioclase (An_{30}), muscovite, calcite, and less commonly chlorite, garnet, and corundum. They differ from the contact metamorphic equivalent lithology by having a

Figure 3-2 Plan view of alteration within the deposit on the
plane of the adit

N

adit

Copper Chief Fault

Alteration Types

- ⬚ Skarn
- ⬛ Silicic
- ⬛ Phyllic
- ⬚ Potassic
- ⬜ Mixed Phyllic–Potassic

Projected Limit of Alteration

0   50   100 m
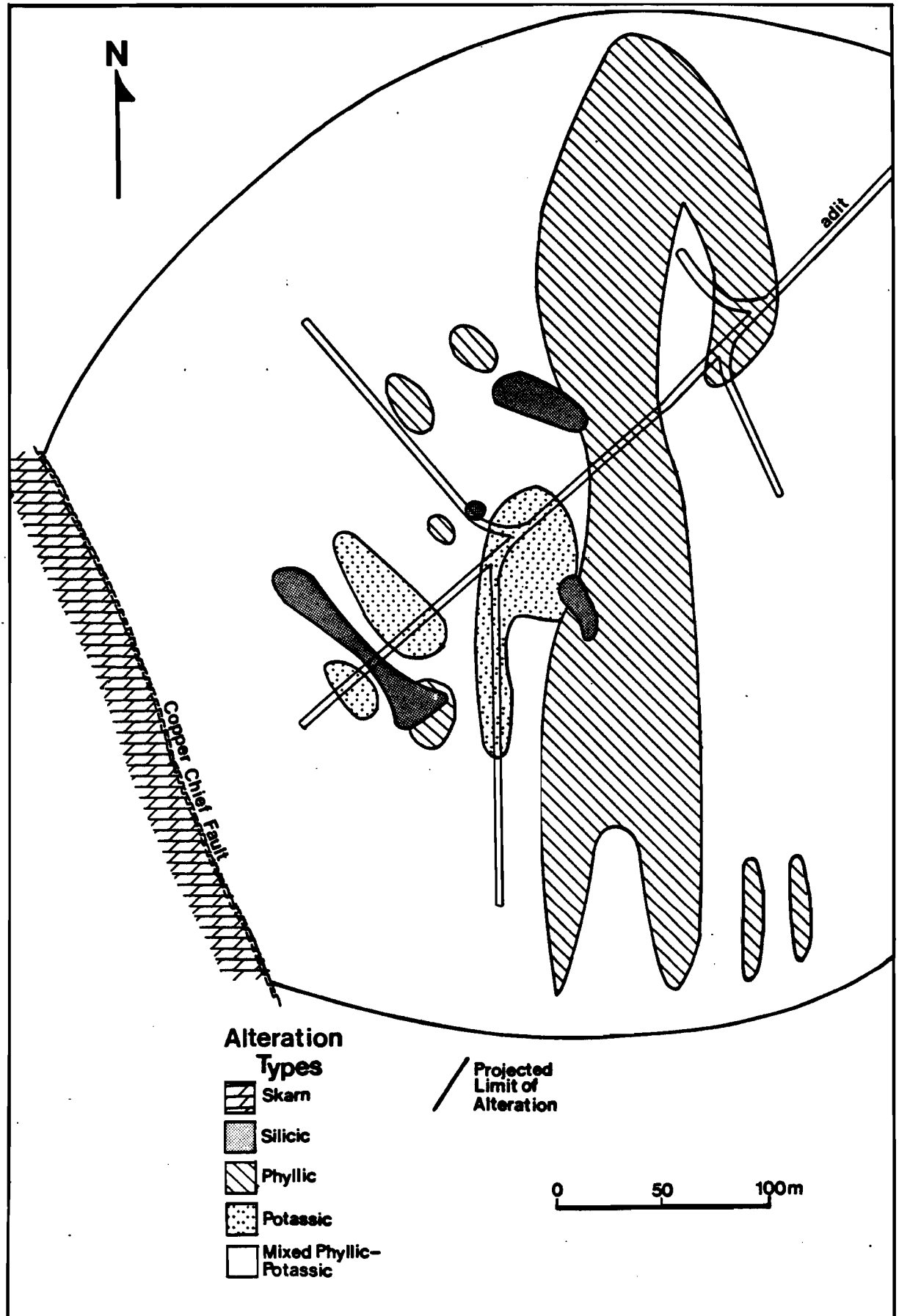
greater modal abundance of biotite and K-feldspar, a lesser modal abundance of chlorite, and a lack of clinozoisite.

The biotite-calcite alteration assemblage is texturally similar to contact metamorphism. Both display compositional layering, and random grain orientation. Haloes of biotite-calcite alteration are not developed around veins, which makes it difficult to establish the relative timing of this event. However, biotite haloes (late potassic alteration) crosscut and replace tremolite-biotite schist. Therefore biotite-calcite alteration probably preceeded late potassic alteration. Alternatively, the two events may have been coeval. If they were coeval, then late potassic alteration represents a higher fluid/rock ratio.

3.1.3 SILICIC ALTERATION

Pervasive silicification by massive quartz replacement as opposed to quartz veins is limited in extent but has been distinguished as quartz stockwork. This alteration-type, which occurs at the center of the deposit (Figs. 3-1 and 3-2), contains relatively high grade molybdenum mineralization. The silicification replaces igneous units and, less commonly, metasedimentary units. Albite, K-feldspar, muscovite, calcite, sphene, rutile, and sulphides are the only minerals present in addition to quartz. Remnant biotite and chlorite have also been recognized, but these are always partially replaced by muscovite, and therefore are considered to be metastable. Plate 3-3 shows a zone of pervasive silicification and quartz veining from the centre of the

Plate 3-1   Skarn (dark green) replacing marble (grey/white)

Plate 3-2   Late potassic alteration crosscutting biotite-
            calcite alteration in a quartz-biotite schist
            (unit 1). The biotite halo is around a quartz-
            albite-K feldspar (stained yellow) vein.
            Sericitized porphyroblasts are present in the
            quartz-biotite schist.

Plate 3-3 Pervasive silicification crosscutting potassic
            alteration. The quartz stockwork crosscuts the
            majority of veins it intersects. The scale is
            approximately 2 m across.
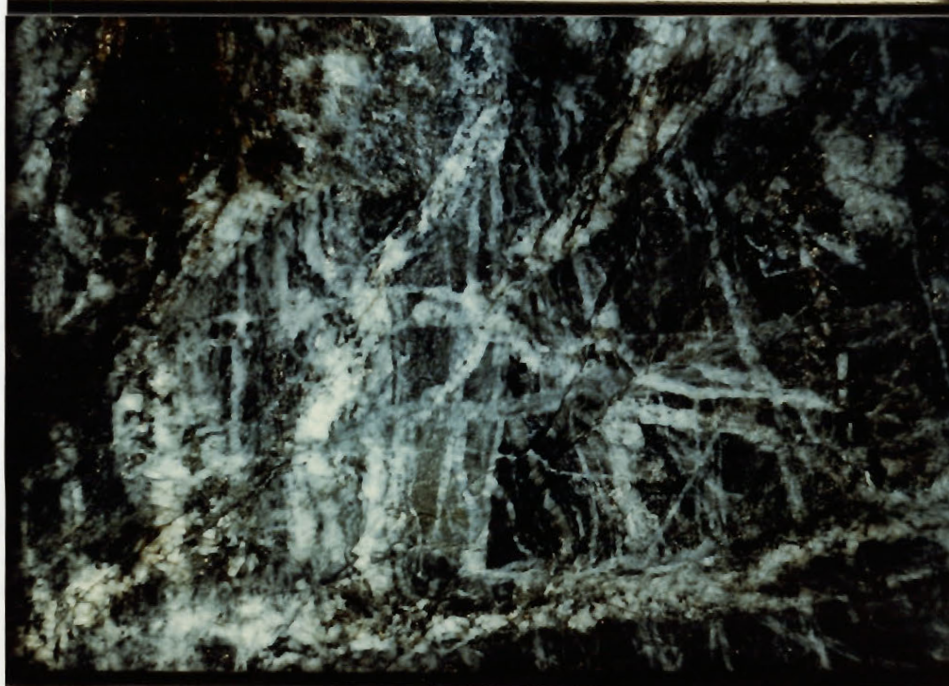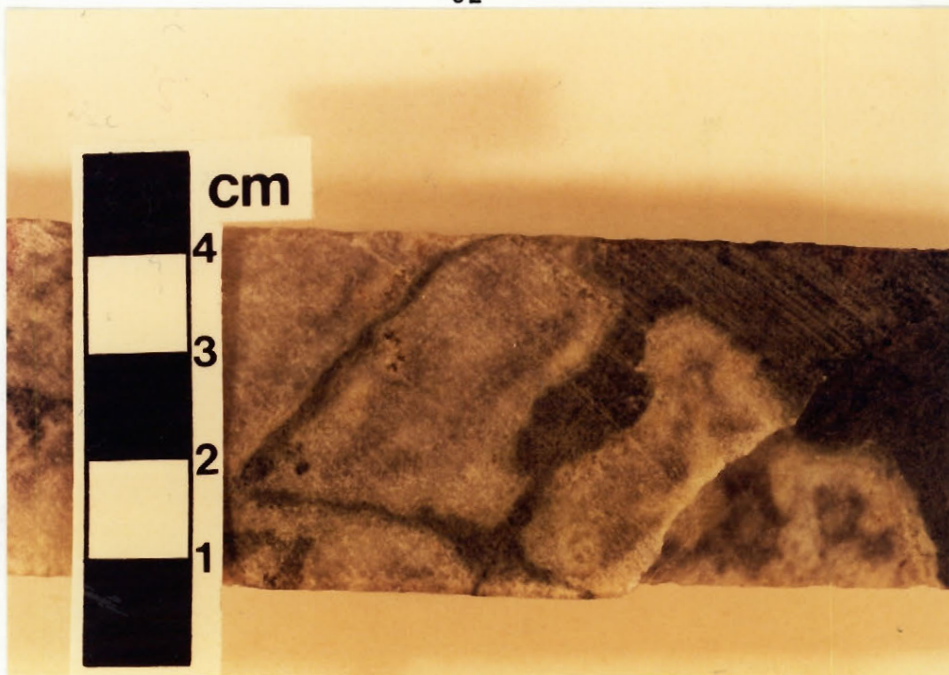
deposit. Here the silicification crosscuts quartz-biotite schist, which was previously affected by potassic alteration.

In partial silicification, a very fine grained silica matrix surrounds coarse grained, partially silicified relict plagioclase crystals (embayed by fine grained quartz). Quartz overgrowths on plagioclase are not observed in fresh igneous samples indicating that this is an alteration texture, and not due to magmatic resorption. Very fine grained K-feldspar can also accompany quartz as groundmass flooding. Most feldspars, even those that are apparently igneous have alkalic compositions indicating that feldspars in silicic alteration zones have generally undergone cationic exchange with hydrothermal solutions. In addition, coarse grained quartz and alkali feldspars are present in veins within pervasively silicified samples, demonstrating that quartz and feldspars were also precipitated from hydrothermal fluids which passed along open fractures.

The amount of vein quartz present in a given volume of rock can be considered as a measure of the degree of silicification, although true alteration (replacement of minerals) may not have occurred. Figure 3-3 shows the volume percent of quartz veins present as determined over 10 meter intervals in the adit and drill core. The shape of the contours of these values correlates well with contours of molybdenum grade, indicating that the degree of silica flooding may be genetically linked to the control of mineralization. Assuming that most of the altering and mineralizing fluids passed along open fractures which became

Figure 3-3   Silicic alteration, quartz vein abundance, and
molybdenum abundance on the plane of the adit.

20-40 % Quartz Veins

>40 % Quartz Veins

Pervasive Silicification

MoS₂ Grade
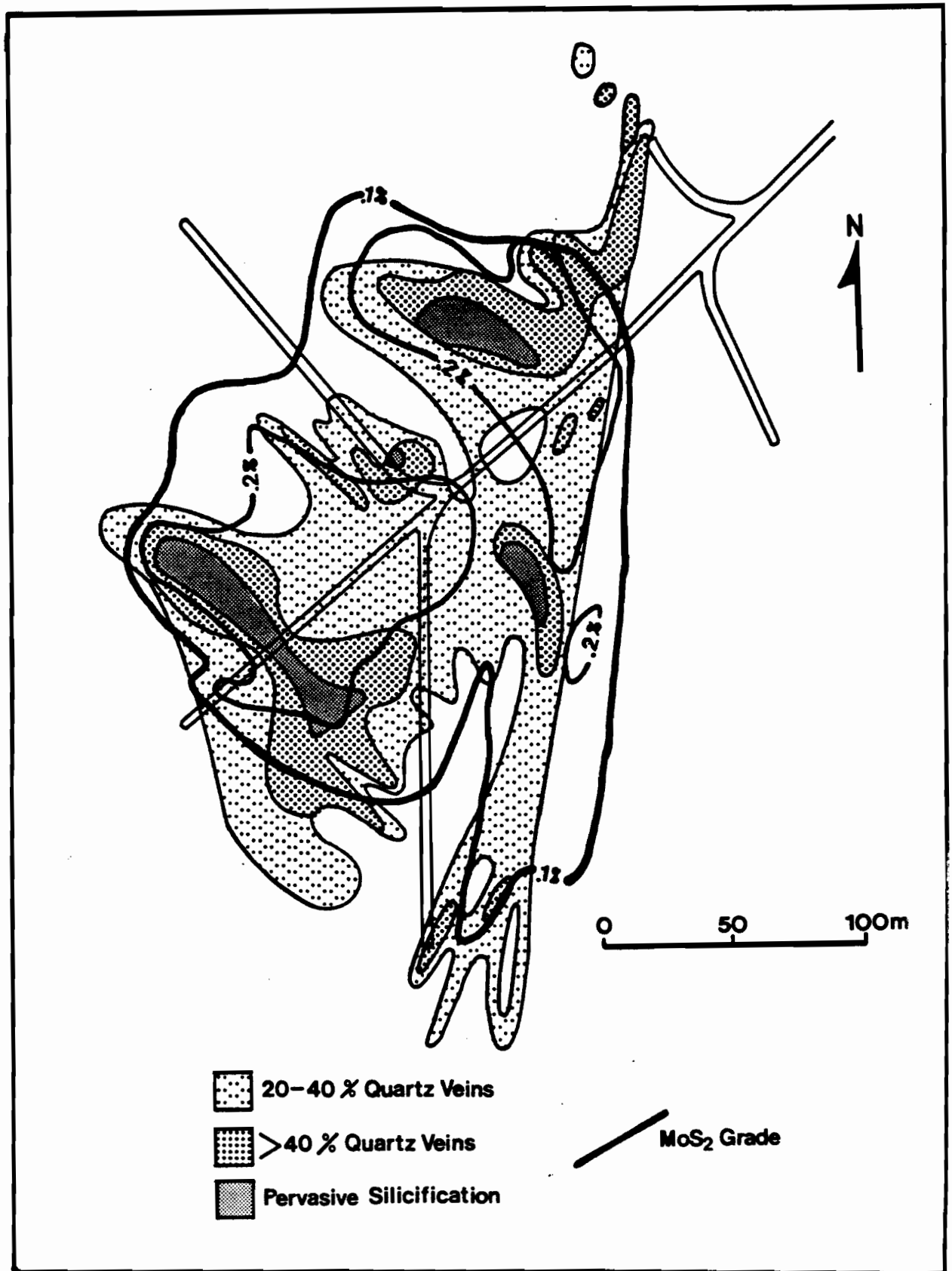
filled by quartz, the areas with high quartz vein densities represent regions of higher fluid/rock ratios. Areas of pervasive silicification are located in the centre of the zones of high grade mineralization and high quartz vein density. Therefore pervasive silicification probably reflects the areas where mineralizing fluids were focussed.

3.1.4 PHYLLIC ALTERATION

Of all the alteration types, phyllic is the easiest to recognise in hand specimen. Haloes around quartz veins, or less commonly around fractures, are sharply defined as the light coloured muscovite contrasts strongly with the dark brown biotite. Plate 3-4 shows phyllic alteration crosscutting quartz-biotite schist. Figure 3-2 displays the distribution of phyllic and potassic alteration on the plan view at the adit level. Pervasive phyllic alteration is generally associated with faults, in particular the Z-fault, but variable amounts of phyllic alteration (mixed alteration on Fig. 3-2) are present throughout the deposit, with the exception of the core, where potassic alteration is dominant.

The phyllic alteration mineral assemblage is typically muscovite with quartz and subordinate K-feldspar, albite, ankerite, pyrite, and rutile. The occurrence of muscovite alone does not constitute phyllic alteration, as muscovite is stable in all alteration types except skarn. Pervasive muscovite replacement of biotite, accompanied by ankerite and pyrite, characterize phyllic alteration. This is unusual if compared to phyllic alteration in porphyry copper deposits,

where feldspars are strongly sericitized (e.g. Lowell and Guilbert, 1970). Thin section inspection of the "aplite dykes" referred to by Boyle and Leitch (1983) shows that these have undergone strong phyllic alteration, and therefore these are probably altered granodiorite and not a separate igneous phase. Dyke/vein features, noted by Boyle and Leitch (1983) can be explained if the fluids from which the vein formed also completely altered the surrounding dyke-rock.

3.2 CHEMISTRY OF ALTERATION

$T-XCO_2$ diagrams were constructed using the method established in Chapter 2. Reactions were written which involve the alteration minerals discussed above. A total confining pressure of 1000 to 2000 bars is interpreted on the basis of fluid inclusion evidence in Chapter 7. Therefore two diagrams, at 1000 and 2000 bars, were constructed (Figs. 3-4 and 3-5). During the early biotite-calcite alteration, the plagioclase had an An_{30} composition, as determined by microprobe analyses, therefore this composition was used in theconstruction of curves involving anorthite, with activity coefficient data taken from Saxena and Ribbe (1972). Reactions used to establish the stability fields of the various alteration assemblages are listed in Chapter 2 (Table 2-2) with several additional reactions tabulated in Table 3-2. The thermodynamic constants A, B, and C are as defined in Chapter 2.

TABLE 3-2 SUMMARY OF ALTERATION MINERAL ASSEMBLAGES

SKARN PROGRADE	SKARN RETROGRADE	BIOTITE-CLACITE TREMOLITE-BIOTITE	BIOTITE-CALCITE QUARTZ-BIOTITE
Clinopyroxene	Tremolite	Tremolite	Biotite
Garnet	Clinozoisite	Biotite	K-feldspar
Quartz	Quartz	Chlorite	Quartz
Calcite	Calcite	Muscovite	Muscovite
Wollastonite	Idocrase	Plagioclase	Calcite
		Quartz	Garnet
		Calcite	Corundum
		Sphene	Chlorite

LATE POTASSIC	SILICIC	PHYLLIC
Biotite	Quartz	Quartz
Albite	Muscovite	Muscovite
Muscovite	Albite	Albite
Quartz	K-feldspar	K-feldspar
Calcite	Calcite	Ankerite
Sphene	Sphene	Rutile
K-feldspar		

TABLE 3-1 ALTERATION REACTIONS

		A	B	C
(10)	$Cc + Q = Wo + CO_2$	-5320	8.66	0.104
(11)	$An + Wo + Cc = Gr + CO_2$	-2350	4.73	0.273
(12)	$Gr + Q = An + 2Wo$	-2970	3.93	-0.169
(13)	$2Cc + Q + An = Gr + 2CO_2$	-7670	13.39	0.377
(14)	$4Zo + Q = 5An + Gr + 2H_2O$	-13106	23.65	-0.329
(15)	$Id + 4Q = Gr + Di + 3Wo + 4H_2O$	-25123	48.61	-0.416
(16)	$3Do + Kf + H_2O = Ph + 3Cc + 3CO_2$	-15738	29.77	0.224
(17)	$Ma + Q = An + And + H_2O$	-4859	9.34	-0.001
(18)	$Ma = An + Co + H_2O$	-5093	9.30	0.016
(19)	$Mu + Q = Kf + And + H_2O$	-4853	8.69	0.016
(20)	$Mu = Co + Kf + H_2O$	-4153	7.39	0.033

An represents anorthite, And andalusite, Cc calcite, Co corundum, Di diopside, Do dolomite, Gr grossularite, Id idocrase, Kf K-feldspar, Ma margarite, Mu muscovite, Ph phlogopite, Q quartz, W wollastonite, Zo zoisite. Reaction (10) is from Greenwood (1967), (11) from Hoscheck (1974), (14) from Boettcher (1970), (15) Hochella et al. (1982), (16) Puhan (1978), (17 and 18) Storre and Nitsch (1974), (19 and 20) Evans (1965). All other reactions are linear combinations of the above.

3.2.1 SKARN ALTERATION

The rarity of plagioclase in skarn indicates that it was almost totally consumed during skarn formation. For reactions such as tr + zo + q = di + an, the anorthite activity must be defined in order to calculate reactions in $T-XCO_2$ space. A plagioclase composition of An_{30} was used to construct Figures 3-4 and 3-5 based on the consistency of plagioclase of this composition elsewhere in the deposit during other early alteration stages. A plagioclase with a composition of An_{50} is present in unaltered marbles, and therefore is the most calcic composition reasonable for the construction of these diagrams. The An_{50} composition will shift zoisite-consuming reactions, e.g. the diopside-anorthite reaction, approximately 20 $^{\circ}$C higher.

The prograde skarn assemblage is clinopyroxene, garnet, calcite, quartz, and rare wollastonite. Therefore the conditions of skarn formation must lie above the diopside and grossular curves (Figs. 3-4, 3-5). As plagioclase and zoisite are both absent, the minimum temperature and XCO_2 cannot be constrained. However, the maximum temperature and XCO_2 can be established using the stability of grossular + quartz. The anorthite-wollastonite reaction restricts the temperature to below 450 $^{\circ}$C at 1000 bars, and below 500 $^{\circ}$C at 2000 bars. The grossular reaction constrains the XCO_2 of skarn formation to less than 0.03 at 1000 to 2000 bars.

The retrograde skarn assemblage is tremolite, calcite, quartz, clinozoisite, and rare idocrase. As with the prograde assemblage, only the maximum temperature and XCO_2 of formation

Figure 3-4   Alteration reactions in $T-XCO_2$ space at 1000

   bars

TOTAL PRESSURE 1000 BARS
AN_{30} PLAGIOCLASE ASSUMED
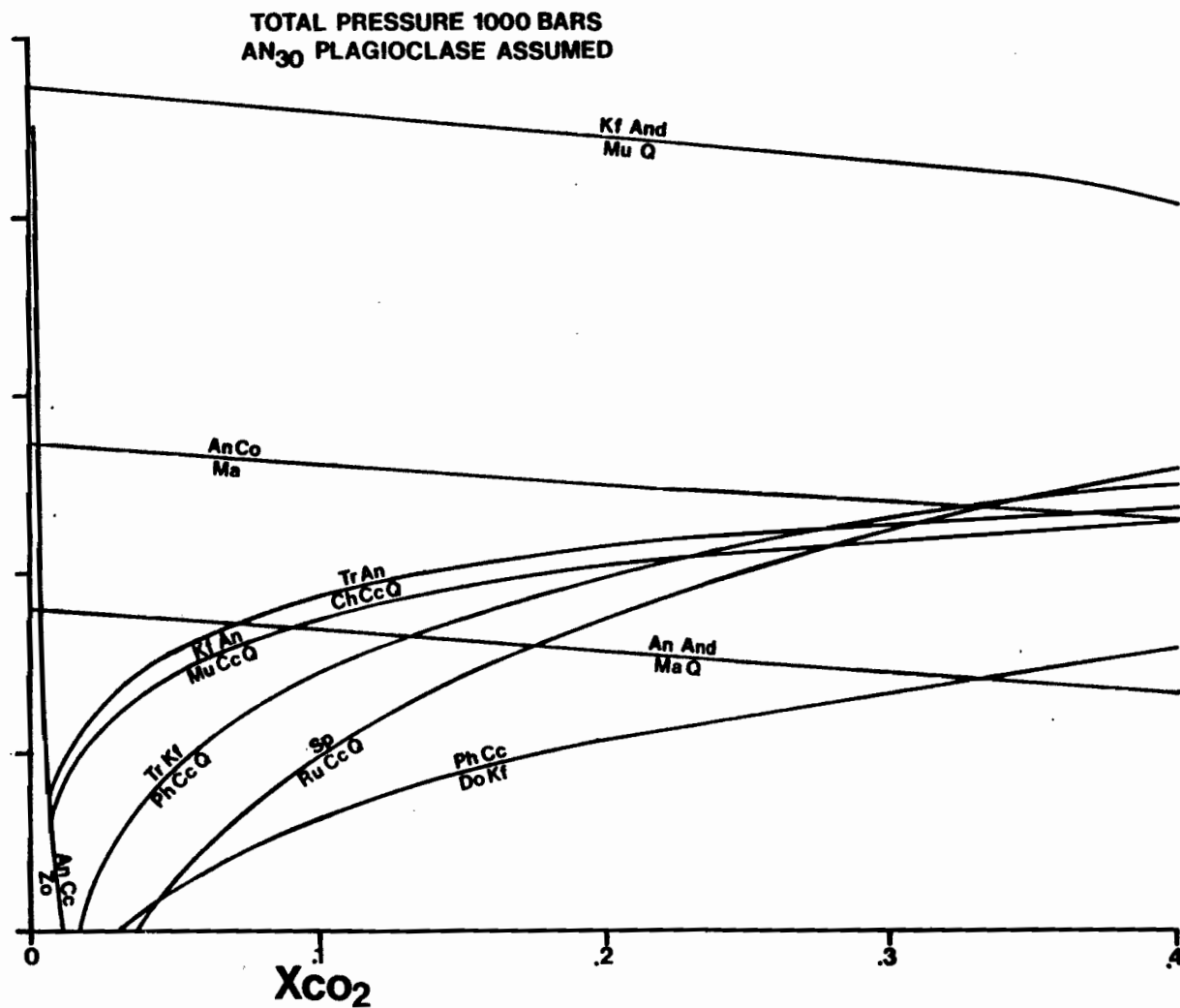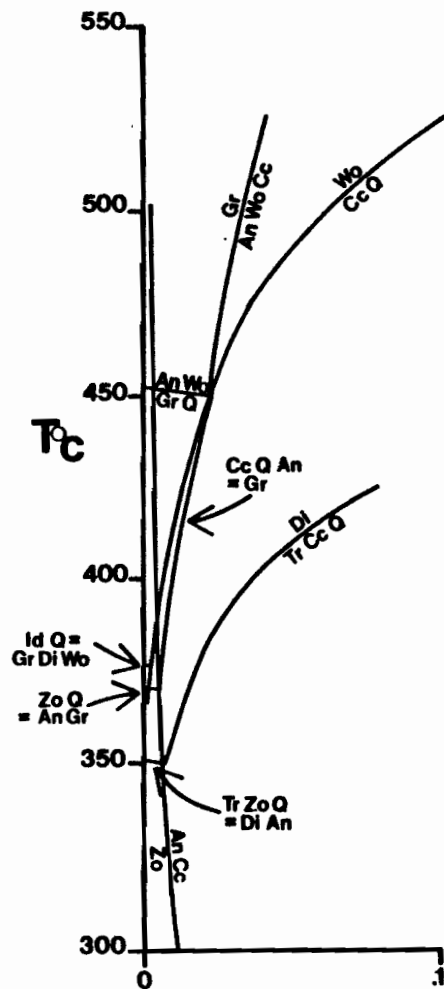
Figure 3-5   Alteration reactions in $T-XCO_2$ space at 2000
bars

TOTAL PRESSURE 2000 BARS
AN_{30} PLAGIOCLASE ASSUMED

$T^{\circ}C$

Gr
AnWo Cc

Wo
Cc Q

AnWo
Gr Q

Gr
Cc Q An

Di
Tr Cc Q

Id Q =
Gr Di Wo

Zo Q
= An Gr

Tr Zo Q
= Di An

Zo

An Cc

600

550

500

450

400

350

0   .1

Kf And
Mu Q

An Co
Ma

Kf An
Mu Cc Q

Tr An
Ch Cc Q

Sp
Ru Cc Q

An And
Ma Q

Tr Kf
Ph Cc Q

Ph Cc
Do Kf

Zo
An Cc

X_{CO_2}

0   .1   .2   .3
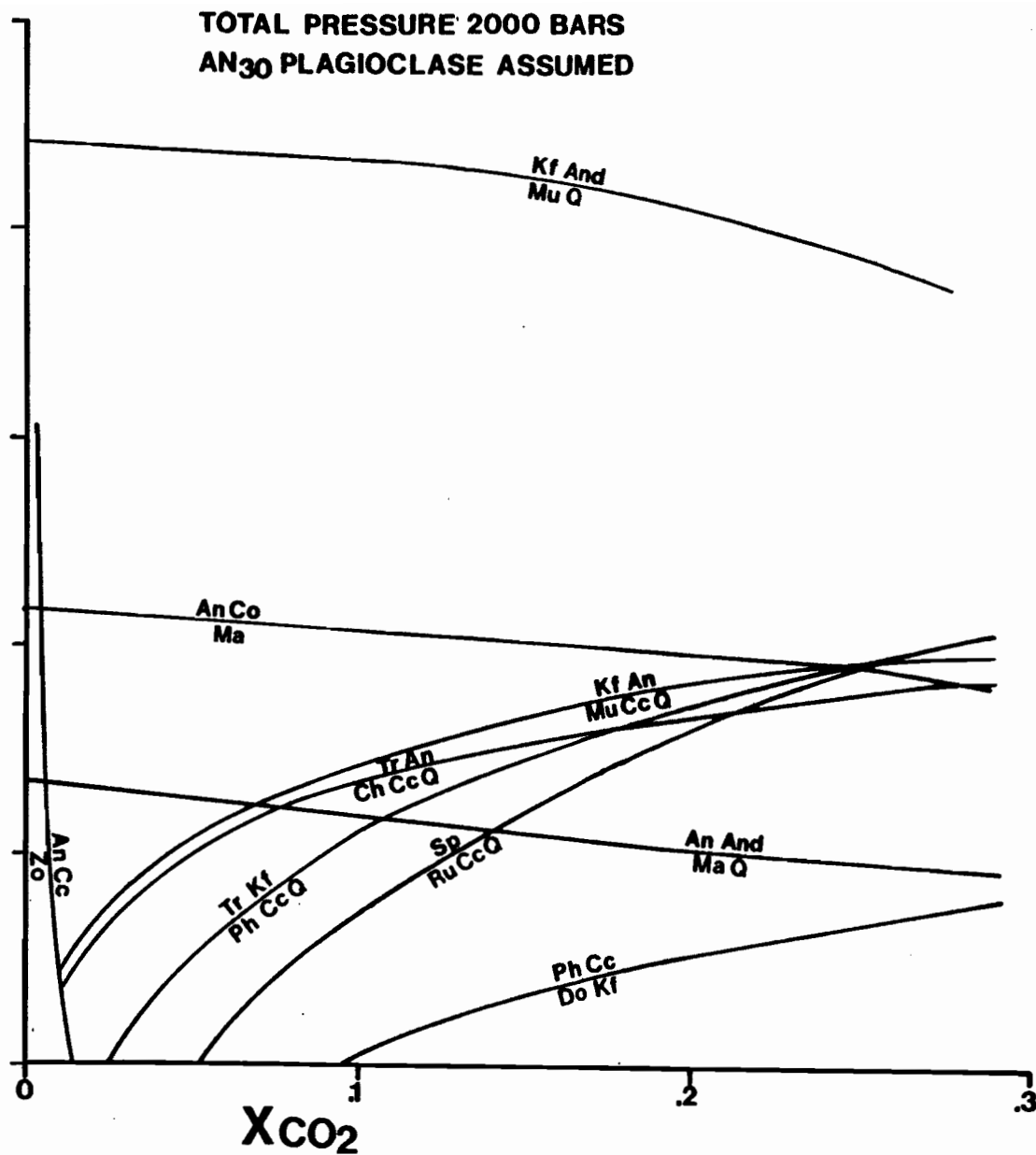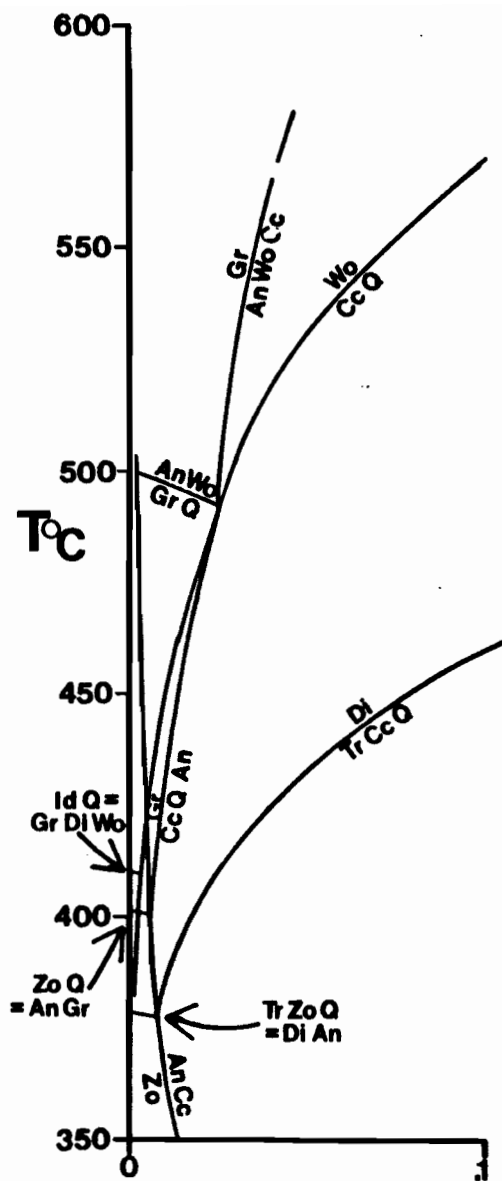
can be established. The stability of idocrase + quartz is restricted by the grossular-diopside-wollastonite reaction. The stability of zoisite + quartz is restricted by the grossular-anorthite reaction, and the stability of tremolite + zoisite + quartz is restricted by the diopside-anorthite reaction. The diopside-anorthite reaction occurs at the lowest temperature of the three reactions. Therefore by using this reaction, the maximum temperature of retrograde skarn formation is 350 ^{o}C at 1000 bars, and 375 ^{o}C at 2000 bars, at a maximum XCO_2 of 0.02 (Figs. 3-4 and 3-5).

As previously discussed, if an An_{50} plagioclase composition is used, the zoisite consuming reactions are raised by approximately 20 ^{o}C (and the An-Cc curve shifts to higher XCO_2 by approximately +0.02). The stability of idocrase + quartz does not involve plagioclase, and constrains the maximum temperature of retrograde skarn formation to 375 and 410 ^{o}C at 1000 and 2000 bars respectively (Figs. 3-4, 3-5). Another possible reaction which involves idocrase + quartz is gr + di = id + q. This reaction curve (not represented on Figs. 3-4, or 3-5) is nearly vertical and terminates at the invariant point (intersection of Reactions 10 and 15 on Figs. 3-4 and 3-5) at the intersection with the wollastonite curve. Therefore the stability of idocrase + quartz indicates that the maximum temperature was 390 ^{o}C at 1000 bars, and 410 ^{o}C at 2000 bars, and that the maximum XCO_2 was 0.02. This is consistent with the estimations using zoisite stability, and therefore the assumption for plagioclase composition is probably reasonable.

3.2.2 BIOTITE-CALCITE ALTERATION

Biotite-calcite alteration, as expressed by tremolite-biotite schists (unit 3) within the area of the deposit have a distinctive mineralogy. The $T-XCO_2$ conditions of tremolite-biotite schist formation must be consistent with conditions defined by the tremolite-anorthite reaction, lie on the low temperature side of the tremolite-K feldspar reaction since the tremolite-biotite schist is K-feldspar absent, and on the high temperature side of the sphene reaction (Fig. 3-4, 3-5). The consistency of mineral compositions, as determined by microprobe analysis, justify the assumption of equilibration between the minerals in the tremolite-biotite schist. Therefore the tremolite-biotite schist formed at approximately 400 ^{o}C with an XCO_2 of approximately 0.25 if 1000 bars was the confining pressure (Fig. 3-4), and at 425 ^{o}C and an XCO_2 of 0.20 at 2000 bars (Fig. 3-5).

Quartz-biotite schists were also affected by biotite-calcite alteration, and $T-XCO_2$ diagrams yeild similar restrictions on the conditions of biotite-calcite alteration. The stability of biotite + calcite + quartz + sphene place restrictions on fluid composition and temperature that are identical to those interpreted from the mineralogical assemblage of the tremolite-biotite schist. As the quartz-biotite schist is chlorite absent, thefluid characteristics cannot be as well constrained. However, the stability field of the observed assemblage overlaps with that of the tremolite-biotite schist. Therefore, it is probable that both lithologies formed under similar $T-XCO_2$ conditions.

Corundum is present in the quartz-biotite schist as anhedral islands within sericitized porphyroblasts (Plate 3-6). A thin layer of margarite (Ca-mica) characteristically separates the corundum from muscovite. At the outer rim of the sericitized porphyroblast muscovite is surrounded by and partially replaced by hydrothermal biotite of the late potassic alteration stage. This suggests that corundum formed prior to late potassic alteration and that the muscovite which encases the corundum did not allow the late potassic alteration fluids to react with the corundum. Any explanation of the early stages of alteration and contact metamorphism must also explain the formation of corundum.

Corundum distribution is restricted to within the zone of pervasive alteration suggesting that it formed solely during hydrothermal alteration. Alternatively it is also possible that it formed during contact metamorphism and that it represents a higher temperature envirnment owing to its close proximaty to the "pluton at depth". However, no other high temperature minerals are present which would indicate that contact metamorphism resulted in higher temperatures in this area. Corundum stability is highly sensitive to changes in pressure. Corundum formed by muscovite breakdown is stable at temperatures above 635 °C at 1000 bars, and 680 °C at 2000 bars (Thompson, 1974). Corundum, if formed from paragonite breakdown is stable at 530 and 565 °C and, if formed from margarite breakdown is stable at 480 and 520 °C, for 1000 and 2000 bars pressure respectively (Thompson, 1974; Storre and Nitsch, 1974). Fluid inclusion evidence (Chapter 7) indicates

Plate 3-4 Phyllic alteration haloes around quartz veins and
           fractures. The vertical bar scale is 1 m.

Plate 3-5 Quartz- clinopyroxene-tremolite vein with a
           clinozoisite halo crosscutting a contact
           metamorphic calcareous schist (unit 3). K-
           feldspar is stained yellow.

Plate 3-6 Photomicrograph (X-polars) of a corundum island
           in a sericitized porphyroblast. Margarite
           separates the corundum from muscovite. Field of
           view is 2.6 mm.
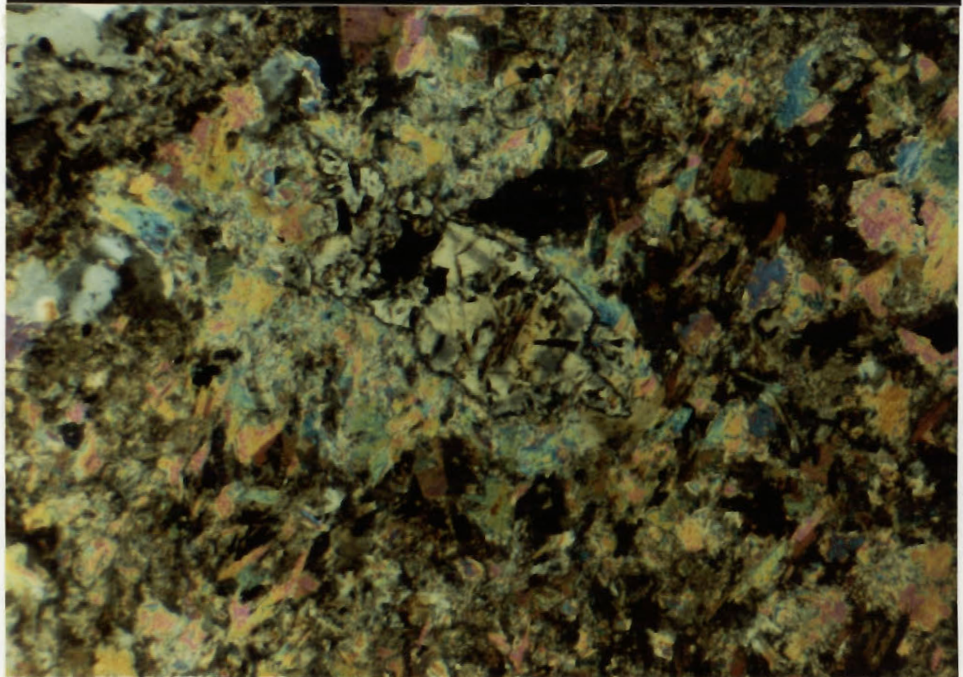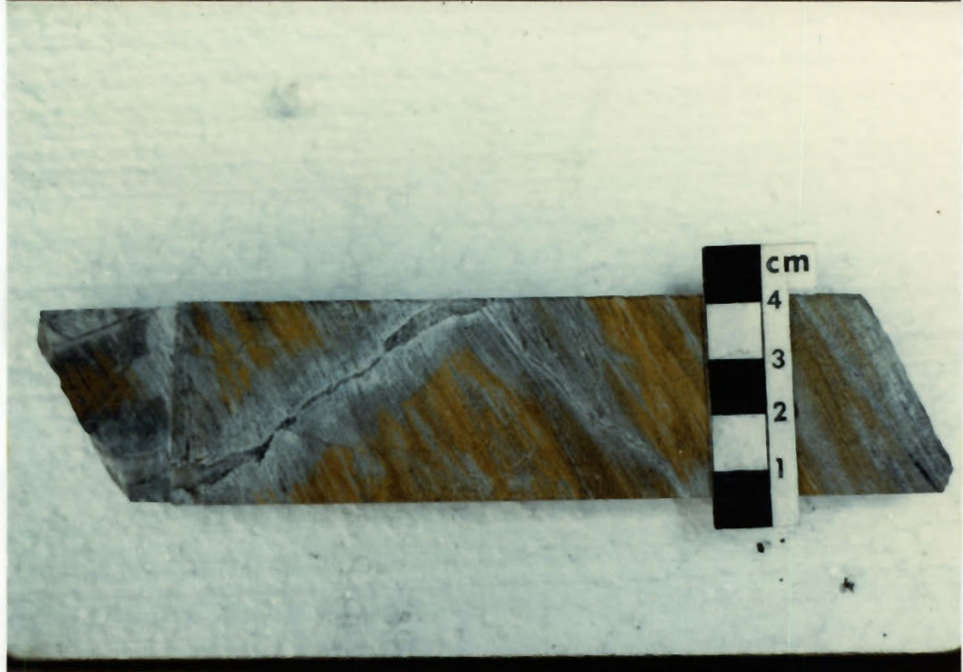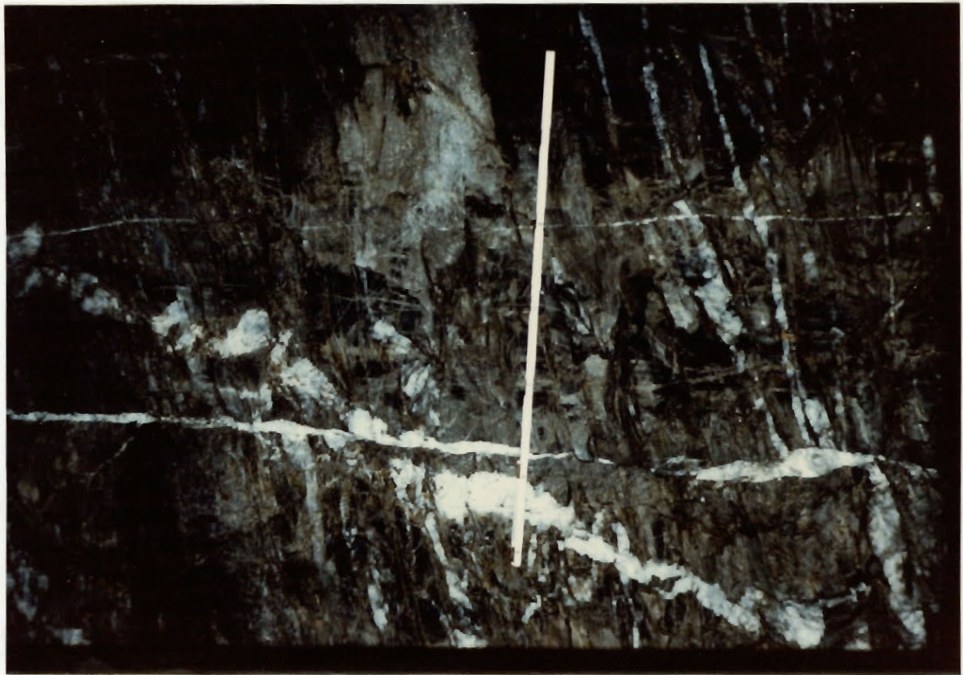
that the confining pressure was 1000 to 2000 bars. Therefore, of the three mica reactions, only the margarite breakdown reaction occurs at temperatures which are reasonable for alteration at Trout Lake.

Anorthite is a co-product with corundum in this reaction, but the matrix plagioclase in the quartz-biotite schists have an An_{30} composition. The effect of a lower anorthite activity on this reaction is to lower the temperature. At 1000 to 2000 bars corundum, coexisting with pure water and An_{30} plagioclase, can form at 430 to 460 ^{o}C (Figs. 3-4 and 3-5), and at lower temperatures for CO_2-H_2O mixtures. While margarite is observed to coexist with corundum, plagioclase is not. Therefore, if corundum formed by a margarite breakdown reaction, it would have to have been a metasomatic reaction. However, the textural relationships between corundum and margarite are suggestive of margarite formation after corundum, not the opposite.

More probably the local environment within the sericitized porphyroblasts was silica undersaturated. Corundum is stable at a temperature of approximately 400 ^{o}C at 1000 to 2000 bars if the fluid phase is silica undersaturated (Hemley et al., 1980). This is possible if the muscovite formed an impermeable barrier to the silica saturated alteration fluids. If, within the closed system of the porphyroblast, the fluids were silica undersaturated, corundum would have formed from an andalusite breakdown reaction. Margarite would have formed by a retrograde metasomatic reaction. In either process, the temperature and XCO_2

-66-

stability field of corundum overlaps with that of biotite-
calcite alteration (Figs. 3-4 and 3-5).

In the quartz-biotite schists, which were affected solely
by contact metamorphism corundum is never present, but
sericitized porphyroblasts are present (Plate 3-7), rarely
with remnant andalusite at the core. Andalusite is probably
of regional metamorphic origin, being sericitized during
contact metamorphism. The breakdown of andalusite + K-
feldspar to form muscovite + quartz (Fig. 3-5) is consistent
with the temperature and pressure of contact metamorphism
estimated in Chapter 2. Andalusite would have been preserved
if K-feldspar was, on a local scale, totally consumed.

3.2.3 LATE POTASSIC ALTERATION

The mineralogy of late potassic alteration is similar to
that of biotite-calcite alteration. Biotite, calcite, quartz,
and sphene are present in both alteration-types. The late
potassic alteration fluid could have existed at $T-XCO_2$
conditions above the sphene reaction and below the tremolite-K
feldspar reaction curve. Clinozoisite is not observed in this
alteration assemblage. In biotite-calcite alteration,the
absence of clinozoisite is significant because plagioclase and
calcite are present. However, in late potassic alteration an
albitic plagioclase is observed, and therefore reactions which
involve plagioclase do not apply to this alteration stage.

Assuming an XCO_2 of 0.10 to 0.20 (XCO_2 maxima established
from fluid inclusion evidence in Chapter 7), the maximum
temperature range is 360 to 425 $^{\circ}C$ at 1000 to 2000 bars, from

the stability of biotite + calcite + quartz (Figs. 3-4, 3-5). However, the XCO_2 was probably lower, which with respect to the above reactions, implies lower temperatures. Therefore, late potassic alteration probably occurred at a lower temperature than biotite-calcite alteration. Rutile inclusions in sphene, observed only in the late potassic alteration, suggest that the temperature was slightly lower than during biotite-calcite alteration, possibly along the sphene curve. However, rutile and sphene may not have equilibrated, as rutile was interpreted to be metastable in some contact metamorphic samples.

3.2.4 SILICIC ALTERATION

Owing to the relatively small number of minerals present in pervasively silicified samples, $T-XCO_2$ diagrams were not found to be useful in the interpretation of the fluid conditions of this alteration type. However, a common observation is that during silicification biotite was replaced in a two-step process. First it was altered to chlorite and sphene, which in turn was altered to muscovite. The presence of sphene in the intermediate step suggests that, during silicification, $T-XCO_2$ conditions were greater than those of the rutile-calcite-quartz stability field. However, as with late potassic alteration, some rutile is present.

3.4.5 PHYLLIC ALTERATION

Phyllic alteration occurred at lower temperatures and/or higher XCO_2 values than any of the previously discussed

events. This is indicated by the presence of rutile +
carbonate + quartz rather than sphene. The carbonate is an
ankerite with approximately equal amounts of iron and
magnesium. Biotite stability, using the phlogopite-calcite
reaction, restricts the conditions of phyllic alteration to
the lower temperature/higher XCO_2 side of that reaction curve.
Using an XCO_2 of 0.10 to 0.20 (established from fluid
inclusion evidence in Chapter 7) the phlogopite-calcite
reaction restricts the conditions of phyllic alteration to a
maximum of 365 ^oC at 1000 (Fig. 3-4), and 380 ^oC at 2000 bars
(Fig. 3-5).

3.5 DISCUSSION

A qualitative chemical potential diagram for potassium
versus magnesium has been constructed, assuming constant
aluminum, to aid interpretation of contact metamorphism and
alteration (Fig. 3-6). At constant temperature and pressure a
maximum of three phases can exist at a given point in
potassium and magnesium chemical potential space for the five
component system K_2O, MgO, Al_2O_3, SiO_2, H_2O (using the phase
rule).

In pelitic quartzites (unit 1) within the aureole
chlorite, muscovite, and biotite are apparently in
equilibrium. During the contact metamorphic to biotite-
calcite alteration stages in unit 1, chlorite was
progressively replaced by biotite reflecting an increase in
the chemical potential of potassium, along the univariant
muscovite-biotite curve. The invariant assemblage biotite +

Figure 3-6 Chemical potential diagram of potassium versus
            magnesium. The arrow represents the chemical
            potential from the contact metamorphic to
            phyllic alteration stages.
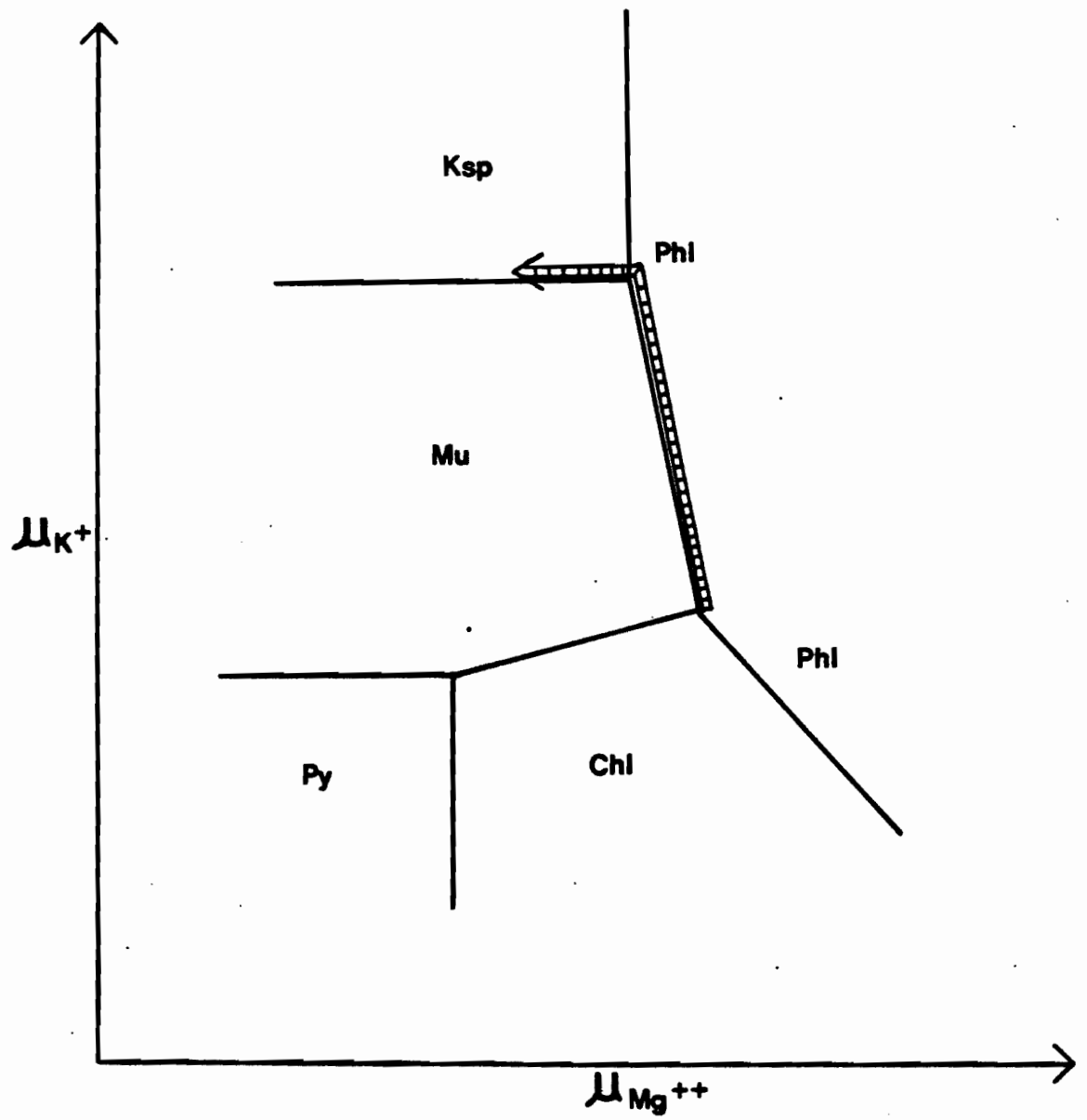
hydrothermal fluids at this stage were water-rich (XCO_2 less than 0.03) and that the temperature was less than 450 to 500 °C for confining pressures of 1000 to 2000 bars respectively. The retrograde skarn assemblage also formed from a water-rich fluid (XCO_2 less than 0.02) at a temperature of less than 390 to 410 °C at 1000 to 2000 bars respectively.

Biotite replacement of tremolite indicates that potassic alteration post-dated skarn alteration. Potassic alteration can be subdivided into two stages: biotite-calcite and late potassic. Biotite-calcite alteration occurred at 400 to 425 °C at 1000 to 2000 bars, at an XCO_2 of 0.20 to 0.25. Biotite-calcite alteration is overprinted by late potassic alteration in the form of quartz-albite veins with biotite haloes. The temperature of late potassic alteration was probably lower than biotite-calcite alteration, but the $T-XCO_2$ conditions cannot be well constrained. It is also possible that biotite-calcite and late potassic alteration were coeval, and late potassic alteration is the result of a higher fluid/rock ratio.

Silicification spatially corelates with molybdenum mineralization and, in the areas of pervasive silicification, both replacement and open-space-filling textures are observed. Alkali feldspars, muscovite, and calcite were also stable during silicification. The conditions of silicic alteration cannot be well constrained by using $T-XCO_2$ diagrams. Phyllic alteration is the youngest hydrothermal event. It is characterized by muscovite replacement of biotite with accessory ankerite, pyrite, alkali feldspars, and rutile. The

stability relations of ankerite + K-feldspar + rutile + quartz
indicate that phyllic alteration occured at lower temperatures
and/or at a higher XCO_2 than previous alteration.

CHAPTER 4: MINERALIZATION

The geological reserves of the Trout Lake deposit are estimated at 50 million tonnes of 0.23 % MoS_2 at a 0.1 % cutoff grade (Boyle and Leitch, 1983). The mineralized zone extends vertically over 1000 m (Fig. 1-6), and is roughly 200 X 300 m in plan view at the adit level (Fig. 1-5). Molybdenite is generally hosted by quartz-feldspar veins, or is associated with silicification. Rarely, molybdenite is observed along "dry" fractures. Zones of scheelite mineralization occur in clinopyroxene-garnet-pyrrhotite skarn adjacent to the deposit.

4.1 STYLES OF MINERALIZATION

As discussed in Chapter 3, there is a strong corelation between quartz vein density and molybdenum grade (Fig. 3-3). Owing to the importance of the relationship between quartz veins and mineralization, a vein study was undertaken to gain insight on the controls of mineralization. Over 1900 veins were described from 19 different stations in the adit and crossdrifts. The method of this study and the interpretation of vein orientations are described at length in Chapter 5. However, in this chapter the nature of the accessory minerals and their relationship to mineralization will be discussed.

Typically a mineralized quartz vein is zoned, with feldspars along the selvages and quartz filling the vein centre (Plate 4-1). The development of euhedral quartz and feldspar crystals, and comb structures suggest open space

filling. It is not uncommon to see veins where multiple openings have resulted in the development of multiple feldspar selvages (Plate 4-1). Molybdenite in quartz veins is generally intergrown with the feldspars or, less commonly, is disseminated in the quartz portion of the veins.

By staining vein feldspars (etching with 70 % hydrofluoric acid and immersing in a saturated sodium cobaltinitrite solution) it was observed megascopically, that molybdenite is dominantly intergrown with albite rather than K-feldspar. In addition, where the two feldspars are intergrown, K-feldspar usually replaces albite (Plate 4-2). Thin section inspection of the molybdenite feldspar intergrowths reveals that albite has been sericitized, particularly at grain boundaries, and the molybdenite grains are actually intergrown with muscovite and calcite, not albite (Plate 4-3). Molybdenite grains disseminated in the quartz portion of the veins are typically intergrown with muscovite and/or calcite. This suggests that molybdenite precipitation is related to sericitization-carbonitization processes. It is therefore concluded that the alkali feldspar-molybdenite association is the result of feldspars having provided favourable sites for molybdenum precipitation to occur. Well developed alteration haloes around mineralized quartz veins are rare. However, some mineralized veins with biotite or muscovite envelopes have been observed.

The association between molybdenite and feldspars is illustrated in Figure 4-1. For each vein station studied, the ratio of veins containing feldspars was determined as a

Plate 4-1   Zoned alkali feldspar-quartz vein.   Molybdenite
            is intergrown with alkali feldspars.   Evidence
            for multiple openings is expressed by a second
            alkali selvage in the centre of the vein.

Plate 4-2   Molybdenite intergrown with albite.   K-feldspar
            (stained yellow) is replacing albite.   Scale is
            in cm.

Plate 4-3   Photomicrograph (X-polars) of molybdenite
            (opaque) intergrown with muscovite and calcite
            at an albite (grey) grain boundary. K-feldspar
            (stained yellow) is replacing albite.   Field
            of view is 0.85 mm.
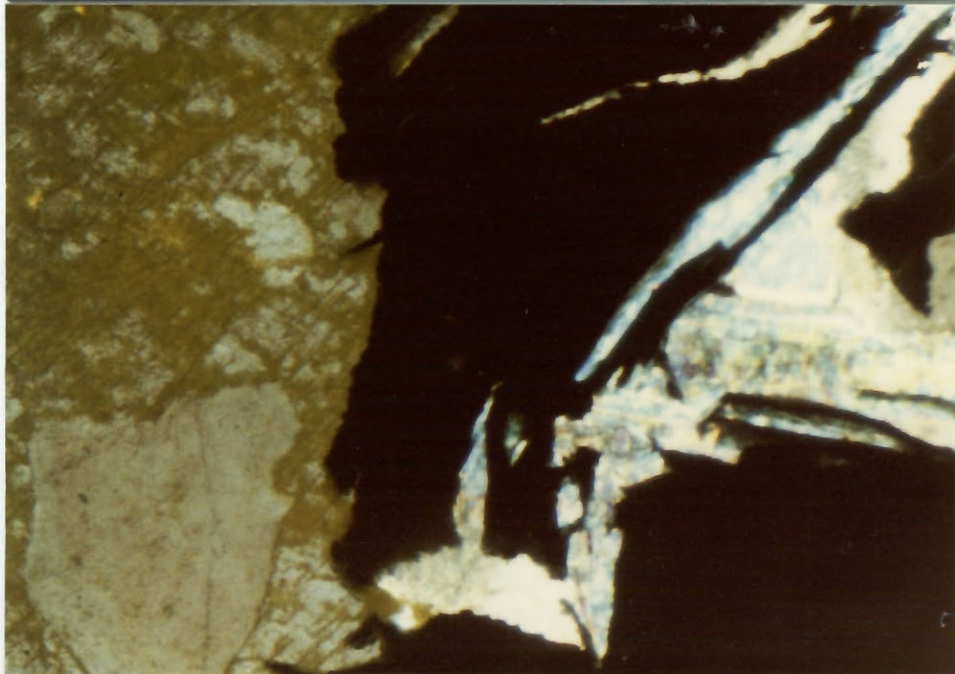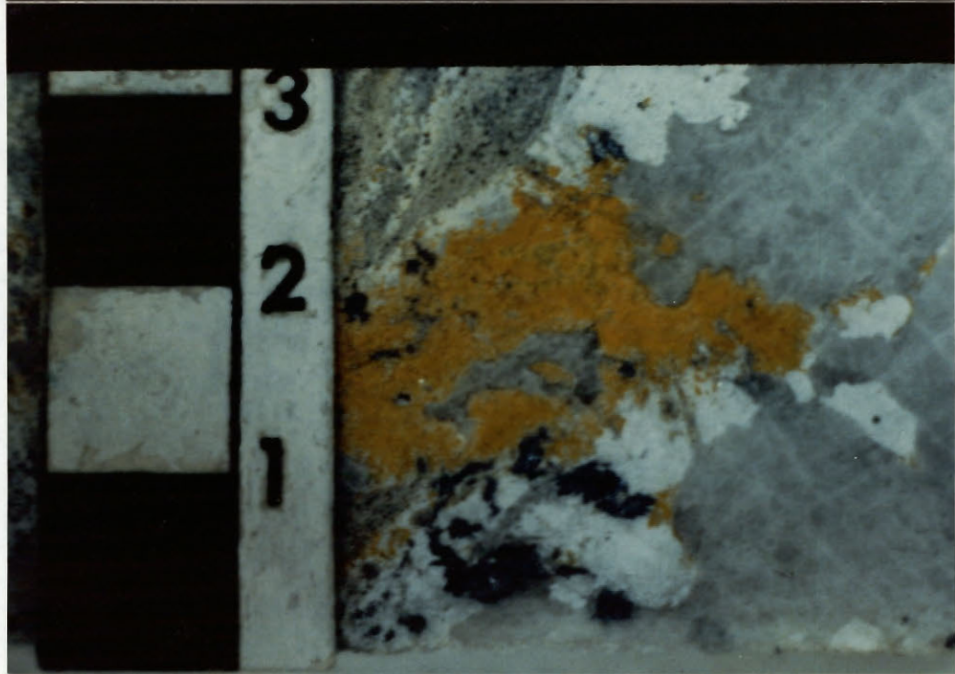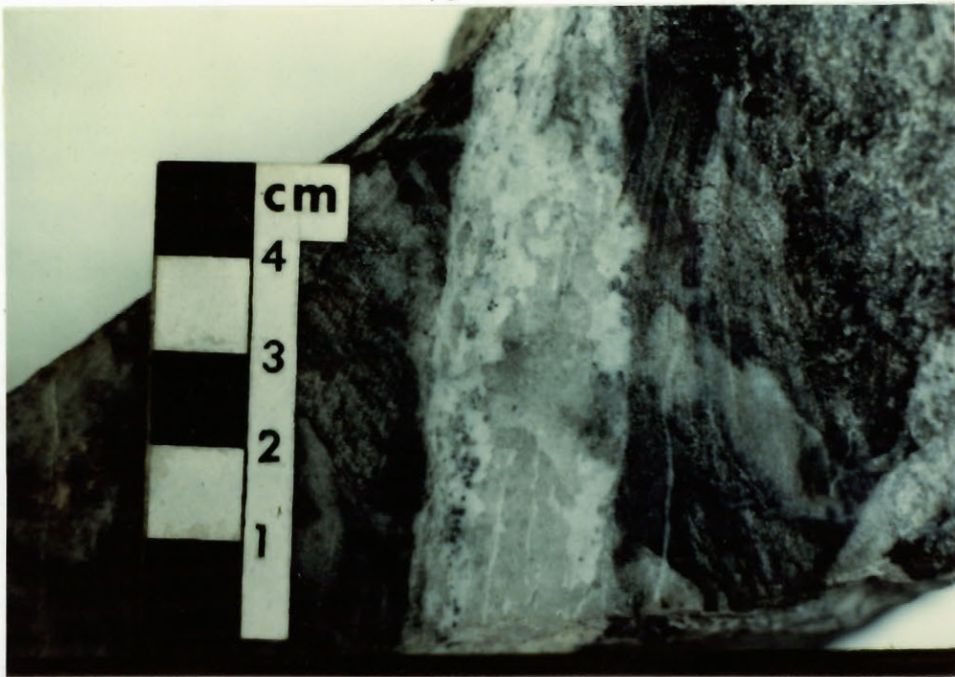
percent of the total number of veins, then these values were contoured. Figure 4-1 also shows a contour plot of the ratio of mineralized veins which contain feldspar to the total number of mineralized veins. By comparing Figure 4-1 to the vein density plot (Fig. 3-3) the following can be concluded: 1) the total density of quartz veins increases from the periphery to the core of the deposit; 2) the percentage of veins with feldspars increases toward the core and 3) the percentage of mineralized veins with feldspars also increases toward the core of the deposit. The strong association between molybdenite and feldspars is thus observed from microscopic to deposit-size scales.

By examining Figure 4-1, it is apparent that mineralization in the igneous host rock differs from that in the metasedimentary host. Both the percentage of veins with feldspars and the percentage of mineralized veins with feldspars is substantially lower in the igneous rocks at the core of the deposit, even though they host significant molybdenum mineralization. The most probable explanation for this lies in the difference in competency between igneous and metasedimentary rock types. The igneous rocks are more brittle due to the lack of foliation and lower sheet silicate content, and this resulted in the development of microfracture systems rather than larger scale vein systems. Microfracturing in the metasediments was impeded by pelitic horizons, evident by the preservation of plagioclase in these horizons, with alkali feldspars present in the more brittle quartz-rich horizons. A greater degree of fluid infiltration occurred in

Figure 4-1   Distribution of % veins with feldspar, and % of mineralized veins with feldspar on the plane of the adit.
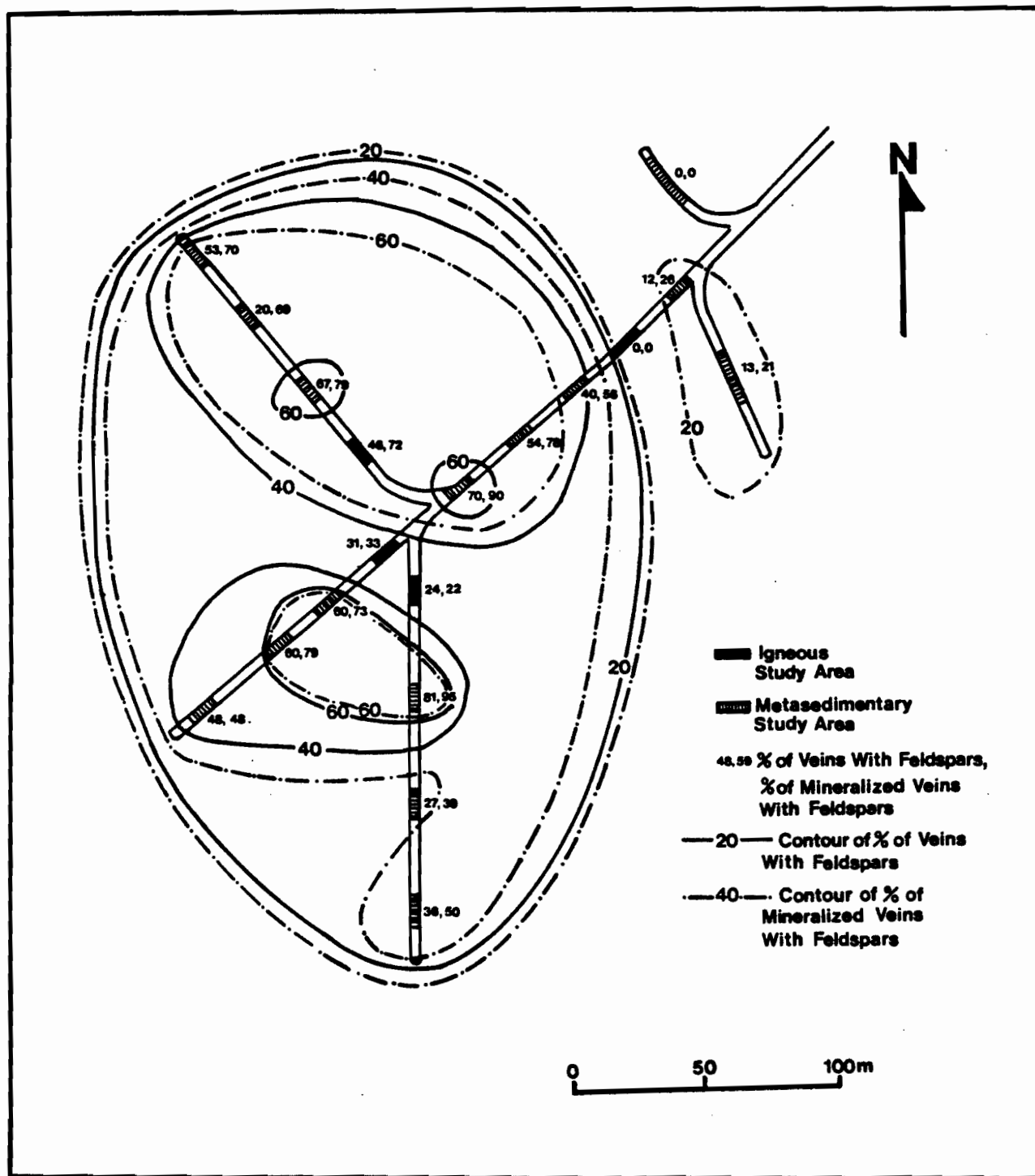
the igneous hosts, as indicated by widespread silicification, albitization, and K-feldspathization. Molybdenite flakes are commonly disseminated in igneous units as a result of the infiltrating fluids. In some instances disseminated molybdenite is concentrated adjacent to quartz veins rather than within them. This texture is rarely observed in metasedimentary rocks owing to their lower permeability. However, a significant proportion of the mineralization hosted by igneous rock is also within quartz or quartz-feldspar veins similar to metasedimentary hosted vein-type mineralization.

Molybdenum mineralization is also associated with intense silicification. This type of mineralization is present either in pervasively silicified rocks or within "high grade dykes", both of which contain relatively high grade mineralization (generally greater than 0.5 % MoS_2). Pervasive silicification replaces both igneous and metasedimentary units as recognised by the remnant material. This intense silica alteration is dominantly within two areas (see plan veiw, Fig. 3-3), both of which contain the highest concentrations of molybdenite in the deposit.

The high grade dykes are similar to pervasive silicification, but are restricted to replacement of small dykes, approximately one meter thick, and are accompanied by abundant molybdenite, locally in excess of 1.0 % MoS_2. Molybdenite appears to be disseminated, but is in fact located along microfractures. These high grade dykes are either within or adjacent to quartz stockwork but, owing to their restricted size and distribution, they have not been

represented on any plan or cross section. Silicification in the high grade dykes is characterized by widespead quartz replacement, including replacement of primary plagioclase, with albitization, K-feldspathization, sericitization, and carbonatization also present (Plates 4-4 and 4-5). In comparing the alteration in high grade dykes to pervasive silicification it can be observed that a greater proportion of primary plagioclase has been preserved in the high grade dykes. In addition, a greater proportion of biotite, and chlorite + sphene (replacement of biotite) has been preserved. However, the matrices of the high grade dykes have been either totally silicified, or replaced by quartz + alkali feldspar.

The timing of silicification in relation to mineralization is unclear. There is certainly a spatial relationship , but silicification may have preceded mineralization, causing the host to be more brittle and to fracture more easily. This would have caused a greater degree offluid infiltration, possibly resulting in more molybdenite precipitation. Alternatively, molybdenite precipitation may have accompanied silicification, with feldspar alteration and dissolution occurring synchronously with mineralization. Textural observations imply that the second hypothesis is more probable. In the high grade dykes molybdenite is preferentially concentrated in areas with higher remnant feldspar contents, rather than in the silicified matrix. If the precipitation of molybdenite is related to the alteration of feldspars, the igneous rocks would provide a better host

for mineralization than the metasedmentary units, as they contain a higher modal percentage of feldspar.

4.2 ACCESSORY MINERALS

Most mineralized quartz veins contain alkali feldspars, muscovite, and calcite. Biotite and chlorite never accompany pervasive silicification, except where remnant grains are preserved, and are rare in quartz veins. The only other non-opaque minerals observed in quartz veins or with pervasive silification are apatite and fluorite. Apatite has only been identified in thin section, and has been observed in both mineralized and barren quartz veins. Characteristically, it forms radiating acicular crystals up to one centimeter in length, often nucleating at vein walls or feldspar edges. The radiating apatite crystals have grown into the centre of the vein, which implies open space filling. No apatite has been identified in pervasively silicified samples but too few thin sections have been examined to establish that apatite is restricted solely to quartz veins. Fluorite is an extremely rare mineral at this deposit. The few grains observed were light green, euhedral, and were filling vugs in phyllically altered rocks.

The only sulphides observed to accompany molybdenite are pyrrhotite, pyrite, and chalcopyrite. Where intergrowths are present, molybdenite always replaces either pyrrhotite or pyrite (Plate 4-6). This suggests that some molybdenite precipitation is the result of the interaction of mineralizing fluids (Mo-rich) with pre-existing sulphides. However, in

Plate 4-4   Quartz Stockwork (pervasive silicification).
            Molybdenite is associated with the alkali
            feldspar layers (K-feldspar is stained yellow)
            rather than the quartz layers.

Plate 4-5   High grade dyke.   Molybdenite is associated with
            strong albitization.   K-feldspathization (stained
            yellow) is weak.

Plate 4-6   Microphotograph (X-polars, reflected light) of
            molybdenite (grey) replacing pyrrhotite
            (cream). Field of view is 2.0 mm.
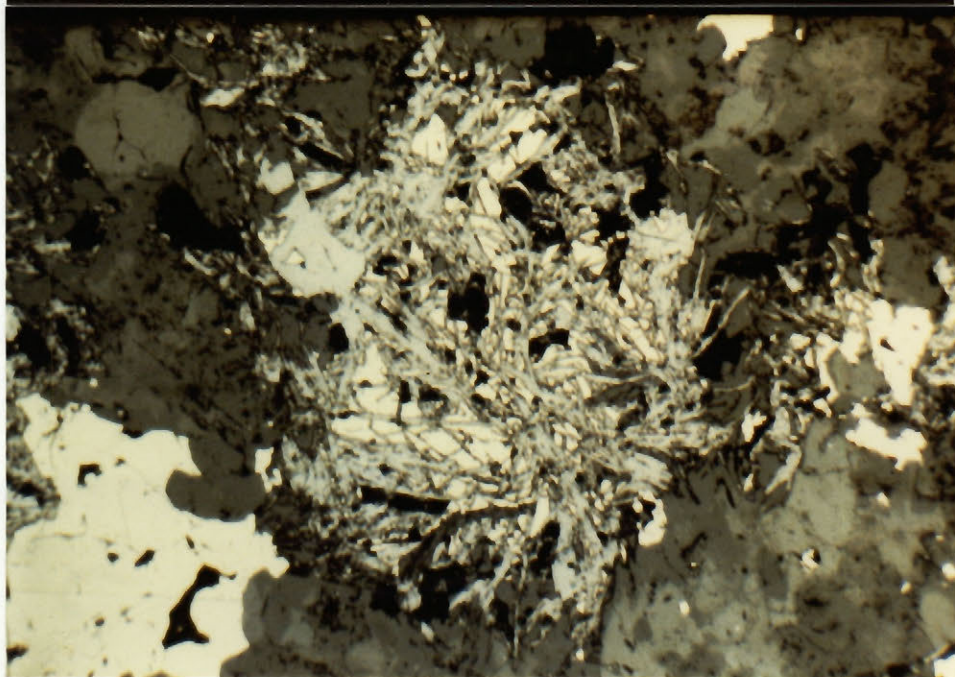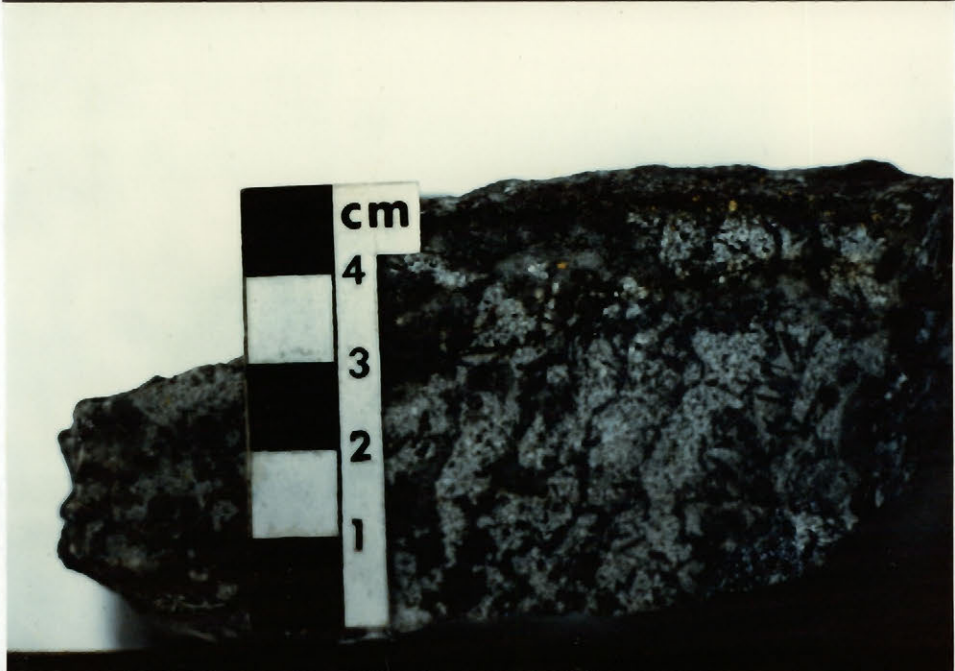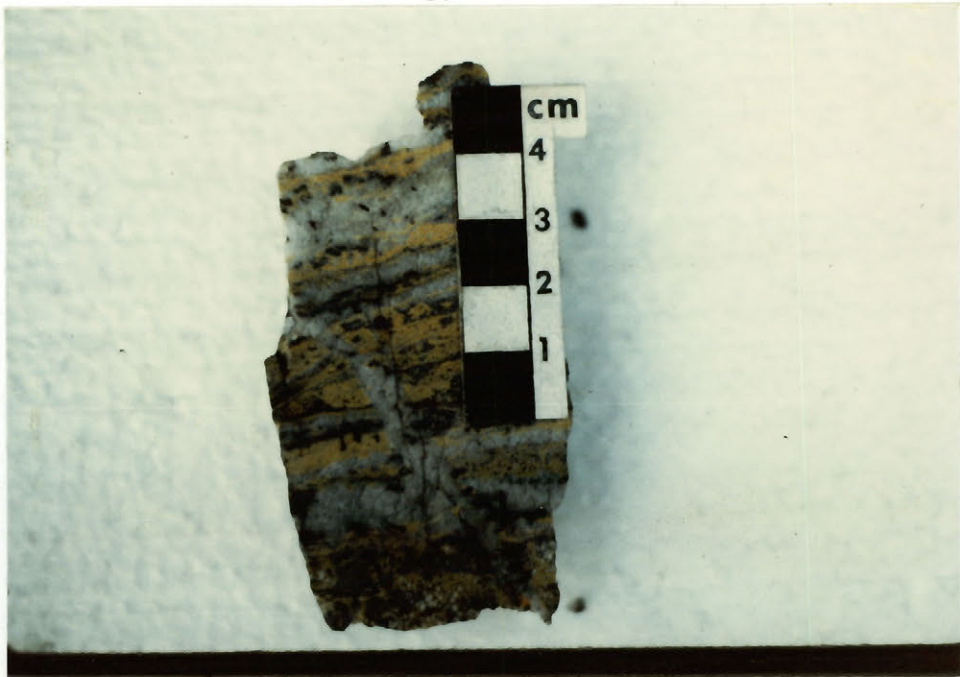
general molybdenite is not intergrown with sulphides, therefore this was not the major mechanism of molybdenite precipitation.

Veins typically contain less than 1 %(by volume) of sulphide minerals, and rarely have total sulphide contents of greater than 5 %. Molybdenite, pyrite, and pyrrhotite are all common in quartz veins whereas chalcopyrite is rare. Pyrite occurs as euhedral cubes 0.5- 2.0 mm, or rarely up to 1.0 cm across. Pyrrhotite occurs as anhedral grains, 0.5-2.0 mm across, and molybdenite generally occurs as rosettes, 0.5-2.0 mm, or rarely up to 5.0 mm across. High grade dykes are characterized by high pyrrhotite contents, up to 10 modal percent. The pyrrhotite occurs in a bladed form due to the alignment of grains along microfractures.

Chalocopyrite is observed as discrete grains in the pyrrhotite-rich high grade dykes and massive pyrrhotite portionsof skarns. In these zones, chalcopyrite also occurs as inclusions in pyrrhotite and pyrite, or shares a common straight boundary at the corners of pyrrhotite grains. Chalcopyrite is rare in quartz veins and, when observed, it is generally as inclusions within pyrrhotite. Pyrrhotite is the dominant sulphide in the skarn unit, was stable during contact metamorphism of the calcareous schists, commonly accompanies veins with biotite haloes and, as discussed above, is characteristic of the high grade dykes. Pyrite was stable during contact metamorphism of quartz-biotite schists, is the dominant accessory sulphide in mineralized quartz veins, is present but less abundant than pyrrhotite in the high grade

dykes, and is characteristically abundant in phyllically altered rocks. Pyrrhotite is absent in phyllically altered samples.

On rare occasions galena and spalerite are observed in quartz veins. Neither galena nor sphalerite have yet been identified in a vein with molybdenum mineralization, nor are these sulphides associated with a particular alteration type.

The abundance of pyrrhotite in veins is concentrically zoned about the occurrence of the high grade dykes, in the centre of the mineralized zone. Figure 4-2 shows the contours of the percentage of veins with pyrrhotite, and the percentage of veins with moderate to excellent molybdenite (greater than approximately 0.5 % MoS_2). Both these contours mimic the molybdenum grade and feldspar contours (Figs. 3-3 and 4-1). Higher pyrrhotite abundance correlates with only one of the two zones of higher molybdenum grades as the adit (from where the data was collected) intersects only one zone. In general, pyrite and molybdenite accompany pyrrhotite-bearing veins, and always accompany pyrrhotite in high grade dykes. Therefore pyrite and pyrrhotite were both stable at the time when molybdenite was precipitated. Pyrite is the only sulphide which formed during later phyllic alteration and therefore the distribution of pyrite does not correlate with that of molybdenite, and is not shown.

4.3 TIMING OF MINERALIZATION AND PARAGENESIS

Molybdenite is present in all phases of alteration but the majority of the molybdenum was deposited relatively late

Figure   4-2   Distribution of % veins with moderate to
               excellent molybdenum mineralization, and %
               veins with pyrrhotite on the plane of the
               adit.
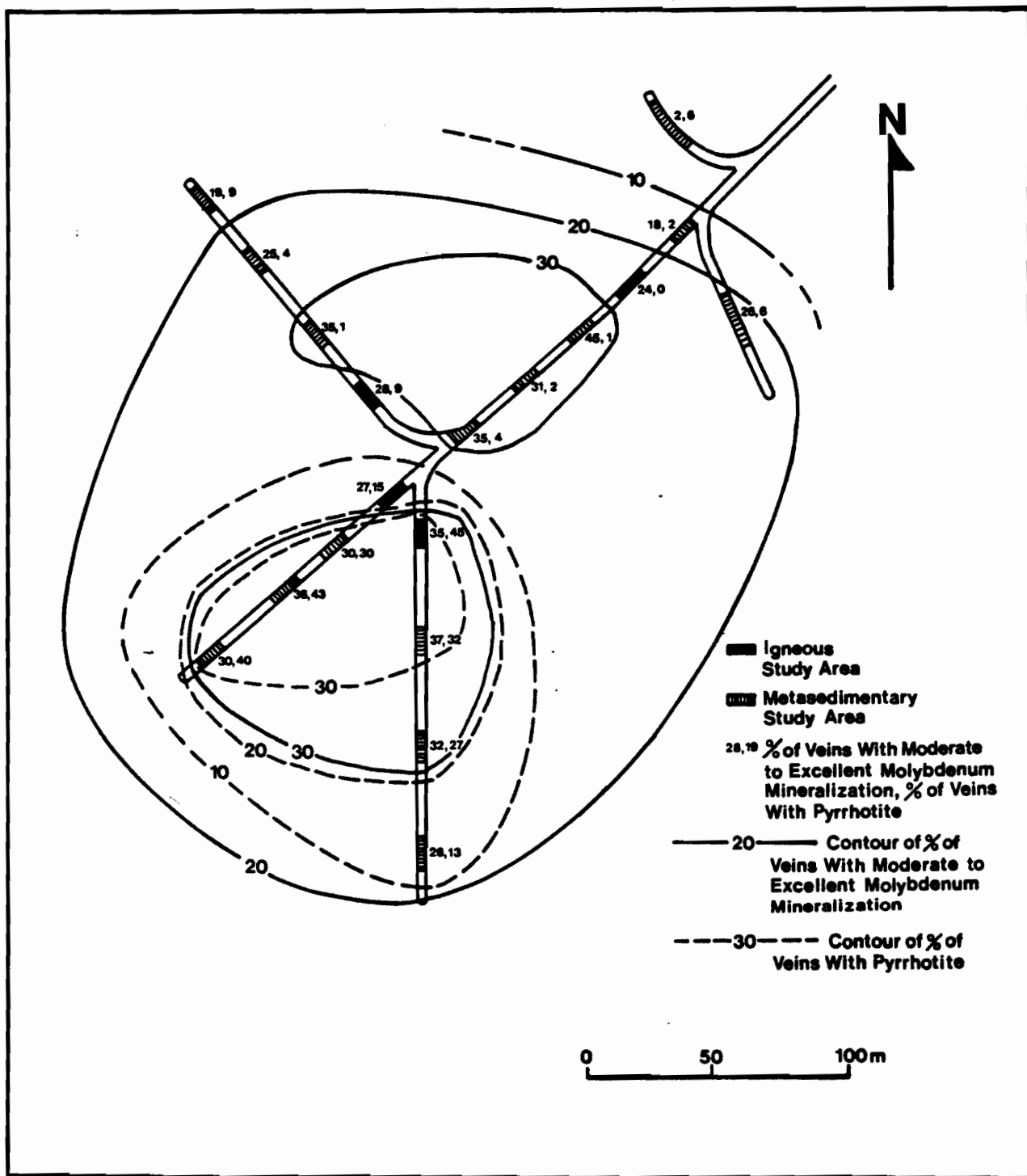
in the history of the deposit. The earliest hydrothermal event after contact metamorphism caused the formation of skarn at low XCO_2 conditions. As both fluids had a similar composition and temperature, possibly some of the skarn formation was synchronous with contact metamorphism. However, quartz-diopside-tremolite-clinozoisite veins are observed to crosscut contact metamorphosed rocks implying that skarn formation was at least in part post contact metamorphic (Plate 3-5). Prograde and retrograde skarn assemblages have been identified, but both formed prior to potassic alteration as biotite replaces retrograde tremolite. Pyrrhotite and chalcopyrite are the dominant sulphide minerals observed in skarns, and are accompanied by scheelite and trace molybdenite.

The next event was biotite-calcite alteration (pervasive potassic). No molybdenite is observed with this alteration type. However, pyrrhotite is commonly disseminated in the tremolite-biotite and quartz-biotite schists, indicating that it was stable at that time. Quartz-albite veins with biotite haloes, representing late potassic alteration, crosscut these schists indicating that they formed later than or possibly at the same time as biotite-calcite alteration. These veins rarely contain molybdenite, but pyrrhotite is commonly present.

The bulk of the mineralization post-dates late potassic alteration and is associated either with quartz-alkali feldspar veins, or silicification. Within this main mineralizing event, veins of similar mineralogy and

Figure 4-3   Sequence of geological events and mineral
            paragenesis.

Sequence of Geological Events

Skarn Alteration

Biotite-Calcite Alteration

Late Potassic Alteration

Silicic Alteration

Phyllic Alteration

Vein-Type Mineralization

Silicification-Type
Mineralization

Skarn Mineralization

Main Granodiorite

Early Granodiorite

Quartz Diorite

Late Granodiorite

Mineral Paragenesis

Tremolite

Clinozoisite

Clinopyroxene

Calcite

Ankerite

Biotite

Muscovite

Plagioclase

Albite

K-feldspar

Quartz

Molybdenite

Pyrrhotite

Pyrite

Chalcopyrite

Scheelite

Time

orientation repeatedly crosscut each other, implying a period of continual refracturing and deposition. The consistency of sulphide and silicate mineralogy suggests that, throughout the mineralizing episode, veins were deposited from a fluid under similar physical and chemical conditions. Zones of pervasive silicification generally have sharp contacts and, at those contacts, the silicification typically cuts the majority of veins that are intersected (Plate 3-3). This implies that the silicification style of mineralization was relatively late in the paragenetic sequence. Pervasive silicification and high grade dykes are both observed to crosscut granodiorite and quartz diorite, demonstrating that pervasive silicification is relatively late in the paragenetic sequence. Crosscutting relationships between quartz veins, granodiorite, and quartz diorite indicate that both the granodiorite and quartz diorite are temporally intramineralization.

The final hydrothermal event is phyllic alteration. The distribution of this alteration type is largely fault controlled, and there is generally an antipathetic relationship between phyllic alteration and mineralization (Boyle and Leitch, 1983). However, significant molybdenum mineralization is present along the strongly sericitized Z fault, indicating that molybdenite remained stable or was only partially leached during phyllic alteration. A summary of the timing of mineralization, alteration, and intrusive events is presented in paragenetic sequence (Figure 4-3).

4.4 TUNGSTEN AND BASE METAL MINERALIZATION

In addition to molybdenum, minor tungsten and base metal mineralization is found peripheral to the Trout Lake deposit. Tungsten mineralization, in the form of scheelite, is generally restricted to zones of skarn alteration, but rarely is observed in quartz-molybdenite veins. The scheelite is disseminated within clinopyroxene-garnet skarn, accompanied by abundant pyrrhotite, which is locally massive, and chalcopyrite. Higher chalcopyrite abundances are associated with massive pyrrhotite, but scheelite abundance does not directly correlate to pyrrhotite abundance.

Two former base and precious metal producers, and several showings are present peripheral to the Trout Lake deposit. In both the former mines and the base metal showings, mineralization occurs in shallowly dipping quartz veins. The Lucky Boy mine (Fig. 1-3) produced 89,800 ounces of silver, 3,284 pounds of copper, and 221,181 pounds of lead from 433 tons of ore mined between the years 1903 and 1912 (Holland, 1952). The dominant ore minerals at the Lucky Boy were galena, sphalerite, tetrahedrite, and native silver. In addition, scheelite from quartz veins at the Lucky Boy was sorted and shipped to Ottawa for treatment in 1942. The Copper Chief mine (Fig. 3-1) produced 1,936 ounces of silver, and 2,672 pounds of lead between the years 1905 and 1917 (Holland, 1952). The occurrence of scheelite in massive pyrrhotite at this deposit was noted by Holland (1952) and was observed in this study. Typical ore minerals found at the Copper Chief deposit are galena, sphalerite, tetrahedrite,

chalcopyrite, pyrrhotite, and scheelite. Scheelite was observed in this study at several locations along the Copper Chief fault in massive pyrrhotite skarn. Scheelite mineralization is apparently continuous from the Trout Lake deposit, northeast along the Copper Chief fault, to at least 100 meters beyond the Copper Chief deposit.

4.5 SUMMARY

Two styles of mineralization are prominent at the Trout Lake deposit. Molybdenite in quartz-feldspar veins is typical of mineralization hosted by the metasediments. Silicified "high grade dykes" or pervasively silicified zones host higher grades of molybdenum mineralization. There is a strong correlation between molybdenum grade and feldspar abundance. Textural evidence suggests that molybdenite precipitation is linked to sericitization-carbonatization reactions, and that feldspars are favourable sites for these processes to occur. Tungsten skarn and vein-type silver-lead-zinc-copper deposits are peripheral to the molybdenum mineralization.

CHAPTER 5:   VEIN ORIENTATIONS, STRUCTURE, AND METALLOGENY

5.1 METHOD OF VEIN STUDY

As a large proportion of the mineralization occurs within quartz veins, the attitudes and mineralogy of quartz veins were recorded in order to investigate the structural controls of molybdenite deposition.   Over 1900 veins were described from 19 different stations within the adit and crossdrifts. Each station covers a 10 meter interval and all veins along one side were measured. Where possible, veins along the back were also measured.   In 1 Drift West and 2 Drift South a 20 meter study interval was used to compensate for the lower vein densities in those areas.   Station locations are shown by Figure 5-1.

For each vein the location, attitude, thickness, intensity of molybdenum mineralization, accessory sulphide, silicate, and carbonate minerals, and crosscutting relationships were recorded.   Owing to the presence of magnetic pyrrhotite compass measurements were unreliable, therefore vein trends were measured as angles from the adit, then later converted to strikes.   Intensity of molybdenum mineralization for each vein was estimated by assigning a grade considering the entire vein and the surrounding country rock.   Grades of less than 0.05 % MoS_2 correspond to veins with absent to trace amounts of molybdenite, and are classified as Type A (sub-economic).   Grades of 0.05-0.20 % MoS2 correspond to moderate molybdenum mineralization, and these veins are classified as Type B (marginally economic).

Grades greater than 0.20 % MoS_2 respresent good to excellent mineralization, and are classified as Type C veins (economic).

5.2 ORIENTATION OF VEINS

Poles to the attitudes of quartz veins were plotted and contoured on equal-area stereonets on the basis of the percentage of points within a one percent area using the CONMAP program of Dr. A. Hynes of McGill University. The result for each study area is shown in Figure 5-1. Five structural orientations are recognised. Type 1 are developed parallel to the regional foliation, northwest-southeast and steeply dipping. Type 2 are perpendicular to the regional foliation, and are also steeply dipping. Type 3 strike north-south, are steeply dipping, and are parallel to the Z fault. Type 4 are sub-horizontal, and finally type 5 strike east-west and are steeply dipping. In a given area the first two structural types are generally present, and the latter three types are weakly developed or absent.

Type 1 veins predominate in the centre of the deposit (Fig. 5-1), but are less strongly developed at the periphery, where type 2 dominate. The strongly developed regional fabric, which pre-dates mineralization, could account for the emplacement of some type 1 veins. However, type 1 veins are observed to cut non-foliated granodiorite. Therefore the stresses which caused this vein orientation were still present during mineralization.

The quartz-biotite schist has well developed quartz segregations in the centre of the deposit, and poorly

developed quartz segregations at the periphery. The development of quartz segregations may have caused the schists to be more brittle, particularly in the direction parallel to foliation. Subsequent fractures and quartz veins would have been developed parallel to foliation. Therefore the development of quartz segregations in the centre of the deposit could account for the prominence of type 1 veins in that area. The timing of quartz segregation development is not totally clear. However, the quartz-biotite schist with quartz segregations is crosscut by veins with biotite haloes, indicating that the formation of quartz segregations was either synchronous with, or prior to late potassic alteration. Areas within the contact metamorphic aureole not affected by late potassic alteration have poorly developed quartz segregations. Therefore the formation of quartz segregations must be post contact metamorphic but prior to or synchronous with potassic alteration.

Adjacent to and east of the Z fault, type 3 veins dominate (parallel the the Z fault) which is not surprising in view of their close proximity to the Z fault. It is also noteworthy that the density of orientations in any one station rarely exceeds 10 percent (per 1% unit area), thus there is also a certain random but subvertical component to vein distribution.

Figure 5-1   Contoured stereonet plots of poles to quartz
             vein orientations from individual stations on
             the plane of the adit.

LEGEND

Quartz Vein
Orientations

○ 1-5%
◍ 5-9%
● >9%

Metasedimentary
Study Area

Igneous
Study Area

Number of Observations
Per Sample Area 98

0 10 20 30 40 50m
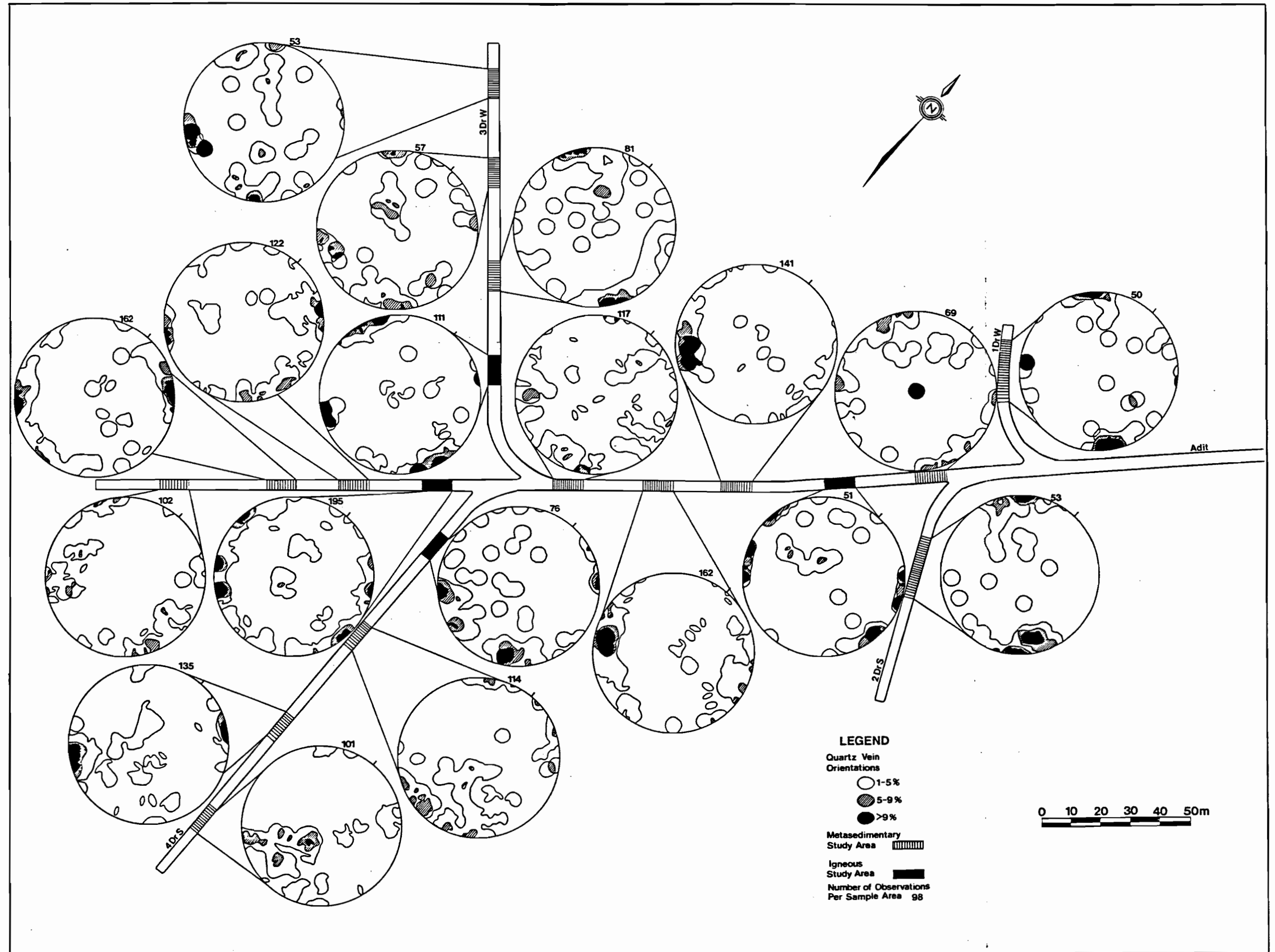
5.3 CROSSCUTTING RELATIONSHIPS

One hundred and ninety crosscutting relationships were recorded which involve veins of structural types 1-5. From these crosscutting relationships the following can be concluded: Each structural type crosscuts and is in turn crosscut by all other types. Veins of the same orientation also crosscut each other, which is evidence of repeated fracturing along a given direction. These relationships are also true for veins with different molybdenum grades and accessory minerals. Crosscutting relationships of veins with the quartz stockwork unit (massive silica replacement) provide furthur evidence for successive generations of veins with similar orientations. Paragenetically, the quartz stockwork is relatively late as it cuts the majority of veins (including all five vein-types) that it intersects (Plate 3-3). However, it is in turn cut by all five vein-types. This suggests that the same stresses were present throughout the genesis of the deposit.

In spite of the evidence for repeated fracturing some useful information can be drawn from the observed crosscutting relations. Type 1 veins are generally early, being the oldest veins in 80 % of the relations in which they are involved (cut by types 2-5). From the plot of type A veins (Figure 5-2) it is apparent that barren to weakly mineralized veins have predominantly a type 1 orientation. Therefore by association, there was probably an early barren stage of quartz vein emplacement which was oriented northwest-southeast. This is similar to the orientation of quartz segregations in the

Figure 5-2   Contoured stereonet plot of the poles to vein
orientations with weak to absent molybdenum
mineralization (Type A).   The number to the
lower right is the number of observations.

N
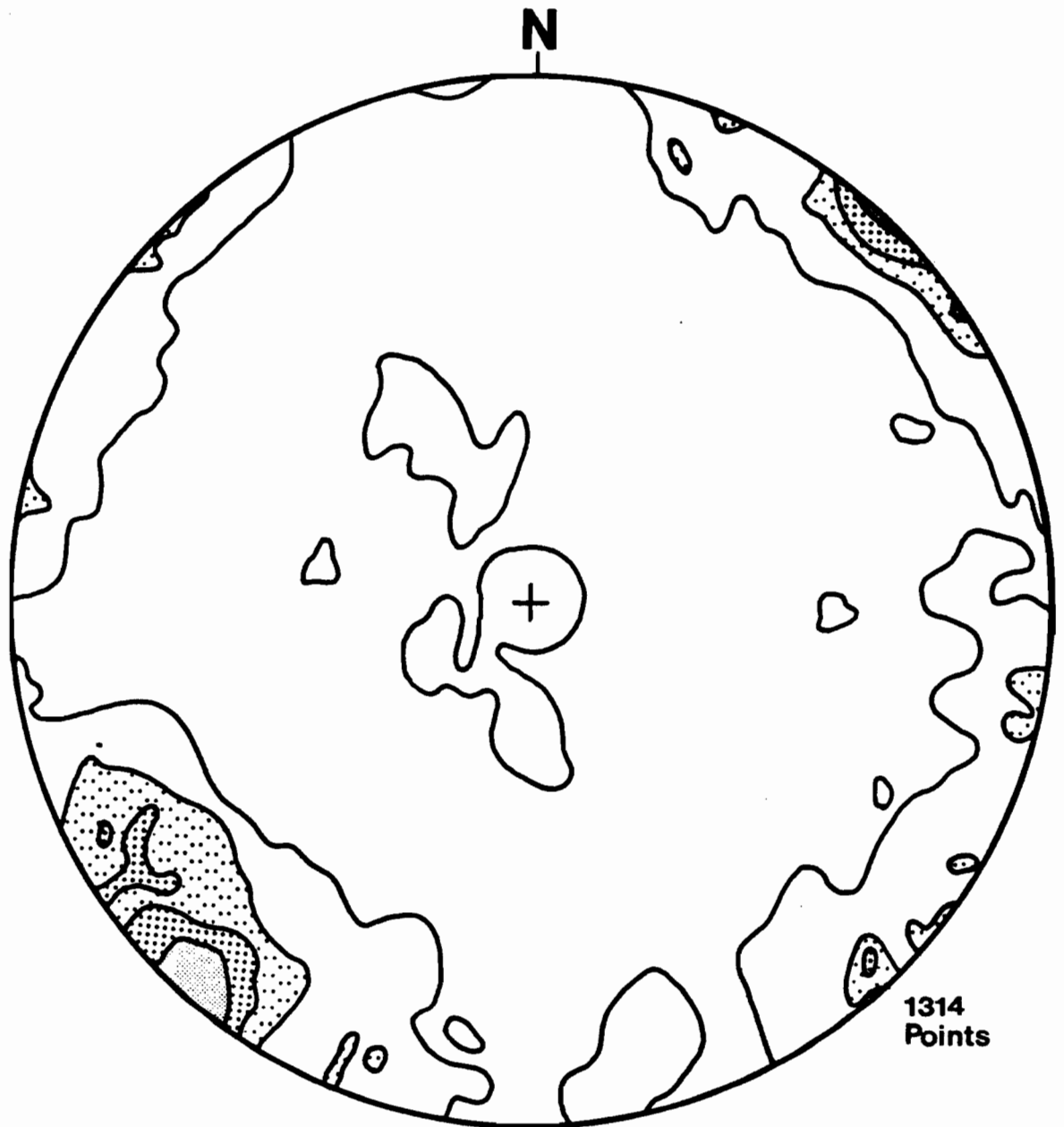
1314
Points

LEGEND

Percentage of Poles Within
a 1% Area

☐	1–3
▦	3–5
▦	5–7
▦	7–9
■	>9
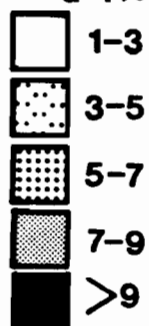
quartz-biotite schist which were developed prior to quartz vein formation, and are parallel to the regional foliation. In terms of molybdenum content, vein types B and C (mineralized) cut type A veins (barren to weakly mineralized) in 68 % of crosscutting relationships recorded, supporting the hypothesis that a large percentage of the barren veins were early.

Figure 5-3 is a stereonet plot of type B (moderately mineralized) veins. The dominant vein population is parallel to foliation (type 1 orientation), with a smaller population perpendicular to foliation (type 2 orientation). Figure 5-4 is a stereonet of type C veins (good to excellent mineralization). These veins are most strongly oriented perpendicular to foliation (type 2), and parallel to foliation (type 1), with a minor set parallel the Z fault (type 3). It was observed that vein types B and C cut type A veins in 68% of the relationships. Therefore there must be a late stage development of type A veins. Too few relationships were recorded to warrant plotting the late stage type A veins on a stereonet. However, structural vein types 4 and 2 were the most abundant, with fewer of vein types 3 and 1.

A final observation is that type 3 veins crosscut type 2 veins in 90 % of the crosscutting relationships observed, indicating that they are relatively late. Type 3 veins are parallel to the Z fault, along which strong sericitic alteration is concentrated. The observation that type 3 veins are relatively late is consistent with sericitic alteration being late in the sequence of geological events. However,

Figure 5-3   Contoured stereonet plot of the poles to
orientations of moderately mineralized veins
(Type B). The number to the lower right is
the number of observations. Symbols are the
same as for Figure 5-2.
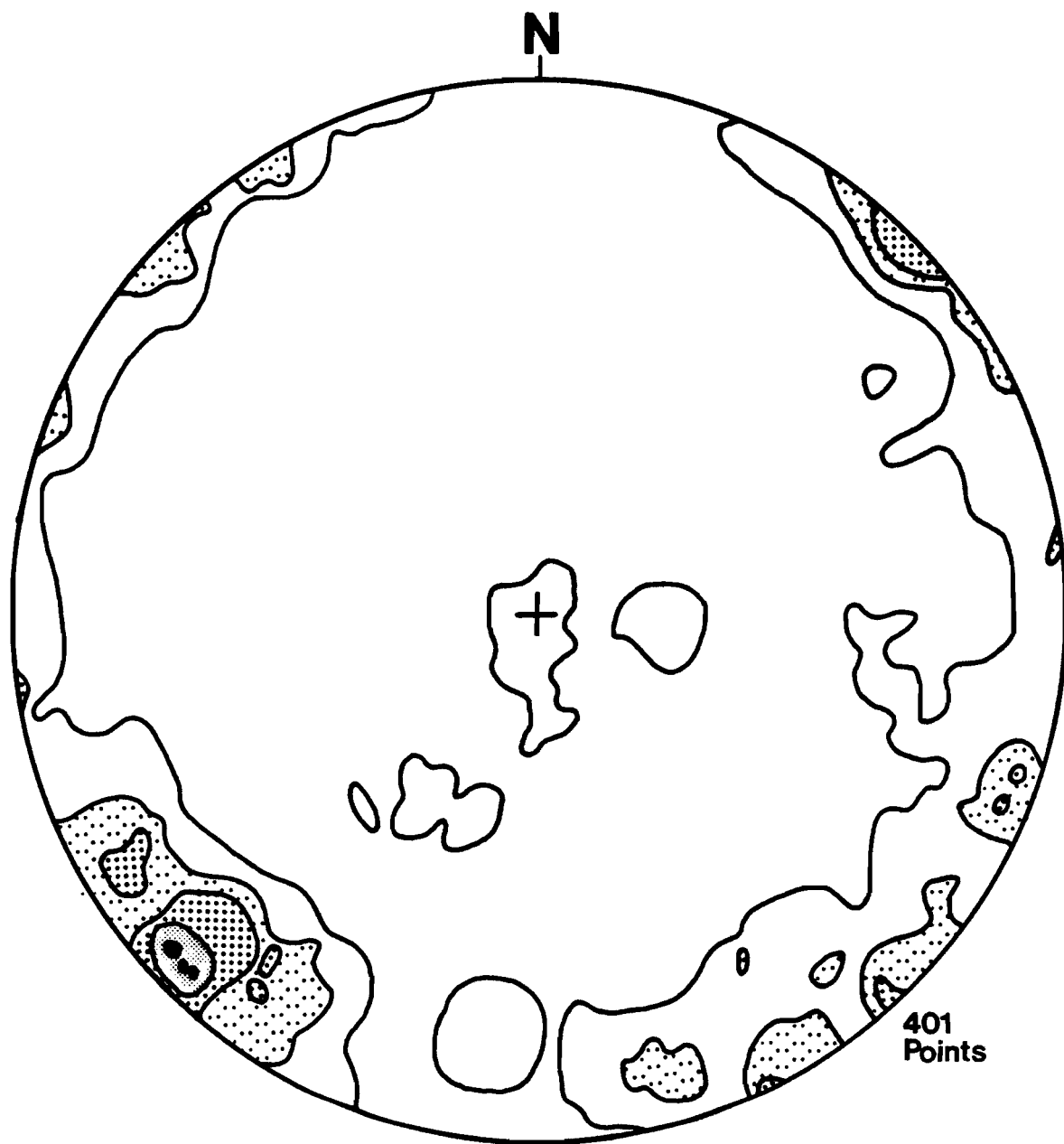
Figure 5-4   Contoured stereonet plot of poles to
              orientations of veins with good to excellent
              molybdenum mineralization (Type C). The
              number to the lower right is the number of
              observations. Symbols are the same as for
              Figure 5-2.

N
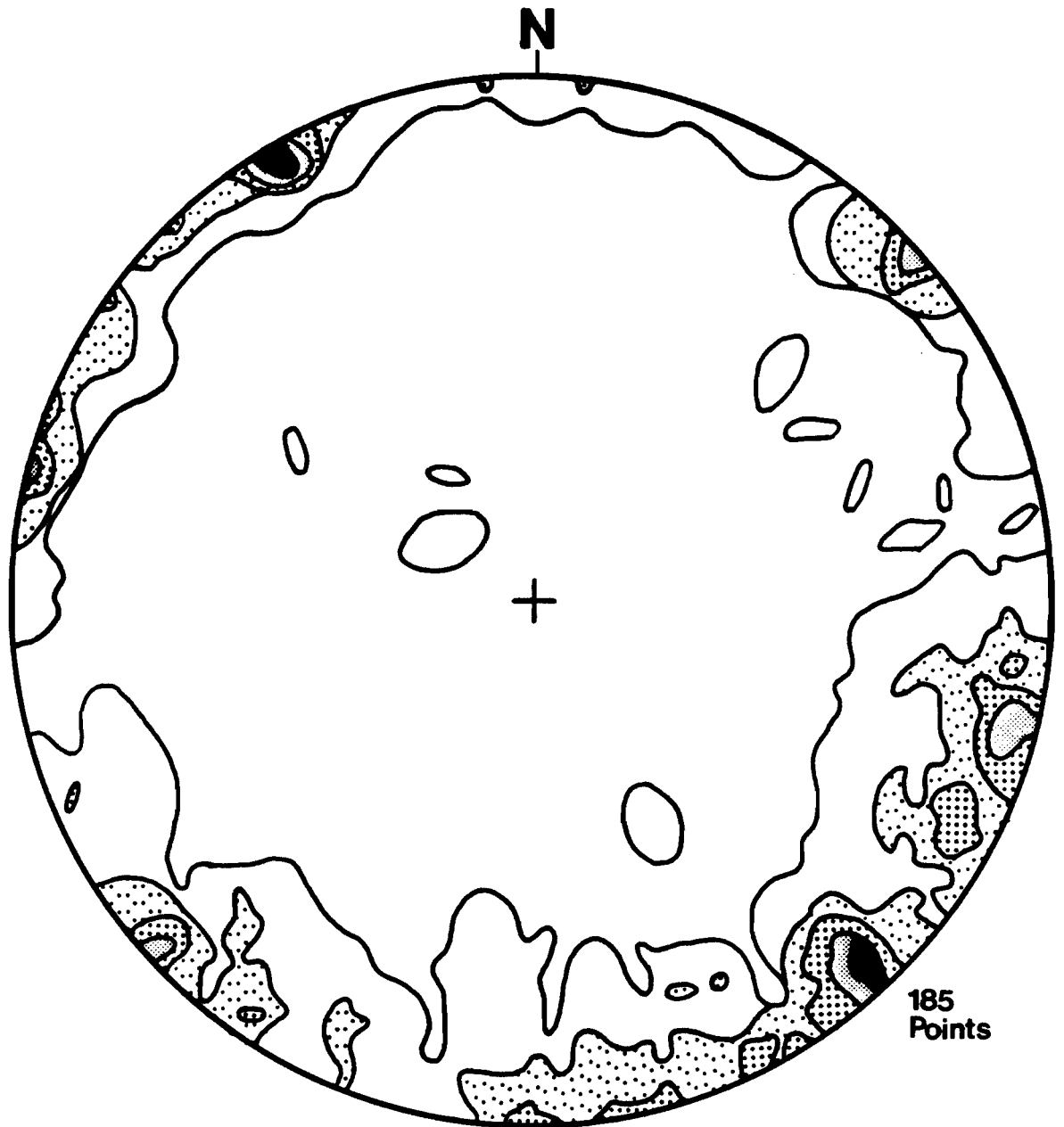
185
Points

sericite alteration is not restricted to type 3 veins, nor is any one alteration type associated solely with a particular orientation.

5.4 ORIENTATION OF FAULTS

Within the area immediately around the deposit several faults are observed or interpreted. The Three-Man, Copper Chief, and Adit faults are parallel to the regional foliation and are steeply dipping. The Z fault cuts the Trout Lake Stock, but also probably pre-dated it, trends north-south and is steeply dipping. The orientations of shears were measured in the adit and then plotted in a manner similar to that used for the veins. Figure 5-5 is a stereonet plot of shears. Two shear orientations are prominent; a steeply dipping north-south set, and a northerly dipping east-west set. A less prominent set is perpendicular to the regional foliation. Thus, shearing coincides with four of the five observed vein orientations.

5.5 REGIONAL STRUCTURE AND METALLOGENY

By inspecting the 1:125,000 geological map of Read and Wheeler (1976) it is apparent that there is a strong northwest-southeast trending regional foliation, and that most faults are parallel to this. North-south, east-west, and northeast-southwest trending faults are less abundant. Therefore the fault pattern at the Trout Lake deposit mimics the regional fault pattern. Figure 5-6 is a stereonet plot of vein attitudes from vein-type lead-zinc-copper-silver-gold

Figure 5-5   Contoured stereonet plot of poles to shear
             orientations. The number to the lower right
             is the number of observations. Symbols are
             the same as for Figure 5-2.

N

101
Points
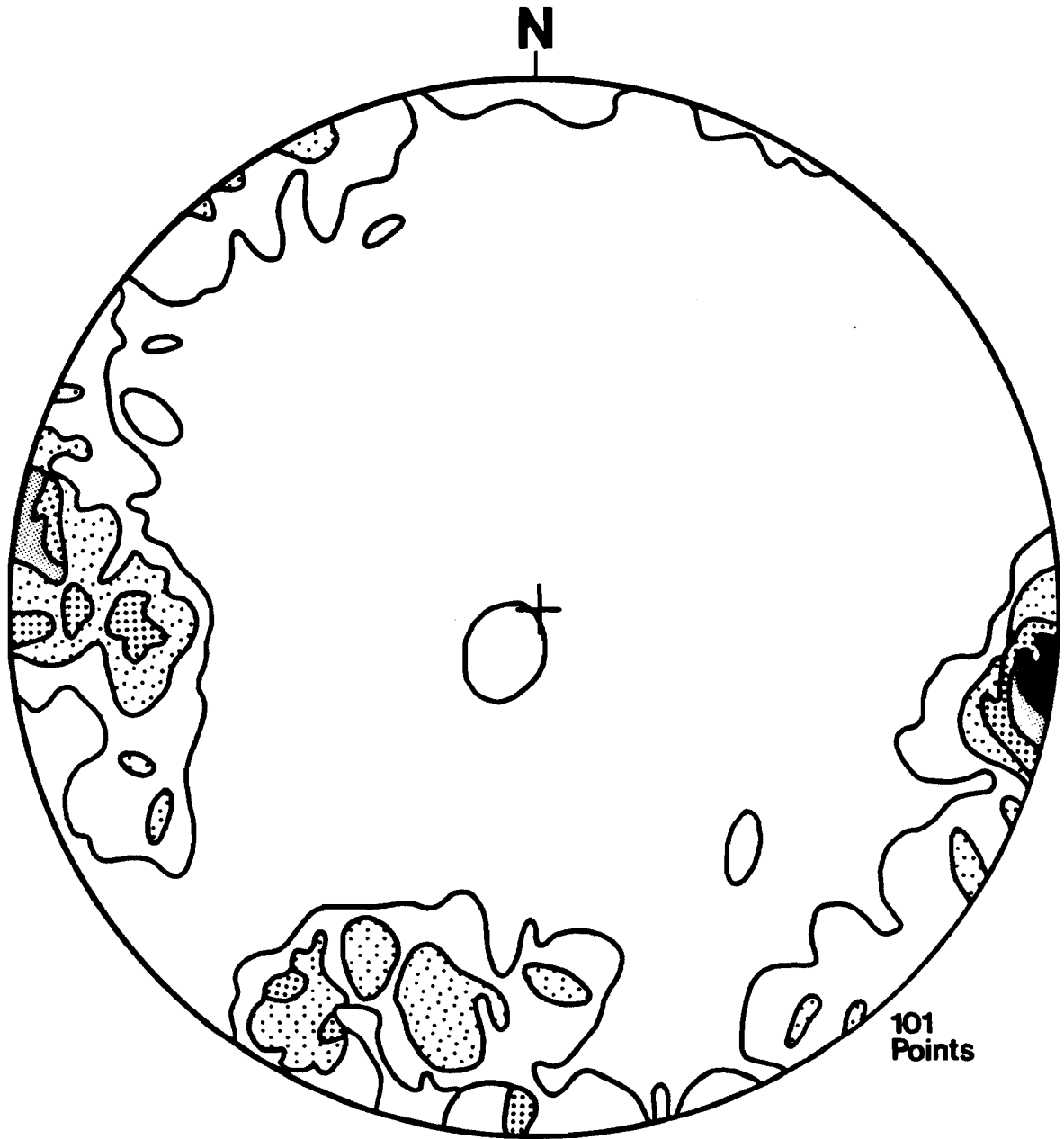
Figure 5-6   Contoured stereonet plot of poles to orientations of veins from regional deposits. Number to the lower right is the number of observations. The data is from Read and Wheeler (1976).

N
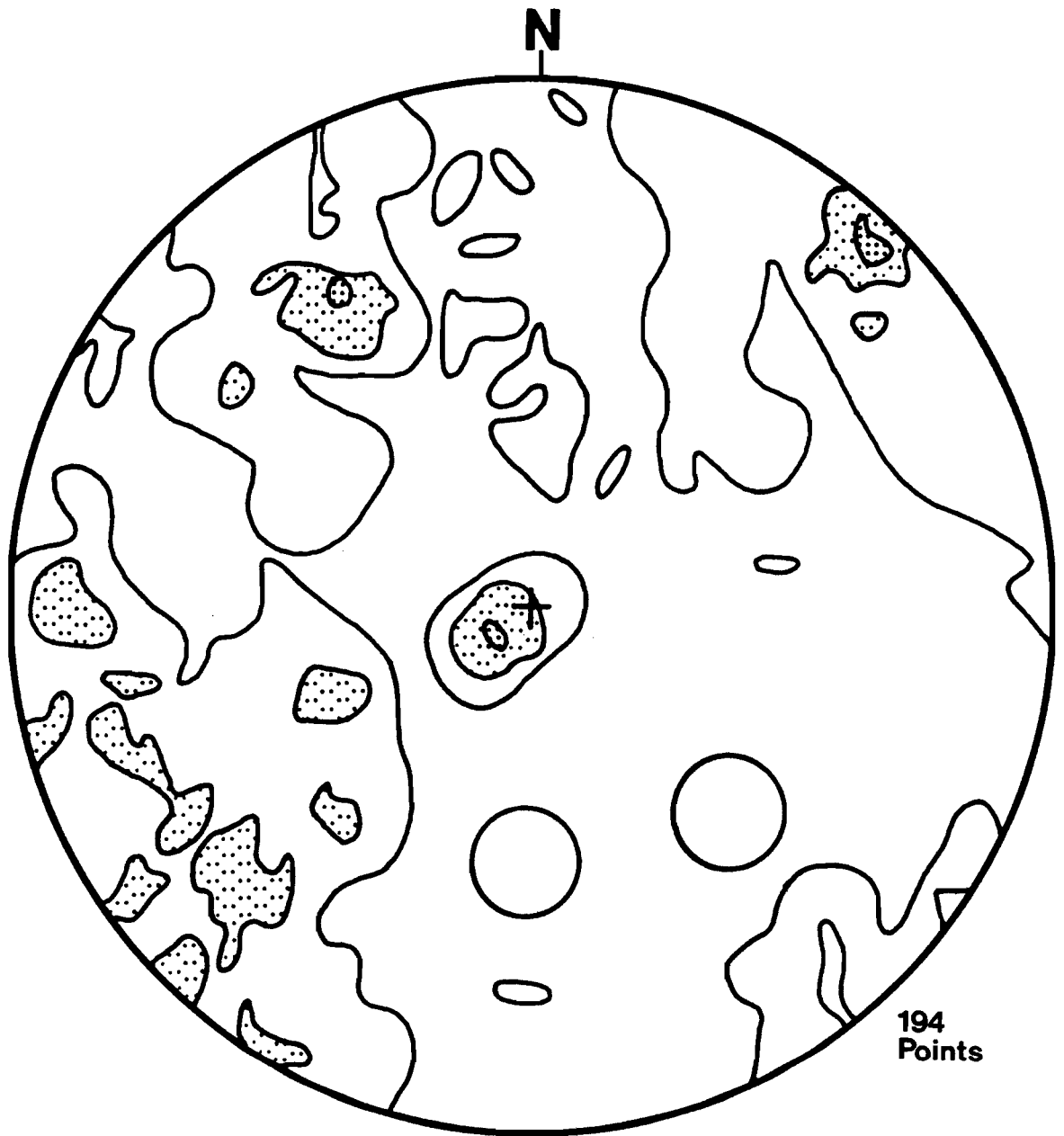
194
Points

deposits within the Lardeau West-Half map area (data from Read and Wheeler, 1976). Four of the five vein-orientation recognised at Trout Lake are also observed in these base and precious metal deposits: parallel to foliation (type 1), perpendicular to foliation (type 2), north-south (type 3), and subhorizontal (type 5).

Two of these deposits, the Copper Chief and Lucky Boy are former producers of Pb-Zn-Ag-Cu-W and are located within the thesis area (Fig. 1-4). It is probable that these deposits are coeval with the Trout Lake deposit owing to their close proximity to the latter deposit, and the continuity of scheelite mineralization between the Copper Chief and Trout Lake deposits. Scheelite may have been remobilized during a later thermal event but the sheelite in the skarns at Trout Lake has the same mode of occurrence as the scheelite in the Copper Chief deposit. At the Lucky Boy deposit scheelite was extracted from quartz veins, but scheelite in quartz veins was also observed at the Trout Lake deposit. Occurrences of galena and sphalerite are rare within the Trout Lake deposit, but their limited presence does indicate that lead and zinc were mobile during the formation of the deposit. Therefore all these deposits are probably part of a single metallogenic event.

5.6 STRESS ANALYSIS

The five vein and fault orientations can be explained in terms of the forces which formed the cordilleran foreland thrust and fold belts from Jurassic to Early Tertiary times

(Monger and Price (1979), Price (1981)). The regional foliation and thrust faults developed perpendicular to the principle compressive stress. Type 1 veins are parallel to the regional foliation, and formed as a result of the plane of weakness caused by that foliation. The north-south and east-west sets (types 3 and 5) are conjugate to the principle stress. During relaxation periods, a tensile northeast-southwest set (type 2; parallel to the dominant stress) formed. The sub-horizontal set (type 4) formed as a result of pressure release due to uplift. Alternatively, Price (1979) proposed that, during the Eocene, the Kootenay Arc underwent ductile spreading related to strike slip motion along the Frazer River and Northern Rocky Mountain Trench faults. The orientation of type 2 veins is prepedicular to the tensile force. The time at which this ductile spreading commenced is poorly constrained. Therefore it is possible that the ductile spreading started in the Mid to Lake Cretaceous, and that type 2 veins are a consequence of the tensile forces.

Within the deposit there is textural evidence which suggests that there were alternating tensile and compressive conditions. Comb textures (Plate 4-1) of the vein-forming minerals indicate open-space filling and a tensile environment. Stronger mineralization (Fig. 5-4) may have resulted from tensile related conduits having a higher fluid/rock ratio. Alternatively, the thickest veins can be interpreted to have formed under the most tensile conditions i.e., they reflect the widest open spaces. A stereonet plot of veins with a thickness of greater than or equal to 10 cm

Figure 5-7   Contoured stereonet plot of the poles to
             orientations of veins which are greater than
             or equal to 10 cm in thickness. Number to
             the lower right is the number of
             observations.

N

70
Points
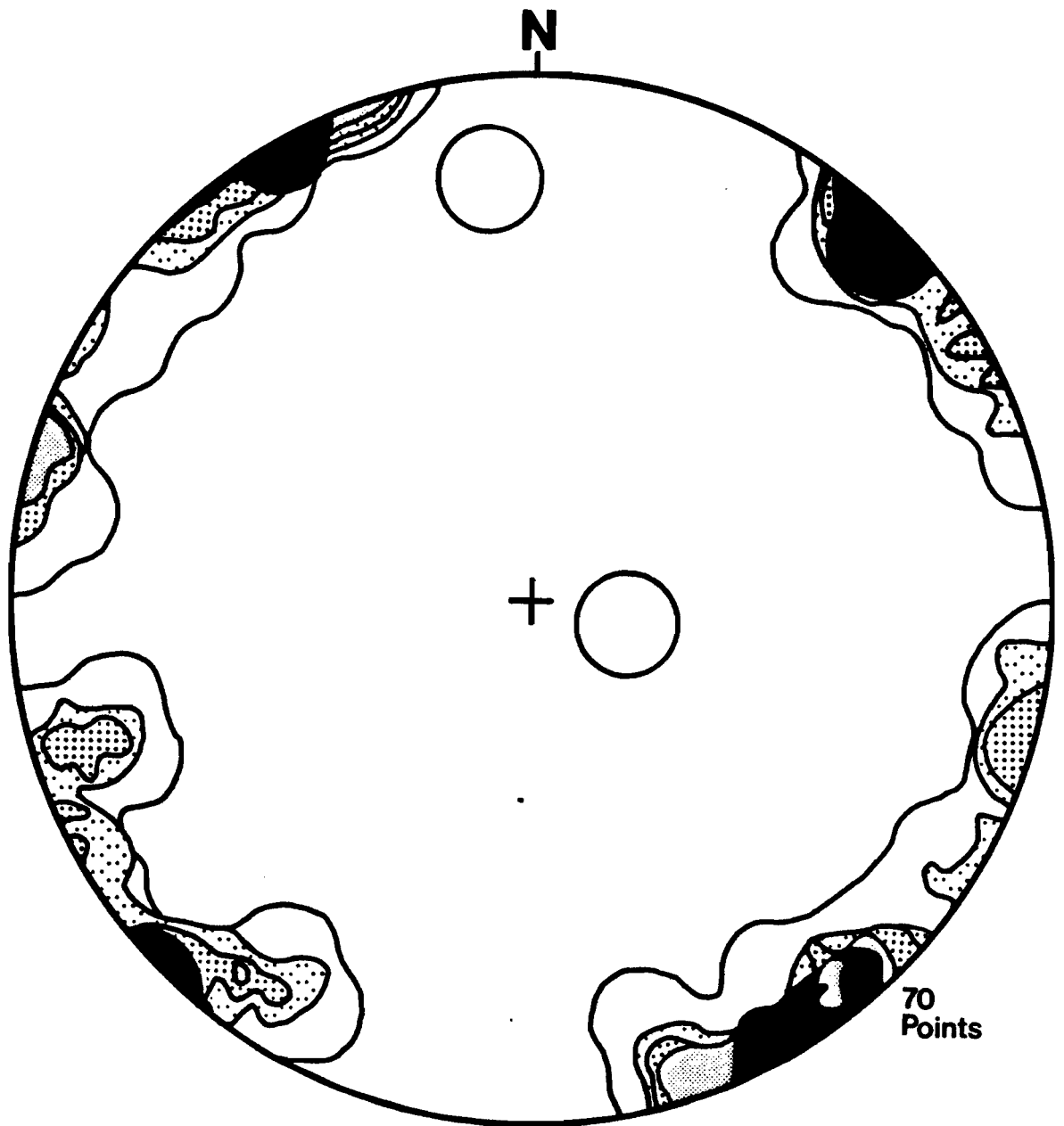
(Figure 5-7) is similar to Figure 5-4. Again the strongest orientation is perpendicular to the regional foliation, representing tensile forces. However within quartz veins, grain boundaries are seriate (Plate 5-1) and, less commonly, quartz stylolites defined by sulphides (Plate 5-2) are present. This implies compression. No structural data indicates that an intrusion at depth significantly altered the stress field in which the deposit formed, and the vein pattern at Trout Lake mimics the regional vein pattern. Therefore regional stresses controlled quartz vein oientations.

5.7 DISCUSSION AND SUMMARY

Five structural orientations are recognised both regionally and within the Trout Lake deposit indicating that the emplacement of the Trout Lake Stock had a negligible effect on the regional stress field, which controlled quartz vein formation at the Trout Lake deposit. The formation of quartz segregations parallel to foliation in the quartz-biotite schist at the centre of the deposit affected the host by making it more brittle. This resulted in a high proportion of quartz veins being emplaced paralled to foliation (type 1) at the centre of the deposit. Veins with weak or absent molybdenum mineralization (type A) correlate with the type 1 orientation. Veins with moderate mineralization (type B) predominantly have a type 1 orientation, and to a lesser extent have a type 2 orientation (perpendicular to foliation). Veins with good to excellent molybdenum mineralization (type C) predominantly have a type 2 orientation, with a subordinant

type 1 orientation.

The following generalizations can be made from the stereonet plots and crosscutting relationships: Early veins are weakly mineralized or devoid of molybdenite, and have a type 1 orientation. Mineralized veins have either a type 1 or 2 orientation, and the proportion with a type 2 orientation increases with molybdenum grade. Type 3 veins (parallel to the Z fault) are relatively late in the vein paragensis. Too few crosscutting relationships of type A veins cutting types B and C were observed to plot on a stereonet. However, structural types 4 (subhorizontal) and 2 predominate in barren veins where they cut mineralized veins, with a smaller number of types 3 and 1. These veins represent a late barren stage of vein emplacement. The limited number of crosscutting relationships involving late stage barren veins is indicative of a low proportion of late stage veins at the deposit.

The observed pattern of vein orientation indicates that the Trout Lake deposit formed dominantly under tensile conditions. This is supported by the prominance of zoned quartz-alkali feldspar veins, interpreted to have formed by open space filling. Numerous vein-type base and precious metal deposits are present in the area surrounding the Trout Lake deposit. The orientations of veins in these deposits mimics the pattern observed at the Trout Lake deposit. The continuity of tungsten mineralization between the Trout Lake deposit and one of these base and precious metal deposits, the Copper Chief, suggests that they are part of the same metallogenic event.

Plate 5-1   Photomicrograph (X-polars) of seriate quartz
            grain boundaries in a quartz vein. Field of
            view is 2.05 mm.

Plate 5-2   Stylolites defined by sulphides in a quartz vein.
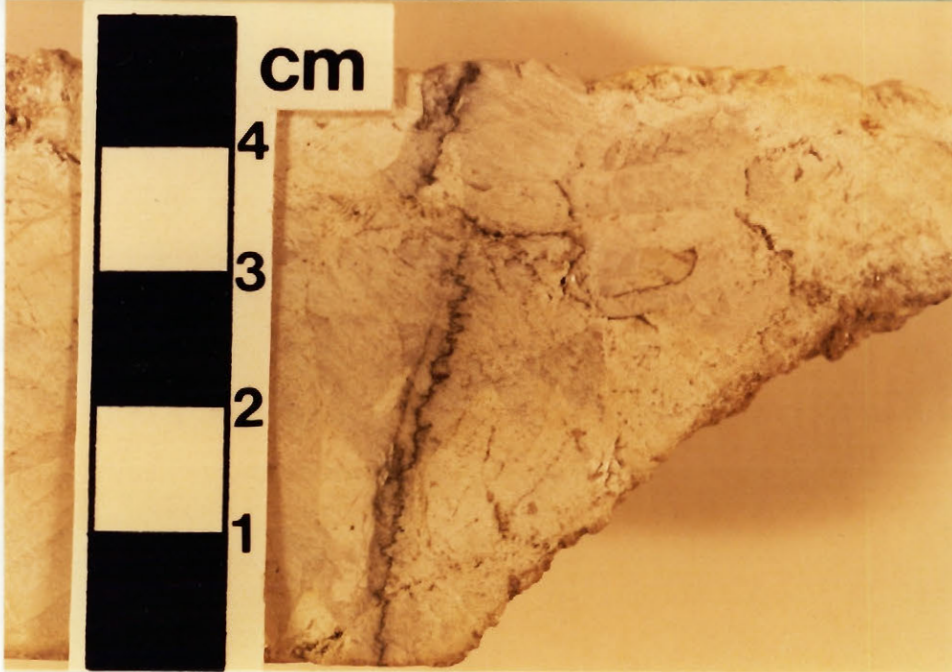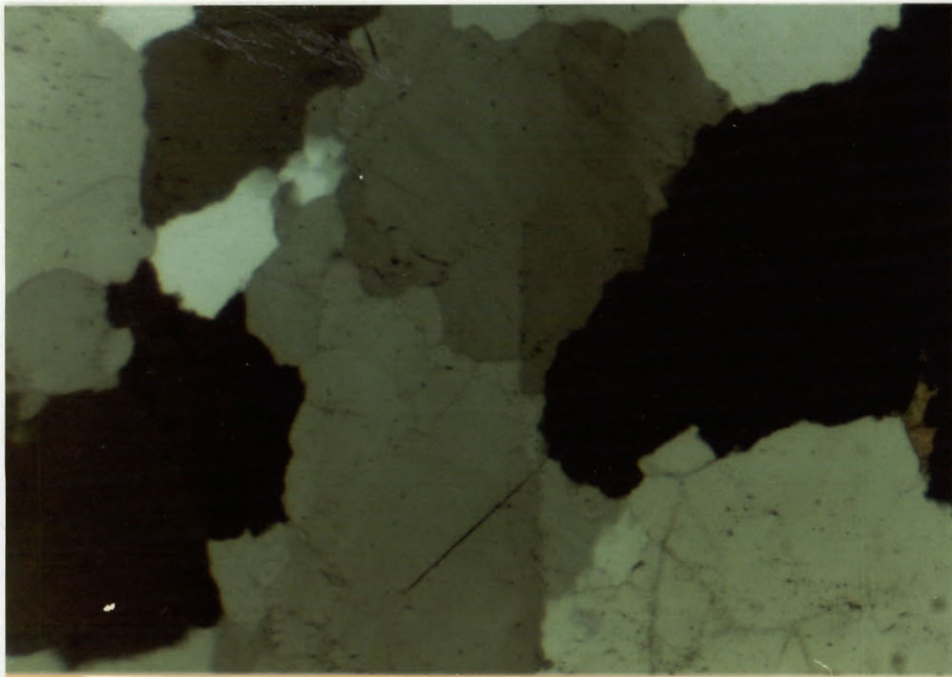
CHAPTER 6: MINERAL CHEMISTRY

The chemical compositions of minerals are controlled by the chemistry and mineralogy of the whole rock of which they comprise a part, the chemical composition of the fluid which they interact with, temperature, and pressure. In order to gain insight into the latter three parameters, microchemical analyses were conducted on various minerals using a CAMEBAX wavelength dispersive electron microprobe.

A 15 kV acceleration voltage, 5.0 nanoampere beam strength, 1 micron beam width, and 30 second counting periods were used. The following standards were used for the respective elements: andradite for Ca, Si, Fe; orthoclase for K, Al; MnTi for Mn, Ti; MgO for Mg; albite for Na; and LiF for F. All data was reduced using a ZAF correction program supplied by the microprobe manufacturer.

Biotite, feldspar, muscovite, and carbonate are present in most phases of alteration and contact metamorphism. Therefore these minerals were selected for analysis as changes in their chemical compositions should reflect changes in the physical and chemical nature of the hydrothermal fluids with which they interacted during the genesis of the deposit.

Fluid inclusions have been observed in all the above minerals (including biotite and muscovite) implying that they were in contact with a hydrothermal fluid. One criterion which can be used to determine whether minerals and coexisting fluids have attained equilibrium is an absence of chemical variability in the mineral. The variation about the median

value of major element oxides for each of the minerals above was generally found to be less than five percent in a given sample or individual grain. Compositional invariability in minerals by itself does not however prove equilibrium. Biotite, feldspar, muscovite, and carbonate analyses are tabulated in Apendices 1,2,3, and 4 respectively.

6.1 BIOTITE

Biotite compostions from within the contact aureole reflect the chemical nature of the lithological unit in which they occur. Compositions of hydrothermal biotites, if different from contact metamorphic biotites, are the result of interaction with hydrothermal fluids. Contact metamorphic biotites from the quartz-biotite schist (unit 1) are enriched in iron and aluminum in comparison to contact metamorphic biotites from the calcareous schist (unit 3). Hydrothermal biotites, which formed during late potassic alteration as haloes around quartz veins have compositions that are intermediate to the two contact metamorphic types. A third biotite type, from biotite-calcite alteration, has been distinguished. These are matrix biotites from schists within the zone of pervasive potassic alteration. Their compositions may reflect interactions with contact metamorphic, biotite-calcite, and late potassic alteration fluids.

All iron is assumed to be in the divalent state since pyrrhotite and ilmenite are accessory phases and magnetite is rare. To test this assumption, biotite stoichiometries were calculated assuming that all iron is ferrous, and that there

is a total of 44 negative charges. Out of 40 representative
biotites, 32 have a calculated cation charge of 44.00 +/-
0.02, and the remainder are within +/- 0.43. If significant
amounts of ferric iron were present the cation totals would be
lower than 44.00. Therefore the assumption of iron being
totally in the ferrous state is valid. By perfect
stoichiometry, 2 filled hydroxyl sites are also implied.

6.1.1 MAGNESIUM-IRON CONTENTS IN BIOTITE

Figure 6-1 is a percent cation plot of magnesium versus
iron in the biotites from Trout Lake.   As mentioned above,
two types of contact metamorphic biotite can be distinguished.
Magnesium-rich biotites are from the calcareous schist (unit
3), and iron-rich biotites are from the pelitic quartzite
(unit 1). Late potassic alteration biotites have compositions
that are intermediate between the two contact metamorphic
types. The biotite-calcite alteration type has compositions
similar to either the contact metamorphic or hydrothermal
types. A reference line with a slope of -1 on Fig. 6-1
demonstrates that there is not a one-to-one Mg-Fe substitution
as the points (in particular those from late potassic
alteration) define a trend with a slope steeper than -1. This
is due to differences in the aluminum contents of the
biotites. Five pairs of coexisting late potassic and biotite-
calcite alteration biotites were analysed. However, the close
spacing of data points in Fig. 6-1 prohibits graphic
representation of their relationships.   Therefore an
additional element (Al) was used to graphically represent

Figure 6-1 Cation % plot of magnesium versus iron in
            biotite.   Crosses represent contact
            metamorphic biotites. Circles represent
            biotite-calcite alteration biotites. Squares
            represent late potassic alteration biotites.

Reference Line
(Slope −1)
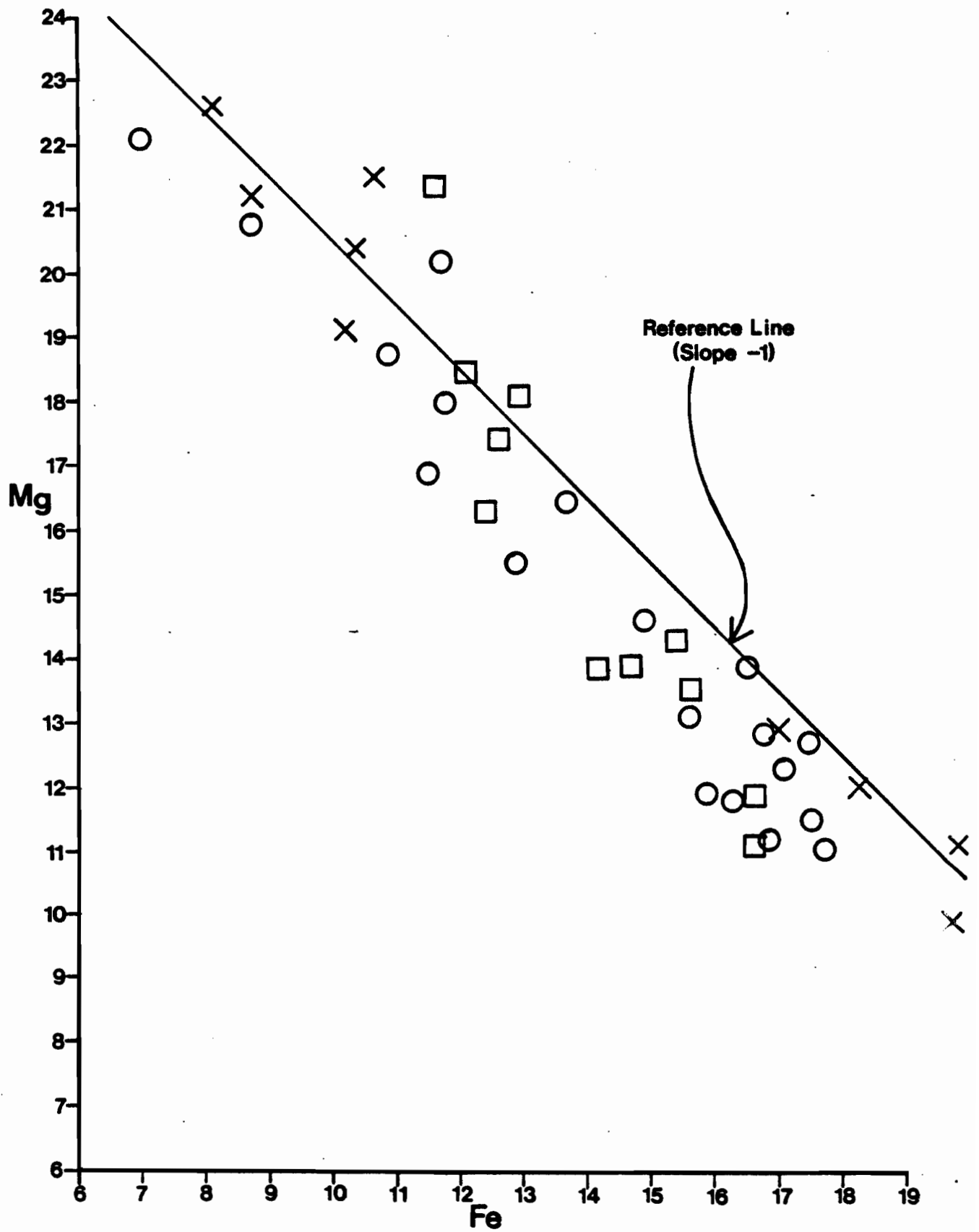
changes in biotite compositions.

Figure 6-2 is a plot of total aluminum as a cation percent versus the mole fraction of magnesium (X_{Mg}; Mg/Mg+Fe). The iron-rich biotites tend to contain more aluminum than magnesium-rich biotites. Again the intermediate composition of late potassic alteration biotites is demonstrated. The tie lines join pairs of late potassic and biotite-calcite alteration biotites from the same sample. Late potassic alteration biotites consistently have an intermediate composition relative to the coexisting Mg-rich or Fe-rich biotite-calcite alteration biotite. The aluminum content of the late potassic alteration biotite is also generally lower. This is probably due to changes in the modal abundance of muscovite, and other aluminous phases, i.e. changes in the form in which aluminum is available.

One tie line joins a pair of late potassic alteration biotites. The two data points represent compositions from the inner and outer edges of a 1 cm thick biotite halo. The biotite composition at the outer edge (furthest from the vein) is more magnesian. This particular halo crosscuts unit 3, and the outer edge biotite has a composition similar to a biotite-calcite alteration biotite from that unit. The biotite from the inner edge (adjacent to the quartz vein) is less magnesian. Therefore the compositional relationships within a biotite halo can be identical to those between coexisting hydrothermal and apparent contact metamorphic biotites. Biotites between the halo edges were also analysed (not plotted in Fig. 6-2, see appendix 1) and their compostions are

Figure 6-2 Cation % plot of aluminum versus magnesium mole

fraction in biotite. Crosses represent contact

metamorphic biotites. Circles represent

biotite-calcite alteration biotites. Squares

represent late potassic alteration biotites.
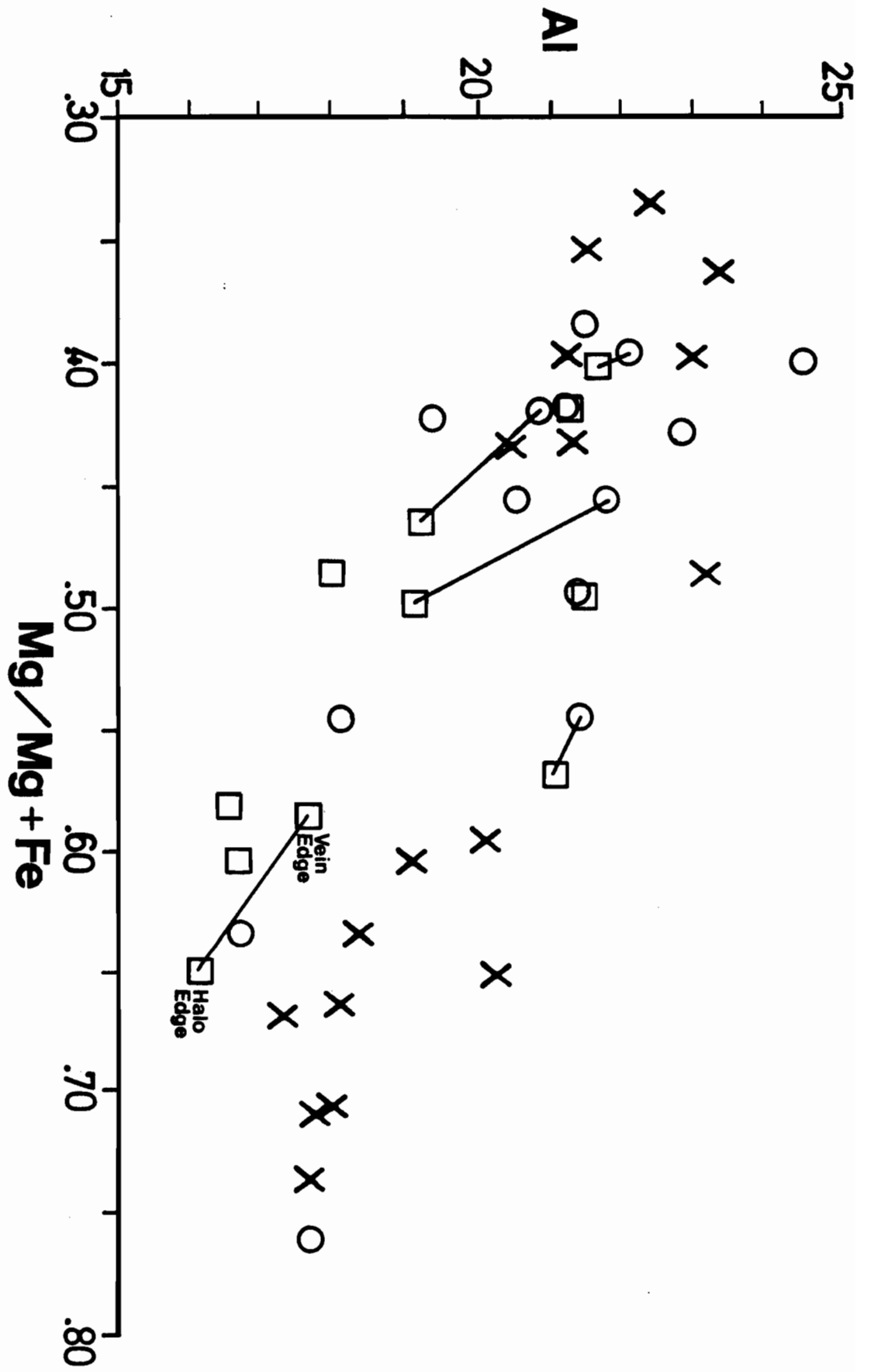
intermediate to compositions at the halo edges. A diffusion-controlled re-equilibration of biotite with the late potassic alteration fluid is the most probable explanation for the progressive iron enrichment. No compositional zoning was observed in biotite haloes developed in the quartz-biotite schist. However, the haloes which overprint the quartz-biotite schist are typically thin (less than 1 cm), whereas haloes in the tremolite-biotite schist are thicker, commonly up to 2 cm. Compositions of contact metamorphic, and to a large extent biotite-calcite alteration biotites are apparently controlled by lithology, whereas late potassic alteration biotite compositions are controlled by the hydrothermal solutions. The question remains, what fluid conditions promote the formation of biotites with intermediate Fe-Mg compositions?

Magnesium enrichment in hydrothermal biotites from porphyry copper deposits is well established e.g. Beane (1974), Chivas (1978). Experimental studies by Schulien (1975) demonstrated that in the case of biotites which have equilibrated with saline solutions, the iron is partitioned into the fluid and the magnesium into biotite. He showed that the degree of partitioning increases with increasing temperature, but did not study the effect of increasing salinity. Bischoff et al. (1981) studied the alteration of greywacke by seawater and brine. They found that the partioning of iron into solution and magnesium into sheet silicates increased with increasing temperature or salinity. An analogous effect is observed in the alteration of basalt by

seawater. Many workers (e.g. Mottl, 1983; Hajash and Archer, 1980) have found Mg-enrichment in chlorites and Fe-enrichment of the fluid during seawater-basalt interaction.

An important parameter controlling the degree of enrichment is the fluid/rock ratio. The highest degree of Mg-enrichment in minerals corresponds to the highest fluid/rock ratio i.e. higher fluid/rock ratios allow for greater equilibration between rock and fluid (Mottl, 1983). Therefore, for conditions where the fluid/rock ratio is high, and the fluid is highly saline, a distillation of iron (or dissolution until saturation) into solution would occur. The magnesium enrichment observed in biotites from porphyry copper deposits can be explained by biotite interaction with highly saline fluids. This is consistent with highly saline orthomagmatic fluids causing early alteration in porphyry copper deposits.

The hydrothermal fluid during late potassic alteration at Trout Lake resulted in biotite compositions that are intermediate to the two contact metamorphic types. The amount of the shift away from contact metamorphic compositions is interpreted as the degree of equilibration of the late potassic alteration biotite with that fluid. Some late potassic alteration biotites have compositions very similar to contact metamorphic types. These compositions are intrepreted to reflect control of Fe-Mg by the rock. Presumably they represent areas of lower fluid/rock ratios. Late potassic alteration biotites with compositions of approximately $X_{Mg} = 0.5$ are at the convergence of Mg-enrichment and Fe-

enrichment trends, and therefore probably represent the most equilibrated compositions, and the areas of highest fluid/rock ratio. However, equilibrium cannot be proved at this point.

At Trout Lake, the late potassic alteration fluids were moderately saline (3 to 15 wt.% NaCl) and had a moderate CO_2 content (between 0.05 and 0.2 XCO_2; see Chapters 3 and 7). It is reasonable to assume that chloride and carbonate complexes controlled the activities of iron and magnesium in solution and the resulting compositional changes in late potassic alteration biotites. Chloride complexing of iron and magnesium in highly saline solutions may result in Mg-enrichment in biotites, as discussed previously. The intermediate compositions of the late potassic alteration biotites could have resulted from the moderately saline nature of the hydrothermal solutions. Alternatively, carbonate complexing may have also influenced iron and magnesium activity. Unfortunately fluid-mineral equilibria processes are not well enough understood to be able to use biotite compositions to calculate physical or chemical parameters for the coexisting fluid.

6.1.2 FLUORINE CONTENTS IN BIOTITE

Figure 6-3 is a plot of the cation percent of fluorine versus X_{Mg} in biotites. It can be seen that the fluorine content of biotite increases with the magnesium content. The logarithim of the ratio of water to hydrogen fluoride fugacities was calculated for each biotite composition in Fig. 6-3 using the method of Gunow et al. (1980). A temperature of

Figure 6-3   Cation % plot of fluorine versus magnesium mole
            fraction in biotite. Crosses represent contact
            metamorphic biotites.   Circles represent
            biotite-calcite alteration biotites. Squares
            represent late potassic alteration biotites.
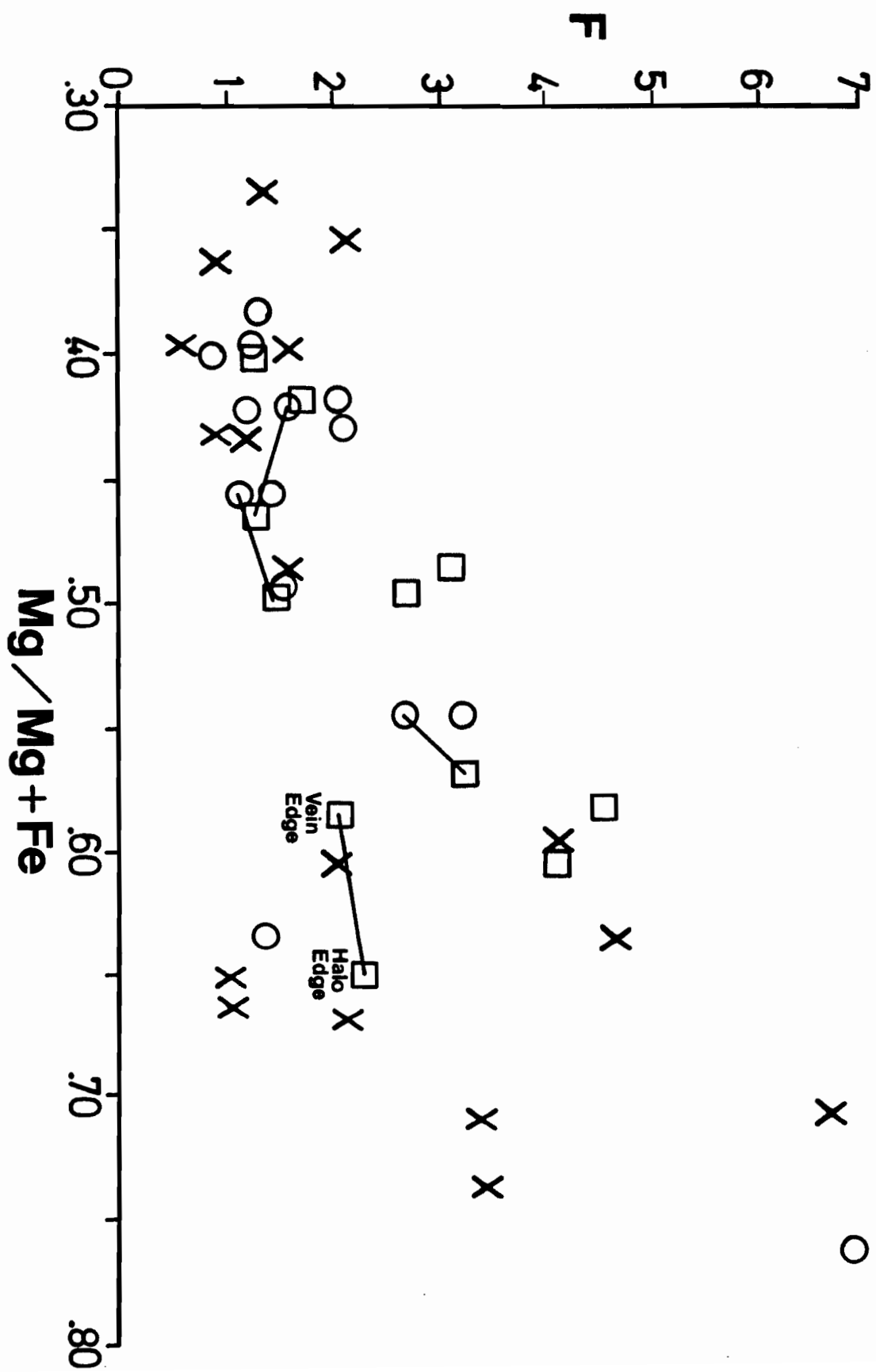
400 ^{o}C, established in Chapter 3 as the temperature of biotite-calcite alteration, was assumed in the calculation. Histograms of the calculated log (f_{H2O}/f_{HF}) of the fluid in equilibrium with the contact metamorphic, biotite-calcite alteration, late potassic alteration, and all biotites, is shown by Figure 6-4 a, b, c, and d respectively. The log fugacity ratios vary from 4.1 to 5.1, and there is no significant difference in the range of log fugacity ratios of the different biotite types. Fluorine contents can vary up to 100 % about the median value in a given sample. A large proportion of this error is due to the analytical technique. The propagation of this error through the fugacity ratio calculations yields an error of +/- 0.3 in the logarithmic fugacity ratio.

The histogram peaks in Figs. 6-4a and 6-4c suggest that there are possible subgroupings of log fugacity ratios. Presumably this would relate to the chemistry of the host lithology, as the fluorinity of the hydrothermal solutions for a given event is expected to be constant. However, there is no relationship between the log fugacity ratio and the chemical composition of the host lithology (Fig. 6-4a), or the chemical composition of the lithologic unit which the hydrothermal biotite overprints (Fig. 6-4c). Therefore the variation of log fugacity ratios is probably the result of a lack of precision in the analytical technique.

Biotites from the Henderson molybdenite deposit in Colorado contain significantly more fluorine. The log fugacity ratio is interpreted to be 3.0 at the core and 4.3 at

Figure 6-4 Histograms of log f_{H2O}/f_{HF}.

                  a) contact metamorphic biotites

                  b) biotite-calcite alteration biotites

                  c) late potassic alteration biotites

                  d) all biotites
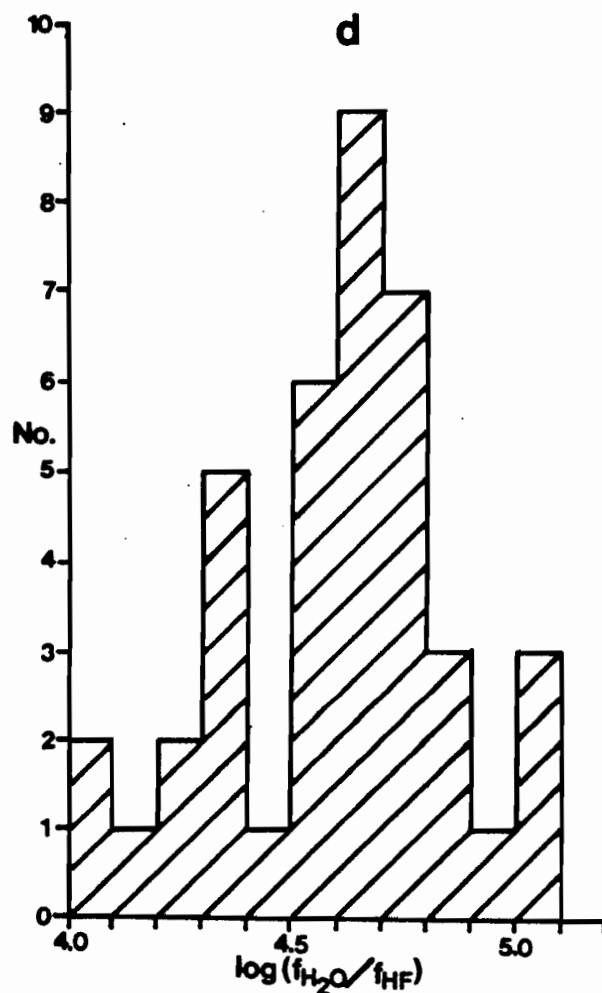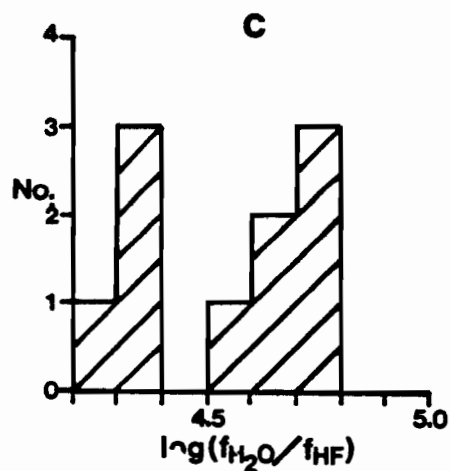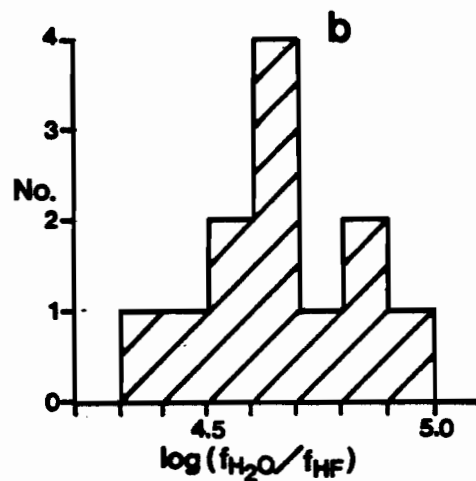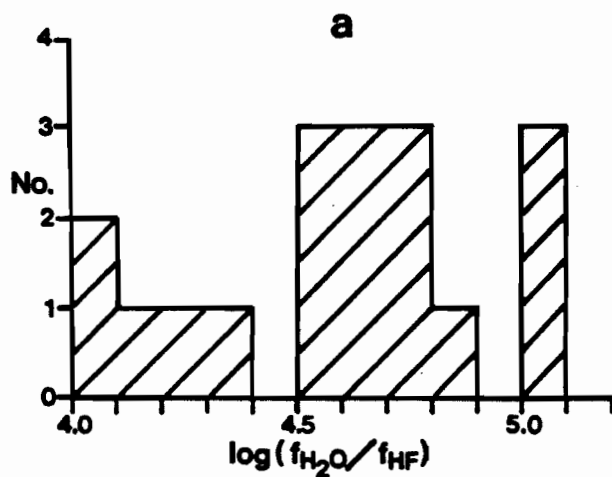
the outer margin (Gunow et al., 1980). Although the precision of fluorine analyses presented in this study are poor, it can be generally concluded that the fluorinity of the Trout Lake system was significantly lower than at Henderson. This is supported by the rarity of fluorite and absence of topaz at the Trout Lake deposit, two common minerals at the Henderson deposit.

6.2 FELDSPARS

The importance of feldspars to mineralization has been discussed in Chapter 4, but feldspars are also present in contact metamorphic rocks, and in all types of alteration. Therefore a systematic feldspar study was undertaken using staining, petrographic, and electron microprobe techniques.

6.2.1 CONTACT METAMORPHIC AND BIOTITE- CALCITE ALTERATION FELDSPARS

The composition of contact metamorphic feldspars was discussed in Chapter 3. The compositions in the calcareous schist (unit 3) are in general An_{50}, and in the pelitic quartzite (unit 1) generally An_{25}, where An_X represents the anorthite mole fraction. Outside the contact metamorphic aureole plagioclase grains are albitic and twinned. Within the aureole plagioclase grains are not twinned and exhibit poikioblastic textures.

Biotite-calcite (pervasive potassic) alteration, is interpreted in Chapter 3 to have formed at a temperature similar to contact metamorphism (approximately 400 ^{o}C), but at

a higher XCO_2. Plagioclase grains with an An_{30} composition are observed in the quartz-biotite and tremolite-biotite schists, both of which are affected by biotite-calcite alteration. Texturally this alteration type is similar to contact metamorphism; the plagioclase grains have a poikioblastic texture with no visible twinning. Figure 6-5 is a histogram of the composition of all plagioclase grains analysed in biotite-calcite altered rocks.

6.2.2 FELDSPARS ASSOCIATED WITH LATE POTASSIC ALTERATION

During subsequent late potassic alteration, iron and magnesium compositions appear to have been controlled by fluid composition and fluid/rock ratios (discussed in section 6.1.1). Only seven microprobe analyses of K-feldspar grains disseminated in unit 1 (potassic alteration) were obtained. The compositions are dominantly Or_{96-97}, where Or_χ represents the orthoclase mole fraction. The remaining analyses are of feldspars from veins with biotite envelopes. These feldspars also formed during the late potassic alteration stage.

The veins with biotite envelopes characteristically have albite at the vein margin and in general do not contain K-feldspar. When K-feldspar is present it is typically near the centre rather than the margin of the vein (Plate 3-2). Histograms of albite and K-feldspar compositions from veins with biotite envelopes are shown by Figure 6-6a and b respectively. A typical albite has an Ab_{97-98} composition, and K-feldspar Or_{97-98}, where Ab_χ and Or_χ are the albite and orthoclase mole fractions respectively.

Figure 6-5   Histogram of plagioclase compositons from
             biotite-calcite alteration. Ab is the albite
             mole fraction.

Figure 6-6   Histograms of feldspar compositions from late
             potassic alteration. Ab is the albite mole
             fraction. Or is the K-feldspar mole fraction.
                    a) albite compositions from quartz veins
                       with biotite haloes
                    b) K-feldspar compositions from quartz
                       veins with biotite haloes
                    c) plagioclase compostions from quartz
                       veins with biotite haloes, and
                       compositions from within the haloes

Figure 6-7   Histograms of albite and K-feldspar compositions
             of feldspars associatied with mineralization.
             Ab is the albite mole fraction. Or is the K-
             feldspar mole fraction.

Fig. 6-5

Fig. 6-6

Fig. 6-7
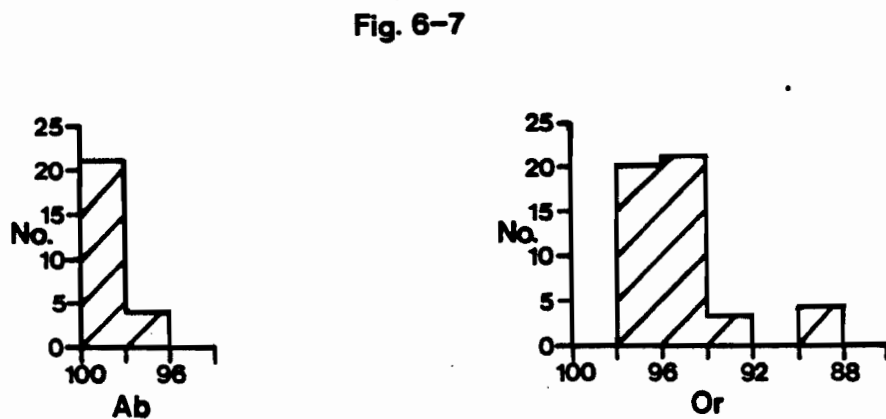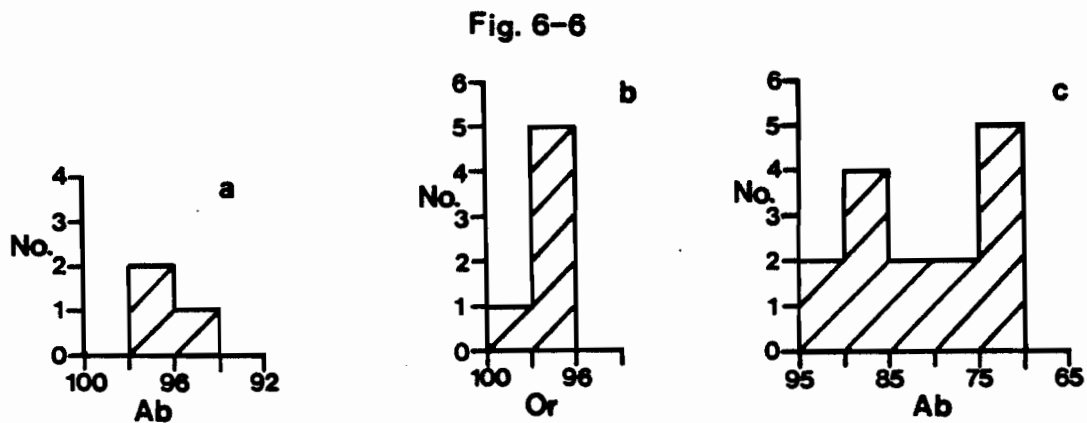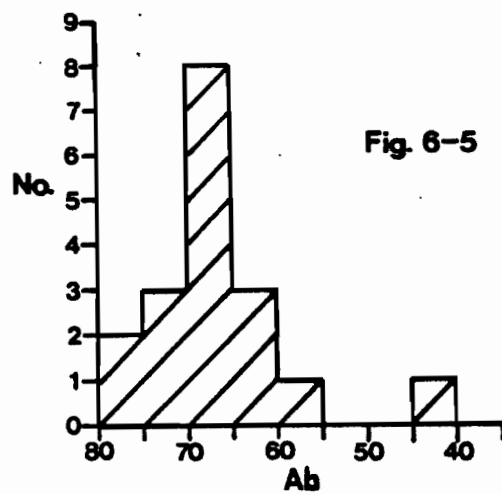
Figure 6-6c shows the compositions of plagioclase in late potassic alteration veins, and in the adjacent halo. Both vein and halo plagioclase grains have compositions which range from An_5 to An_{25}. They are interpreted to represent the partial re-equilibration of An_{30} plagioclase during late potassic alteration. The fact that these plagioclase grains have compositions that are intermediate between the vein (albite) and biotite-calcite alteration (An_{30}) compositions suggests that they formed by replacement of An_{30} plagioclase, and not by direct precipitation from a hydrothermal solution. Because these plagioclase grains are presently within a quartz veins it is implied that veins must have formed by a dissolution and partial replacement process in addition to open-space filling.

6.2.3 FELDSPARS ASSOCIATED WITH MINERALIZATION

Figure 6-7 is a histogram of alkali feldspar compositions that are present in mineralized veins and mineralized zones of silicification. The albites have an Ab_{97-100} composition, and the K-feldspars a composition of Or_{93-98}. A small population of K-feldspars with an Or_{90} composition was also observed. There are no apparent textural or chemical differences between vein feldspars and feldspars from silicified zones. Therefore no distinction will be made between these feldspar types, and they will be treated collectively as feldspars associated with mineralization.

A variety of textures are observed in the alkali feldspars associated with mineralization. Albite or

chessboard twinning (Plate 6-1) is commonly observed although more typically albite is cloudy, and not twinned. No twinned K-feldspar from this type of alteration has been observed. K-feldspar replacement of albite is commonly observed (Plate 6-1), both in thin sections, and in hand specimens with the aid of staining. With massive K-feldspar replacement, patches of remnant albite are generally scattered throughout the grain. Where less intense K-feldspathization is present, K-feldspar is observed to replace albite along fractures or cleavage planes (Plate 4-3).

Where one feldspar replaces another it is dominantly K-feldspar that replaces albite. The opposite is rarely observed. In some quartz veins successive feldspar bands are observed. Both albite and K-feldspar are present in the feldspar bands. This suggests that the quartz veins underwent multiple stages of opening, and that the albite and K-feldspar formed almost synchronously from the same hydrothermal solution.

Alkali vein feldspars are generally coarse grained, up to 1 cm, and line the walls of quartz veins. However, alkali feldspars which accompany silica flooding (silicification) are very fine grained. Plate 6-2 shows quartz-K feldspar flooding of granodiorite. In other samples quartz-albite or quartz-albite-K feldspar flooding is present. In silicified granodiorite, it is interesting that plagioclase phenocrysts are embayed by quartz and not by alkali feldspar (Plate 6-3). No consistent paragensis could be established regarding the relative timing of silicification and alkali feldspathization.

Plate 6-1   Photomicrograph (X-polars) of "chessboard"
             twinned albite replaced by K-feldspar along
             fractures and cleavage planes. Field of view
             is 0.85 mm.

Plate 6-2a   Photomicrograph (plane polarized light) of
             quartz-K fledspar flooding in granodiorite.
             Field of view is 0.53 mm.

Plate 6-2b   Photomicrograph (X-polars) of quartz-K feldspar
             flooding in granodiorite. Field of view is
             0.53 mm.
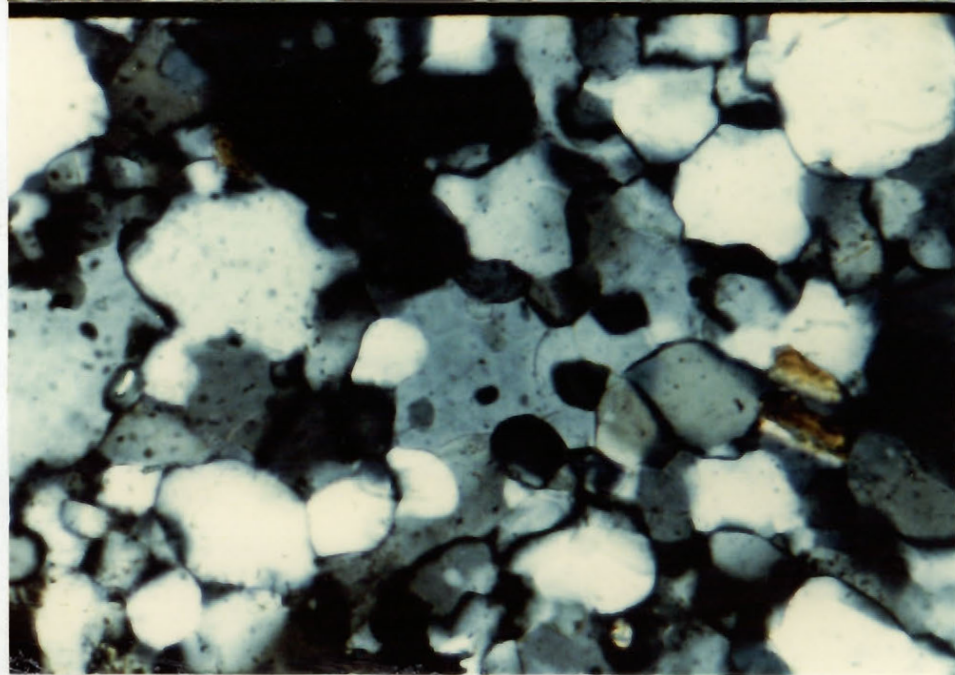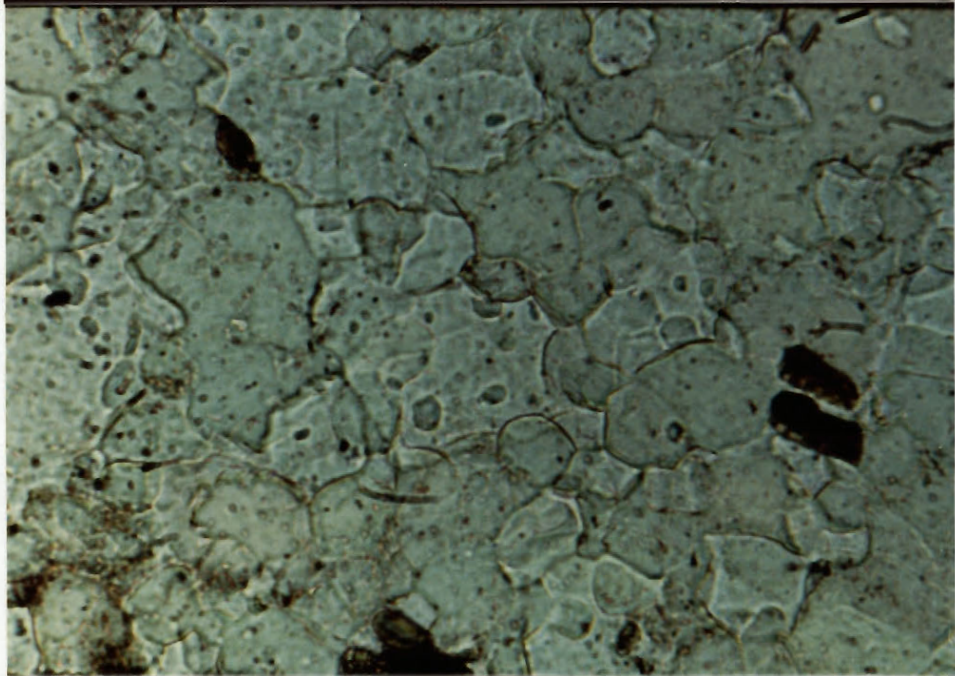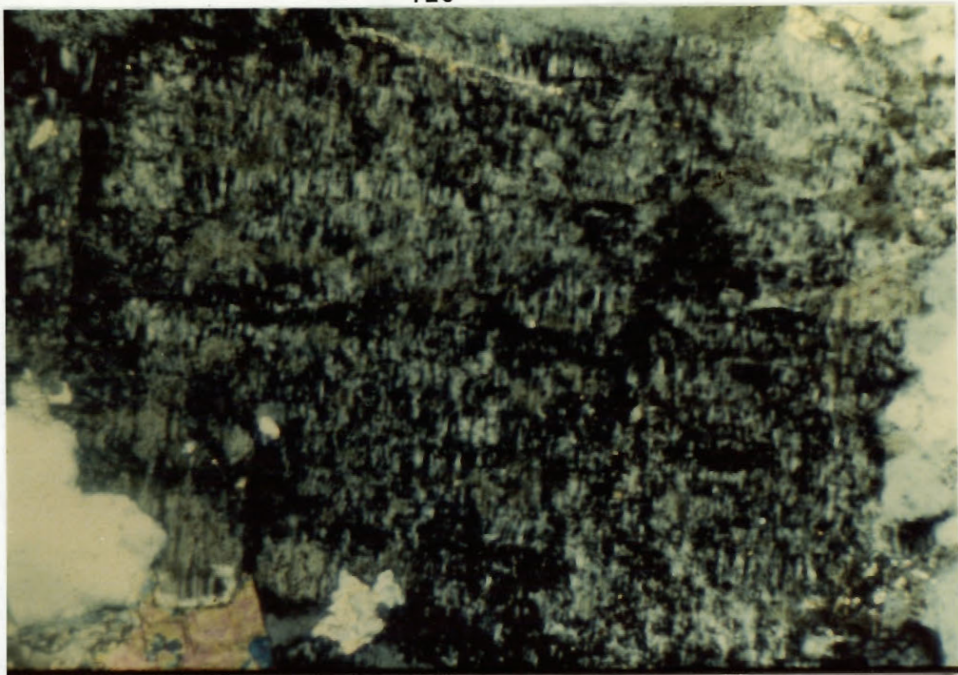
Plate 6-3 Photomicrograph (X-polars) of quartz overgrowths
          on a plagioclase phencryst in granodiorite.
          Field of view 2.05 mm.

Plate 6-4a Photomicrograph (plane polarized light) of
            microcline (cloudy) flooding in a phyllically
            altered schist. Field of view 2.05 mm.

Plate 6-4b Photomicrograph (X-polars) of microcline (tarton
            twinning) flooding in a phyllically altered
            schist. Field of view 2.05 mm.

However, silicification may have preceeded alkali feldspathization and mineralization.

6.2.4   PHYLLIC ALTERATION FELDSPARS

The compositions of alkali feldspars associated with phyllic alteration are similar to those in other stages. Albite has an Ab_{95-100} composition, and K-feldspar is Or_{95-98} (Fig. 6-8). Texturally, albite in phyllic alteration is similar to albite in other alteration types (discussed above) i.e. it is generally cloudy, twins are developed locally, and it is commonly replaced by K-feldspar. However, K-feldspar grains in phyllically altered rocks commonly exhibit tartan twinning, a texture rarely observed elsewhere in the deposit. Twinning has been observed in fine grained interstitial "matrix flooded" grains (Plate 6-4), or in overgrowths on earlier feldspars in both igneous and metasedimentary hosts. Locally some feldspar grains are strongly sericitized but this is not characteristic of phyllic alteration. Therefore it is concluded that albite, K-feldspar, and muscovite were all stable during phyllic alteration.

6.2.5   INTERPRETATION OF FELDSPAR COMPOSITIONS

The An_{25} composition of contact metamorphic plagioclase in the pelitic quartzite is consistent with the interpretation that contact metamorphism occurred at approximately 400 °C. At this temperature albite, anorthite, and peristerite are the stable subsolidus phases (Smith, 1983). However, the An_{50} plagioclase composition observed in the calcareous
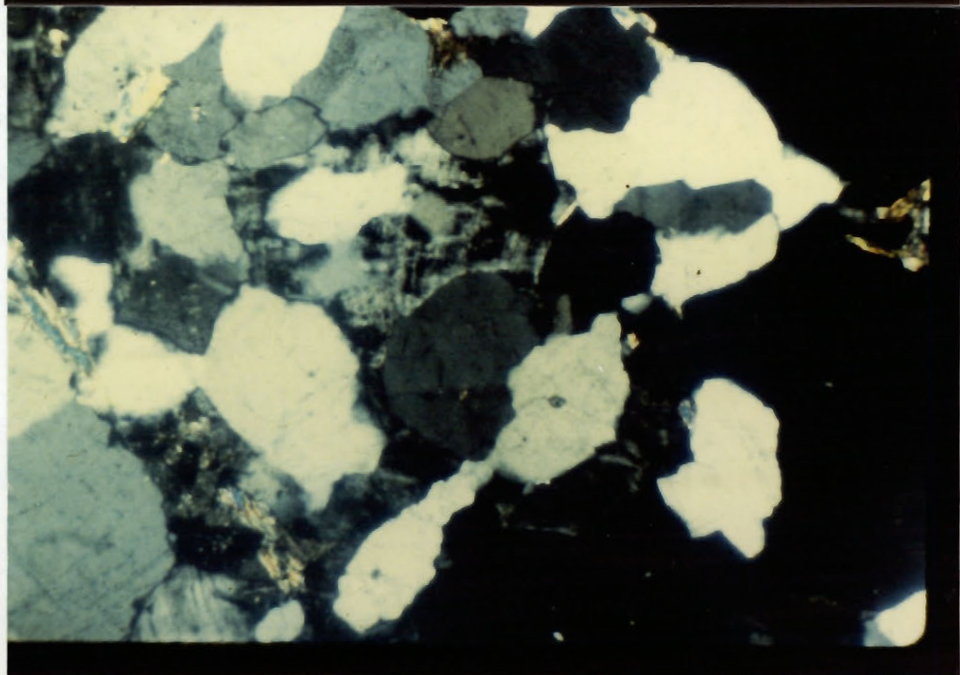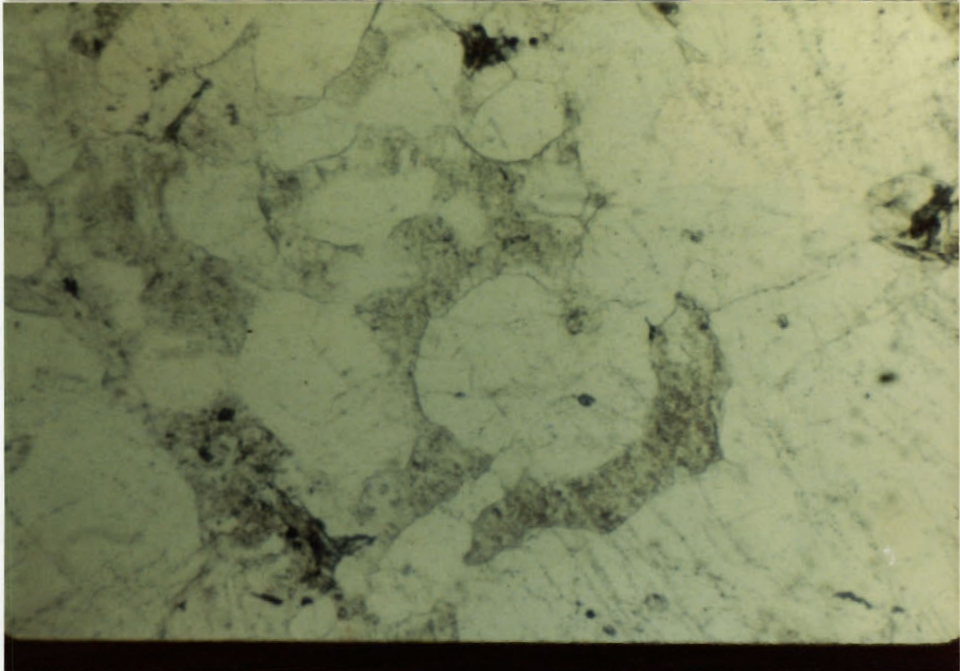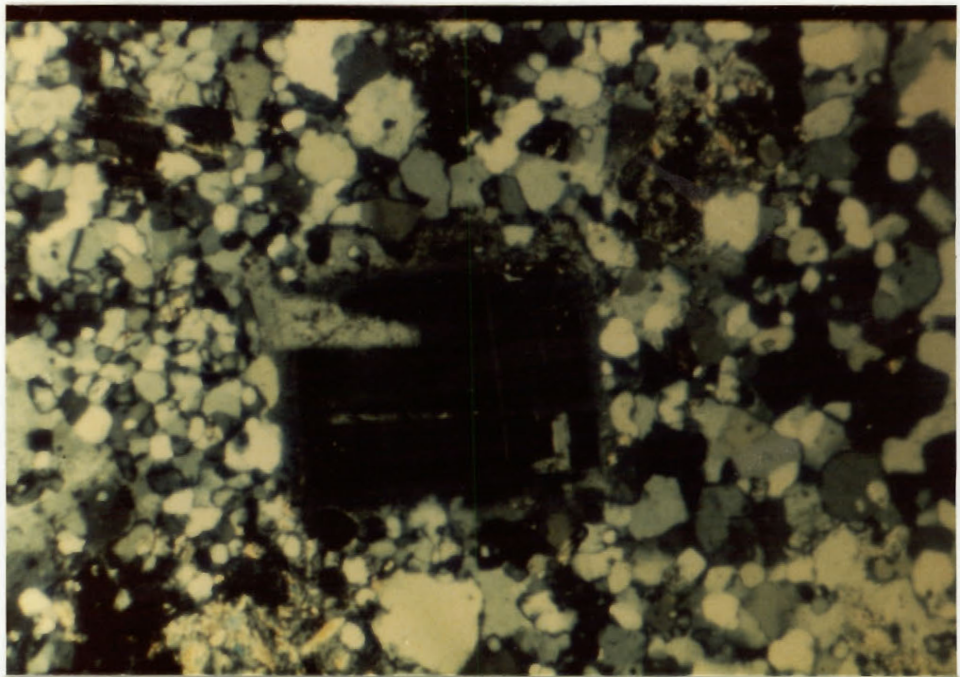
metasediments may represent metastablity. Ideally, a plagioclase with an An_{50} composition is stable at approximately 800 ^oC (Smith, 1983). The more calcic plagioclases are found in more calcareous sediments, i.e. are a result of higher calcium activity. At high calcium activities, peristerite and anorthite should be thecoexisting stable phases at 400 ^oC, with albite and anorthite being the phases below 400 ^oC. The bulk calcium content of the metasediments resulted in the formation of calcic plagioclase and, as the calcic plagioclase does not have an anorthitic composition, it may therefore have formed metastably. Alternatively, the plagioclase may be comprised of submicroscopic intergrowths of albite and anorthite.

During biotite-calcite alteration an An_{25-35} plagioclase formed at a temperature similar to that of contact metamorphism. If this composition represents equilibration of plagioclase with the hydrothermal fluids during biotite-calcite alteration then the fluids were probably not significantly below 4CC ^oC, otherwise the plagioclase would have been converted wholely or partially to albite.

The plagioclase observed adjacent to or within veins with biotite alteration envelopes retained a significant anorthite component (An_{5-25}),(Fig. 6-6). This is interpreted as a partial re-equilibration of the plagioclase from biotite-calcite alteration with a late potassic alteration fluid. If the pre-existing An_{25-35} plagioclase was at, or nearly at equilibrium, the destruction of plagioclase during potassic alteration indicates a lower temperature. Alternatively, if

the An_{25-35} plagioclase from biotite-calcite alteration was metastable, the transition from plagioclase to albite during late potassic alteration could represent a higher fluid/rock ratio i.e. conditions that better facilitate equilibration.

The K-feldspars and albites observed in late potassic and phyllic alteration, and those associated with mineralization all have a similar range of compositions. Using the argument presented above, the lack of an anorthite component in albites from phyllic alteration or mineralization implies that either a lower temperature or a higher fluid/rock ratio existed during these events in comparison to biotite-calcite alteration.

From the discussion in Chapter 3, it is interpreted that potassic and phyllic alteration occurred at different temperature and XCO_2 conditions. The alkali feldspars from the different hydrothermal events have similar compositions. This suggests a similar K/Na/Ca ratio in each solution, or alternatively, that they all re-equilibrated with a late hydrothermal fluid, presumably the phyllic alteration fluid. Using the observed range of compositions and the two feldspar geothermometer (Whitney and Stormer, 1977) a temperature of 300-400 °C is estimated (Fig. 6-9) assuming equilibrium conditions at 1000 bars of pressure.

Two alkali feldspars coexisting with a fluid at a given temperature and pressure are stable at only one given K/Na ratio for the fluid (Lagache and Weisbrod, 1977). At 400 °C and 1000 bars the K/Na ratio of a saline fluid co-existing with two alkali feldspars is a maximum of 0.14, and possibly

Figure 6-8   Histograms of albite and K-feldspar compositions
            from phyllic alteration.   Ab is albite mole
            fraction.   Or is K-feldspar mole fraction.

Figure 6-9   Two-feldspar geothermometer from Whitney and
            Stormer (1977).   Solid line is for microcline
            and the dotted line for sanidine.   The solid
            square represents the compostional range
            observed in alkali feldspars at Trout
            Lake.

Fig. 6-8
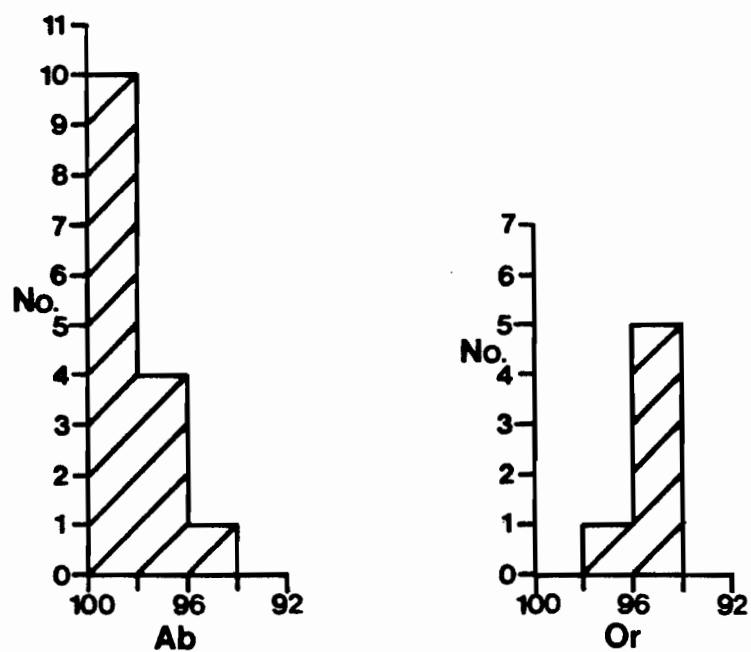
Fig. 6-9
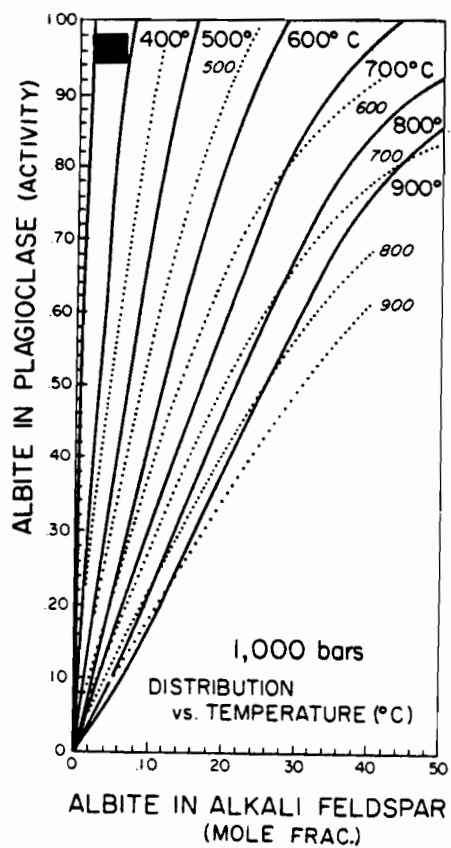
lower for dilute salt solutions (Lagache and Weisbrod, 1977). At a lower temperature, the K/Na ratio of the fluid must be even lower for two alkali feldspars to coexist stably. The addition of CO_2 to the KCl-NaCl-two feldspar system complicates interpretation. If sodium and potasium are in solution as carbonate complexes the K/Na ratio of the fluid must be lower than that for chlorine complexes for two alkali feldspars to form stably (Iiyama, 1965). Fluid inclusion evidence (Chapter 7) suggests that the fluids at Trout Lake were moderately saline and had a moderate XCO_2. Unfortunately the relative importance of chlorine versus carbonate complexing of sodium and potassium in high temperature multicomponent solutions is poorly understood. However, it can be stated that the maximum K/Na ratio of the potassic and phyllic alteration, and mineralizing fluids was probably not greater than 0.14. If the temperature of the various fluids was lower than 400 ^{o}C or the alkali metals were in part complexed by carbonate, the fluids must have had a K/Na ratio lower than 0.14. For phyllic alteration at least, the K/Na ratio was probably lower than 0.14. In addition, albite, K-feldspar, and muscovite coexist throughout the history of the deposit. By using data from Montoya and Hemley (1975) it can be concluded that if temperature decreased and XCO_2 increased over time, then the K/Na activity ratio decreased and K/H activity ratio increased over time.

6.3 MUSCOVITE COMPOSITIONS

The subsolidus phase relationships between muscovite and paragonite are analagous to those of the alkali feldspar system (Thompson, 1974). At higher temperatures, muscovite and K-feldspar will contain more sodium, and albite and paragonite more potassium. A muscovite is stoichiometrically dioctahedral if there are 4.0 octahedral cations. Iron and magnesium can also substitute into muscovite in a reaction such as $Mg^{+2} + Si^{+4} = 2Al^{+3}$. All the muscovites observed at Trout Lake are phengitic (excess octahedral cations), possibly the result of a reaction such as $3Mg^{+2} = 2Al^{+3}$. Figure 6-11 is a plot of the mole fraction of muscovite (K/K+Na) versus the octahedral cation total. Sodium can affect the degree of iron and magnesium substitution as greater sodium contents allow greater tetrahedral rotation, thereby increasing the amount of iron and magnesium that can be substituted into the structure (Zussman, 1979).

Muscovites at Trout Lake have the following characteristics (Fig. 6-11): contact metamorphic muscovites generally have a higher paragonite component; the calcareous schists are typically more phengitic and the pelitic quartzites less phengitic; hydrothermal muscovites have a smaller paragonite component, but a variable degree of octahedral filling; muscovites, specifically from phyllic alteration, have a very large number of octahedral cations. The high iron and magnesium contents in muscovites from phyllic alteration are presumably the result of iron and magnesium having been released during biotite destruction, or

Figure 6-10   Mole fraction of muscovite/paragonite versus
              the octahedral cation total.   Crosses
              represent contact metamorphic muscovites.
              Solid circles represent vein muscovites. Open
              circles represent biotite-calcite alteration
              muscovites. Triangles represent phyllic
              alteration muscovites.
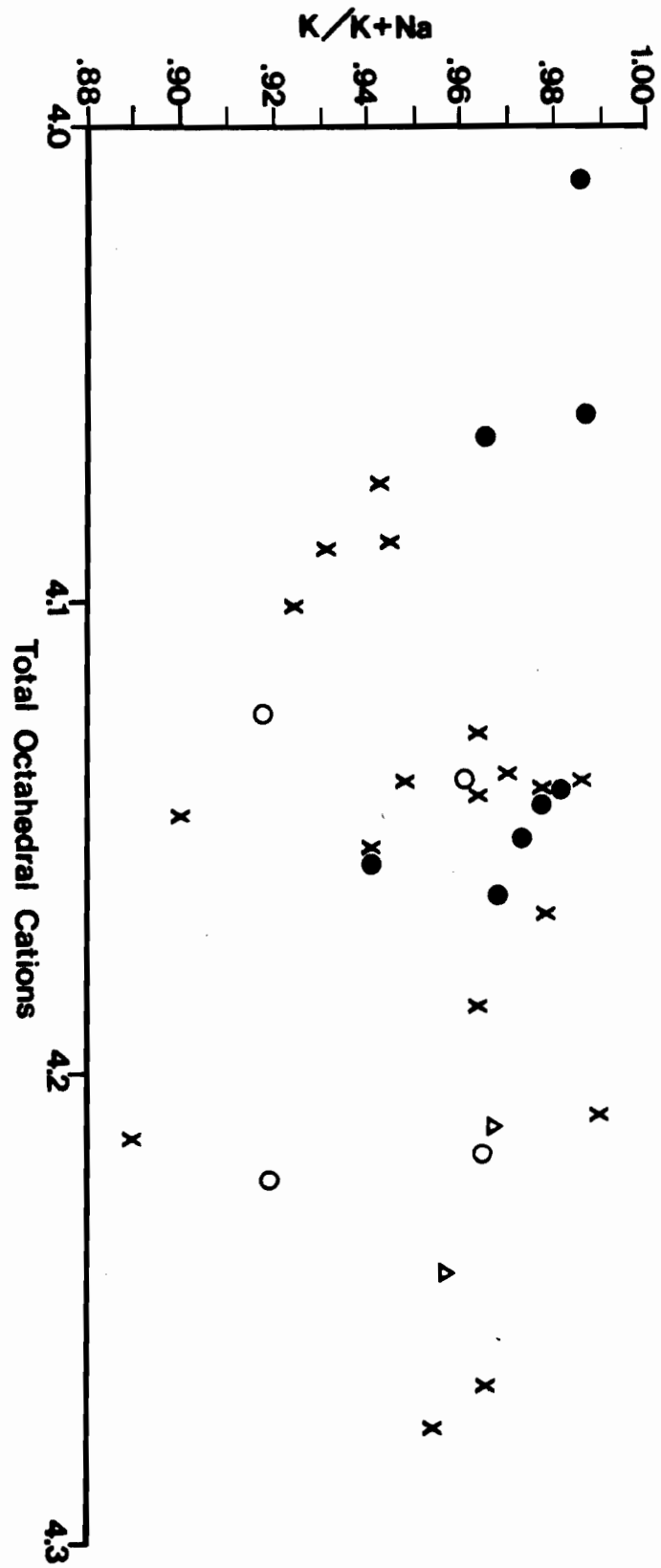
iron and magnesium having resisted solvation during biotite replacement by muscovite.

The lower sodium content in hydrothermal muscovite relative to contact metamorphic muscovite is consistent with the interpretation given for the feldspars, that hydrothermal alteration occurred at a lower temperature than contact metamorphism. However, the variation of phengitic muscovite composition with temperature and pressure is not well enough constrained to make a more qualitative interpretation.

6.4 CARBONATE COMPOSITIONS

Carbonate compositions were investigated using staining (alizarin red and potassium ferricyanide) and electron microprobe techniques. Ankerite is the only carbonate observed in phyllic alteration. Calcite is present in all other alteration types, and contact metamorphic rocks. Microprobe analyses indicate that the calcites are nearly end-member $CaCO_3$ (0.96-1.00 calcite mole fraction) with small siderite, magnesite, and rhodochrosite mole fractions. Ankerite has a variable composition; 0.50-0.57 calcite mole fraction, 0.15-0.24 siderite mole fraction, 0.21-0.31 magnesite mole fraction, and 0.00-0.04 rhodochrosite mole fraction. The Fe/Fe+Mg ratio varies from 0.33 to 0.53. If ankerite is saturated with respect to iron and magnesium, the Fe/Mg ratio should be constant for a given temperature and constant iron and magnesium activities in solution (Bickle and Powell, 1977). The variation of ankerite compositions at Trout Lake suggests that either ankerite formed under

disequilibrium conditions, or that it was not fully saturated with respect to iron or magnesium. The latter is more probable since there is no coexisting siderite or magnesite.

6.5 SUMMARY

Biotite compositions during contact metamorphism and biotite-calcite alteration were controlled by the chemistry and mineralogy of the host lithological unit. During subsequent late potassic alteration, fluid composition and fluid/rock ratios tended to control biotite chemistry. Two trends, either Mg or Fe-enrichment, represent Mg-Fe exchange between biotites and hydrothermal fluids. The largest deviations away from the contact metamorphic compositions are interpreted to represent conditions of higher fluid/rock ratios. The intermediate compositions of the biotites which are "most equilibrated" are probably due to the effects of chloride or, less likely, carbonate complexing of iron and magnesium.

Plagioclase is observed in contact metamorphic rocks, and accompanies the earliest form of alteration, biotite-calcite. Their compositions are consistent with the interpretation that these events occurred at approximately 400 ^{o}C, although contact metamorphic plagioclase from calcareous schists may be metastable. Subsequent alteration and vein feldspars are alkalic, and were formed at lower temperatures, 300-400 ^{o}C. The muscovite-paragonite system is analagous to the K feldspar-albite system, and the compositions of alteration muscovites also indicate that alteration events occurred at

temperatures lower than contact metamorphism. Calcite is the only carbonate mineral observed in the contact metamorphic to mineralization events. During subsequent phyllic alteration ankerite formed as a result of biotite destruction or replacement.

CHAPTER 7: FLUID INCLUSIONS

7.1 INTRODUCTION

Fluid inclusions were investigated to aid in the interpretation of the physical and chemical nature of the hydrothermal fluids which formed late potassic and phyllic alteration, and mineralization. An S.G.E. model III heating-freezing stage was employed to determine melting and homogenization temperatures of fluid inclusions. The stage was calibrated for temperatures in the -100 to +400 °C range using the melting temperatures of various known standards. A summary of the fluid inclusion data is presented in Appendix 5. All melting and homogenization temperatures have been corrected to the true temperature using the calibration curve. Both the CO_2 homogenization and the melting data are generally accurate to +/- 0.2 °C, whereas the H_2O and H_2O-CO_2 homogenization data are generally accurate to +/- 1.0 °C. Fluid inclusions in quartz from three different sample groups were examined using doubly-polished sections: 1) late potassic alteration, represented by quartz veins with biotite haloes 2) mineralization, represented by mineralized quartz veins and mineralized pervasive silicic alteration 3) phyllic alteration, represented by quartz veins with muscovite haloes and quartz veins from zones of pervasive phyllic alteration.

7.2 DESCRIPTION OF INCLUSIONS

Inclusions were categorized as primary, pseudosecondary, and secondary, using the criteria of Roedder (1979). Two

compositional types were observed: 1) liquid-vapour H_2O, and 2) H_2O-CO_2.

7.2.1 PRIMARY INCLUSIONS

Primary inclusions are rare. Only type 1 primary inclusions were identified. They range from 5 to 30 microns in diameter. Most however, are 10 to 30 microns in diameter. They are either rhomboidally or spheroidally shaped in three dimensions (Plate 7-1), and tend to occur as clusters in certain discrete quartz grains. This suggests that not all quartz grains formed during the same event and that these inclusions represent an early hydrothermal event. The clusters of inclusions are probably due to necking down. The size of the vapour bubble varies from 20 to 80 volume percent at 25 °C. This variability is likely due to necking down.

7.2.2 PSEUDOSECONDARY INCLUSIONS

Pseudosecondary inclusions are more commonly observed. Both pseudosecondary type 1 and type 2 inclusions have been identified. They are commonly less than 5 microns across, which is too small for accurate microthermometric analysis. Larger pseudosecondary inclusions, 5 to 20 microns in diameter, generally have rounded or irregular shapes (Plate 7-2). They have little depth in the third dimension, and therefore are lensoid. Many pseudosecondary inclusions exhibit necking down textures (Plate 7-3), and therefore were not analysed. Type 1 inclusions are the dominant type observed in group 1 samples (late potassic alteration), with a

Plate 7-1   Photomicrograph (plane polarized light) of a
             primary H_2O liquid/vapour (type 1) inclusion.
             Field of view 220 microns.

Plate 7-2   Photomicrograph (plane polarized light) of
             pseudosecondary H_2O-CO_2 inclusions (type 2).
             Field of view 220 microns.

Plate 7-3   Photomicrograph (plane polarized light) of
             necking down textures (centre of picture) in
             pseudosecondary inclusions. Field of view 220
             microns.
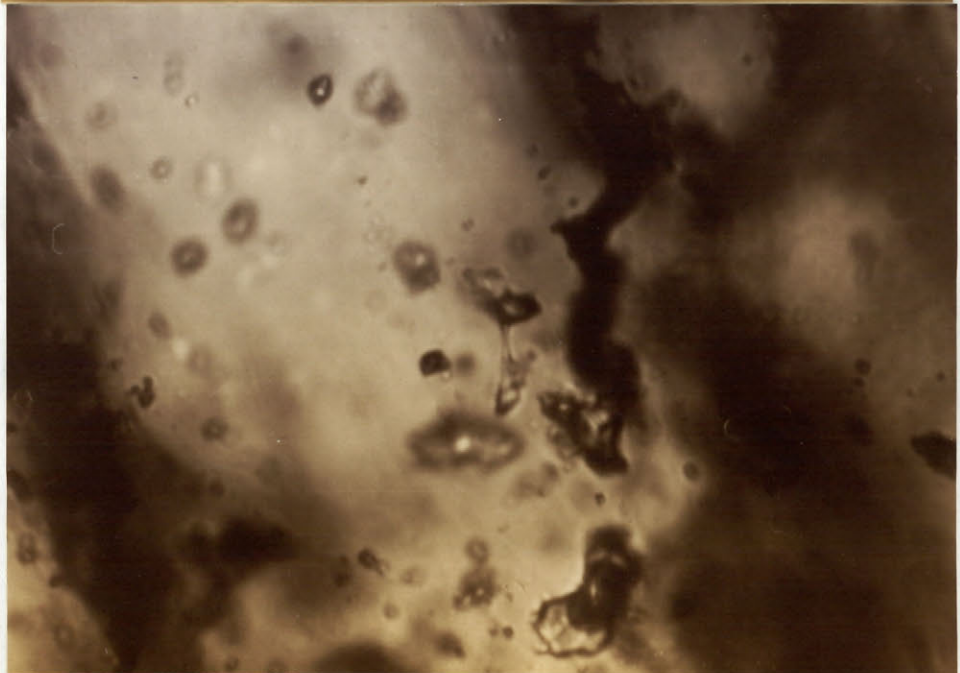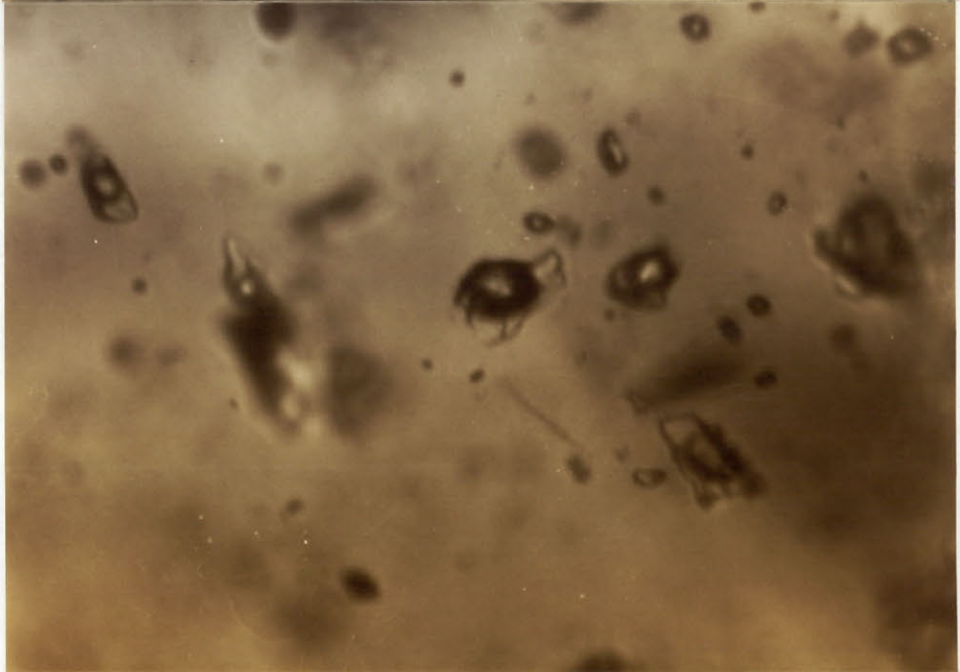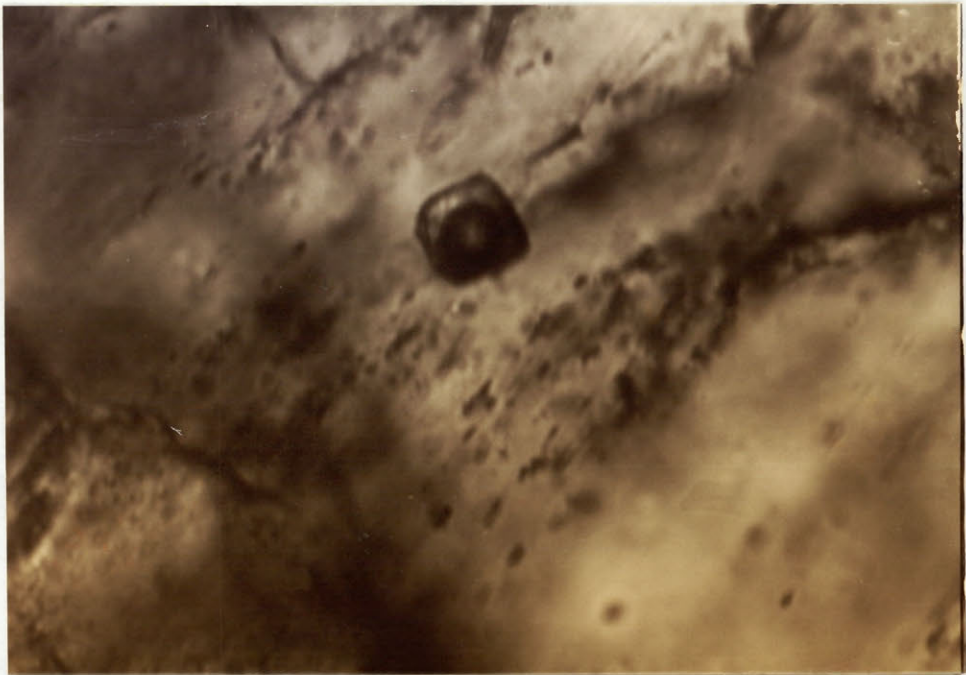
subordinate type 2 population. Both type 1 and type 2 inclusions are common in group 2 samples (mineralized quartz veins-silicic alteration), with type 2 predominating. Only type 2 inclusions have been identified in group 3 samples (phyllic alteration). Pseudosecondary type 1 inclusions generally have a vapour bubble which comprises 10 to 20 volume percent of the inclusion (estimated at 25 $^{\circ}$C). However, pseudosecondary type 2 inclusions display a variation of 10 to 90 volume percent CO_2 estimated at 25.0 +/- 5.0 $^{\circ}$C (Fig. 7-1). A histogram of the volume percent CO_2 in inclusions from late potassic alteration quartz veins (group 1) shows a peak at 30 to 40 vol. % CO_2. Inclusions from mineralized quartz veins and silicification (group 2) show a broad peak at 20 to 60 vol.% CO_2. Inclusions from phyllic alteration quartz veins (group 3) show a peak at 20 to 30 vol. % CO_2.

The majority of pseudosecondary type 2 inclusions contain 20 to 60 vol.% CO_2, which represents the most probable H_2O-CO_2 ratio at the time of trapping. The true H_2O-CO_2 ratio at the time of trapping may be even more restricted if necking down caused the variation of H_2O-CO_2 ratios. The volume percent CO_2 data shows a large spread, which may be reflecting necking down. The widest scatter occurs in group 2 inclusions. Therefore these inclusions underwent a greater degree of necking down, or the necking down in these inclusions occurred under different subcritical conditions than the other groups.

Alternatively, variations in H_2O-CO_2 ratios can be explained by fluid mixing, or by the trapping of immiscible fluids. The predominace of type 1 inclusions in group 1

samples (late potassic) and type 2 inclusions in group 2
samples (mineralization), and the occurrence of only type 2
inclusions in group 3 samples (phyllic) suggests mixing
between type 1 and type 2 fluids. The two fluids may have had
separate sources, or alternatively the type 2 fluid may have
resulted from CO_2 enrichment during wallrock interaction.
Generally it is not possible to distinguish between inclusion
types when the inclusion is smaller than 5 microns. The
relative abundances of inclusion types are therefore based on
the compositions of inclusions greater than 5 microns across.
If the distribution of inclusion types less than 5 microns is
different from those greater than 5 microns, the above
interpretations are erroneous. Unfortunately this problem
cannot be resolved.

7.2.3 SECONDARY INCLUSIONS

The majority of inclusions in Trout Lake quartz are
secondary, and are less than 5 microns in diameter. Both type
1 and type 2 secondary inclusions were observed, and range up
to 10 microns in diameter. They generally have a spheroidal
or lensoidal shape. The long axes of lensoidal secondary
inclusions are commonly perpendicular to the plane of the
fractures (Plate 7-4). Liquid-vapour and H_2O-CO_2 ratios in
secondary type 1 and 2 inclusions are similar to those in
pseudosecondary inclusions (see Appendix 5). The number of
observations is too few to warrant the construction of
histograms.

Plate 7-4   Photomicrograph (plane polarized light) of
             secondary inclusions oriented perpendicular to
             the fracture plane.   Field of view 220
             microns.
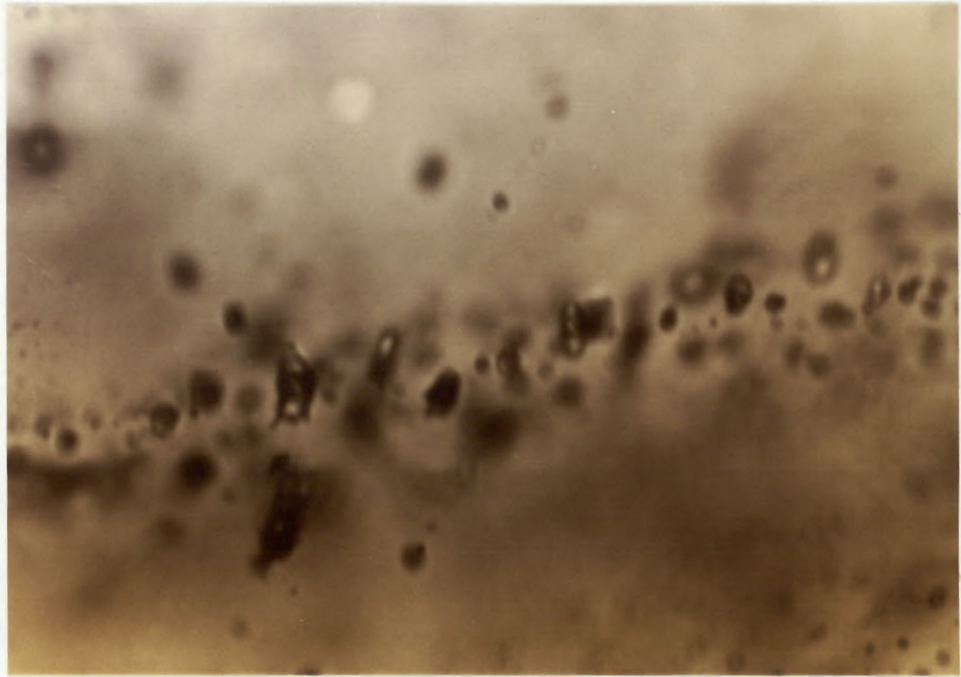
7.3 MICROTHERMOMETRIC DATA

7.2.1 H_2O HOMOGENIZATION AND MELTING TEMPERATURES

Microthermometric observations from only six primary type 1 inclusions were obtained. All six were from group 2 samples, and these inclusions homogenized to the liquid phase. The homogenization temperatures are evenly distributed between 270 and 370 °C (Fig. 7-2). However, melting temperatures of ice are very consistent, ranging from -1.4 to -1.8 °C. This corresponds to a salinity range of 2 to 3 wt. % NaCl equivalent (Potter et al.,1978).

Similar homogenization temperatures for pseudosecondary type 1 inclusions were obtained from group 1 and 2 samples. Therefore, data from these two groups were plotted together (Figure 7-2). Homogenization temperatures range from 180 to 300 °C, with peaks at 200 to 210 and 250 to 260 °C. Homogenization temperatures of secondary type 1 inclusions from groups 1 and 2 (Figure 7-3) range from 200 to 310 °C. The temperature distribution of this histogram mimics Figure 7-2. Only eight melting temperatures were obtained from pseudosecondary type 1 inclusions (five from group 1, three from group 2), and two from secondary type 1 inclusions (both from group 2). The number of melting observations is too small to determine if the salinity varies between sample groups. Melting temperatures in pseudosecondary inclusions range from -2.0 to -11.0 °C, and both secondary inclusions melted at -5.2 °C. This corresponds to a salinity range of 3 to 15 wt. % NaCl equivalent (Potter et al.,1978). No dominant

Figure 7-1   Histograms of volume % CO_2 in H_2O-CO_2 (type 2)
              inclusions from

                   a) late potassic alteration (group 1)

                   b) silicification-mineralization (group 2)

                   c) phyllic alteration (group 3)

Plate 7-2 Histograms of homogenization temperatures of H_2O
           (type 1) pseudosecondary, and primary (solid
           bars) inclusions.

Plate 7-3   Histogram of homogenization temperatures of
             secondary H_2O (type 1) inclusions.

Fig. 7-1
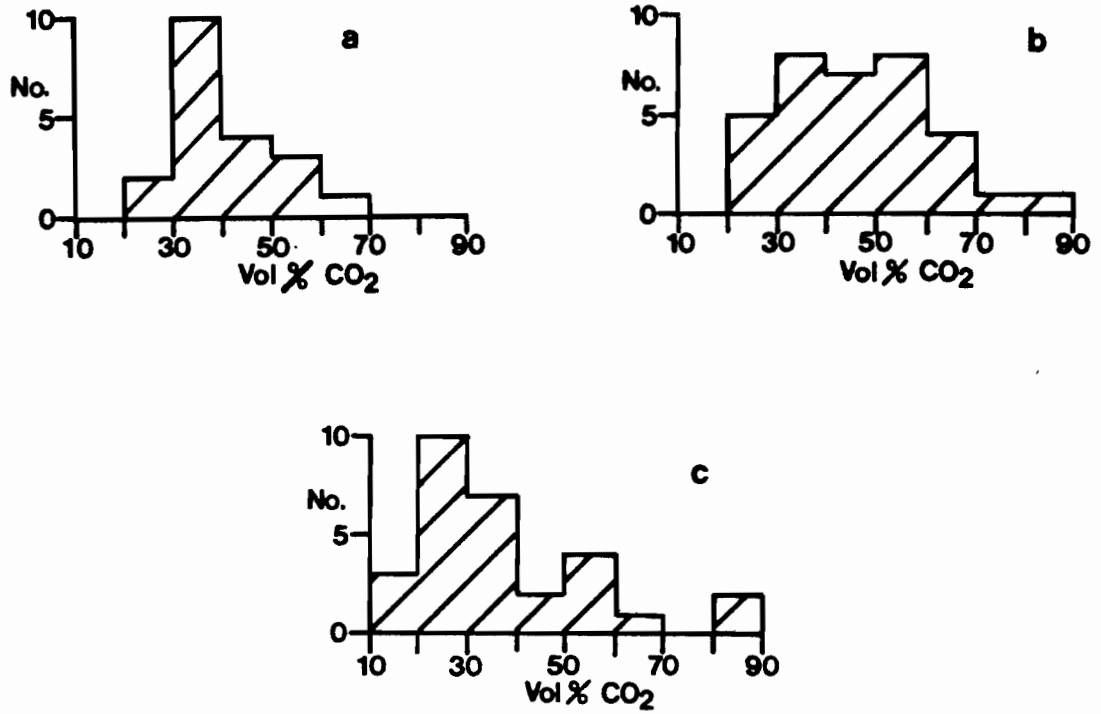
Fig. 7-2
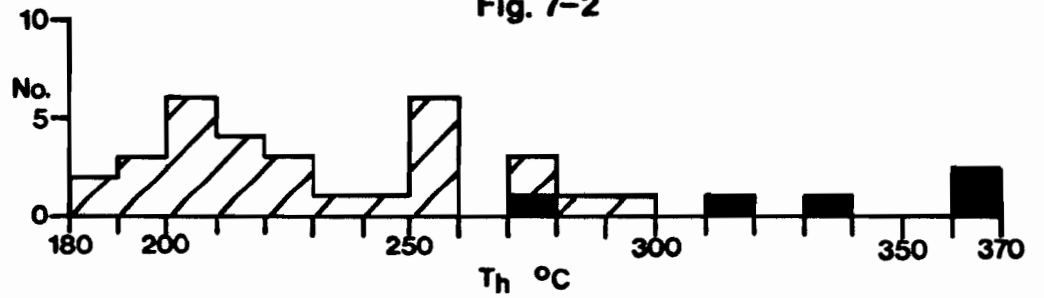
Fig. 7-3
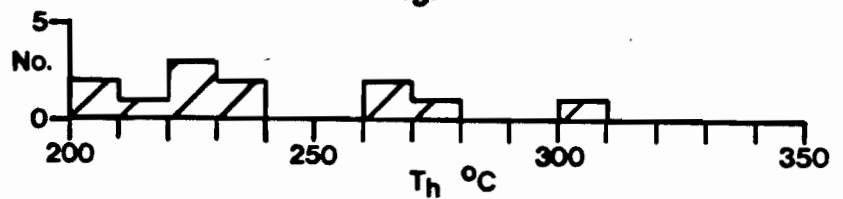
melting temperature is apparent.

During one freezing experiment a double freezing of the aqueous solution was observed. Collins (1979) suggests that double freezing is the result of clathrate formation, then ice formation, and indicates the presence of CO_2. Therefore some type 1 inclusions probably contain minor CO_2 at concentration levels too low to form a separate CO_2 phase (the CO_2 is concentrated in the vapour phase). This is consistent with a fluid mixing model for the deposit.

7.3.2 CO_2 HOMOGENIZATION AND MELTING TEMPERATURES

Group 1 inclusions show a broad range of CO_2 homogenization temperatures (Fig. 7-4), +0 to +27 ^oC, with a peak at +22 to +25 ^oC. Group 2 homogenization temperatures (Fig. 7-4) range from +5 to +22 ^oC, with the majority of the inclusions in the +15 to +22 ^oC range. Group 3 homogenization temperatures (Fig. 7-4) range from +15 to +30 ^oC, with a peak at +28 ^oC. Secondary type 2 inclusions have similar homogenization temperatures, but are not represented graphically (see Appendix 5).

The melting temperature of the CO_2 phase was commonly lower than -56.6 ^oC, the melting temperature of pure CO_2. The presence of methane lowers the melting temperature of CO_2 (Burruss, 1981). A phase change at -95 ^oC, with gradual sublimation at higher temperatures was commonly observed, which is consistent with the CH_4 liquid-vapour transition and CO_2-CH_4 solid-vapour solvus in the CO_2-CH_4 system (Burruss, 1981). Therefore it is concluded that methane caused the

depressed melting temperatures. The presence of both CO_2 and CH_4 was confirmed by Raman spectroscopic analysis (I. Samson, 1984 unpub. data).

The mole fractions of methane (XCH_4) within the CO_2 portions of type 2 inclusions were calculated using the method of Swanenberg (1979). Group 1 and 2 inclusions show a major XCH_4 peak at 0.03, with a smaller peak at 0.10 to 0.20 (Fig. 7-5). Group 3 inclusions contain negligible methane (Fig. 7-5).

The clathrate melting temperatures of all pseudosecondary type 2 inclusions range from +4.0 to +11.0 °C (Fig. 7-6). The clathrates melt in the presence of liquid CO_2, liquid H_2O, and vapour, which are invariant conditions on Figure 7-7. The invariant point shifts to lower temperature with the addition of NaCl. Therefore the salinities are 0.0 to 10.0 wt.% NaCl equivalent if the inclusion compositions can be represented by the system H_2O-CO_2-NaCl (Collins, 1979). However, the addition of CH_4 to this system will shift clathrate melting to higher temperatures (Collins, 1979).

Figure 7-8 is a plot of clathrate melting temperature versus XCH_4. In inclusions where CH_4 is absent, clathrates melt from +7.0 to +9.0 °C, which corresponds to salinities of 3.0 to 6.0 wt.% NaCl equivalent (Collins, 1979). All group 3 inclusions plotted on Fig. 7-8 are methane-free as are two group 2 inclusions. The rest of the data points are from methane-bearing group 1 and 2 inclusions. If salinity was constant, a positive slope would be defined by the points on Fig.7-8 as higher melting temperatures result from increased

Figure 7-4 Histograms of CO_2 homogenization temperatures
            from type 2 inclusions
                    a) late potassic alteration
                    b) mineralization-silicification
                    c) phyllic alteration

Figure 7-5 Histograms of X_{CH4} in type 2 inclusions
                    a) late potassic alteration
                    b) mineralization-silicification
                    c) phyllic alteration

Fig. 7-4
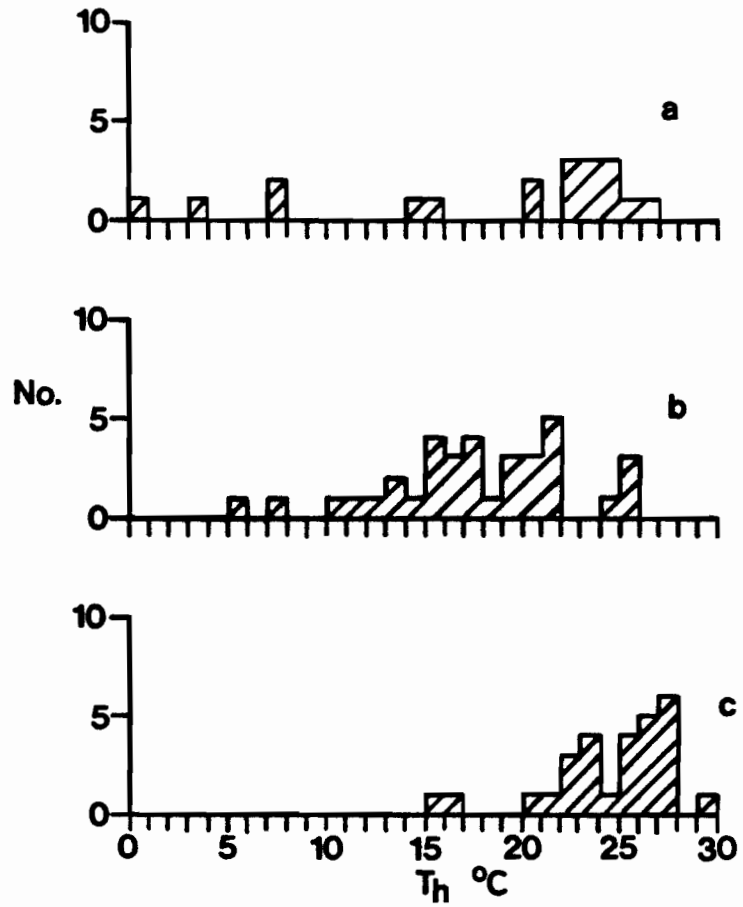
Fig. 7-5
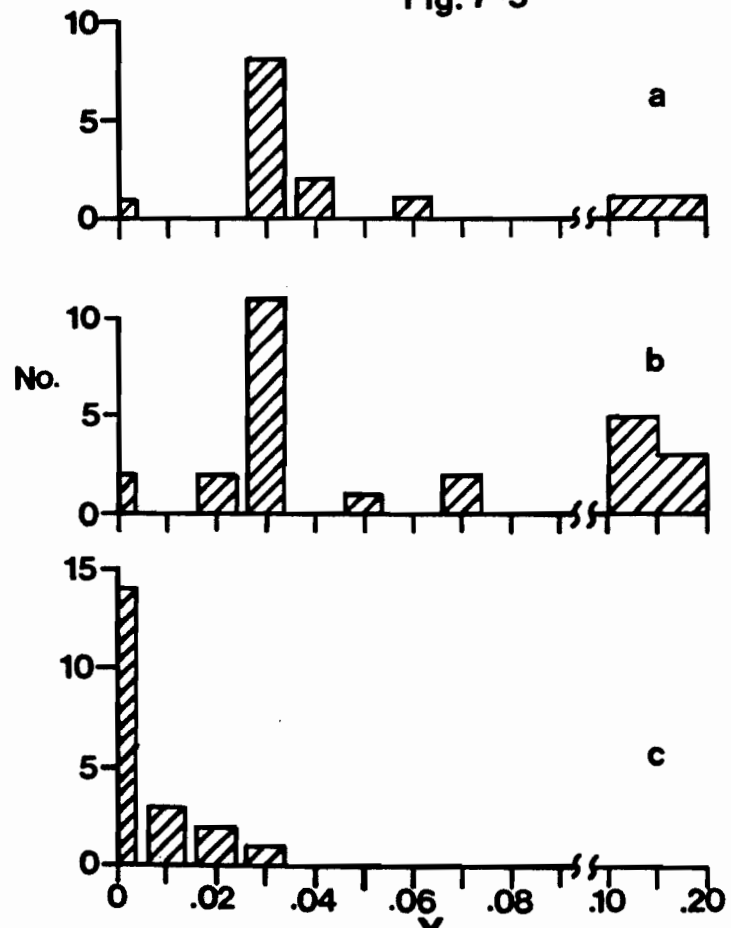
methane contents. The lack of such a positive slope implies that group 2 inclusions are generally more saline than 3.0 to 6.0 wt.% NaCl equivalent. Only one group 1 inclusion is plotted on Fig. 7-8, therefore no statement can be made about the general salinity of this group of inclusions.

7.3.3 CALCULATION OF XCO$_2$

A knowledge of the methane content and the CO$_2$ homogenization temperature for each inclusion allows calculation of the density of the CO$_2$-rich phase, using the method of Swanenberg (1979). These densities are calculated as a "CO$_2$ equivalent" i.e. the density if the CO$_2$-rich phase is pure CO$_2$, and all densities calculated are listed in Appendix 5. The mole fraction of carbon dioxide (XCO$_2$) of individual inclusions can be calculated using the volume percentage of CO$_2$, the density of the CO$_2$ phase, and the following assumptions: 1) CO$_2$ and H$_2$O are mutually insoluble at 25 ^{o}C. The solubility of H$_2$O into CO$_2$ is less than 0.6 mole %, and CO$_2$ into H$_2$O less than 3.0 mole % at this temperature (Burruss, 1981). Therefore this assumption is reasonable. 2) The density of the CO$_2$ phase is proportional to the molar volume of CO$_2$, i.e. the CO$_2$ phase may be treated as pure CO$_2$ and not a CO$_2$-CH$_4$ mixture. This is reasonable as the density is calculated as an equivalent CO$_2$ density. 3) The density of water at 25 ^{o}C is 1.0 g/cm^3, and this density is proportional to the molar volume of water. The addition of a salt to pure water raises the fluid density. However, this will not significantly affect XH$_2$O, e.g a 12 wt. % NaCl CO$_2$-

Figure 7-6   Histogram of clathrate melting temperatures

Figure 7-7   Phase relations in the C-O-H-NaCl system (from
             Collins, 1979).

Fig. 7-6
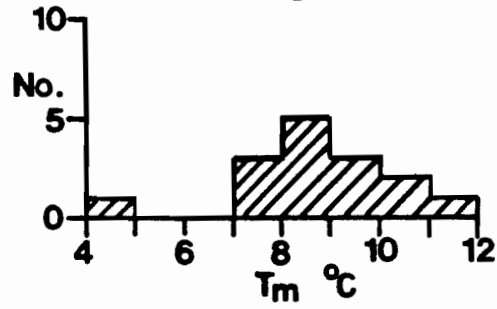
Fig. 7-7
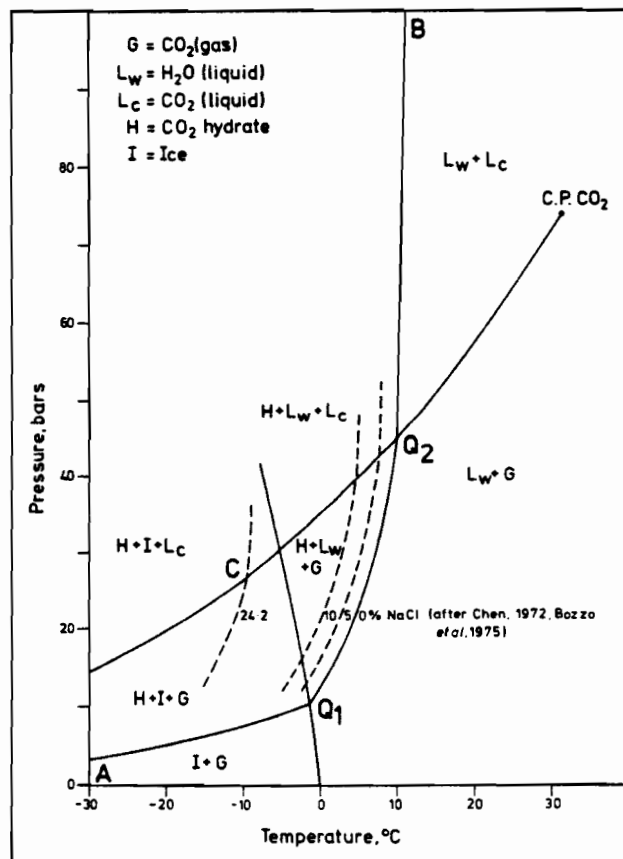
free solution has an XH_2O of 0.960.   4)   The   volume percentage of a phase is proportional to its mole fraction.

Based on the above assumptions, the molar proportions of CO_2 and H_2O of each inclusion were determined by dividing the phase densities by the corresponding molecular weights, and multiplying the results by the volume percentages of the phases.   The molar proportions were normalised to 1 to yield XCO_2.   A sample calculation is given below.

SAMPLE CALCULATION

Density of CO_2 = 0.70 g/cm^3 Density of H_2O = 1.0 g/cm^3

mol. wt. of CO_2 = 44.01 g/mol   mol. wt. of H_2O = 18.02 g/mol

30 vol.% CO_2 at 25 ^{0}C   70 vol.% H_2O at 25 ^{0}C

$$\text{Molecular proportion of } CO_2 = (0.70/44.01) \times 0.3 = 0.00477$$

$$\text{Molecular proportion of } H_2O = (1.0/18.02) \times 0.7 = 0.0388$$

$$XCO_2 = 0.00477/(0.00477+0.0388) = 0.109$$

Group 1 inclusions show an XCO_2 range of 0.05 to 0.25, with a peak at 0.10 to 0.15 (Fig. 7-9).   Group 2 inclusions show an XCO_2 range of less than 0.05 to 0.60, with a peak at 0.15 to 0.20 (Fig. 7-9).   Group 3 inclusions show an XCO_2 range of less than 0.05 to 0.65, with a peak at 0.05 to 0.10 (Fig. 7-9).   The lowest XCO_2 calculated is 0.04, which is near the minimum CO_2 concentration for the existence of a separate CO_2 phase at room temperature (less than 0.03, Burruss, 1981). As minor CO_2 is interpreted to be present in type 1

Figure 7-8 X_{CH4} versus clathrate melting temperature. Open circles represent late potassic alteration. Solid circles represent mineralization-silicification. Square represent phyllic alteration.

Figure 7-9 X_{CO2} in type 2 inclusions

        a) late potassic alteration

        b) mineralization-silicification

        c) phyllic alteration

Fig. 7-8
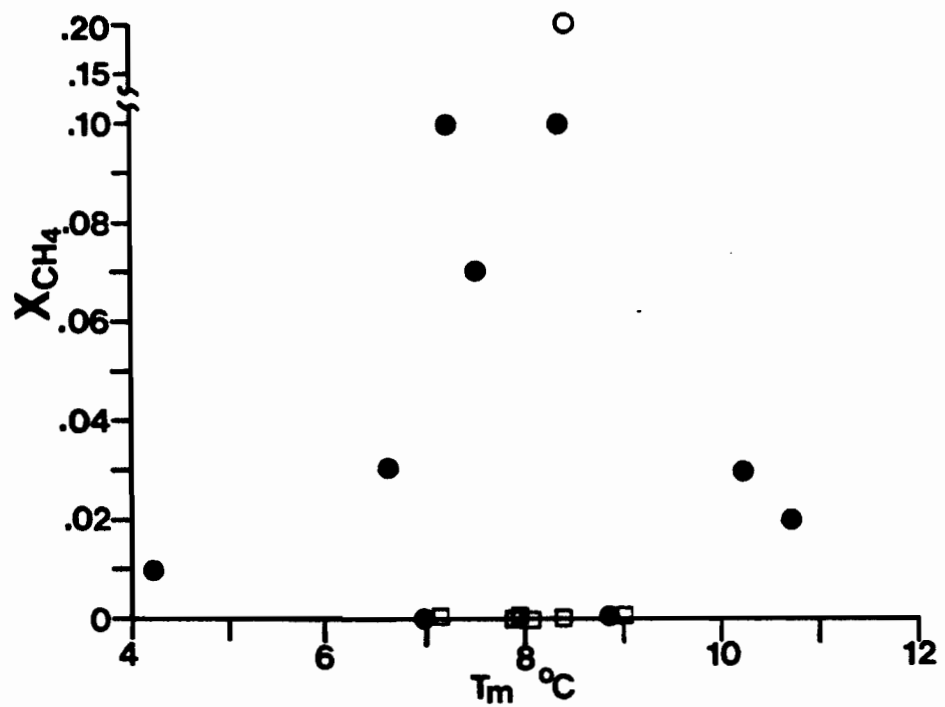
Fig. 7-9
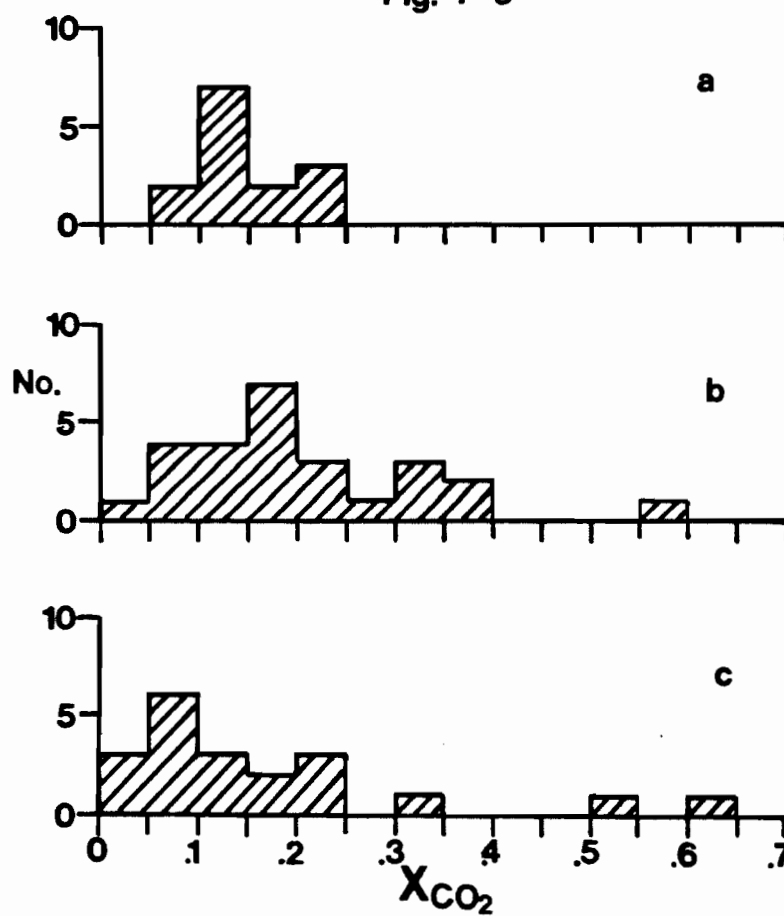
inclusions, there may be a compositional continuum between type 1 and type 2 inclusions. If such a continuum exists, it cannot be entirely explained by necking down, and a certain degree of fluid mixing is implied.

7.3.4 BULK DENSITIES

The density of the CO_2 phase for each type 2 inclusion was calculated using the method of Swanenberg (1979), as previously discussed. The density of the H_2O phase is less certain. From the ice melting temperatures of type 1 inclusions, and the clathrate melting temperatures of type 2 inclusions, the salinity range of inclusions trapped at Trout Lake is 2.0 to 15.0 wt. % NaCl. Therefore three different bulk densities were calculated for each pseudosecondary type 2 inclusion, assuming that 0.0, 6.0, and 12.0 wt. % NaCl is present in the H20 portion of the inclusion (Figures 7-10, 7-11, and 7-12 respectively). These salinities are convenient because they correspond approximately to the range of salinities observed in this study and to currently available P-T-XCO_2 data, to be discussed later, is availiable for these compositions. The densities of 0.0, 6.0, and 12.0 wt.% NaCl-H_2O solutions at 25 $^{\circ}C$ are 1.0, 1.040, and 1.084 g/cm^3 respectively (Potter and Brown, 1977). The density of the CO_2 phase was multiplied by the volume percentage of CO_2 in the inclusion, then added to the appropriate water density multiplied by the H_2O volume percentage at 25 $^{\circ}C$ to yield the inclusion bulk density.

For type 2 inclusions, containing 0.0 wt.% NaCl in the

Figures 7-10, 7-11, 7-12 Bulk densities of type 2
inclusions,calculated assuming 0, 6, and 12
wt. % NaCl in solution respectively.

    a) late potassic alteration

    b) mineralization-silicification

    c) phyllic alteration

Fig. 7-10
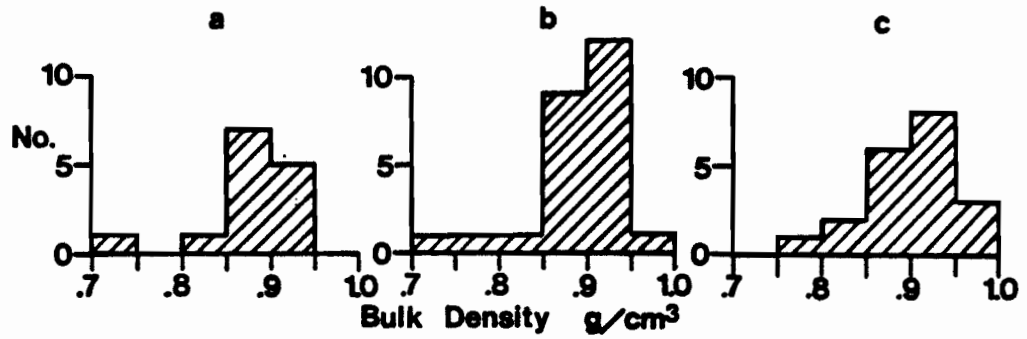
Fig. 7-11
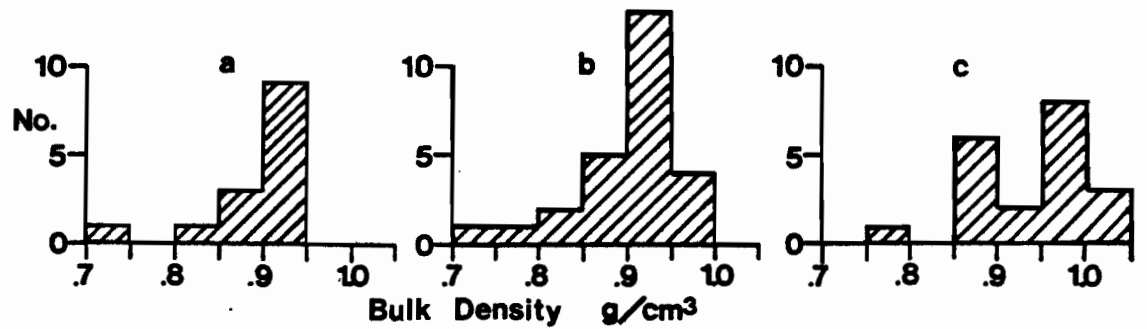
Fig. 7-12
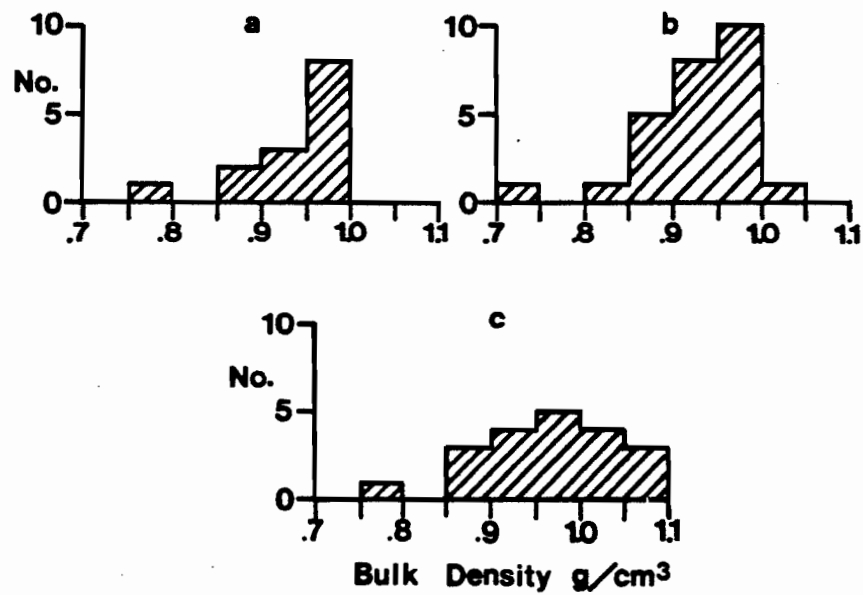
H_2O fraction (Fig. 7-10) the bulk density ranges from 0.70 to 1.00 g/cm^3, with a frequency maximum at 0.85 to 0.95 g/cm^3. At 6.0 wt. % NaCl (Fig. 7-11) the frequency maximum is between 0.90 and 1.00 g/cm^3. At 12 wt. % NaCl (Fig. 7-12) the frequency maximum is between 0.95 and 1.05 g/cm^3.

7.3.5 CO_2-H_2O HOMOGENIZATION AND DECREPITATION TEMPERATURES

The CO_2-H_2O homogenization and decrepitation temperatures of pseudosecondary type 2 inclusions are not presented graphically, but are listed in Appendix 5. Carbon dioxide-water homogenizations are rarely obtained. This is a result of the nature of the molar volume of carbon dioxide, which increases rapidly at temperatures above 250 ^{O}C (Malinin, 1974), causing brittle failure and decrepitation. However, when H_2O-CO_2 homogenizations are observed, the CO_2 bubble always shrinks and homogenizes into the water phase. Leroy (1979) demonstrated that internal pressures of up to 1200 bars are required to decrepitate 12 to 13 micron size inclusion in quartz, and up to 2700 bars for smaller inclusions. Therefore, if type 2 inclusions were trapped as homogeneous fluids, a minimum trapping pressure of approximately 1000 bars is implied. Inclusions near fractures were not analysed. However, quartz generally does contain fractures, which may cause decrepitation at lower internal pressures.

The molar volume of carbon dioxide reaches a maximum at approximately 450 ^{O}C (Malinin, 1974). Therefore if a subcritical H_2O-CO_2 fluid was trapped at a temperature lower than 450 ^{O}C, decrepitiation cannot be used to estimate

trapping pressures, as the inclusions may be heated to conditions above the trapping temperature and the internal pressure would exceed the trapping pressure. No homogenizations were observed in group 1 inclusions, but decrepitation temperatures ranged from 250 to 294 $^{\circ}$C. One homogenization was observed of a group 2 inclusions at 278 $^{\circ}$C. Decrepitation temperatures ranged from 220 to 300 $^{\circ}$C. Four homogenizations were observed in group 3 inclusions at 267, 278, 289, and 335 $^{\circ}$C. Decrepitation temperatures range from 240 to 280 $^{\circ}$C.

7.4   INTERPRETATIONS

Most of the histograms presented in this chapter display scatter, e.g. in H_2O/CO_2 ratios and H_2O homogenization temperatures. There are three explanations for the scatter: 1) Inclusions leaked after forming. This is possible, however inclusions near fractures were not analysed 2) The quartz trapped heterogeneous fluids while growing. 3) Inclusions necked down after forming. Inclusions with necking down textures were not analysed. Textural evidence of necking down is however, not always present. Roedder (1981) states that variable homogenization temperatures or H_2O/CO_2 ratios in otherwise similar inclusions is alternative evidence for necking down. The degree of variability in inclusion data will depend on whether the necking down process occurred before or after fluid immiscibility took place.

As necking down textures are common, it is considered that at least some of the scatter in histograms is due to

necking down. Useful information can be obtained from these inclusions in spite of the necking down. Roedder (1981) demonstrated that the homogenization temperature of an inclusion prior to necking down will be intermediate to the homogenization temperatures of the necked down parts of the original inclusion. The observed variability in this study of inclusion bulk density, XCO_2, and homogenization temperatures may therefore reflect this process. Fluid mixing between type 1 and type 2 inclusions may result in inclusions with an XCO_2 of less than 0.20, but cannot explain inclusions with an XCO_2 of greater than 0.20 (the maximum XCO_2 of the H_2O-CO_2 fluid). This must be a result of necking down or the trapping of immiscible fluids.

7.4.1 INTERPRETATIONS OF H_2O-CO_2-NaCl INCLUSIONS

The possible trapping pressures of fluids at Trout Lake are restricted to the conditions discussed in Chapter 2, 500 to 2000 bars. The majority of type 2 inclusions have an XCO_2 composition of 0.10 to 0.20. Using a maximum XCO_2 of 0.20, and a maximum pressure of 2000 bars, the maximum temperature of late potassic alteration is 425 °C (cf Chapter 3). Similarly the maximum temperature of phyllic alteration is 375 °C. Therefore the maximum trapping temperature of type 2 inclusions is 425 °C for group 1 samples, and 375 °C for group 3 samples.

It is necessary to examine phase diagrams for the appropriate systems, with the above restrictions, in order to determine whether the H_2O-CO_2 fluids at the Trout Lake deposit

were trapped at critical, subcritical, or supercritcal conditions, and at what temperature and pressure the trapping occurred. Figures 7-13 to 7-16 show phase relationships in P-T space for the H_2O-CO_2-NaCl system at various salinities, as calculated by Bowers and Helgeson (1983a). Homogenization temperatures of inclusions trapped at critical or supercritical conditions in a given system will lie along the solvus.

In the pure H_2O-CO_2 system (Fig. 7-13), a fluid with an XCO_2 between 0.1 and 0.2 will intersect the H_2O-CO_2 solvus at 200 to 300 °C for pressures between 500 and 2000 bars. This solvus is at too low a temperature to explain all the homogenization and decrepitation data. At 6.0 wt. % NaCl (Fig. 7-14) this fluid will intersect the solvus at 1000 to 2000 bars at a temperature of 250 to 400 °C (at lower pressures the solvus is intersected at too low a temperature to explain homogenization and decrepitation data). A 12.0 wt. % NaCl fluid (Fig.7-15), with the same P-T restrictions, will intersect the solvus between 1000 and 2000 bars, at 300 to 500 °C (at lower pressures the solvus is intersected at an unreasonable temperature). The solvus temperature at 1000 bars and XCO_2 of 0.20 is 500 °C, which is significantly higher than the interpreted maximum alteration temperature (425 °C). Lower solvus temperatures are obtained by increasing pressure and/or decreasing XCO_2. At 20 wt. % NaCl (Fig. 7-16) the solvus is at an unreasonably high temperature for supercritical trapping of fluids in the above range of pressure and XCO_2. It should be noted however that the

Figure 7-13 The H_2O-CO_2 system (from Bowers and Helgeson, 1983a).
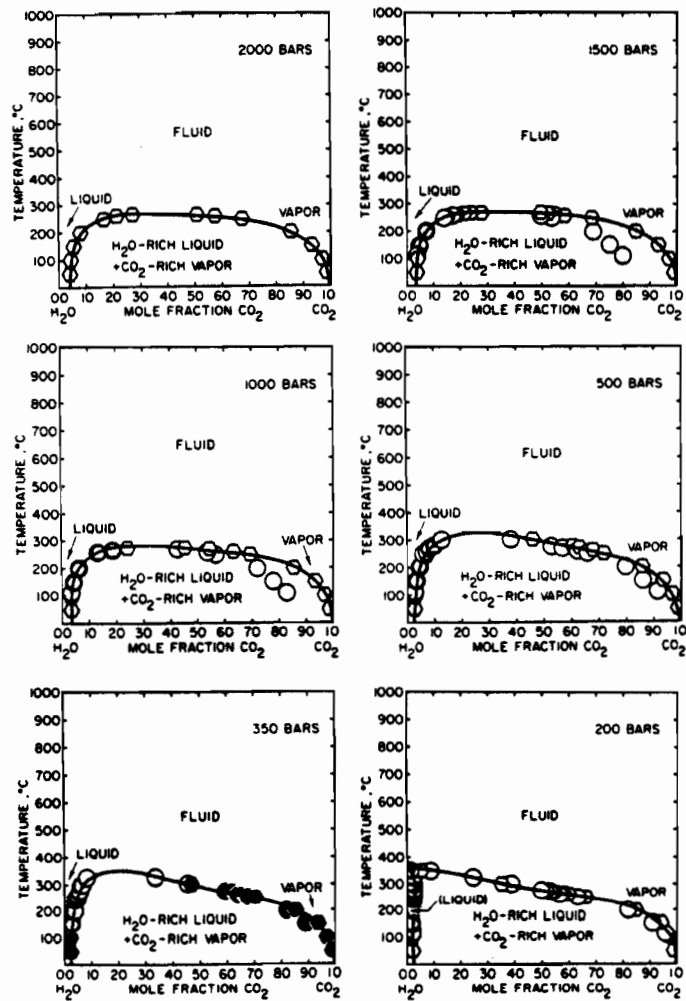
Figure 7-14   The H_2O-CO_2-NaCl (6 wt. %) system (from Bowers
and Helgeson, 1983a)
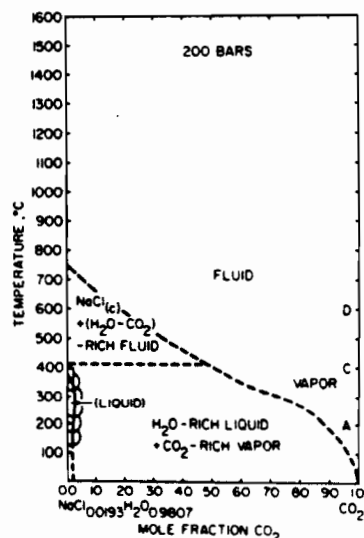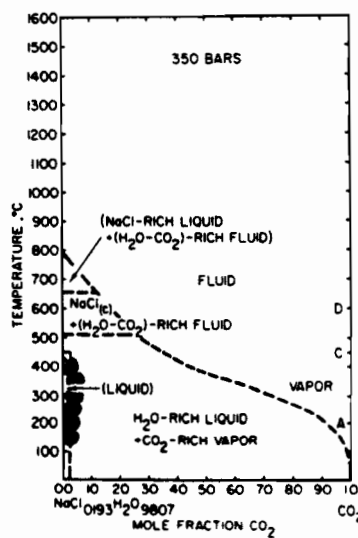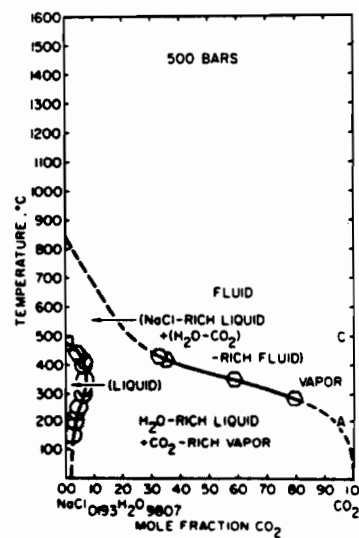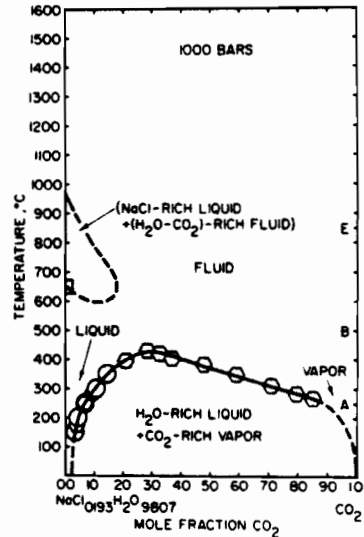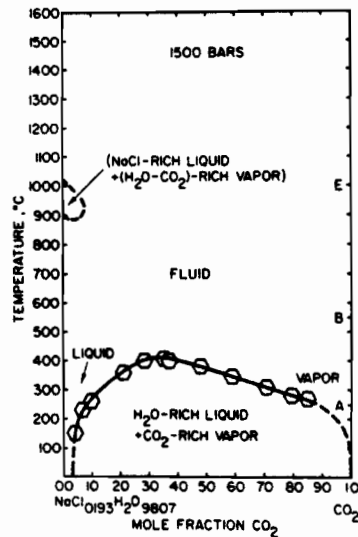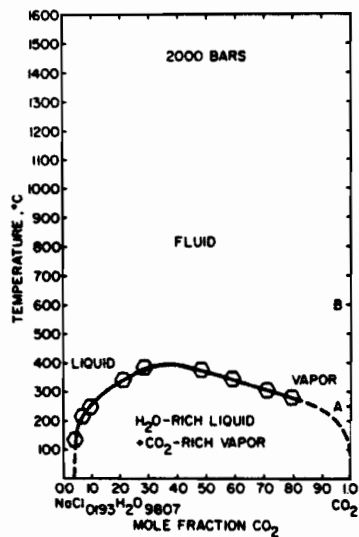
Figure 7-15   The H_2O-CO_2-NaCl (12 wt. %) system (from Bowers
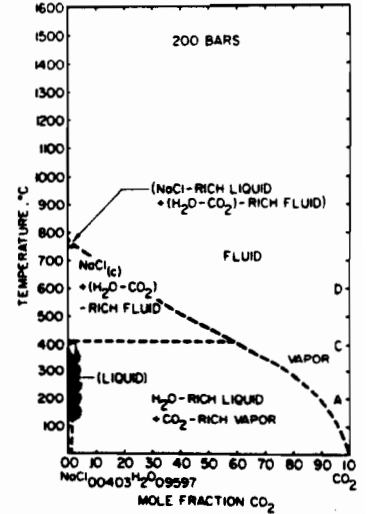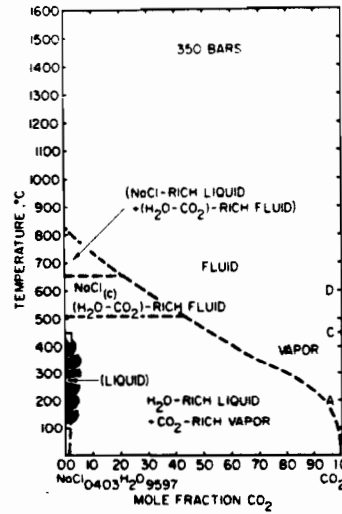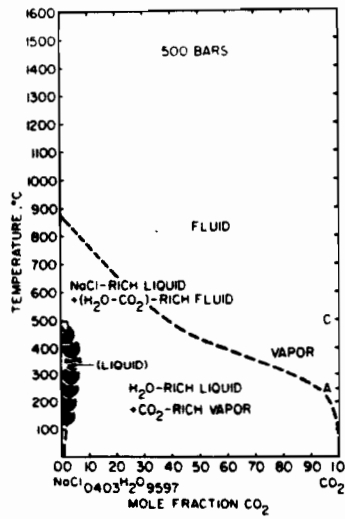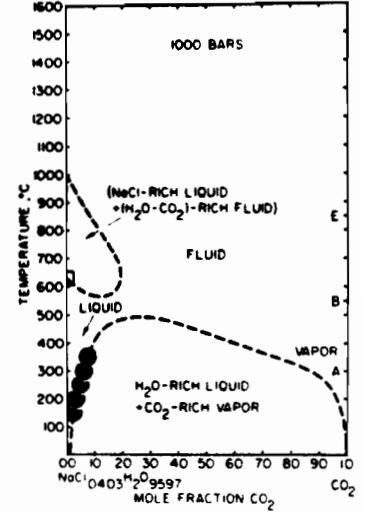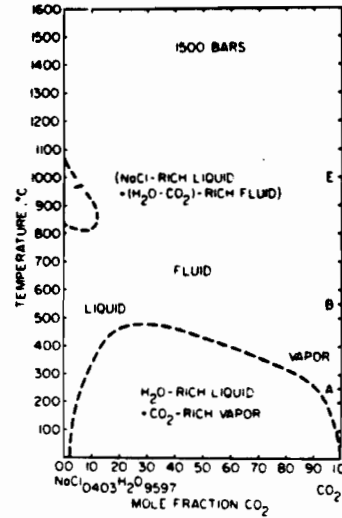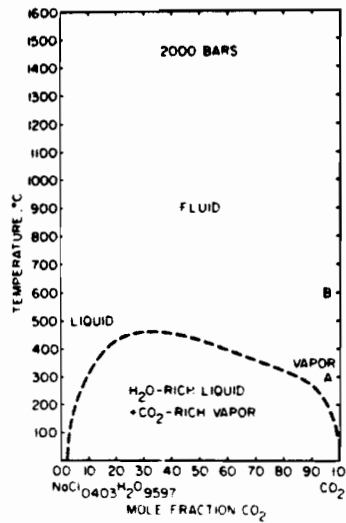
and Helgeson, 1983a)

Figure 7-16   The H_2O-CO_2-NaCl (20 wt. %) system (from Bowers and Helgeson, 1983a).
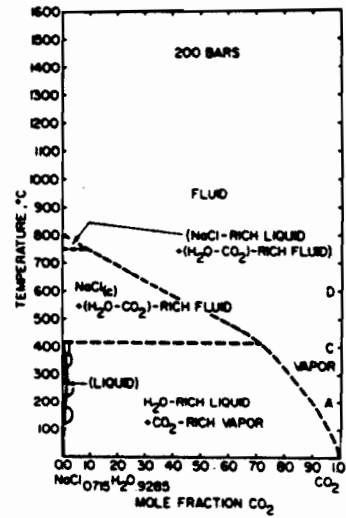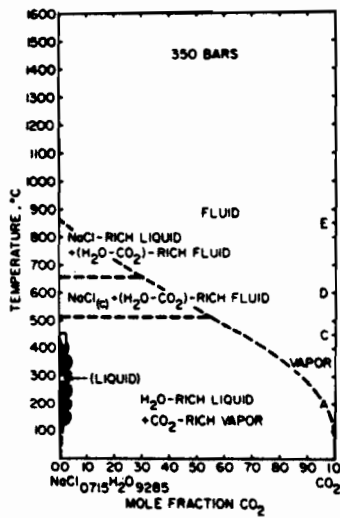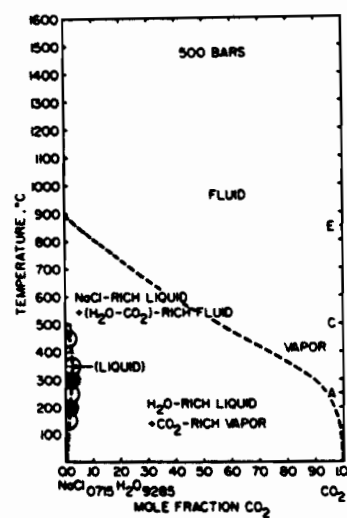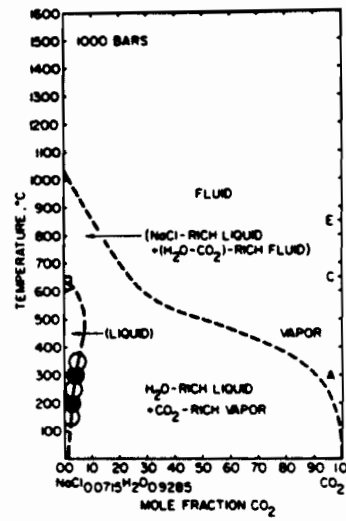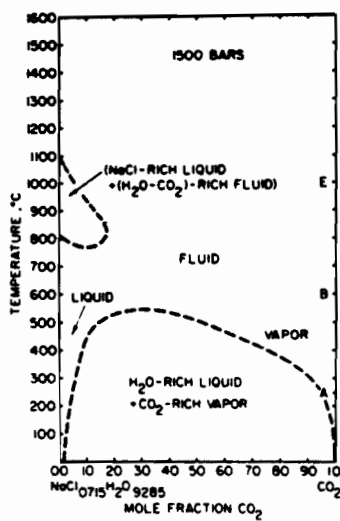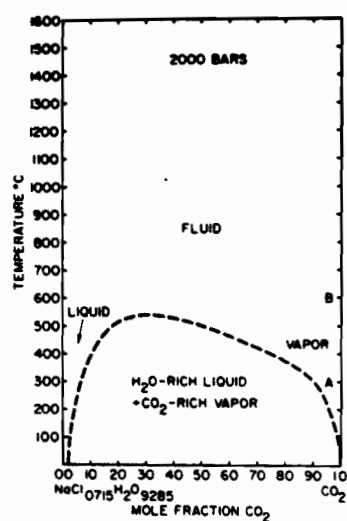
maximum salinity determined for any inclusion was 15wt.% NaCl equivalent.

It may be concluded that many of the inclusions may have formed supercritically, but that those having salinities at the high end of the computed range (2 to 15 wt. % NaCl equivalent) or at higher XCO_2 may be better explained by subcritical entrapment.

If inclusions were trapped under subcritical conditions the composition of the trapped inclusion would be dependent on the fluid flow rate, and the cohesive forces between the immiscible fluid droplets. Higher fluid flow rates result in greater mechanical mixing. If the immiscible droplets are infinitely small, the trapped fluids would be effectively homogeneous, whereas larger droplets that have coalesced will produced heterogeneous fluids. A discussion of the physical behavior of immiscible fluids is beyond the scope of this study. However it seem intuitively probable that the entrapment of subcritical fluids will result in widely varying inclusion compositions. If type 2 inclusions were trapped at subcritical conditions, a fluid with an XCO_2 composition of 0.10 to 0.20, would coexist with an immiscible fluid having an XCO_2 composition of 0.30 to 0.90 at the various possible pressures and salinities considered. Using the lever rule, it can be shown that only small quantities of CO_2-rich fluid would be produced at subcritical conditions for the lower salinity-XCO_2 combination of the above fluid composition (depending on how far below the solvus the subcritical conditions lie). Therefore the rarity of CO_2-rich inclusions

does not rule out the possibility that inclusions were trapped at subcritical conditions. Isochoric pressure-temperature diagrams for the system H_2O-CO_2-$NaCl$ (Fig. 7-17) from Bowers and Helgeson (1983a,b) can be used to furthur constrain the pressure and temperature of alteration and mineralization if the assumption is made that the fluid was trapped as a critical or supercritical phase.

At 0.0 wt. % NaCl, the isochores for the observed compositional range (0.85 to 0.95 g/cm^3) in type 2 inclusions intersect the two phase region at too low a temperature to explain the majority of homogenization and decrepitation temperatures. If an XCO_2 composition of 0.20 is used, the solvus is expanded, and the homogenization and decrepitation temperatures can be explained. At 6.0 wt. % NaCl the homogenization-decrepitation and bulk density data imply a minimum trapping pressure of 1000 to 2000 bars, and minimum trapping temperature of 270 to 380 ^oC. The solvus at 12 wt. % NaCl is slightly above most homogenization temperatures. However this diagram can explain the decrepitation temperatures, which are approximately 300 ^oC. Using the 12.0 wt.% NaCl diagram, the minimum trapping pressure is 1300 to 2000 bars, and minimum trapping temperature is 320 to 420 ^oC. Given a salinity of at least 6 wt. % NaCl equivalent, the H_2O-rich limb of the H_2O-CO_2 solvus is at XCO_2 compositions of less than 0.05 for pressures significantly lower than 1000 bars. Therefore group 1 and 2 inclusions formed at a minimum pressure of 1000 bars. Group 3 inclusions are less saline, and all pressures in the 500 to 2000 bar range must be

Figure 7-17   Isochores in the H_2O-CO_2 system at $XCO_2 = 0.1$ for 0 wt. % NaCl, 6 wt. % NaCl, and 12 wt. % NaCl (from Bowers and Helgeson, 1983b). Solid line represents the two-phase solvus at $XCO_2 = 0.2$ projected using data from Bowers and Helgeson (1983a).

E

$X_{CO_2} = 0.1$
$X_{NaCl} = 0.0$

LIQUID + VAPOR

F

$X_{CO_2} = 0.10$
$X_{NaCl} = 0.0193$

LIQUID + VAPOR

G

$X_{CO_2} = 0.1$
$X_{NaCl} = 0.0403$

LIQUID + VAPOR
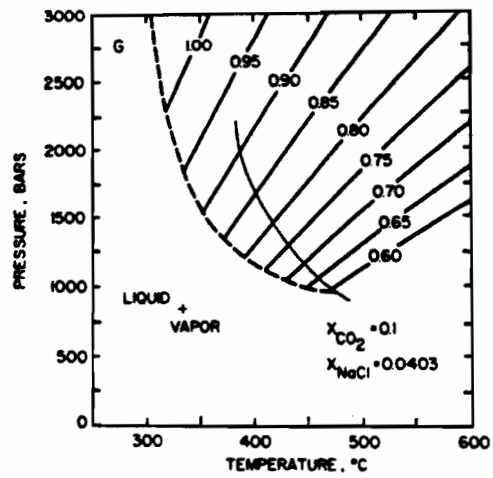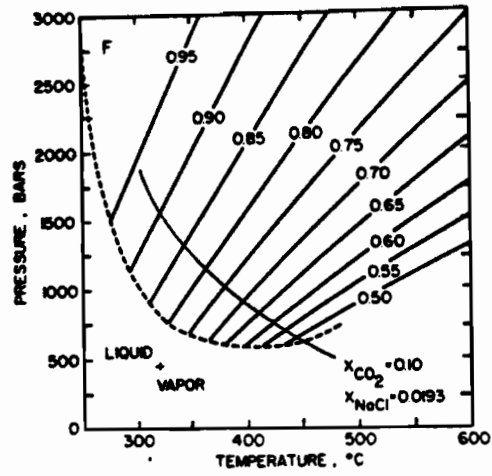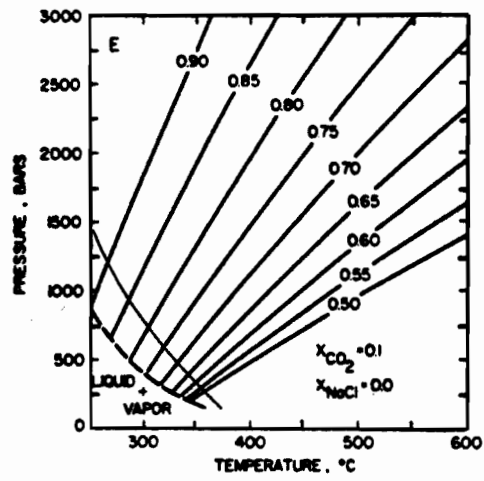
considered possible.

Using the interpretations from Chapter 3, phyllic alteration fluids were at a temperature lower than 375 ^{o}C. Clathrate melting temperatures indicate a lower salinity than the preceding alteration events, less than 6 wt. % NaCl equivalent. At an XCO_2 range of 0.10 to 0.20, and a salinity range of 0.0 to 6.0 wt. % NaCl equivalent, the phyllic alteration fluids could have been trapped either as a single phase or as immiscible fluids. If immiscible fluids were trapped, the H_2O-CO_2 homogenization temperature represents the maximum trapping temperature, whereas if supercritical fluids were trapped the homogenization is a minimum temperature. The lowest H_2O-CO_2 homogenization temperature observed is 267 ^{o}C. If this inclusion represents an immiscible fluid, the homogenization temperature is very close to the lowest temperature solvus that is possible. Therefore it represents the minimum trapping temperature, and thus phyllic alteration occurred at 267 to 375 ^{o}C. Using the 6 wt.% NaCl solvus, the minimum trapping pressure is 1000 bars, but lower trapping pressures are possible if the solutions were less saline.

Both salinity, and XCH_4 values are higher in the late potassic alteration and mineralizing fluids reltive to phyllic alteration fluids and, as previously discussed, probably reflect mixing. Mineral assemblage data from Chapter 3 indicate that these events occurred at higher temperatures than phyllic alteration, although lower than 425 ^{o}C. At temperatures greater than 267 ^{o}C (the minimum temperature of phyllic alteration), an XCO_2 of 0.10 to 0.20, bulk densities

of 0.85 to 1.00 g/cm^3, and salinities of 6.0 to 12.0 wt.% NaCl equivalent, the solvus conditions vary enough that the trapping of either a two-phase or single phase fluid is possible. However, if immiscible fluids were trapped at temperatures significantly below the solvus, much more compositional variation would be expected. Therefore if immiscible fluids were trapped, the fluids were nearly at critical conditions. As the phase equilibria are also consistent with the trapping of supercritical fluids, it is reasonable to conclude that the inclusions were trapped under critical or supercritical conditions. Many type 2 inclusions from groups 1 and 2 decrepitate at temperatures near 300 °C, and the sole homogenization of these groups of inclusions was at 278 °C. Therefore the minimum solvus temperature is approximately 300 °C. Using the phase equilibria in Figure 7-16, and the appropriate bulk densities, the minimum trapping pressure is 1000 bars.

7.4.2 INTERPRETATIONS OF H$_2$O-NaCl INCLUSIONS

Primary type 1 inclusions have widely varying liquid/vapour ratios, but a consistent salinity of 2 to 3 wt. % NaCl equivalent. Given a salinity of 2 to 3 wt. % NaCl equivalent, the critical pressure is approximately 200 bars (Holloway, 1981). Therefore the fluids must have been trapped supercritically. The necking down process must have occurred at some time after the formation of the deposit, during regional uplift, when the fluids were subcritical. In addition, these inclusions may have leaked during the necking

down processes, owing to the difference between the internal and external pressure. This would explain the widely varying homogenization temperatures, and assuming that it was liquid (not vapour) which leaked, explains why homogenization temperatures are higher in comparison to pseudosecondary type 1 inclusions.

Histograms of pseudosecondary type 1 inclusions display the greatest degree of scatter. The consistency of liquid/vapour ratios suggests that if necking down occurred, it was before vapour-liquid phase separation, and that no leakage occurred. Therefore necking down or leakage cannot explain the variation in homogenization temperatures. Either the H_2O-NaCl fluids were trapped at different temperatures, or were originally inhomogeneous. If type 1 inclusions were trapped at different temperatures, different histogram peaks would be expected. Although two temperature peaks are apparent on Figure 7-2, they are only fifty degrees apart, and the range of homogenization temperatures cannot be totally explained by different trapping temperatures. The homogenization temperature variation probably represents differences in CO_2 contents. The observation of double freezing temperatures suggests that some type 1 inclusions contain CO_2. Variable H_2O/CO_2 ratios in the vapour phase will result in different homogenization temperatures.

The majority of pseudosecondary type 1 inclusions homogenize between 180 and 260 $^{\circ}$C, and less commonly up to 310 $^{\circ}$C. Given that these fluids were trapped supercritically, and that CO_2 contents caused the variation in homogenization

temperatures, all homogenization temperature must be considered as possible minimum trapping temperatures, although 180 to 260 °C is the most probable range. Figure 7-18 is a P-T plot of phase and density relations in the H2O-NaCl system constructed using data from Haas (1976), Potter and Brown (1977), and Sourirajan and Kennedy (1962). Owing to the variation of possible salinities, isochores were constructed for fluids that range from 2.0 to 15.0 wt. %NaCl. Assuming that type 1 inclusions were trapped at 1000 to 2000 bars and that 425 °C is the maximum temperature, the trapping temperatures were 240 to 425 °C for inclusion that homogenized between 180 and 260 °C.

Using H_2O-NaCl isochores, and a homogenization temperature of 310 °C, the maximum temperature of 425 °C is intersected at approximately 1000 bars. Therefore the highest homogenization temperatures reflect a lower trapping pressure, or alternatively are anomalously high owing to processes which change homogenization temperatures, such as leakage, or volume change.

7.5 DISCUSSION AND SUMMARY

Two compositional types of inclusions have been identified: liquid-vapour H_2O (type 1), and H_2O-CO_2 (type 2). Some type 1 inclusions are interpreted to be primary, but these are rare. However, variable liquid/vapour ratios indicate that these inclusions have necked down at relatively low pressures, have probably leaked, and that homogenization temperatures therefore are not useful. The low salinities are

Figure 7-18   Isochores in the H_2O-NaCl system constructed using 0.5 (2.84 wt. %), 1.0 (5.52 wt. %), and 3.0 (14.92 wt. %) molal NaCl data from Haas (1976), Potter and Brown (1977), and Sourirajan and Kennedy (1962).
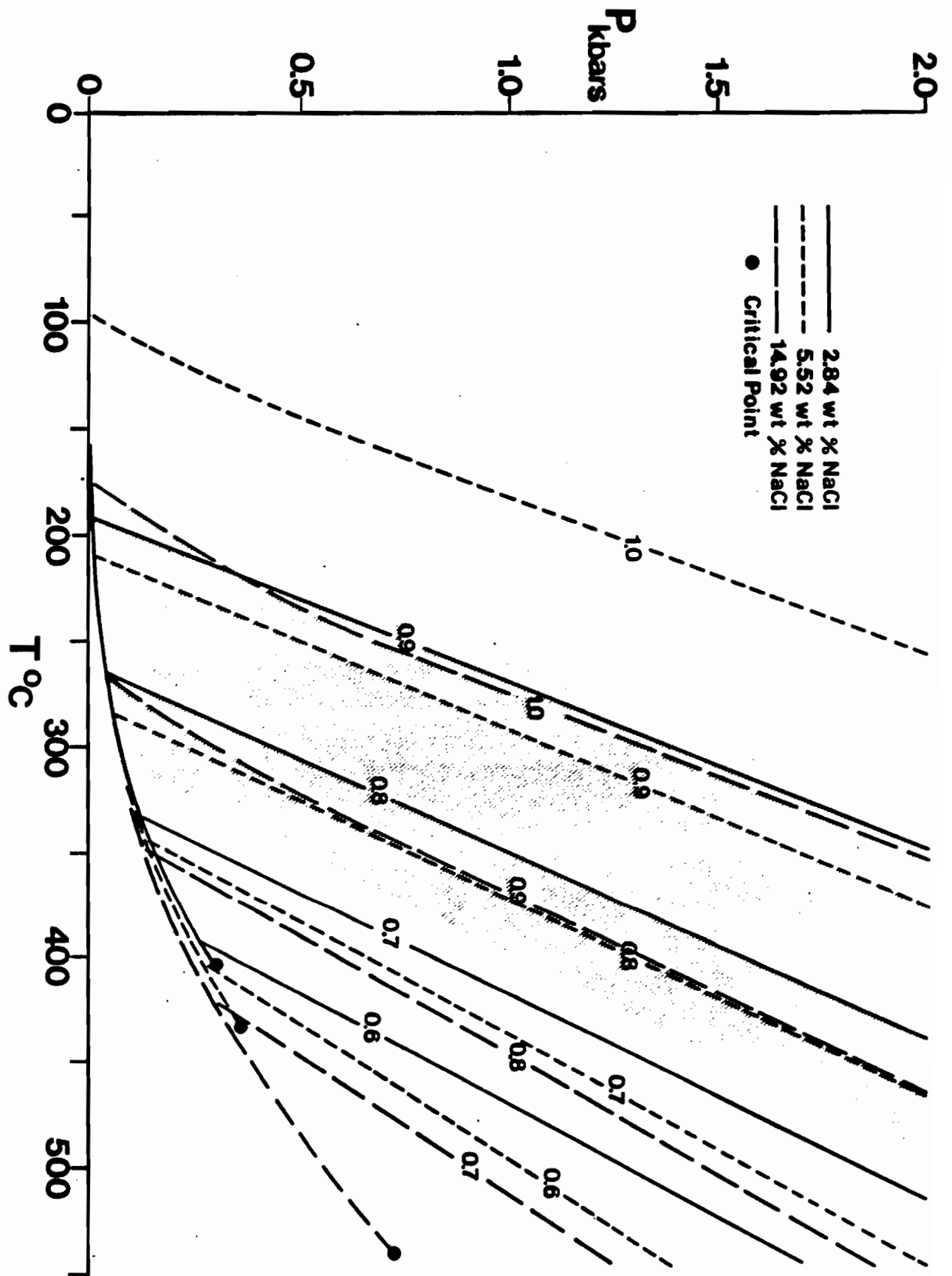
consistent with interpretations in Chapter 3 that late potassic alteration biotites interacted with hydrothermal solutions of low to moderate salinity.

Pseudosecondary and secondary inclusions of both compositional types have been identified. Histograms of microthermometric data contain significant scatter, and this scatter is attributed to necking down, or compositional variation. In spite of necking down or compositional variation, the following has been interpreted for the fluids that were present during late potassic alteration, mineralization, and phyllic alteration: 1) The confining pressure was 1000 to 2000 bars, although pressures as low as 500 bars are possible for phyllic alteration. 2) Mineral assemblage data from Chapter 3 place restrictions on the maximum temperature. Therefore the fluids were at a temperature of 250 to 425 ^{o}C. 3) Fluid salinities were 2.0 to 15.0, and more probably 6.0 to 12.0 wt. % NaCl for late potassic alteration and mineralization, and less than 6.0 wt. % NaCl for phyllic alteration 4) The XCO_2 values of type 2 inclusions are 0.10 to 0.20.

The origin of type 1 inclusions is debatable. Phase equilibria diagrams (Figs. 7-13 to 7-16) demonstrate that an H_2O-rich fluid cannot coexist stably with fluids of 0.10 to 0.20 XCO_2 compositions. In group 1 samples, type 1 inclusions commonly occur in areas devoid of type 2 inclusions. If necking down of type 2 inclusions had produced type 1 inclusions then some type 2 inclusions would be expected near type 1 inclusions. Therefore necking down cannot explain

the formation of type 1 inclusions. The fact that group 1 samples contain mainly type 1 inclusions, group 2 contain mainly type 2 inclusions, and group 3 contain only type 2 inclusions suggests fluid mixing. This is consistent with the early fluids being H_2O-rich, and later fluids having moderate CO_2 contents, as interpreted in Chapter 3.

If mixing occurred, type 1 inclusions should contain variable CO_2 contents. Analysis of CO_2 contents in type 1 inclusions, such as by Raman spectroscopy, is necessary to determine whether mixing occurred, i.e. variable CO_2 contents indicate mixing. Both types of inclusions are present in certain samples, or even certain quartz grains. Therefore if mixing did not occur, it is implied that different inclusion types formed at different times, for which there is no textural evidence. Homogenization and phase equilibria data suggest that type 1 and 2 inclusions were trapped at a similar temperature, assuming a similar trapping pressure.

Group 1 and 2 inclusions contain significant methane, whereas group 3 inclusions are methane free. Clathrate melting and XCH_4 data (Fig. 7-8) indicate that group 2 (and possible group 1) inclusions are more saline than group 3 inclusions. The addition of salts and/or methane to the H_2O-CO_2 system expands the two-phase solvus. If inclusions were trapped as supercritical fluids, it is possible that group 1 and 2 inclusions were trapped at higher pressures and temperatures than group 3 inclusions, owing to the different solvus conditions for the different fluids. Although it cannot be conclusively determined whether type 2 inclusions

formed under super or subcritical conditions, critical to supercritical conditions are favoured.

A minimum trapping pressure of 1000 bars is interpreted for potassic alteration and mineralization, whereas lower pressures are possible for phyllic alteration. Unfortunately, fluid inclusions are not particularly useful in constraining the temperature. The possible temperature range for the late potassic and phyllic alteration and mineralization events is 250 to 425 ^oC. The following model is proposed to explain the mineralogical (from Chapter 3) and fluid inclusion data: 1) Initially, during contact metamoprhism and skarn alteration, the fluid was H_2O-rich, supercritical, at pressures of 1000 to 2000 bars, and temperatures of 350 to 425 ^oC. 2) Mixing of supercritical H_2O-rich (dominant) and H_2O-CO_2 (subordinate) fluids occurred during late potassic alteration at similar pressures, and similar or lower temperatures than skarn formation. 3) Mixing of supercritical H_2O-rich (subordinate) and H_2O-CO_2 (dominant) fluids occurred during mineralization at pressures and temperatures similar to late potassic alteration. 4) A lower temperature and possibly lower pressure supercritical H_2O-CO_2 fluid was present during phyllic alteration.

CHAPTER 8: EVOLUTION OF THE DEPOSIT

Molybdenum mineralization at the Trout Lake deposit is spatially associated with the Trout Lake Stock. More specifically the mineralization is associated with small neck-like multiphase stocks which are adjacent to the main granodiorite body. Crosscutting relationships indicate that molybdenum mineralization both pre- and post-dates the emplacement of these small neck-like multiphase stocks. The following sequence of thermal events has been established: contact metamorphism, followed by skarn, potassic, silicic, and phyllic alteration. Molybdenum mineralization is associated with silicic alteration although minor molybdenite is present with other alteration types. The small neck-like multiphase stocks were emplaced prior to pervasive silicification and probably after potassic alteration (as they are not affected by potassic alteration). Therefore the evolution of the deposit can be grouped into three major episodes: 1) contact metamorphism and early alteration (skarn and potassic); 2) mineralization and silicic alteration; 3) late (phyllic) alteration.

8.1 CONTACT METAMORPHISM AND EARLY ALTERATION

Mineral assemblages in calcareous pelites surrounding the Trout Lake Stock define a contact metamorphic aureole. The distribution of isograds and mineral stability data indicate that heat transfer was advective, that the fluid composition was H_2O-rich (XCO_2 less than 0.05), and that the temperature

was approximately 400 $^{\circ}$C. The fluid composition and temperature is based on the assumption that contact metamorphism occurred at a lithostatic pressure of 2000 bars. Lithostatic and hydrostatic pressure have been estimated elsewhere within the region by previous studies.

The lateral extent of the isograds indicate that contact metamorphism must have resulted from the emplacement of a larger, and presumably parental, magma at depth. The lack of chill margins in the Trout Lake Stock (or contact hornfels) indicate that it was possibly emplaced into pre-heated rock (i.e. the contact aureole was developed around a "pluton at depth" prior to the emplacement of the Trout Lake Stock). The small neck-like multiphase stocks were intramineralization in timing, and were therefore emplaced after the contact aureole formed.

Skarn alteration assemblages overprint contact metamorphic rocks. However, the composition and probably the temperature of the skarn-forming fluids is similar to the contact metamorphic fluids. Biotite replacement of tremolite indicates that potassic alteration post-dates skarn formation. Biotite-calcite alteration is considered to be pervasive potassic alteration. A low fluid/rock ratio during biotite-calcite alteration is indicated by the chemical compositions of biotite, which appear to have been controlled by the rock, and the preservation of An_{30} plagioclase. The biotite-calcite mineral assemblages indicate that the XCO_2 of the coexisting fluid was higher than during contact metamorphism, at approximately 0.20 in calcareous horizons. This is probably

the result of mineral reactions controlling fluid composition, which is consistent with low fluid/rock ratios. Mineral stabilities in $T-XCO_2$ space indicate that the temperature was similar to contact metamorphism, at approximately 400 °C.

Biotite-calcite alteration is overprinted by late potassic alteration, characterized by biotite haloes around quartz-albite veins. The iron-magnesium compositions of late potassic alteration biotites appear to have been controlled by the fluid, suggesting that the fluid/rock ratio was relatively high. The overprinting of biotite-calcite alteration by biotite haloes does not necessarily imply that these are separate temporal events. The former event may reflect a low degree of infiltration and mineral reactions buffering fluid composition, with the latter event the result of higher fluid/rock ratios. However, the stability relations of biotite + calcite + quartz at water-rich conditions and the dominance of H_2O-rich fluid inclusions in late potassic alteration quartz veins (indicating a low XCO_2), suggest that late potassic occurred at temperatures lower than biotite-calcite alteration.

Fluid inclusions from quartz veins associated with late potassic alteration are dominantly of low to moderate salinity and H_2O-rich, with a subordinate H_2O-CO_2 population. These two compositions could not have resulted from the immiscible separation of a single fluid. There is no textural evidence to support their having been trapped at different times, nor, owing to the distribution of inclusion types, can they be explained by a necking down process. Therefore the two types

of inclusions probably represent fluid mixing, and the proportions of H_2O-rich (dominant), and H_2O-CO_2 (subordinate) inclusions reflect the ratio of the two fluids in the mixture.

In summary, the contact metamorphic to biotite-calcite alteration stages probably all occurred at a similar temperature. Low XCO_2 contents in the contact metamorphic and skarn fluid are interpreted to be the result of an external control of fluid composition. Higher XCO_2 contents in the biotite-calcite alteration fluids are interpreted to be the result of mineral reactions controlling fluid composition. Late potassic alteration probably occurred at a lower temperature and XCO_2 than biotite-calcite alteration.

8.2 MINERALIZATION AND SILICIC ALTERATION

The bulk of the molybdenum mineralization formed between the late potassic and phyllic alteration events. Molybdenite is generally present within quartz veins, or within zones of pervasive silicification. With both styles, there is a strong association between molybdenite and alkali feldspars (dominantly albite). Molybdenite is typically intergrown with muscovite and/or calcite at alkali feldspar grain boundaries. In addition, pervasively silicified granodiorite and quartz diorite have higher contents of molybdenite than metasedimentary hosts. This is probably due to the combined effect of higher alkali feldspar contents, and higher fluid/rock ratios. The presence of sphene in silicified rocks suggests that the temperature was higher and/or XCO_2 was lower than during phyllic alteration, where

rutile + ankerite + quartz was stable.

Consider now the nature of a cooling hydrothermal fluid. At high temperatures, above approximately 200 ^{o}C, salts are not completely dissociated, e.g. as an HCl solution cools from 400 to 300 ^{o}C, the lower temperature results in greater dissociation and higher hydrogen and chloride ion activities (Helgeson, 1969). However, different salts have different dissociation constants. Potassium chloride is more dissociated than sodium chloride at temperatures less than 350 ^{o}C (Helgeson, 1969). Hydrochloric acid is more strongly associated than either KCl or NaCl at temperatures less than 350 ^{o}C (Helgeson, 1969). Therefore if a fluid in the isobaric closed system H2O-KCl-NaCl-HCl was cooled from 400 to 300 ^{o}C, the activities of potassium, sodium, hydrogen, and chlorine ions would all increase, and the K^{+}/Na^{+} and K^{+}/H^{+} activity ratios would increase.

The stability of muscovite and K-feldspar in contact metamorphic rocks and all stages of alteration is evidence that the K^{+}/H^{+} activity ratio increased over time (decreasing temperature). The stability of albite and K-feldspar in all stages of alteration indicates that the K^{+}/Na^{+} ratio decreased over time (if temperature decreased after late potassic alteration), the opposite of a dissociation controlled evolution. However, the K^{+}/Na^{+} activity ratio is not controlled soley by the dissociation of salts. It is likey that the K-Na exchange which occurred during sericitization of albite, or K depletion caused by muscovite precipitation resulted in a decrease of the K^{+}/Na^{+} activity ratio over time.

The following can be stated about the nature of molybdenum in aqueous solutions: 1) molybdate complexes have a solubility of several thousand ppm (dominantly as $HMoO_4^-$) in slighty acidic solutions at 350 $^\circ$C, and that the solubility is approximately 10^6 times lower at 300 $^\circ$C (Smith et al., 1980). 2) fluorine can complex with molybdenite, but the solubilities are much lower than molybdate complexes (Smith et al., 1980). The hydrothermal fluids at Trout Lake are interpreted to have had a relatively low fluorine activity, therefore fluorine is not to be considered an important complexing agent in the Trout Lake mineralizing fluids. 3) chlorine and sulphur complexes of molybdenum are not important at geologically reasonable conditions (Smith et al.,1980). 4) at room temperature, the solubility of K_2MoO_4 is approximately four times greater than Na_2MoO_4 (Dean and Wilkinson, 1983). 4) the solubility of molybdenite decreases with increasing acidity (Kolonin et al.,1975). Therefore, molybdate complexes were probably responsible for the transportation of molybdenum in the solutions which formed the Trout Lake deposit. Decreasing temperature, decreasing K^+/Na^+ activity ratios, and increasing acidity each favour the precipitation of molybdenite, and all are interpreted as having occurred during the evolution of the hydrothermal fluids at the Trout Lake deposit.

The textural relationships between molybdenite, muscovite-calcite, and alkali feldspars must be explained in order to propose a mechanism for molydenite precipitation. Consider the fluid-mineral reactions that occurred at an albite grain boundary. Hydrogen ions were locally consumed,

and K-Na exchange occurred during the sericitization of albite. Molybdenum, if complexed as a molybdate, must have been reduced from a +6 to a +4 valence in order to precipitate as molybdenite, which also involves the consumption of hydrogen. Possible half-reactions for molybdenite precipitation are written below.

e.g. $3 H^+ + HMoO_4^- + 2 H_2S(aq) + 2 e^- = MoS_2 + 4 H_2O$

or $5 H^+ + HMoO_4^- + 2 HS^- + 2 e^- = MoS_2 + 4 H_2O$
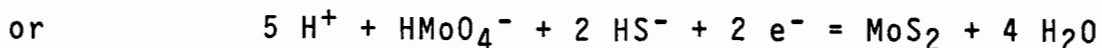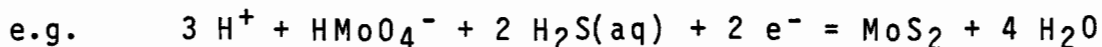
The precipitation of calcite (intergrown with molybdenite) may have resulted from the locally lowered hydrogen ion activity, i.e. this promotes the decoupling of carbonate complexes. If temperature drop was the only cause of molybdenite precipitation, an association between molybdenite and muscovite-calcite would not have occurred, unless the saturation temperature of these minerals was reached synchronously. If increasing acidity caused molybdenite precipitation, intergrowths with muscovite would not be expected, as the local environment around the precipitating molybdenite would be depleted with respect to hydrogen ions. However, if the pH was externally controlled and the hydrogen ion diffusion was fast enough, the pH of the local precipitation environment would not be different from the surrounding hydrothermal fluids. Although the precipitation of molybdenite was probably due to a combination of several factors, textural relationships indicate that K-Na exchange in the local precipitation enviroment may have been a significant factor. The above half-reactions of molybdenite precipitation and a reaction for the sericitization of albite

can be combined to give possible mechanisms for the precipitation of molybdenite at the Trout Lake deposit. Electrons produced by the reduction of Mo^{+6} are consumed by oxygen to produce O_2.

e.g. $3 NaAlSi_3O_8 + HMoO_4^- + K^+ + 3 H^+ + 2 H_2S (aq) =$

$KAl_3Si_3O_{10}(OH)_2 + MoS_2 + 6 SiO_2 + 3 Na^+ + 3 H_2O + 0.5 O_2$

or $3 NaAlSi_3O_8 + HMoO_4^- + K^+ + 5 H^+ + 2 HS^- =$

$KAl_3Si_3O_{10}(OH)_2 + MoS_2 + 6 SiO_2 + 3 Na^+ + 3 H_2O + 0.5 O_2$
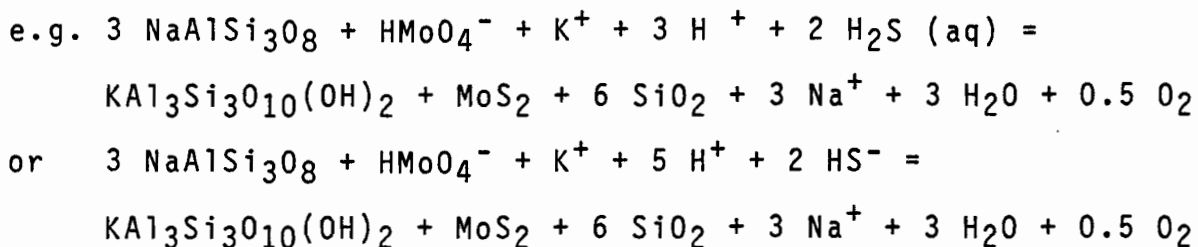
The above argument is based on the tendancies of reactions in simple systems. Computer modelling in the proper multicomponent system (e.g. Brimhall, 1980) is necessary to prove whether these reactions are possible for the fluid conditions of the Trout Lake deposit.

8.3 LATE ALTERATION

Phyllic alteration post-dates mineralization and is characterized by muscovite + ankerite + pyrite. The stability of rutile + quartz + ankerite + K-feldspar indicates that phyllic alteration occurred at higher XCO_2 and/or lower temperature than the preceding events. Muscovite primarily replaced biotite rather than feldspars. This may be a consequence of higher chlorine activity, the result of salt dissociation at lower temperatures. Higher chlorine activity may have caused iron and magnesium to be leached from biotite, leaving residual muscovite.

Another possible biotite breakdown reaction is related to an increase in sulphur fugacity:

annite $+ 3 S_2 =$ orthoclase $+ 3$ pyrite $+ H_2O + 1.5 O_2$
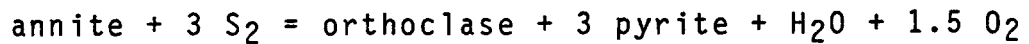
The lack of pyrrhotite and abundance of pyrite may indicate a higher sulphur fugacity during phyllic alteration than previous alteration. Stoichiometric aluminum in Trout Lake biotite is greater than 1.0 (i.e. they have a siderophyllite component). Therefore, owing to the high aluminum activity, muscovite rather than orthoclase-pyrite replacement of biotite could have occurred. At some locations up to 10 % modal K-feldspar accompanies phyllic alteration, indicating that orthoclase-pyrite replacement of biotite may also have occurred. However the above explanation does not take into account the activity of iron and magnesium activities in solution, one of the variables controlling biotite stability. Therefore, if the replacement of biotite is to be explained, both the above processes must be combined to calculate the stability field of biotite in a multicomponent system. This type of chemical modelling is beyond the scope of this study.

Frost (1979) demonstrated that the XCH_4 present in a C-O-H fluid is highly dependant upon oxygen fugacity. At fixed hydrogen and oxygen fugacities XCH_4 increases as temperature decreases (Eugster and Skippen, 1967). The H_2O-CO_2 fluid inclusions from the late potassic alteration and mineralization stages contain signifcant amounts of methane, but negligible methane is present in fluid inclusions from the phyllic alteration stage. As phyllic alteration did not occur at higher temperature, the low XCH_4 contents of inclusions from this stage reflect a higher oxygen fugacity.

Fluid inclusion evidence suggests that there was mixing

of H_2O-rich and H_2O-CO_2 fluids during the emplacement of the deposit. If the H_2O-rich fluid had a relatively low oxygen fugacity, and the H_2O-CO_2 fluid had a relatively high oxygen fugacity, then conceivably, during mixing the two fluids diffusion of oxygen between fluids occurred (the fluids could not have mixed totally otherwise only one inclusion type would have been trapped), resulting in the lowering of the oxygen fugacity in the H_2O-CO_2 fluid. During phyllic alteration a single H_2O-CO_2 fluid was present, therefore the oxygen fugacity remained high. Alternatively, the higher oxygen fugacity in phyllic alteration may have resulted from wallrock interaction. However, the pervasive nature, and fault controlled distribution of phyllic alteration suggests high fluid/rock ratios, which is inconsistent with the rock controlled the fluid composition.

8.4 GENETIC MODELS

Fluid inclusion evidence from the late potassic to phyllic alteration stages indicates that there was a progressive CO_2 enrichment in the hydrothermal fluids due to the mixing of an early H_2O-rich fluid with a later H_2O-CO_2 fluid. Contact metamorphic and skarn mineralogy reflect equilibration with an H_2O-rich fluid. Fluid inclusion and mineral stability data indicate that phyllic alteration is a consequence of an interaction with an H_2O-CO_2 fluid. Based on fluid inclusion evidence, late potassic alteration and silicification-mineralization formed from a mixed H_2O-rich and H_2O-CO_2 fluid. The relative abundance of the two types of

fluid inclusions in these alteration types is consistent with progressive CO_2 enrichment in the fluid mixture with time. A temperature decrease is interpreted to have occurred between contact metamorphism-skarn formation and late potassic alteration. Temperature-XCO_2 relationships in the hydrothermal fluids which followed are less certain.

Two models are proposed to explain the fluid evolution from the late potassic to phyllic alteration stages. 1) The temperature decreased between biotite-calcite and late potassic alteration, then XCO_2 increased by isothermal fluid mixing. In this model late potassic alteration minerals interacted with an H_2O-rich fluid mixture which, considering the stability of biotite + calcite + quartz, suggests a temperature maximum of 350 °C (assuming XCO_2 was less than 0.10). Silicic and phyllic alteration can be explained by an increase in XCO_2, as the fluid mixing proceeded toward a single H_2O-CO_2 fluid. 2) Temperature decreased and XCO_2 increased synchronously after biotite-calcite alteration. In this model the late potassic alteration minerals must have equilibrated with a higher XCO_2 fluid in comparison to the XCO_2 required in the first model. The fluid composition would be a mixture of H_2O-rich infiltrating fluids and CO_2-rich fluids produced by mineral reactions. Silicic and phyllic alteration are the result of decreasing temperature and increasing XCO_2 until a single H_2O-CO_2 fluid was present (phyllic alteration).

8.5 TECTONICS AND METALLOGENY

The similarity of vein orientations between the Trout Lake deposit and vein-type base and precious metal deposits in the surrounding area indicate that the fractures, in which the veins formed, developed as a result of similar stresses. This suggests that the emplacement of the Trout Lake Stock did not significantly alter the regional stress field. The orientation of veins, and the interpretation from vein textures that they filled open spaces, suggests that the Trout Lake deposit formed under tensile conditions.

Mathews (1983) proposed that, in the Kootenay Arc to the south, a Late Cretaceous to Early Tertiary non-penetrative thermal event reset potassium and argon isotopes in potassic minerals. Ohmoto and Rye (1970) suggest an early Tertiary age for the formation of the Bluebell lead-zinc deposit, also in the southern Kootenay Arc, which is similar to the lead-zinc deposits in the Trout Lake area. Considering the above, two explanations for the mineralization observed in the deposit and surrounding area are proposed. The Trout Lake deposit could have formed in the mid-Cretaceous (the age of many other granodiorites in the region), pre-dating the base and precious metal event, implying therefore that the K-Ar date of 76 Ma by Boyle and Leitch (1983, p.117) is due to partial resetting by the Tertiary thermal event. The second possibility is that molybdenum and lead-zinc mineralization are associated with the same Late Cretaceous event and reflect deeper and shallower levels of emplacement respectively. The second hypothesis seems more likely owing to the apparent genetic

relationships between the Trout Lake, Copper Chief, and Lucky Boy deposits. This metallogenic event may have been continuous from the Late Cretaceous to the Early Tertiary Periods. Furthur dating of the mineralization and alteration at these deposits is needed to clarify the timing of molybdenum and base metal deposition.

CHAPTER 9:   CONCLUSIONS

The Trout Lake stockwork molybdenum deposit is spatially associated with a small Late Cretaceous (76 Ma.) granodiorite-quartz diorite stock. The stock intruded the Lardeau Group of metasediments, which had previously been affected by Jurassic regional metamorphism and deformation. Contact metamorphic aureoles are present around the Trout Lake Stock, and a small quartz diorite dyke southwest of the Trout Lake Stock. The distribution and extent of the isograds indicate that contact metamorphism must have resulted from the intrusion of a larger pluton at depth, and that heat transfer was advective. The fluids involved in contact metamorphism had a temperature of 360 to 400 $^\circ$C, and an XCO_2 of less than 0.05, assuming lithostatic pressure (2000 bars).

Skarn deposits are developed peripheral to the Trout Lake deposit, and are localized at the intersection of faults with limestone. Prograde and retrograde skarn assemblages have been distinguished. Assuming a pressure at 1000 to 2000 bars, prograde skarn formation occurred at a maximum temperature of 450 to 500 $^\circ$C, and at an XCO_2 less than 0.03. The retrograde skarn formed at a maximum temperature of 390 to 410 $^\circ$C, and at an XCO_2 of less than 0.02 assuming a pressure of 1000 and 2000 bars respectively. The fluid composition is similar to that present during contact metamorphism. Skarn formation at least in part post-dates contact metamorphism, and pre-dates potassic alteration. Skarn is interpreted to have formed at approximately 400 $^\circ$C as the preceeding and subsequent events

were at this temperature.

Biotite-calcite (pervasive potassic) alteration follows skarn in the sequence of geological events. Calc-silicate reactions in T-XCO2 space, and the stability of corundum and plagioclase indicate that the temperature was approximately 400 ^{o}C, and that the XCO_2 was approximately 0.20. Fluid and biotite compositions in this alteration stage were controlled by the bulk chemistry of the rock.

Late potassic alteration probably post-dates biotite-calcite alteration. Fluid inclusions from quartz veins associated with potassic alteration are dominantly H_2O-rich, with a subordinate population of H_2O-CO_2 inclusions. Microthermometric observations indicate an XCO_2 of 0.10 to 0.20 in the H_2O-CO_2 inclusions. It is interpreted that these two fluids mixed. All fluid inclusions were most likely trapped as supercritical fluids. The possibility that the fluids were subcritical cannot be ruled out. However, they could not have been trapped at conditions significantly below the two-phase solvus. Homogenization and decrepitation temperatures, combined with phase equilibria in the H_2O-CO_2-NaCl system indicate that potassic alteration fluids were at a pressure of 1000 to 2000 bars, a temperature of 250 to 425 ^{o}C, and a salinity of 2 to 15 (and most likely greater than 6) wt. % NaCl equivalent. The extrapolation of densities of H_2O-rich inclusions along the appropriate isochores indicates a similar trapping temperature range assuming the same range of trapping pressures. The observed mineral assemblages restrict the temperature to 360 to 425 ^{o}C if the CO_2 range was 0.10 to

0.20. At these conditions late potassic alteration could have been synchronous with biotite-calcite alteration, and would represent a higher degree of infiltration. However, the fluid inclusion evidence from late potassic alteration suggests that the bulk composition of this fluid mixture was H_2O-rich, probably at an XCO_2 less than 0.10. The H_2O-rich composition of the late potassic alteration fluid and the stability relations of the alteration assemblage suggest that this event occurred at a a lower temperature than biotite-calcite alteration.

Biotite compositions from late potassic alteration suggest that they were strongly influenced by the chemical composition of the hydrothermal fluids, which were of low to moderate salinity. Additionally, biotite compositions indicate a higher fluid/rock ratio during late potassic alteration. The formation of alkali feldspars indicates that temperatures were lower and/or fluid/rock ratios were higher than during biotite-calcite alteration.

Silicic alteration, with which the bulk of mineralization is associated, follows late potassic alteration in the sequence of geological events. Highest molybdenum grades are associated with the zones of strongest silicification. These zones are interpreted as areas where the fluid/rock ratio was higher. Molybdenite is intergrown with muscovite and calcite at alkali feldspar grain boundaries. This suggests that the precipitation of molybdenite is linked to sericitization-carbonitization processes, and that alkali feldspars are favourable sites for this processes to occur. The range of

possible temperatures and pressures at which mineralization occurred is similar to that of late potassic alteration. Fluid inclusions are dominantly H_2O-CO_2 type, with a subordinate H_2O-rich population. This is consistent with progressive CO_2 enrichment as a result of fluid mixing. Decreasing temperature, pH, and K^+/Na^+ activity ratios all favour the precipitation of molybdenite. All of these processes are interpreted to have occurred during the evolution of the deposit, but the latter process may have been the most significant, as it explains the observed textural relationships.

Phyllic alteration is the youngest geological event recognized. Fluid inclusions from quartz veins associated with phyllic alteration are solely H_2O-CO_2 types. This is interpreted to represent a single fluid, the end product of fluid mixing where the proportion of the H_2O-CO_2 fluid is at a maximum. The low methane content of these inclusions, compared to the H_2O-CO_2 inclusions from the late potassic alteration and mineralization stages, suggests that the oxygen fugacity was higher during phyllic alteration than during the preceeding events.

The hydrothermal fluids are interpreted to have cooled between the contact metamorphic-skarn and late potassic alteration stages. Two models are proposed to explain the evolution of the hydrothermal fluids from the late potassic to phyllic alteration stages. Fluid mixing which occurred between the late potassic to phyllic alteration stages was either isothermal as XCO_2 increased, or there was a

synchronous decrease in temperature and increase in XCO_2.

Five structural orientations of veins and faults are recognised regionally and within the Trout Lake deposit. This suggests that regional stresses controlled the quartz vein orientations, and that the emplacement of the Trout Lake Stock did not significantly alter the local stress field. The similarity of vein orientations regionally and within the deposit, and the apparent genetic relationship between the Trout Lake and Copper Chief deposits suggest that both are part of the same metallogenic event. Vein orientations and textures indicate that the Trout Lake deposit formed under tensile conditions.

REFERENCES

Archibald, D.A., Glover, J.K., Price, R.A., and Carmichael, D.M., 1983, Geochronolgy and Tectonic Implications of Magmatism and Metamorphism; Southern Kootenay Arc and Neighbouring Regions, Southeastern British Columbia: Part I; Jurassic to Mid-Cretaceous: Can. Jour. Earth Sci., vol. 20, pp. 1891-1913.

Beane, R.E., 1974, Biotite Stability in the Porphyry Copper Environment: Econ. Geol., vol. 69, pp. 241-256.

Best, N.F., 1978, Mixed Volitile Equilibria in Greenschist Facies Metabasalts: In Progress in Experimental Petrology. 4th Report, Natural Environment Research Concil, Manchester, University, Published Series D, No. 11, pp. 337-379.

Bickle, M.J., and Powell, R., 1977, Calcite-Dolomite Geothermometry for Iron-Bearing Carbonates: Contrib. Mineral. Petrol., vol. 59, pp. 281-292.

Bischoff, J.L., Radtke, A.S., and Rosenbauer, R.J., 1981, Hydrothermal Alteration and Chloride Complexing on Metal Solubilization at 200 ^{o}C and 350 ^{o}C: Econ. Geol., vol 76, pp. 659-676.

Boettcher, A.L., 1970, The System $CaO-Al_2O_3-SiO_2-H_2O$ at High Pressures and Temperatures: Jour. Petrol., vol. 11, pp. 337-379.

Bowers, T.S., and Helgeson, H.C., 1983a, Calculation of the Thermodynamic and Geochemical Consequences of Nonideal Mixing in the System H_2O-CO_2-NaCl on Phase Relations in Geologic Systems: Equation of State for H_2O-CO_2-NaCl Fluids at High Pressures and Temperatures: Geochim. Cosmochim. Acta, vol. 47, pp. 1244-1275.

Bowers, T.S., and Helgeson, H.C., 1983b, Calculation of Thermodynamic and Geochemical Consequences of Nonideal Mixing in the System H_2O-CO_2-NaCl on Phase Relations in Geologic Systems: Metamorphic Equilibria at High Pressures and Temperatures: Am. Mineral., vol. 68, pp. 1059-1075.

Boyle, H.C. and Leitch, C.H.B., 1983, Geology of the Trout Lake Molybdenum Deposit, B.C.: Can. Inst. Min. Metal. Bull., Vol. 76, No. 849, pp. 115-124.

Brimhall, G.H., 1980, Deep Hypogene Oxidation of Porphyry Copper Potassium Silicate Protore at Butte, Montana: A Theoretical Evaluation of the Copper Remobilization Hypothesis: Econ. Geol., vol. 75, pp. 384-409.

Brock, R.W., 1903, Trout Lake District: Geol Sur. Can. Summary Report Part A, pp. 71-72.

Burnham, C.W., Holloway, J.R., and Davis, N.F., 1969, Thermodynamic Properties of Water to 1000 $^{\circ}$C and 10,000 bars: Geol. Soc. Am. Sp. Pap. 132, 96 p.

Burruss, R.C., 1981, Analysis of Phase Equilibria in C-O-H-S Fluid Inclusions: In Mineral. Assoc. Can. Short Course Handb., vol. 6, L.S. Hollister and M.L. Crawford eds., pp. 39-74.

Chivas, A.R., 1978, Porphyry Copper Mineralization at the Koloula Igneous Complex, Guadalcanal, Solomon Islands: Econ. Geol., vol. 73, pp. 645-677.

Collins, P.L.F., 1979, Gas Hydrates in CO_2-Bearing Fluid Inclusions and the Use of Freezing Data for Estimation of Salinity: Econ. Geol., vol. 74, pp. 1435-1444.

Dawson, G.M., 1889, Geol. Sur. Can. Annual Report 1888-1889, vol. IV, pp. B5-B65.

Dean, K.J., and Wilkinson, G.R., 1983, Precision Raman Investigation of the v_1 Mode of Vibration of SO_4^{-2}, WO_4^{-2}, and MoO_4^{-2} in Aqueous Solution of Different Concentrations: Jour. Raman Spectr., vol. 14, no. 2, pp. 131-134.

Eugster, H.P., and Skippen, G.B., 1967, Igneous amd Metamorphic Reactions Involving Gas Equilibria: In Researches in Geochemistry, vol. 2, P. Abelson ed., pp. 492-520.

Evans, B.W., 1965, Application of a Reaction-Rate Method to the Breakdown Equilibria of Muscovite and Muscovite Plus Quartz: Am. Jour. Sci., vol. 263, pp. 647-667.

Ferry, J.M., 1983, Regional metamorphism of the Vassalboro Formation, South-Central Maine, U.S.A.: Jour. Geol. Soc. London, vol. 140, pp. 551-576.

Frost, B.R., 1979, Mineral Equilibria Involving Mixed Volatiles in a C-O-H Fluid Phase: The Stabilities of Graphite and Siderite: Am. Jour. Sci., vol. 279, pp. 1033-1059.

Fyles, J.T., and Eastwood, G.E.P., 1962, Geology of the Ferguson Area, Lardeau District, British Columbia: B.C. Dept. Mines Bull. 45, 92 p.

Greenwood, H.J., 1967, Wollastonite: Stability in H_2O-CO_2 Mixtures and Occurrence in a Contact-Metamorphic Aureole Near Salmo, British Columbia, Canada: Am. Mineral., vol. 52, pp. 1669-1680.

Greenwood, H.J., 1975, Buffering of Pore Fluids by Metamorphic Reactions: Am. Jour. Sci., vol. 275, pp. 573-593.

Gunow, A.J., Ludington, S., and Munoz, J.L., 1980, Fluorine in Micas from the Henderson Molybdenite Deposit, Colorado: Econ. Geol., vol. 75, pp. 1127-1137.

Haas, J.L., 1976, Thermodynamic Properties of the Coexisting Phases and Thermochemical Properties of the NaCl Component in Boiling NaCl Solutions: U.S.G.S. Bull. 1421-B, 71 p.

Hajash, A., and Archer, P., 1980, Experimental Seawater/Basalt Interactions: Effects of Cooling: Contrib. Mineral. Petrol., vol. 75, pp. 1-13.

Helgeson, H.C., 1969, Thermodynamics of Hydrothermal Systems at Elevated Temperatures and Pressures: Am. Jour. Sci., vol. 267, pp. 729-804.

Hemley, J.J., Montoya, J.W., Marinenko, J.W., and Luce, R.W., 1980, Equlibria in the System $Al_2O_3-SiO_2-H_2O$ and Some General Implications for Alteration/Mineralization Processes: Econ. Geol., vol. 75, pp. 210-228.

Hewitt, D.A., 1973, Stability of the Assemblage Muscovite-Calcite-Quartz: Am. Mineral., vol. 58, pp. 785-791.

Hewitt, D.A., 1975, Stability of the Assemblage Phlogopite-Calcite-Quartz: Am. Mineral., vol. 60, pp. 391-397.

Hochella, M.F., Liou, J.G., Keskinen, M.J., and Kim, H.S., 1982, Synthesis and Stability Relations of Magnesium Idocrase: Econ. Geol., vol. 77, pp. 798-808.

Holland, S.S., 1952, Lucky Boy and Copper Chief (Major Exploration Ltd.): B.C. Minister of Mines Ann. Rept. 1953, pp. 144-145.

Holloway, J.R., 1981, Compositions and Volumes of Supercritical Fluids in the Earth's Crust: Mineral. Assoc. Can. Short Course Handb., vol. 6, L.S. Hollister and M.L. Crawford eds., pp. 13-38.

Hoschek, G., 1974, Gehlenite Stability in the System $CaO-Al_2O_3-SiO_2-H_2O$: Contrib. Mineral. Petrol., vol. 47, pp. 245-254.

Hunt, J.A., and Kerrick, D.M., 1977, The Stability of Sphene: Experimental Redetermination and Geological Implications: Geochim. Cosmochim. Acta, vol. 41, pp. 279-288.

Iiyama, J.T., 1965, Influence des Anions sur les Equilibres d'Echange d'Ions Na-K dans les Feldspaths Alcalins a 600 ^{0}C sous une Pression de 1000 Bars: Bull. Soc. Franc. Mineral. Crist., vol. 88, pp. 618-622.

Jacobs, G.K., and Kerrick, D.M., 1981, Devolatization Equilibria in H_2O-CO_2 and H_2O-CO_2-NaCl Fluids: An Experimental and Thermodynamic Evaluation at Elevated Pressures and Temperatures: Am. Mineral., Vol. 66, pp. 1135-1153.

Kerrick, D.M., 1974, Review of Metamorphic Mixed-Volatile (H_2O-CO_2) Equilibria: Am. Mineral., vol. 59, pp. 729-762.

Kolonin, G.R., Shironosova, G.P., and Laptev, Yu.V., 1975, Experimental Checking of Thermodynamic Diagrams of the Stability of W, Mo, and Bi Minerals Under Hydrothermal Conditions: Fortschr. Miner., vol. 52, pp. 161-167.

Lagache, M., and Weisbrod, A., 1977, The System: Two Alkali Feldspars-KCl-NaCl-H_2O at Moderate to High Temperatures and Low Pressures: Contrib. Mineral. Petrol., vol. 62, pp. 78-101.

Leroy, J., 1979, Contribution a l'Etalinnage de la Pression Interne des Inclusion Fluides lor de Leur Decrepitation: Bull. Mineral., vol. 102, pp. 584-593.

Lowell, J.D., and Guilbert, J.M., 1970, Lateral and Vertical Alteration-Mineralization Zoning in Porphyry Ore Deposits: Econ. Geol., vol 65, pp. 373-408.

Malinin, S.D., 1974, Thermodynamics of the H_2O-CO_2 System: Geochem. Intern., vol. 11, pp. 1060-1085.

Mathews, W.H., 1983, Early Tertiary Resetting of Potassium-Argon Dates in the Kootenay Arc, Southeastern British Columbia: Can. Jour. Earth Sci., vol. 20, pp. 867-872.

Miller, F.K., and Engels, J.C., 1975, Distribution and Trends of Discordant Ages of Plutonic Rocks of Northeastern Washington and Northern Idaho: Geol. Soc. Am. Bull., vol. 86, pp. 517-528.

Monger, J.W.H., and Price, R.A., 1979, Geodynamic Evolution of the Canadian Cordillera-Progress and Problems: Can. Jour. Earth Sci., vol. 16, pp. 770-791.

Montoya, J.W., and Hemley, J.J., 1975, Activity Relations and Stabilities in Alkali Feldspar and Mica Alteration Reactions: Econ. Geol., vol. 70, pp. 577-594.

Mottl, M.J., 1983, Metabasalts, Axial Hot Springs, and the Structure of Hydrothermal Systems at Mid-Ocean Ridges: Geol. Soc. Am. Bull., vol. 94, pp. 161-180.

Norton, D., and Knight, J., 1977, Transport Phenomena in Hydrothermal Systems: Cooling Plutons: Am. Jour. Sci., vol. 277, pp. 937-981.

Ohmoto, H., and Rye, R.O., 1970, The Bluebell Mine, British Columbia. I. Mineralogy, Paragenesis, Fluid Inclusions, and the Isotopes of Hydrogen, Oxygen, and Carbon: Econ. Geol., vol. 65, pp. 417-437.

Potter, R.W., and Brown, D.L., 1977, The Volumetric Properties of Aqueous Sodium Chloride Solutions from 0° to $500\ ^oC$ at Pressures up to 2000 Bars Based on a Regression of Available Data in the Literature: U.S.G.S. Bull. 1421-C, 36 p.

Potter, R.W., Clynne, M.A., and Brown, D.L., 1978, Freezing Point Depression of Aqueous Solium Chloride Solutions: Econ. Geol., vol. 73, pp. 284-285.

Price, R.A., 1979, Intercontinental Ductile Crustal Spreading Linking the Fraser River and Northern Rocky Mountain Trench Fault Zones, South-Central British Columbia and Northeastern Washington: Geol. Soc. Am., Abstr. with Progr., vol. 11, No. 7, p. 499.

Price, R.A., 1981, The Cordilleran Foreland Thrust and Fold Belt in the Southern Canadian Rocky Mountains: in Thrust and Nappe Tectonics, K.R. McClay and N.J. Price eds., Geol. Soc. London Sp.Pap. 9, pp. 427-448.

Psutka, J.F., Read, P.B., and Fyles, J.T., 1982, Stratigraphy, Structure, and Metamorphism Trout Lake Molybdenum Deposit and Vicinity: unpub. rept. for Geotex Consultants Ltd., 24p.

Puhan, D., 1978, Experimental Study of the Reaction Dolomite + K-Feldspar + H_2O = Phlogpite + Calcite + CO_2 at the Total Gas Pressures of 4000 and 6000 Bars: N. Jb. Miner. Mh., Vol. 3, pp. 110-127.

Read, P.B., 1973, Petrology and Structure of Poplar Creek Map-Area, British Columbia: Geol. Sur. Can. Bull. 193, 143 p.

Read, P.B., 1976, Lardeau Map-Area (82 K West Half) British Columbia: Geol. Sur. Can. Pap. 76-1A, pp. 95-96.

Read, P.B., and Brown, R.L., 1981, Columbia River Fault Zone: Southeastern Margin of the Shuswap and Monashee Complexes, Southern British Columbia: Can. Jour. Earth Sci., vol. 18, pp. 1127-1145.

Read, P.B., and Wheeler, J.O., 1976, Geology and Mineral Deposits, Lardeau West-Half: Geol. Sur. Can. open-file 288.

Reesor, J.E., 1973, Geology of the Lardeau Map Area, East Half, British Columbia: Geol. Sur. Can. Mem. 369, 129 p.

Rice, J.M., 1977, Progressive Metamorphism of Impure Dolomitic Limestone in the Marysville Aureole, Montana: Am. Jour. Sci., vol. 277, pp. 1-24.

Roedder, E., 1979, Fluid Inclusions as Samples of Ore Fluids: in Geochemistry of Hydrothermal Ore Deposits, H.L. Barnes ed., pp. 684-737.

Saxena, S.K., and Ribbe, P.H., 1972, Activity-Composition Relations in Feldspars: Contrib. Mineral. Petrol., vol. 37, pp. 131-138.

Schulien, S., 1975, Determination of the Equilibrium Constant and the Enthalpy of Reaction for the Mg^{+2}-Fe^{+2} Exchange Between Biotite and a Salt Solution: Fortschr. D. Mineral., vol. 52, pp. 133-139.

Slaughter, J., Kerrick, D.M., and Wall, V.J., 1975, Experimental and Thermodynamic Study of Equilibria in the System $CaO-MgO-SiO^2-H^2O-CO^2$: Am. Jour. Sci., vol. 275, pp. 143-162.

Smith, J.V., 1983, Phase Equilibria of Plagioclase: in Feldspar Mineralogy, 2nd edition, Mineral. Soc. Am. Short Course, vol. 2, P.H. Ribbe ed., pp. 223-239.

Smith, R.W., Norman, D.I., and Popp, C.J., 1980, Calculated Solubility of Molybdenite in Hydrothermal Solutions: Geol. Soc. Am. Abstr. with Prog., Vol. 12, No. 7, p. 525.

Sourirajan, S., and Kennedy, G.C., 1962, The System $H_2O-NaCl$ at Elevated Temperatures and Pressures: Am. Jour. Sci., vol. 260, pp. 115-141.

Storre, B., and Nitsch, K.H., 1972, Die Reaktion 2 Zoisit + 1 CO_2 = 3 Anorthit + 1 Calcit + 1 H_2O: Contrib. Mineral. Petrol., vol. 35, pp. 1-10.

Storre, B., and Nitsch, K.H., 1974, Zur Stabilitat von Margarit in System $CaO-Al_2O_3-SiO_2-H_2O$: Contrib. Mineral. Petrol., vol. 43, pp. 1-24.

Swanenberg, H.E.C., 1979, Phase Equilibria in Carbonic Systems, and Their Application to Freezing Studies of Fluid Inclusions: Contrib. Mineral. Petrol., vol. 68, pp. 303-306.

Thompson, A.B., 1974, Calculation of Muscovite-Paragonite-Alkali Feldspar Phase Relations: Contrib. Mineral. Petrol., vol. 44, pp. 173-194.

Walker, J.F., and Bancroft, M.F., 1929, Lardeau Map-Area, British Columbia: General Geology: Geol. Sur. Can. Mem. 161, pp. 1-16.

Westra, G., and Keith, S.B., 1981, Classification and Genesis of Stockwork Molybdenum Deposits: Econ. Geol., vol. 76, pp. 844-873.

Whitney, J.A., and Stormer, J.C., 1977, The Distribution of $NaAlSi_3O_8$ Between Coexisting Microcline and Plagioclase and its Effect on Geothermometric Calculations: Am. Mineral., vol. 62, pp. 687-691.

Williams-Jones, A.E., 1981, Thermal Metamorphism of Siliceous Limestone in the Aureole of Mount Royal, Quebec: Am. Jour. Sci., vol. 281, pp. 673-696.

Williams-Jones, A.E., 1982, Patapedia: an Appalachian Calc-Silicate Hosted Copper Prospect of Porphyry Affinity: Can. Jour. Earth Sci., vol. 19, pp. 438-455.

Zussman, J., 1979, The Crystal Chemistry of the Micas: Bull. Mineral., v. 102, pp. 5-13.

APPENDIX 1

ELECTRON MICROPROBE ANALYSES OF BIOTITES

Metased are grains of contact metamorphic or apparent contact metamorphic origin.

Halo are grains within biotite haoles around quartz veins.

Ign are grains from the granodiorite or quartz diorite units.

N.A. is not analysed.

* indicates representative analysis used in figures in the text.

Sample 26 + 90

	(1)	(2)*	(3)	(4)	(5)	(6)	(7)	(8)
SiO_2	34.77	34.56	34.46	34.93	35.01	37.62	34.70	34.57
TiO_2	2.06	1.63	1.62	1.37	1.68	0.19	2.19	1.94
Al_2O_3	18.61	18.32	18.95	18.40	18.40	16.01	17.83	17.74
MgO	8.38	8.17	8.24	8.31	8.53	11.92	7.96	7.71
FeO	21.94	22.15	21.90	22.35	21.78	19.14	22.44	22.99
MnO	0.43	0.49	0.38	0.40	0.35	0.38	0.39	0.36
F	0.34	0.19	0.32	0.06	0.36	0.86	0.28	0.21
Cl	0.01	0.04	0.05	0.04	0.02	0.09	0.05	0.05
CaO	0.01	0.00	0.00	0.01	0.00	0.08	0.01	0.01
Na_2O	N.A.	N.A.	N.A.	N.A.	N.A.	N.A.	N.A.	N.A.
K_2O	9.94	9.62	9.33	9.84	9.49	9.67	9.79	9.55
TOT.	96.49	95.17	95.25	95.71	95.63	95.95	95.64	95.13

(1)-(8) metased

Sample 1346

	(1)	(2)*	(3)	(4)	(5)	(6)	(7)
SiO_2	35.32	34.87	35.08	34.82	35.96	35.23	33.72
TiO_2	2.93	2.67	2.75	2.71	2.96	3.49	2.47
Al_2O_3	18.07	17.84	18.50	17.36	16.48	16.49	17.99
MgO	9.43	9.53	9.44	9.70	9.90	9.32	8.59
FeO	20.73	20.23	19.45	20.12	19.51	20.17	21.28
MnO	0.15	0.00	0.08	0.17	0.05	0.04	0.06
F	0.58	0.47	0.34	0.62	0.60	0.66	0.56
Cl	0.07	0.07	0.01	0.07	0.09	0.09	0.02
CaO	0.01	0.00	0.00	0.01	0.00	0.00	0.00
Na_2O	N.A.	N.A.	N.A.	N.A.	N.A.	N.A.	N.A.
K_2O	9.60	9.27	9.04	8.67	8.61	9.02	9.30
TOT.	96.89	94.95	94.71	94.22	94.15	94.51	94.00

(1),(2),(4)-(6) at vein contact   (3),(7) metased

	Sample 1446		Sample 1498			Sample 1504	
	(1)	(2)	(1)*	(2)		(1)	(2)*
SiO_2	35.71	35.45	36.09	36.32		34.49	33.61
TiO_2	3.43	2.96	3.48	2.96		2.22	1.39
Al_2O_3	16.24	16.29	16.02	15.57		19.80	21.47
MgO	7.78	7.68	11.51	11.78		7.91	7.81
FeO	23.37	23.07	17.11	17.11		20.32	20.87
MnO	0.52	0.50	0.28	0.34		0.10	0.25
F	0.75	0.72	0.90	1.03		0.07	0.29
Cl	N.A.	N.A.	0.02	0.03		N.A.	N.A.
CaO	0.03	0.02	0.00	0.02		0.01	0.00
Na_2O	0.08	0.00	N.A.	N.A.		0.07	0.22
K_2O	9.80	9.97	9.60	9.34		10.13	9.99
TOT.	97.72	96.67	95.01	94.51		95.11	95.89

1446 (1),(2) ign   1498 (1),(2) metased   1504 (1),(2) metased

Sample 1 Dr. W. 18

	(1)	(2)	(3)	(4)	(5)	(6)	(7)*
SiO_2	38.72	39.07	37.51	38.19	38.80	38.69	38.47
TiO_2	2.50	1.91	2.19	2.37	1.84	2.51	1.82
Al_2O_3	14.87	15.14	15.32	15.51	15.80	15.69	15.12
MgO	14.50	14.27	14.18	14.22	14.79	14.16	14.47
FeO	14.93	14.87	14.98	15.11	14.80	15.07	14.97
MnO	0.46	0.48	0.43	0.52	0.49	0.50	0.45
F	1.04	0.65	0.70	0.63	1.06	0.63	0.46
CaO	0.00	0.04	0.02	0.01	0.00	0.04	0.05
Na_2O	0.10	0.07	0.05	0.08	0.00	0.03	0.09
K_2O	10.22	10.31	10.45	10.38	10.11	10.35	10.12
TOT.	97.32	96.80	95.81	97.03	97.69	97.64	96.01

(1)-(7) metased

Sample 4Dr.S. 13

	(1)	(2)	(3)	(4)	(5)	(6)	(7)	(8)
SiO_2	32.17	34.18	34.09	33.64	32.87	34.40	33.04	34.48
TiO_2	2.38	2.69	2.96	2.70	2.70	2.94	2.95	2.83
Al_2O_3	18.91	18.68	18.82	18.81	19.05	19.26	20.41	19.79
MgO	8.05	7.77	7.92	7.64	8.19	7.95	7.64	8.43
FeO	22.82	22.21	21.10	22.24	20.72	20.07	20.83	19.86
MnO	0.06	0.10	0.15	0.06	0.22	0.10	0.29	0.50
F	0.20	0.57	0.22	0.29	0.67	0.42	0.41	0.63
Cl	0.04	0.03	0.03	0.03	0.04	0.02	0.03	0.04
CaO	0.04	0.00	0.00	0.00	0.03	0.00	0.00	0.01
Na_2O	0.06	0.07	0.11	0.07	0.08	0.08	0.12	0.16
K_2O	9.02	9.61	9.24	9.68	10.08	9.49	9.80	10.40
TOT.	93.74	95.91	94.64	95.17	94.65	94.66	95.34	97.08

	(9)*	(10)	(11)*	(12)	(13)	(14)	(15)
SiO_2	33.74	34.06	34.31	35.32	34.08	34.16	33.69
TiO_2	2.76	3.26	3.26	3.27	3.40	3.47	2.25
Al_2O_3	19.10	19.11	18.76	18.01	18.88	18.33	18.75
MgO	7.83	7.77	7.59	8.23	7.59	7.69	8.13
FeO	21.25	21.01	20.19	20.26	20.87	22.38	20.93
MnO	0.04	0.31	0.25	0.22	0.11	0.02	0.07
F	0.41	0.50	0.41	0.11	0.52	0.27	0.27
Cl	0.03	0.03	0.07	0.02	0.03	0.04	0.02
CaO	0.00	0.01	0.00	0.00	0.00	0.00	0.02
Na_2O	0.09	0.13	0.12	0.06	0.16	0.07	0.02
K_2O	9.70	10.31	10.29	10.44	10.11	10.10	10.11
TOT.	94.93	96.50	95.24	95.94	95.76	96.52	94.24

(1)-(9) metased   (10)-(15) halo

Sample 4 Dr. S. 83

	(1)	(2)	(3)*	(4)	(5)
SiO_2	33.83	35.48	35.18	36.74	37.61
TiO_2	2.23	1.76	1.45	3.17	2.60
Al_2O_3	19.16	20.76	19.18	16.28	16.06
MgO	8.71	10.13	10.32	11.74	11.76
FeO	20.98	18.20	18.72	16.60	16.28
MnO	0.06	0.33	0.36	0.34	0.26
F	0.23	0.57	0.50	1.09	0.93
CaO	0.00	0.02	0.01	0.00	0.00
Na_2O	0.12	0.21	0.01	0.06	0.09
K_2O	9.58	10.23	10.47	9.79	10.24
TOT.	94.92	97.69	96.19	95.82	95.84

(1)-(5) metased

Sample 81-15 410

	(1)	(2)	(3)	(4)*	(5)*	(6)	(7)
SiO_2	34.56	34.50	35.45	34.98	36.81	37.06	36.56
TiO_2	2.60	2.50	2.68	2.04	2.54	2.96	3.12
Al_2O_3	19.11	18.79	19.17	19.16	16.83	16.86	15.73
MgO	8.82	8.83	9.07	9.16	9.95	10.78	9.99
FeO	20.37	18.54	19.92	19.45	17.90	18.76	17.21
MnO	0.50	0.50	0.57	0.48	0.40	0.43	0.36
F	0.63	0.00	0.53	0.37	0.48	0.59	0.70
CaO	0.00	0.03	0.02	0.02	0.03	0.00	0.02
Na_2O	0.00	0.01	0.09	0.14	0.20	0.24	0.07
K_2O	10.10	9.95	9.99	10.20	10.23	10.10	9.68
TOT.	96.70	93.66	97.48	96.01	95.38	97.76	93.42

(1)-(4) metased (5)-(6) halo (7) vein

Sample 81-15 494

	(1)*	(2)	(3)	(4)*
SiO_2	35.65	34.92	35.80	35.28
TiO_2	2.56	3.12	2.90	2.64
Al_2O_3	19.18	18.07	19.94	18.85
MgO	8.50	8.77	8.39	8.27
FeO	21.11	20.59	20.65	20.44
MnO	0.22	0.10	0.16	0.26
F	0.58	0.48	0.74	0.68
CaO	0.03	0.00	0.00	0.00
Na_2O	0.13	0.04	0.06	0.08
K_2O	10.45	10.29	10.21	10.35
TOT.	98.42	96.36	98.86	96.84

(1)-(3) halo (4) metased

Sample 81-23 18

	(1)	(2)*	(3)
SiO_2	35.76	35.55	34.16
TiO_2	1.98	2.64	1.86
Al_2O_3	20.07	19.44	20.59
MgO	9.57	10.00	9.67
FeO	19.30	18.20	21.21
MnO	0.59	0.51	0.38
F	0.48	0.91	0.57
CaO	0.06	0.05	0.04
Na_2O	0.13	0.03	0.22
K_2O	10.35	10.06	8.40
TOT.	98.29	97.39	97.10

(1)-(3) halo

Sample 81-32 39

	(1)*	(2)	(3)	(4)
SiO_2	38.40	38.77	37.60	38.36
TiO_2	2.06	2.72	2.07	2.90
Al_2O_3	15.75	15.36	16.20	15.49
MgO	13.78	13.00	13.20	12.95
FeO	16.15	16.58	17.42	16.66
MnO	0.38	0.42	0.51	0.42
F	1.45	1.73	0.92	1.61
CaO	0.03	0.14	0.00	0.00
Na_2O	0.10	0.13	0.27	0.18
K_2O	10.44	10.00	10.17	9.94
TOT.	98.53	98.86	98.36	98.51

(1)-(4) halo

Sample 81-33 90

	(1)	(2)	(3)	(4)	(5)
SiO_2	35.43	35.17	34.51	34.70	34.79
TiO_2	4.14	3.41	3.24	3.74	3.64
Al_2O_3	14.86	15.22	17.79	16.90	17.31
MgO	9.44	9.54	8.44	8.22	7.77
FeO	21.13	22.63	22.11	22.68	21.43
MnO	0.31	0.27	0.28	0.29	0.31
F	0.73	0.87	0.66	0.69	0.45
Cl	0.05	0.10	0.04	0.03	0.09
CaO	0.00	0.04	0.06	0.08	0.00
Na_2O	0.04	0.02	0.12	0.12	0.06
K_2O	10.14	9.17	8.53	8.15	8.89
TOT.	96.26	96.44	95.78	95.61	94.74

(1)-(5) igneous

Sample 81-42 92

	(1)	(2)*
SiO_2	37.01	36.10
TiO_2	3.33	3.58
Al_2O_3	16.57	15.98
MgO	10.78	9.80
FeO	18.17	18.51
MnO	0.09	0.08
F	1.20	1.04
CaO	0.01	0.00
Na_2O	0.15	0.16
K_2O	10.24	10.53
TOT.	97.53	95.77

81-42 (1)-(2) halo

Sample 81-44 46.5

	(1)	(2)*
SiO_2	34.83	34.64
TiO_2	2.23	1.54
Al_2O_3	19.49	20.33
MgO	8.21	8.42
FeO	20.31	19.96
MnO	0.24	0.16
F	0.49	0.71
CaO	0.00	0.00
Na_2O	0.17	0.18
K_2O	10.10	10.31
TOT.	96.10	96.25

81-44 (1)-(2) metased

Sample 81-55 19

	(1)	(2)*	(3)	(4)*	(5)
SiO_2	34.89	36.43	34.90	33.99	34.48
TiO_2	2.61	3.55	3.53	2.89	2.76
Al_2O_3	19.65	17.08	19.79	18.35	18.81
MgO	8.20	9.46	8.08	8.57	8.37
FeO	20.71	19.45	20.57	21.08	21.40
MnO	0.51	0.30	0.55	0.39	0.36
F	0.68	0.42	0.66	0.53	0.41
CaO	0.00	0.00	0.01	0.00	0.00
Na_2O	0.11	0.10	0.09	0.06	0.02
K_2O	10.27	10.33	10.09	10.13	10.05
TOT.	97.61	97.11	98.28	96.00	96.62

(1),(4) metased   (2),(3),(5) halo

Sample 81-60 203.5

	(1)*	(2)	(3)	(4)	(5)	(6)*	(7)	(8)
SiO_2	38.13	38.16	38.43	38.80	36.23	36.62	37.08	36.51
TiO_2	1.41	1.60	1.63	1.86	2.84	3.29	1.50	1.64
Al_2O_3	14.60	15.08	15.71	14.81	16.06	15.87	15.52	16.49
MgO	15.34	15.30	14.79	14.62	12.48	12.87	13.72	13.49
FeO	14.73	15.43	15.36	15.42	16.32	16.29	15.95	16.12
MnO	0.18	0.23	0.15	0.21	0.25	0.20	0.17	0.18
F	0.79	1.36	1.27	1.09	0.91	0.70	1.13	1.22
Cl	0.04	0.05	0.03	0.00	0.08	0.03	0.03	0.06
CaO	0.01	0.02	0.00	0.00	0.03	0.03	0.01	0.01
Na_2O	0.00	0.04	0.07	0.08	0.13	0.12	0.08	0.12
K_2O	9.83	9.77	9.81	9.63	9.96	9.82	9.45	9.82
TOT.	94.06	97.05	97.27	96.51	95.28	95.84	94.62	95.63

Sample 81-60 203.5

	(9)	(10)	(11)	(12)
SiO_2	36.60	36.96	37.65	37.89
TiO_2	2.37	2.46	2.33	2.59
Al_2O_3	16.28	15.35	15.99	15.97
MgO	13.25	13.80	13.82	13.69
FeO	16.27	15.60	15.87	16.12
MnO	0.21	0.17	0.21	0.20
F	0.43	0.91	0.88	0.61
Cl	0.05	0.02	0.05	0.04
CaO	0.00	0.00	0.00	0.02
Na_2O	0.17	0.08	0.10	0.11
K_2O	9.95	9.66	9.56	9.26
TOT.	95.57	95.41	96.46	96.46

(1)-(12) halo

Sample 81-64 188

	(1)	(2)*	(3)	(4)*	(5)
SiO_2	36.77	37.33	36.29	35.36	36.16
TiO_2	1.10	1.07	0.78	2.47	2.36
Al_2O_3	19.99	19.79	19.33	19.64	19.41
MgO	11.72	12.12	11.91	11.23	11.12
FeO	15.93	16.44	16.83	16.70	16.66
MnO	0.24	0.26	0.02	0.16	0.20
F	0.91	1.14	0.71	1.11	0.62
CaO	0.00	0.04	0.00	0.00	0.04
Na_2O	0.18	0.03	0.00	0.09	0.34
K_2O	10.43	10.82	10.57	10.28	10.20
TOT.	97.27	98.83	97.03	97.06	97.11

(1)-(3) halo   (4)-(5) metased

Sample 82-16

	(1)	(2)*
SiO_2	38.10	38.56
TiO_2	1.08	1.48
Al_2O_3	16.25	16.46
MgO	14.42	16.17
FeO	14.17	14.28
MnO	0.60	0.50
F	1.16	0.77
CaO	0.02	0.08
Na_2O	0.00	0.20
K_2O	10.39	10.54
TOT.	96.19	98.98

82-16 (1)-(2) metased

Sample 82-21

	(1)	(2)	(3)*
SiO_2	37.83	38.34	37.50
TiO_2	1.98	1.68	1.99
Al_2O_3	18.13	19.13	18.29
MgO	13.18	14.38	13.64
FeO	13.93	12.70	13.02
MnO	0.15	0.06	0.12
F	0.30	0.23	0.37
CaO	0.03	0.07	0.02
Na_2O	0.07	0.04	0.07
K_2O	10.46	10.23	10.33
TOT.	96.71	96.85	95.36

82-21 (1)-(3) metased

Sample 82-28

	(1)	(2)*	(3)	(4)	(5)
SiO_2	39.72	38.53	38.14	39.72	40.10
TiO_2	1.44	1.52	1.81	1.24	1.29
Al_2O_3	14.69	16.79	16.37	16.84	16.86
MgO	17.82	16.98	15.53	17.05	17.23
FeO	10.93	10.83	12.03	11.02	11.27
MnO	0.32	0.54	0.36	0.33	0.37
F	2.17	1.24	1.15	2.11	1.61
CaO	0.08	0.03	0.03	0.01	0.02
Na_2O	0.29	0.02	0.06	0.05	0.05
K_2O	10.45	10.69	10.86	9.32	10.63
TOT.	97.92	96.92	96.32	97.69	99.35

82-28 (1)-(5) metased

Sample 82-43

	(1)*	(2)	(3)
SiO_2	38.74	39.19	38.46
TiO_2	1.62	1.40	1.71
Al_2O_3	16.28	17.24	17.08
MgO	14.55	15.37	14.58
FeO	13.12	12.48	13.10
MnO	0.24	0.19	0.24
F	0.37	0.53	0.49
CaO	0.00	0.01	0.03
Na_2O	0.08	0.16	0.11
K_2O	9.95	10.29	10.47
TOT.	94.94	96.85	96.27

82-43 (1)-(3) metased

Sample 82-76

	(1)	(2)	(3)*
SiO_2	35.11	33.05	33.96
TiO_2	1.73	1.22	1.35
Al_2O_3	20.26	19.82	20.63
MgO	9.62	9.91	9.90
FeO	19.20	19.83	18.61
MnO	0.17	0.13	0.22
F	0.50	1.08	0.54
CaO	0.01	0.02	0.02
Na_2O	0.10	0.06	0.26
K_2O	10.31	9.51	10.20
TOT.	97.01	94.63	95.67

(1)-(3) metased

Sample 82-77

	(1)	(2)*	(3)
SiO_2	34.80	34.12	35.30
TiO_2	2.80	2.29	2.63
Al_2O_3	17.69	18.80	18.90
MgO	8.48	9.00	9.00
FeO	20.82	21.10	21.82
MnO	0.38	0.47	0.44
F	0.61	0.30	0.12
CaO	0.02	0.00	0.00
Na_2O	0.33	0.15	0.12
K_2O	10.37	10.25	10.66
TOT.	96.30	96.48	99.00

Sample 82-78

	(1)*	(2)	(3)	(4)	(5)	(6)
SiO_2	38.50	39.01	35.52	36.23	36.62	37.40
TiO_2	1.37	0.83	1.62	1.72	1.52	0.34
Al_2O_3	16.38	17.11	17.56	17.06	17.25	18.27
MgO	15.49	16.20	9.39	12.21	9.93	15.12
FeO	11.30	12.39	20.22	15.86	20.19	11.34
MnO	0.25	0.35	0.27	0.31	0.27	0.30
F	1.19	0.93	0.79	0.78	0.45	1.76
CaO	0.02	0.00	0.06	0.01	0.04	0.04
Na_2O	0.21	0.21	0.01	0.23	0.08	0.09
K_2O	10.30	10.72	10.03	10.15	9.97	9.91
TOT.	94.96	97.75	95.46	94.55	96.33	94.56

(1)-(2), (6) metased (3)-(5) ign

Sample 82-91

	(1)*	(2)	(3)
SiO_2	36.87	36.67	39.97
TiO_2	1.99	2.28	1.08
Al_2O_3	17.20	16.91	15.31
MgO	12.80	12.57	15.53
FeO	14.93	15.63	11.93
MnO	0.20	0.20	0.14
F	0.70	0.65	1.50
CaO	0.07	0.02	0.10
Na_2O	0.05	0.04	0.13
K_2O	10.42	10.44	9.66
TOT.	95.23	95.43	95.35

82-91 (1)-(3) metased

Sample 82-101B

	(1)	(2)	(3)	(4)*	(5)	(6)	(7)	(8)
SiO_2	35.58	32.69	35.45	32.29	32.80	35.39	34.73	34.36
TiO_2	1.47	1.16	1.80	1.09	1.20	1.15	1.19	1.07
Al_2O_3	17.30	19.33	19.13	19.92	20.11	19.35	19.84	18.80
MgO	8.48	7.86	8.05	7.57	7.79	8.55	7.54	8.34
FeO	21.58	22.98	21.00	23.73	22.83	20.46	19.50	21.11
MnO	0.34	0.39	0.29	0.36	0.35	0.29	0.24	0.38
F	0.54	0.18	0.00	0.30	0.00	0.48	0.24	0.89
CaO	0.06	0.05	0.10	0.04	0.06	0.11	0.07	0.00
Na_2O	0.00	0.15	0.11	0.02	0.02	0.11	0.11	0.17
K_2O	9.44	9.99	9.55	8.87	8.46	8.23	8.24	9.57
TOT.	94.78	94.76	95.47	94.19	93.63	94.13	91.71	94.68

(1)-(8) metased

Sample 82-115; Sample 82-116; Sample 82-117

	(1)	(2)	(3)*	(1)	(2)*	(1)*	(2)
SiO_2	32.86	32.52	32.14	35.84	36.11	35.09	32.02
TiO_2	1.75	1.17	1.67	1.79	2.30	1.83	1.20
Al_2O_3	20.09	20.11	18.87	19.49	18.62	17.47	16.70
MgO	7.15	7.79	6.59	11.70	12.36	8.64	9.17
FeO	22.70	20.85	23.37	14.58	14.99	20.15	19.90
MnO	0.20	0.20	0.17	0.36	0.33	0.30	0.31
F	0.16	0.77	0.43	1.63	1.44	0.39	0.86
CaO	0.01	0.00	0.02	0.03	0.01	0.00	0.04
Na_2O	0.08	0.07	0.05	0.07	0.13	0.03	0.10
K_2O	9.85	10.19	9.98	10.31	10.22	9.59	9.94
TOT.	94.84	93.67	93.28	95.81	96.51	93.49	93.15

82-115, 82-116, 82-117 metased

Sample 82-121

	(1)	(2)	(3)	(4)
SiO$_2$	37.91	38.20	37.90	37.95
TiO$_2$	1.83	1.95	1.30	1.70
Al$_2$O$_3$	14.80	14.34	14.40	13.89
MgO	13.59	13.73	14.51	14.18
FeO	16.03	16.05	15.94	16.25
MnO	0.07	0.10	0.07	0.03
F	0.30	0.00	0.16	0.26
CaO	0.04	0.01	0.05	0.04
Na$_2$O	0.09	0.10	0.18	0.20
K$_2$O	10.24	10.53	10.17	10.25
TOT.	94.90	95.01	94.70	94.73

82-121 (1)-(4) metased

Sample 82-127

	(1)	(2)*	(3)
SiO$_2$	33.65	33.37	33.92
TiO$_2$	2.68	2.56	1.80
Al$_2$O$_3$	18.97	18.39	19.08
MgO	6.94	7.47	8.38
FeO	21.43	21.37	19.80
MnO	0.28	0.10	0.16
F	0.25	0.42	0.90
CaO	0.02	0.02	0.05
Na$_2$O	0.12	0.13	0.07
K$_2$O	10.22	10.35	10.02
TOT.	94.56	94.18	94.18

82-127 (1)-(3) metased

Sample 82-131

	(1)*	(2)
SiO$_2$	35.60	37.12
TiO$_2$	2.30	1.66
Al$_2$O$_3$	16.90	17.26
MgO	13.65	13.75
FeO	14.12	14.23
MnO	0.28	0.31
F	1.62	1.68
CaO	0.03	0.00
Na$_2$O	0.04	0.11
K$_2$O	10.69	10.35
TOT.	95.23	96.47

82-131 (1),(2) metased

Sample 82-132

	(1)	(2)	(3)	(4)*
SiO$_2$	36.22	34.88	36.53	36.28
TiO$_2$	3.67	3.47	3.36	3.43
Al$_2$O$_3$	16.07	18.45	17.28	16.67
MgO	8.65	8.22	8.46	8.68
FeO	20.39	21.19	21.57	21.17
MnO	0.58	0.58	0.53	0.09
F	0.61	0.51	0.19	0.40
CaO	0.66	0.02	0.03	0.01
Na$_2$O	0.01	0.06	0.18	0.19
K$_2$O	9.96	10.05	10.34	8.29
TOT.	97.45	97.43	98.46	97.40

82-132 (1) ign (2)-(4) metased

Sample 82-144

	(1)*	(2)	(3)
SiO$_2$	38.04	37.58	37.53
TiO$_2$	1.33	1.76	1.34
Al$_2$O$_3$	17.19	17.94	17.19
MgO	17.05	15.96	17.07
FeO	9.53	9.95	9.44
MnO	0.41	0.37	0.34
F	2.53	1.97	2.97
CaO	0.00	0.04	0.01
Na$_2$O	0.15	0.13	0.11
K$_2$O	10.53	9.57	10.66
TOT.	96.76	95.26	96.67

82-144 (1)-(3) metased

Sample 82-145

	(1)	(2)	(3)*
SiO$_2$	36.02	37.05	36.03
TiO$_2$	1.24	1.32	1.12
Al$_2$O$_3$	16.73	15.90	16.78
MgO	15.88	16.22	15.41
FeO	12.12	10.63	11.45
MnO	0.40	0.40	0.41
F	2.75	2.68	2.35
CaO	0.00	0.04	0.06
Na$_2$O	0.17	0.06	0.14
K$_2$O	10.23	10.56	10.11
TOT.	95.55	94.87	93.85

82-145 (1)-(3) metased

Sample 82-147

	(1)	(2)*	(3)
SiO$_2$	34.14	33.03	33.76
TiO$_2$	3.04	2.95	2.51
Al$_2$O$_3$	17.86	18.64	17.31
MgO	7.33	7.06	7.40
FeO	21.39	23.02	22.77
MnO	0.00	0.10	0.01
F	1.16	0.70	2.51
CaO	0.04	0.04	0.01
Na$_2$O	0.00	0.08	0.02
K$_2$O	9.55	9.76	9.58
TOT.	94.52	95.38	94.38

82-147 (1)-(3) metased

Sample 82-152

	(1)	(2)	(3)*
SiO$_2$	34.34	33.92	32.12
TiO$_2$	2.73	2.83	2.98
Al$_2$O$_3$	19.20	19.68	19.81
MgO	7.89	7.71	7.76
FeO	21.05	20.32	21.06
MnO	0.27	0.36	0.27
F	0.42	0.00	0.53
CaO	0.01	0.00	0.00
Na$_2$O	0.07	0.10	0.07
K$_2$O	10.13	9.96	9.90
TOT.	96.10	94.88	94.50

82-152 (1)-(3) metased

APPENDIX 2

ELECTRON MICROPROBE ANALYSES OF FELDSPARS

Metased are grains of contact metamorphic or apparent contact metamorphic origin.

Ign are grains of apparent igneous origin

Xan represents anorthite mole fraction

Xab represents albite mole fraction

Xor represents orthoclase mole fraction

Sample 1164

	(1)	(2)	(3)	(4)	(5)	(6)
SiO_2	67.47	68.08	68.32	68.79	68.01	69.03
Al_2O_3	19.72	19.50	19.47	19.28	19.51	19.19
FeO	0.00	0.10	0.04	0.00	0.00	0.02
CaO	0.40	0.31	0.02	0.02	0.00	0.00
Na_2O	10.86	10.48	11.12	10.66	11.29	10.84
K_2O	0.11	0.12	0.06	0.10	0.06	0.08
TOT.	98.56	98.59	99.02	98.85	98.88	99.16
Xan	.02	.01	.00	.00	.00	.00
Xab	.97	.98	1.00	.99	1.00	.99
Xor	.01	.01	.00	.01	.00	.01

(1)-(6) hydrothermal

Sample 1369

	(1)	(2)	(3)	(4)	(5)	(6)	(7)	(8)
SiO_2	67.17	69.05	68.45	67.94	63.48	67.96	67.39	64.58
Al_2O_3	19.87	19.71	19.94	19.80	18.71	19.71	20.05	18.19
FeO	0.07	0.07	0.09	0.24	0.00	0.00	0.00	0.11
CaO	0.25	0.02	0.15	0.18	0.00	0.03	0.62	0.00
Na_2O	9.67	10.27	9.90	10.64	0.40	10.03	9.98	0.46
K_2O	0.18	0.04	0.08	0.08	15.79	0.08	0.09	16.93
TOT.	97.21	99.16	98.60	98.98	98.38	97.81	98.13	100.26
Xan	.01	.00	.01	.01	.00	.00	.03	.00
Xab	.98	1.00	.99	.99	.04	.99	.96	.04
Xor	.01	.00	.00	.00	.96	.01	.01	.96

(1)-(8) hydrothermal

Sample 1369   Sample 1446

	(9)		(1)	(2)	(3)
SiO_2	67.82		58.87	60.69	58.71
Al_2O_3	19.34		24.61	24.43	25.54
FeO	0.02		0.06	0.09	0.03
CaO	0.25		6.77	6.16	7.15
Na_2O	10.52		7.03	7.74	6.85
K_2O	0.23		0.35	0.20	0.02
TOT.	98.19		97.69	99.32	98.46
Xan	.01		.34	.30	.36
Xab	.97		.64	.69	.63
Xor	.02		.02	.01	.01

1369 (9) hydrothermal   1446 (1)-(3) ign

Sample 1498

	(1)	(2)	(3)	(4)	(5)	(6)	(7)	(8)
SiO_2	64.28	64.07	64.48	63.57	68.76	63.86	64.56	63.18
Al_2O_3	18.34	18.33	18.31	18.25	19.79	18.55	18.40	18.46
FeO	0.00	0.03	0.03	0.06	0.01	0.00	0.00	0.00
CaO	0.00	0.00	0.01	0.00	0.10	0.00	0.03	0.02
Na_2O	0.33	0.50	0.54	0.34	11.49	0.34	0.44	0.73
K_2O	16.91	16.87	17.00	16.87	0.08	16.97	17.05	16.04
TOT.	99.86	99.80	100.36	99.08	100.23	99.72	100.48	98.43
Xan	.00	.00	.00	.00	.01	.00	.00	.00
Xab	.03	.04	.05	.03	.98	.03	.04	.07
Xor	.97	.96	.95	.97	.01	.97	.96	.93

(1)-(8) hydrothermal

Sample 1498

	(9)	(10)	(11)	(12)	(13)	(14)	(15)
SiO_2	62.53	65.23	64.15	65.05	64.26	62.91	63.99
Al_2O_3	18.35	18.58	18.52	18.19	18.23	18.41	18.26
FeO	0.00	0.00	0.06	0.00	0.02	0.00	0.00
CaO	0.06	0.01	0.03	0.02	0.01	0.03	0.08
Na_2O	0.52	2.17	1.07	0.44	0.34	1.14	0.47
K_2O	15.65	15.09	15.48	17.10	17.50	15.65	16.86
TOT.	97.12	101.08	99.32	100.80	100.38	98.14	99.65
Xan	.00	.00	.00	.00	.00	.00	.00
Xab	.05	.18	.10	.04	.03	.10	.04
Xor	.95	.82	.90	.96	.97	.90	.96

(9)-(11) hydrothemal, (12)-(15) metased

Sample 1503

	(1)	(2)	(3)	(4)	(5)	(6)	(7)
SiO_2	63.15	64.62	64.56	68.10	62.97	69.26	63.76
Al_2O_3	18.40	18.35	18.38	19.31	18.16	19.64	18.16
FeO	0.09	0.00	0.00	0.00	0.00	0.11	0.00
CaO	0.00	0.00	0.00	0.08	0.04	0.24	0.00
Na_2O	0.25	0.34	0.30	11.58	0.63	11.72	0.29
K_2O	16.73	17.35	17.10	0.06	16.63	0.06	16.95
TOT.	98.62	100.66	100.34	99.14	98.43	101.03	99.16
Xan	.00	.00	.00	.01	.00	.02	.00
Xab	.02	.03	.03	.99	.05	.97	.03
Xor	.98	.97	.97	.00	.95	.00	.97

(1)-(7) hydrothermal

Sample 1504

	(1)	(2)	(3)	(4)	(5)	(6)	(7)	(8)	(9)	(10)	(11)	(12)
SiO_2	69.88	63.24	69.31	64.16	67.75	68.13	64.12	61.91	59.55	68.80	68.91	66.84
Al_2O_3	19.55	18.23	19.45	18.36	19.25	19.29	18.51	23.51	25.19	19.60	19.92	20.84
FeO	0.01	0.00	0.00	0.06	0.00	0.00	0.06	0.00	0.30	0.02	0.00	0.00
CaO	0.06	0.00	0.02	0.00	0.06	0.01	0.00	4.52	6.33	0.06	0.05	0.25
Na_2O	11.15	4.52	10.66	3.86	11.43	11.05	0.37	8.92	6.35	11.27	11.38	9.78
K_2O	0.09	16.68	0.07	16.56	0.09	0.07	17.02	0.24	0.35	0.06	0.15	0.06
TOT.	100.73	98.60	99.52	99.53	98.57	98.55	100.07	99.12	98.06	99.81	100.40	97.77
Xan	.00	.00	.00	.00	.00	.00	.00	.22	.35	.00	.00	.01
Xab	.99	.04	1.00	.04	.99	1.00	.03	.77	.63	1.00	.99	.98
Xor	.01	.96	.00	.96	.01	.00	.97	.01	.02	.00	.01	.01

(1)-(7) hydrothermal   (8) metased   (9),(12) metased   (10),(11) hydro

Sample 1 Dr.W. 18

	(1)	(2)	(3)
	60.41	61.01	60.06
	25.12	24.83	24.91
	0.02	0.07	0.11
	6.44	5.90	6.20
	7.30	7.34	8.06
	0.08	0.09	0.06
	99.37	99.24	99.40
	.33	.31	.30
	.67	.69	.70
	.00	.00	.00

(1)-(3) metased

Sample 3 DrW 117

	(1)	(2)	(3)	(4)	(5)	(6)	(7)
SiO_2	68.04	64.25	64.95	64.96	66.97	64.99	64.44
Al_2O_3	19.50	18.21	21.22	18.51	19.84	18.43	18.42
FeO	0.02	0.05	0.00	0.11	0.00	0.01	0.05
CaO	0.00	0.00	2.36	0.07	0.12	0.04	0.01
Na_2O	11.54	0.34	9.96	0.71	11.30	0.43	0.49
K_2O	0.08	16.84	0.43	16.78	0.07	16.85	17.10
TOT.	99.19	99.69	98.92	101.15	98.29	100.74	100.51
Xan	.00	.00	.11	.00	.01	.00	.00
Xab	1.00	.03	.86	.06	.99	.04	.04
Xor	.00	.97	.03	.94	.00	.96	.96

(1)-(7) hydrothermal

Sample 4Dr.S. 13

	(1)	(2)	(3)
SiO_2	58.57	57.31	62.58
Al_2O_3	25.64	25.94	22.61
FeO	0.37	0.30	0.01
CaO	7.22	7.89	4.17
Na_2O	6.71	6.52	8.36
K_2O	0.19	0.28	0.24
TOT.	98.70	98.24	97.97
Xan	.37	.39	.21
Xab	.62	.59	.77
Xor	.01	.02	.02

(1)-(3) metased

Sample 4Dr.S. 83

	(1)	(2)	(3)	(4)	(5)	(6)	(7)
SiO_2	65.18	64.32	63.45	68.38	63.73	63.93	63.11
Al_2O_3	18.33	18.59	18.28	19.15	18.30	18.04	18.42
FeO	0.04	0.05	0.07	0.00	0.00	0.00	0.01
CaO	0.00	0.00	0.06	0.01	0.00	0.00	0.07
Na_2O	0.49	0.37	0.59	10.11	0.47	0.49	0.93
K_2O	15.91	16.35	16.24	0.08	16.17	16.42	15.39
TOT.	99.95	99.68	98.69	97.73	98.67	98.88	97.93
Xan	.00	.00	.00	.00	.00	.00	.00
Xab	.04	.03	.05	.99	.04	.04	.08
Xor	.96	.97	.95	.01	.96	.96	.92

(1)-(7) hydrothermal

Sample 81-15 410

	(1)	(2)	(3)	(4)	(5)	(6)
SiO_2	59.72	59.40	62.87	68.96	58.94	62.74
Al_2O_3	25.29	25.40	18.87	18.95	25.67	22.27
FeO	0.13	0.02	0.04	0.38	0.12	0.04
CaO	6.66	5.00	0.05	0.58	6.52	2.81
Na_2O	7.20	8.12	0.59	10.36	7.04	9.19
K_2O	0.13	0.09	15.76	0.08	0.12	0.10
TOT.	99.20	98.24	98.18	99.33	98.50	97.19
Xan	.34	.25	.00	.03	.34	.14
Xab	.65	.74	.05	.96	.65	.85
Xor	.01	.01	.95	.01	.01	.01

(1)-(4),(6) hydrothermal   (5) metased

Sample 81-15 494

	(1)	(2)	(3)	(4)	(5)	(6)
SiO_2	63.35	67.67	63.49	64.68	65.54	63.43
Al_2O_3	18.58	19.92	22.82	18.38	18.62	18.52
FeO	0.00	0.03	0.00	0.05	0.00	0.02
CaO	0.01	0.46	3.38	0.00	0.00	0.00
Na_2O	0.45	10.80	9.06	0.38	0.38	0.60
K_2O	16.65	0.14	0.20	16.09	16.62	16.30
TOT.	99.14	99.05	99.01	99.63	101.20	98.95
Xan	.00	.02	.17	.00	.00	.00
Xab	.04	.97	.82	.03	.03	.05
Xor	.96	.01	.01	.97	.97	.95

(1),(2),(6) metased   (3)-(5) hydrothermal

Sample 81-23 18

	(1)	(2)	(3)	(4)	(5)	(6)	(7)	(8)	(9)	(10)
SiO_2	68.99	62.22	59.02	63.62	64.73	64.51	69.61	60.46	67.58	64.82
Al_2O_3	20.35	18.66	25.55	18.84	18.48	18.63	19.85	25.56	19.90	18.67
FeO	0.11	0.05	0.02	0.00	0.00	0.00	0.00	0.09	0.00	0.00
CaO	0.73	0.01	6.90	0.00	0.00	0.00	0.07	6.29	0.11	0.00
Na_2O	10.22	0.33	7.42	0.41	0.36	0.33	10.98	7.43	10.60	0.42
K_2O	0.05	15.01	0.19	15.62	16.46	15.29	0.10	0.10	0.08	15.04
TOT.	100.45	96.28	99.10	98.49	100.03	98.75	100.61	99.94	98.27	99.06
Xan	.04	.00	.34	.00	.00	.00	.00	.31	.01	.00
Xab	.96	.03	.65	.04	.03	.03	.99	.68	.99	.04
Xor	.00	.97	.01	.96	.97	.97	.01	.01	.00	.96

(1)-(7) hydrothermal   (8) metased   (9),(10) hydrothermal

Sample 81-32 39

	(1)	(2)	(3)	(4)	(5)	(6)	(7)	(8)
SiO_2	53.60	58.12	59.66	62.62	61.63	63.47	67.00	62.46
Al_2O_3	29.13	26.06	24.53	23.20	23.87	24.49	21.49	23.18
FeO	0.07	0.02	0.13	0.15	0.01	0.02	0.00	0.04
CaO	11.81	8.16	6.46	4.35	5.35	3.33	1.80	2.69
Na_2O	4.68	6.77	7.68	7.78	8.11	7.54	9.62	9.00
K_2O	0.10	0.12	0.09	1.43	0.16	1.07	0.12	0.90
TOT.	99.37	99.25	98.56	99.53	99.11	99.93	100.03	98.28
Xan	.58	.40	.32	.22	.26	.18	.09	.13
Xab	.41	.59	.68	.70	.73	.75	.90	.81
Xor	.01	.01	.00	.08	.01	.07	.01	.05

(1)-(3) metased   (4)-(8) hydrothermal

Sample 81-33 90

	(1)	(2)	(3)	(4)	(5)	(6)	(7)	(8)
SiO_2	64.88	66.24	68.55	65.95	63.13	64.64	64.51	65.15
Al_2O_3	21.08	20.87	19.40	21.34	22.73	21.53	18.16	18.26
FeO	0.16	0.04	0.04	0.01	0.06	0.10	0.03	0.00
CaO	2.00	1.83	0.13	2.01	4.00	1.28	0.00	0.04
Na_2O	10.26	10.59	11.64	10.22	9.17	10.02	0.34	0.57
K_2O	0.22	0.12	0.06	0.30	0.14	0.81	16.94	16.92
TOT.	98.60	99.69	99.82	99.82	99.23	98.38	99.98	100.93
Xan	.10	.09	.01	.09	.19	.06	.00	.00
Xab	.89	.90	.99	.89	.80	.89	.03	.05
Xor	.01	.01	.00	.02	.01	.05	.97	.95

(1)-(8) hydrothermal

Sample 81-33 90

	(9)	(10)	(11)	(12)	(13)
SiO_2	69.68	63.81	64.60	63.21	64.54
Al_2O_3	19.38	18.04	18.33	17.95	24.79
FeO	0.00	0.03	0.00	0.00	0.13
CaO	0.18	0.00	0.00	0.06	1.42
Na_2O	11.16	0.44	1.25	0.51	8.29
K_2O	0.17	17.22	16.06	16.92	2.93
TOT.	100.57	99.54	100.24	98.64	102.09
Xan	.01	.00	.00	.00	.07
Xab	.98	.04	.11	.04	.75
Xor	.01	.96	.89	.96	.18

(9)-(13) hydrothermal

Sample 81-42 92

	(1)	(2)	(3)	(4)	(5)	(6)	(7)	(8)
SiO_2	68.47	64.22	67.25	68.94	63.67	67.84	68.92	65.89
Al_2O_3	19.31	18.15	18.98	19.61	18.10	19.24	19.59	18.89
FeO	0.01	0.00	0.00	0.08	0.02	0.00	0.00	0.01
CaO	0.00	0.00	0.03	0.02	0.00	0.01	0.03	0.00
Na_2O	11.71	0.31	11.27	11.70	0.28	11.69	11.78	7.41
K_2O	0.08	17.48	0.23	0.09	17.22	0.10	0.07	17.29
TOT.	99.58	100.17	97.76	100.45	99.29	98.87	100.39	99.68
Xan	.00	.00	.00	.00	.00	.00	.00	.00
Xab	1.00	.03	.99	.99	.02	.99	1.00	.60
Xor	.00	.97	.01	.01	.98	.01	.00	.40

(1)-(8) hydrothermal

Sample 81-42 92

	(9)	(10)	(11)	(12)	(13)	(14)
SiO_2	64.07	63.62	63.91	63.55	63.46	62.69
Al_2O_3	18.24	18.08	18.14	17.68	18.10	18.49
FeO	0.00	0.00	0.11	0.03	0.00	0.12
CaO	0.00	0.00	0.02	0.00	0.00	0.02
Na_2O	0.28	0.29	0.81	0.40	0.36	0.92
K_2O	17.29	17.15	15.98	16.89	17.16	15.35
TOT.	99.88	99.14	98.97	98.55	99.08	97.59
Xan	.00	.00	.00	.00	.00	.00
Xab	.02	.03	.07	.04	.03	.08
Xor	.98	.97	.93	.96	.97	.92

(9)-(14) hydrothermal

Sample 81-44 46.5

	(1)	(2)
SiO_2	69.85	67.88
Al_2O_3	19.64	19.47
FeO	0.03	0.04
CaO	0.06	0.02
Na_2O	10.00	10.20
K_2O	0.06	0.07
TOT.	99.64	97.68
Xan	.00	.00
Xab	.99	1.00
Xor	.01	.00

(1)-(2) hydrothermal

Sample 81-55 19

	(1)	(2)	(3)	(4)	(5)	(6)	(7)	(8)
SiO_2	63.14	68.35	63.35	64.29	60.58	64.56	69.04	60.80
Al_2O_3	18.77	19.88	22.75	19.00	24.23	18.80	20.81	24.57
FeO	0.05	0.00	0.00	0.05	0.08	0.02	0.13	0.13
CaO	0.00	0.31	3.97	0.00	5.83	0.00	1.00	5.96
Na_2O	0.42	10.42	9.19	0.39	7.83	0.30	9.72	8.17
K_2O	16.46	0.08	0.09	16.37	0.22	16.59	0.08	0.17
TOT.	98.84	99.04	99.34	100.09	98.77	100.27	100.78	99.84
Xan	.00	.02	.19	.00	.29	.00	.05	.28
Xab	.04	.98	.80	.04	.70	.01	.94	.71
Xor	.96	.00	.01	.96	.01	.99	.01	.01

(1)-(4),(6),(7) hydrothermal   (5),(8) metased

Sample 81-55 19

	(9)	(10)	(11)	(12)	(13)	(14)	(15)
SiO_2	63.23	60.00	65.47	64.55	61.47	66.10	58.71
Al_2O_3	24.53	24.94	21.90	18.35	24.57	22.62	24.68
FeO	0.00	0.00	0.01	0.00	0.08	0.00	0.12
CaO	4.12	6.37	2.65	0.00	5.12	2.89	5.73
Na_2O	5.71	7.89	9.26	0.48	8.03	9.10	7.91
K_2O	0.13	0.18	0.13	16.70	0.32	0.18	0.13
TOT.	97.72	99.77	99.42	100.08	99.58	100.89	97.29
Xan	.28	.31	.14	.00	.26	.15	.28
Xab	.71	.68	.86	.04	.72	.84	.71
Xor	.01	.01	.01	.96	.02	.01	.01

(9),(11),(12) hydrothermal   (10),(13)-(15) metased

Sample 81-64 188

	(1)	(2)
SiO_2	66.71	66.40
Al_2O_3	20.61	20.47
FeO	0.03	0.07
CaO	1.46	1.50
Na_2O	10.27	10.00
K_2O	0.10	0.10
TOT.	99.19	98.53
Xan	.07	.08
Xab	.92	.92
Xor	.01	.01

(1),(2) metased

Sample 81-70 48

	(1)	(2)	(3)	(4)	(5)	(6)	(7)	(8)	(9)
SiO_2	64.21	62.53	68.89	68.91	63.64	69.12	63.18	69.38	64.37
Al_2O_3	18.86	19.36	20.22	20.10	18.69	19.83	18.86	19.91	18.54
FeO	0.13	0.00	0.00	0.01	0.07	0.02	0.03	0.00	0.00
CaO	0.00	0.00	0.03	0.21	0.00	0.03	0.07	0.01	0.00
Na_2O	0.41	0.46	10.43	10.71	0.23	11.75	1.41	11.17	0.30
K_2O	15.50	16.02	0.08	0.10	13.52	0.12	15.30	0.06	16.28
TOT.	99.11	98.38	99.85	100.05	96.15	100.88	98.85	100.52	99.50
Xan	.00	.00	.00	.01	.00	.00	.00	.00	.00
Xab	.04	.04	.99	.98	.03	.99	.12	1.00	.03
Xor	.96	.96	.01	.01	.97	.01	.88	.00	.97

(1)-(8) hydrothermal   (9) hydrothermal

Sample 82-16

	(1)	(2)	(3)
SiO_2	54.53	54.04	63.07
Al_2O_3	28.00	26.66	19.13
FeO	0.08	0.43	0.12
CaO	10.77	9.38	0.74
Na_2O	4.75	5.69	1.01
K_2O	0.11	0.33	15.57
TOT.	98.37	97.05	99.78
Xan	.55	.47	.03
Xab	.44	.51	.09
Xor	.01	.02	.88

(1)-(3) metased

Sample 82-28

	(1)	(2)	(3)	(4)	(5)	(6)	(7)	(8)
SiO_2	55.40	58.63	63.15	66.34	66.04	54.70	53.59	57.46
Al_2O_3	27.57	25.75	17.67	20.90	21.24	28.87	28.84	26.60
FeO	0.59	0.13	0.92	0.01	0.15	0.04	0.08	0.11
CaO	9.78	7.53	0.18	1.81	2.01	11.07	11.26	8.27
Na_2O	5.65	6.88	0.45	10.78	10.17	4.98	5.05	6.29
K_2O	0.47	0.66	15.95	0.03	0.25	0.13	0.16	0.18
TOT.	99.46	99.58	98.33	99.83	99.85	99.78	98.99	98.91
Xan	.47	.36	.01	.09	.10	.55	.55	.42
Xab	.50	.60	.04	.91	.89	.44	.44	.57
Xor	.03	.04	.95	.00	.01	.01	.01	.01

(1)-(8) metased

Sample 82-43

	(1)	(2)
SiO_2	68.75	66.92
Al_2O_3	19.26	19.30
FeO	0.06	0.04
CaO	0.12	0.05
Na_2O	12.50	12.20
K_2O	0.10	0.08
TOT.	100.79	98.59
Xan	.00	.00
Xab	.99	1.00
Xor	.01	.00

(1),(2) metased

Sample 82-76

	(1)	(2)	(3)	(4)	(5)	(6)	(7)
SiO_2	65.66	64.35	62.16	68.17	65.16	68.30	66.31
Al_2O_3	21.15	22.09	24.15	19.34	22.14	19.20	22.33
FeO	0.00	0.13	0.10	0.03	0.03	0.14	0.06
CaO	2.12	3.29	5.33	0.02	2.03	2.22	3.75
Na_2O	10.14	9.03	8.43	11.20	9.43	8.74	8.87
K_2O	0.11	0.17	0.11	0.06	0.59	0.03	0.08
TOT.	99.18	99.05	100.28	98.81	99.39	98.69	101.38
Xan	.10	.17	.26	.00	.10	.12	.19
Xab	.89	.82	.74	1.00	.86	.87	.81
Xor	.01	.01	.00	.00	.04	.01	.00

(1),(2) hydrothermal   (3)-(7) metased

Sample 82-77

	(1)	(2)	(3)	(4)	(5)	(6)
SiO_2	65.38	64.01	63.17	62.98	65.21	60.76
Al_2O_3	21.35	22.11	23.66	23.15	20.68	23.82
FeO	0.03	0.11	0.02	0.09	0.02	0.07
CaO	2.48	3.02	5.16	4.45	1.81	5.41
Na_2O	9.59	9.53	7.61	8.13	9.22	7.55
K_2O	0.12	0.07	0.24	0.21	0.15	0.16
TOT.	98.95	98.84	99.86	99.01	97.10	97.75
Xan	.12	.15	.27	.23	.10	.28
Xab	.87	.85	.72	.76	.89	.71
Xor	.01	.00	.01	.01	.01	.01

Sample 82-78

	(1)	(2)	(3)	(4)
SiO_2	60.46	59.49	55.89	58.31
Al_2O_3	24.09	24.07	27.32	25.13
FeO	0.16	0.00	0.00	0.03
CaO	6.01	6.11	9.50	6.75
Na_2O	8.17	8.28	5.96	7.42
K_2O	0.25	0.08	0.10	0.10
TOT.	99.14	98.03	99.01	97.81
Xan	.29	.29	.47	.33
Xab	.70	.71	.53	.66
Xor	.01	.00	.00	.01

(1),(2) igneous   (3),(4) metased

Sample 82-91

	(1)	(2)	(3)	(4)
SiO_2	65.19	64.98	54.34	56.04
Al_2O_3	18.31	21.46	27.88	26.50
FeO	0.00	0.05	0.00	0.00
CaO	0.02	2.80	10.72	8.78
Na_2O	0.53	9.14	5.22	6.46
K_2O	16.66	0.08	0.12	0.14
TOT.	100.71	98.51	98.29	98.19
Xan	.00	.14	.52	.42
Xab	.05	.85	.47	.57
Xor	.95	.01	.01	.01

82-91 (1)-(4) metased

Sample 82-101B

	(1)	(2)	(3)
SiO_2	68.89	69.42	67.65
Al_2O_3	19.86	19.50	19.65
FeO	0.11	0.06	0.08
CaO	0.06	0.02	0.06
Na_2O	10.60	11.59	11.11
K_2O	0.09	0.13	0.06
TOT.	99.61	100.72	98.69
Xan	.00	.00	.00
Xab	.99	.99	.99
Xor	.01	.01	.01

82-101B (1)-(3) metased

Sample 82-115

	(1)	(2)	(3)	(4)	(5)
SiO_2	61.14	64.36	62.23	62.99	64.96
Al_2O_3	24.00	21.96	23.57	23.62	21.17
FeO	0.03	0.05	0.01	0.28	0.00
CaO	5.34	2.58	4.95	4.57	2.04
Na_2O	8.44	9.03	8.69	8.70	10.16
K_2O	0.10	0.66	0.21	0.10	0.10
TOT.	99.05	98.64	99.68	100.25	98.44
Xan	.26	.13	.24	.22	.10
Xab	.74	.83	.75	.77	.89
Xor	.00	.04	.01	.01	.01

(1)-(5) metased

Sample 82-116

	(1)	(2)	(3)	(4)	(5)	(6)
SiO_2	64.95	61.07	67.97	61.01	65.94	67.37
Al_2O_3	21.73	23.56	19.84	23.12	20.95	19.50
FeO	0.18	0.00	0.19	0.10	0.17	0.19
CaO	1.50	4.88	0.14	4.57	1.93	0.06
Na_2O	9.42	8.62	10.70	8.38	9.82	11.06
K_2O	1.11	0.21	0.38	0.56	0.17	0.07
TOT.	98.89	98.34	99.22	97.75	98.98	98.25
Xan	.07	.24	.01	.23	.10	.00
Xab	.86	.75	.97	.74	.89	.99
Xor	.07	.01	.02	.03	.01	.01

(1),(2) hydrothermal   (3)-(6) metased

Sample 82-117

	(1)	(2)	(3)	(4)	(5)
SiO_2	62.06	58.70	65.78	67.87	52.17
Al_2O_3	24.46	25.25	21.34	19.49	29.97
FeO	0.24	0.12	0.00	0.01	0.12
CaO	5.08	6.96	2.50	0.63	12.24
Na_2O	8.13	7.38	9.91	10.56	4.44
K_2O	0.09	0.15	0.08	0.07	0.09
TOT.	100.05	98.57	99.60	98.64	99.03
Xan	.25	.34	.12	.03	.60
Xab	.74	.65	.87	.96	.39
Xor	.01	.01	.01	.01	.01

(1),(2),(5) metased   (3),(4) hydrothermal

Sample 82-121

	(1)	(2)
SiO_2	68.31	69.29
Al_2O_3	19.22	19.50
FeO	0.14	0.15
CaO	0.15	0.03
Na_2O	10.89	10.57
K_2O	0.09	0.06
TOT.	98.80	99.60
Xan	.01	.00
Xab	.99	1.00
Xor	.00	.00

82-121 (1),(2) metased

Sample 82-127

	(1)	(2)	(3)	(4)
	65.37	67.77	64.44	65.64
	21.12	20.53	21.85	21.63
	0.07	0.08	0.02	0.08
	1.85	0.95	2.20	2.48
	8.76	10.74	10.23	8.95
	0.10	0.16	0.11	0.13
	97.86	100.24	99.04	98.93
	.10	.05	.11	.13
	.89	.94	.89	.86
	.01	.01	.00	.01

82-127 (1)-(4) metased

Sample 82-131

	(1)	(2)	(3)
SiO_2	67.11	63.03	63.65
Al_2O_3	23.36	23.30	22.78
FeO	0.03	0.03	0.05
CaO	1.38	4.06	4.26
Na_2O	10.42	8.05	8.66
K_2O	0.09	0.10	0.27
TOT.	100.45	98.58	99.86
Xan			.21
Xab			.77
Xor			.02

82-131 (1)-(3) metased

Sample 82-132

	(1)	(2)	(3)
	62.35	55.93	66.56
	23.74	26.27	21.39
	0.01	0.10	0.08
	5.08	8.72	1.64
	9.22	6.92	11.35
	0.34	0.08	0.43
	100.74	98.02	101.45
	.23	.41	.07
	.75	.59	.91
	.02	.00	.02

82-132 (1)-(3) metased

Sample 82-144

	(1)	(2)	(3)
SiO_2	64.48	67.63	69.86
Al_2O_3	23.05	20.97	20.59
FeO	0.02	0.01	0.03
CaO	3.88	1.58	2.52
Na_2O	8.63	10.07	8.82
K_2O	0.08	0.13	0.08
TOT.	100.14	100.38	101.88
Xan	.20	.08	.14
Xab	.80	.91	.86
Xor	.00	.01	.00

82-144 (1)-(3) metased

Sample 82-145

	(1)	(2)	(3)
	67.38	56.55	64.88
	21.30	26.58	21.50
	0.05	0.01	0.04
	1.60	8.82	6.38
	9.92	6.32	5.45
	0.07	0.19	0.10
	100.33	98.47	98.35
	.08	.43	.39
	.91	.56	.60
	.01	.01	.01

82-145 (1)-(3) metased

Sample 82-147

	(1)	(2)	(3)	(4)	(5)
SiO_2	66.39	68.96	68.56	67.31	68.50
Al_2O_3	19.76	19.80	19.42	19.60	20.42
FeO	0.00	0.07	0.06	0.00	0.06
CaO	0.04	0.27	0.09	0.24	0.08
Na_2O	11.42	10.84	10.54	11.00	11.03
K_2O	0.11	0.08	0.07	0.10	0.09
TOT.	97.73	100.03	98.74	98.24	100.18
Xan	.00	.01	.01	.01	.00
Xab	.99	.98	.99	.98	.99
Xor	.01	.01	.00	.01	.01

Sample 82 152

	(1)	(2)	(3)	(4)	(5)	(6)	(7)
SiO_2	65.67	65.57	68.83	67.86	65.04	66.80	69.49
Al_2O_3	22.45	18.19	19.10	20.06	22.28	18.45	20.71
FeO	0.22	0.07	0.19	0.03	0.14	0.02	0.08
CaO	0.81	0.03	1.68	0.79	3.00	0.00	0.24
Na_2O	8.63	0.84	8.40	10.51	9.35	0.53	9.12
K_2O	1.75	16.32	0.78	0.13	0.16	16.72	0.13
TOT.	99.53	100.99	98.97	99.40	99.96	102.53	99.76
Xan	.05	.00	.10	.04	.15	.00	.01
Xab	.84	.07	.85	.95	.84	.05	.98
Xor	.11	.93	.05	.01	.01	.95	.01

(1)-(7) metased

APPENDIX 3

ELECTRON MICROPROBE ANALYSES OF MUSCOVITES

Metased are grains of contact metamorphic or apparent contact metamorphic origin.

* indicates representative analyses used in figures in the text.

Sample 1369

	(1)	(2)	(3)*	(4)
SiO_2	48.25	51.30	49.42	46.54
TiO_2	2.93	0.21	0.70	0.61
Al_2O_3	31.36	32.82	30.53	27.78
MgO	1.60	2.03	2.81	3.80
FeO	1.76	1.93	3.11	4.39
MnO	0.03	0.04	0.03	0.04
F	0.18	0.64	0.39	0.13
CaO	0.00	0.00	0.01	0.00
Na_2O	0.20	0.24	0.21	0.40
K_2O	9.59	9.13	9.73	11.09
TOT.	95.89	98.34	96.92	94.76

(1)-(4) from phyllic alteration zone

Sample 1504

	(1)	(2)*	(3)*	(4)	(5)	(6)	(7)
SiO_2	48.19	50.22	46.98	45.46	48.87	45.20	48.40
TiO_2	0.05	0.14	0.28	0.36	0.49	0.14	0.33
Al_2O_3	32.84	30.95	37.19	34.59	30.62	37.29	37.06
MgO	1.05	1.47	0.57	0.78	2.65	0.51	0.61
FeO	2.65	3.88	1.15	1.55	2.71	0.61	1.03
MnO	0.06	0.00	0.00	0.02	0.01	0.08	0.00
F	0.25	0.63	0.00	0.28	0.21	0.36	0.21
CaO	0.01	0.00	0.08	0.00	0.03	0.24	0.02
Na_2O	0.11	0.19	0.25	0.41	0.16	0.25	0.46
K_2O	9.51	9.25	9.38	9.08	8.87	8.35	10.00
TOT.	94.71	96.79	95.89	92.53	94.64	93.03	98.10

(1),(2) hydrothermal   (3)-(7) metasedimentary

Sample 3 DrW 117   Sample 4 DrS 83   Sample 81-15 410

	(1)*		(1)	(2)*	(3)	(4)*	(5)			(1)*
SiO_2	47.02		49.30	48.36	48.86	51.07	50.09		SiO_2	48.77
TiO_2	0.91		0.07	0.00	1.78	0.03	0.00		TiO_2	0.37
Al_2O_3	28.98		32.84	35.62	27.67	29.35	31.17		Al_2O_3	30.92
MgO	3.92		1.54	0.54	2.70	2.92	0.76		MgO	2.83
FeO	3.52		1.39	0.83	3.03	2.61	0.62		FeO	2.62
MnO	0.00		0.05	0.00	0.11	0.05	0.11		MnO	0.09
F	0.68		0.00	0.13	0.49	0.72	0.00		F	0.23
CaO	0.03		0.03	0.00	0.15	0.01	0.02		CaO	0.03
Na_2O	0.30		0.19	0.22	0.13	0.61	1.79		Na_2O	0.23
K_2O	11.27		9.22	9.52	10.08	10.65	9.89		K_2O	9.59
TOT.	96.67		94.64	95.23	94.98	98.02	95.44		TOT.	95.67

3DrW117 vein ser
4DrS83 (1),(2) hydrothermal (3)-(5) metasedimentary

81-15 410 (1) metasedimentary

Sample 81-32-39

	(1)*	(2)	(3)
	50.59	50.09	45.87
	0.00	0.02	0.01
	33.46	31.06	37.79
	1.35	2.92	0.02
	1.83	1.68	0.45
	0.00	0.00	0.08
	0.29	0.26	0.00
	0.00	0.03	0.01
	0.11	0.13	0.20
	11.64	11.02	11.15
	99.26	97.22	95.56

81-32 39   (1)-(3) hydro

Sample 81-42 92.5

	(1)*	(2)*	(3)	(4)	(5)	(6)
SiO_2	49.32	47.56	48.99	50.02	48.88	48.12
TiO_2	0.45	0.07	0.48	0.26	0.06	0.91
Al_2O_3	28.96	37.23	30.53	30.16	36.79	29.42
MgO	3.00	0.76	3.16	4.00	0.57	4.20
FeO	2.45	.058	3.30	2.37	0.61	4.25
MnO	0.02	0.04	0.05	0.02	0.00	0.00
F	0.57	0.02	0.37	0.53	0.00	0.52
CaO	0.00	0.00	0.00	0.00	0.00	0.00
Na_2O	0.15	0.10	0.13	0.20	0.12	0.13
K_2O	10.15	11.15	10.66	10.78	11.09	10.93
TOT.	95.08	97.51	97.67	98.33	98.13	98.53

(1)-(6) hydrothermal

Sample 81-44 46.5

	(1)	(2)	(3)	(4)	(5)*
SiO_2	48.98	49.48	47.63	49.89	49.92
TiO_2	0.10	0.46	1.90	0.82	0.25
Al_2O_3	31.57	31.74	29.51	31.90	32.62
MgO	2.18	1.69	2.31	2.36	1.97
FeO	1.48	2.03	2.37	1.58	1.54
MnO	0.00	0.01	0.05	0.02	0.00
F	0.58	0.51	0.44	0.21	0.58
CaO	0.00	0.01	0.00	0.00	0.00
Na_2O	0.23	0.10	0.19	.019	.018
K_2O	9.64	10.65	9.30	9.88	10.14
TOT.	94.76	96.68	93.70	96.84	97.21

(1)-(5) hydrothermal

Sample 81-55 19

	(1)*	(2)
SiO_2	47.99	46.87
TiO_2	0.62	1.30
Al_2O_3	34.81	35.44
MgO	1.07	0.57
FeO	1.67	1.16
MnO	0.00	0.00
F	0.39	0.56
CaO	0.02	0.00
Na_2O	0.39	0.56
K_2O	10.13	8.95
TOT.	97.08	94.84

(1),(2) metased

Sample 81-64 188

	(1)*	(2)	(3)	(4)	(5)*
SiO_2	49.33	48.53	47.57	46.73	46.28
TiO_2	0.78	1.42	0.29	1.20	0.73
Al_2O_3	33.20	35.49	33.74	33.91	35.17
MgO	1.62	0.87	0.97	0.86	0.75
FeO	1.70	1.05	0.89	1.13	0.99
MnO	0.04	0.05	0.00	0.00	0.03
F	0.04	0.22	0.00	0.00	0.00
CaO	0.02	0.00	0.00	0.00	0.00
Na_2O	0.39	0.48	0.50	0.46	0.51
K_2O	9.42	9.74	8.86	8.83	8.59
TOT.	96.53	97.84	92.82	93.12	93.04

(1) hydrothermal   (2)-(5) metasedimentary

Sample 82-16

	(1)*
SiO_2	49.72
TiO_2	0.00
Al_2O_3	34.83
MgO	1.60
FeO	1.43
MnO	0.11
F	0.06
CaO	0.01
Na_2O	0.14
K_2O	9.88
TOT.	97.78

Sample 82-21

	(1)*	(2)	(3)
SiO_2	47.99	48.59	53.97
TiO_2	0.61	0.61	0.17
Al_2O_3	34.96	34.42	28.77
MgO	1.54	1.68	3.63
FeO	1.16	1.20	1.47
MnO	0.01	0.02	0.00
F	0.00	0.02	0.20
CaO	0.00	0.00	0.00
Na_2O	0.44	0.58	0.25
K_2O	10.92	10.77	10.28
TOT.	97.53	97.90	98.74

Sample 82-28

	(1)*
SiO_2	51.92
TiO_2	0.05
Al_2O_3	32.20
MgO	3.04
FeO	1.13
MnO	0.01
F	0.47
CaO	0.01
Na_2O	0.10
K_2O	10.12
TOT.	99.05

82-16, 82-21, and 82-28   metased

Sample 82-43

	(1)	(2)	(3)*
SiO$_2$	49.02	48.59	47.90
TiO$_2$	2.05	0.83	0.85
Al$_2$O$_3$	30.75	31.89	31.39
MgO	3.01	3.33	3.64
FeO	2.04	1.69	2.63
MnO	0.02	0.05	0.06
F	0.00	0.09	0.11
CaO	0.00	0.00	0.04
Na$_2$O	0.33	0.29	0.32
K$_2$O	10.42	10.48	10.11
TOT.	97.64	97.25	97.06

82-43 (1)-(3) metased

Sample 82-76

	(1)*	(2)	(3)
SiO$_2$	47.04	45.38	49.82
TiO$_2$	0.25	0.27	0.02
Al$_2$O$_3$	36.63	35.64	30.87
MgO	0.84	0.95	2.65
FeO	1.00	1.15	1.72
MnO	0.00	0.00	0.00
F	0.31	0.24	0.39
CaO	0.00	0.01	0.01
Na$_2$O	0.50	0.56	0.40
K$_2$O	10.12	9.96	9.75
TOT.	96.68	94.16	95.62

82-76 (1)-(3) metased

Sample 82-77

	(1)	(2)*	(3)
SiO$_2$	46.84	47.23	47.56
TiO$_2$	0.43	0.33	0.37
Al$_2$O$_3$	35.91	36.62	35.59
MgO	0.83	0.68	1.12
FeO	1.53	1.34	1.22
MnO	0.06	0.00	0.00
F	0.03	0.25	0.15
CaO	0.00	0.01	0.00
Na$_2$O	0.32	.037	0.37
K$_2$O	9.62	8.99	9.68
TOT.	95.57	95.83	96.06

82-77 (1)-(3) metased

Sample 82-78

	(1)*	(2)
SiO$_2$	52.30	50.47
TiO$_2$	0.18	0.27
Al$_2$O$_3$	30.13	28.83
MgO	3.82	5.13
FeO	1.18	2.82
MnO	0.00	0.05
F	0.38	0.73
CaO	0.02	0.04
Na$_2$O	0.05	0.06
K$_2$O	8.80	9.48
TOT.	96.85	97.87

82-78 (1),(2) metased

Sample 82-91

	(1)	(2)*	(3)
SiO$_2$	51.55	51.32	49.41
TiO$_2$	0.06	0.09	0.37
Al$_2$O$_3$	32.32	32.37	31.21
MgO	1.99	2.33	2.40
FeO	1.83	1.83	1.74
MnO	0.06	0.01	0.00
F	0.14	0.14	0.53
CaO	0.00	0.08	0.14
Na$_2$O	0.10	0.17	0.28
K$_2$O	9.40	8.92	9.57
TOT.	97.45	97.28	95.66

82-91 (1)-(3) metased

Sample 82-101

	(1)	(2)	(3)*
SiO$_2$	48.38	47.72	46.67
TiO$_2$	0.15	0.28	0.29
Al$_2$O$_3$	35.34	35.96	34.49
MgO	0.93	0.71	1.09
FeO	2.13	1.48	2.56
MnO	0.01	0.00	0.06
F	0.08	0.23	0.28
CaO	0.02	0.02	0.00
Na$_2$O	0.74	0.30	0.68
K$_2$O	9.26	8.12	8.29
TOT.	97.04	94.80	94.42

82-101 (1),(3) metased

Sample 82-115

	(1)*	(2)	(3)
SiO$_2$	48.34	47.17	48.95
TiO$_2$	0.49	0.29	0.24
Al$_2$O$_3$	34.21	36.38	33.08
MgO	1.46	1.14	1.60
FeO	2.24	1.99	1.72
MnO	0.01	0.05	0.03
F	0.18	0.00	0.20
CaO	0.02	0.00	0.00
Na$_2$O	0.67	0.44	0.46
K$_2$O	9.38	9.77	9.80
TOT.	97.00	97.23	96.10

82-115 (1)-(3) metased

Sample 82-116

	(1)	(2)*	(3)
SiO$_2$	52.48	50.02	49.22
TiO$_2$	0.09	0.58	0.32
Al$_2$O$_3$	30.23	34.63	35.61
MgO	3.60	1.73	1.20
FeO	1.99	1.35	1.08
MnO	0.05	0.04	0.01
F	0.50	0.00	0.00
CaO	0.00	0.01	0.02
Na$_2$O	0.07	0.23	0.20
K$_2$O	9.92	9.51	9.48
TOT.	98.93	98.11	97.13

82-116 (1)-(3) metased

Sample 82-117

	(1)*	(2)
SiO$_2$	49.38	45.96
TiO$_2$	0.09	0.24
Al$_2$O$_3$	35.23	33.38
MgO	1.25	1.59
FeO	1.27	3.44
MnO	0.00	0.06
F	0.23	0.35
CaO	0.00	0.01
Na$_2$O	0.23	0.09
K$_2$O	9.39	9.27
TOT.	97.07	94.37

82-117 (1),(2) metased

Sample 82-127

	(1)	(2)*	(3)	(4)	(5)
SiO$_2$	48.39	46.03	44.88	45.96	44.76
TiO$_2$	0.34	0.35	1.13	0.21	0.19
Al$_2$O$_3$	35.61	35.66	35.77	34.82	35.66
MgO	0.77	0.71	0.52	0.63	0.73
FeO	1.36	1.03	1.11	1.16	1.00
MnO	0.00	0.02	0.01	0.00	0.01
F	0.30	0.08	0.00	0.00	0.35
CaO	0.01	0.00	0.00	0.00	0.08
Na$_2$O	0.46	0.50	0.58	0.56	0.26
K$_2$O	9.62	9.25	9.87	8.41	9.15
TOT.	96.86	93.62	93.86	91.76	92.18

(1)-(5) metasedimentary

Sample 82-131

	(1)*	(2)	(3)
SiO_2	49.50	47.58	47.17
TiO_2	0.01	0.10	0.36
Al_2O_3	32.05	34.20	29.26
MgO	2.56	1.04	4.62
FeO	1.66	1.53	3.25
MnO	0.05	0.09	0.07
F	0.53	0.17	0.56
CaO	0.05	0.03	0.03
Na_2O	0.15	0.15	0.11
K_2O	9.79	10.01	9.94
TOT.	96.34	94.90	95.37

82-131 (1)-(3) metased

Sample 82-132

	(1)*	(2)*	(3)
SiO_2	50.49	48.01	45.92
TiO_2	0.70	0.45	0.00
Al_2O_3	29.45	30.77	39.12
MgO	3.33	2.27	0.23
FeO	2.83	3.06	1.25
MnO	0.06	0.09	0.00
F	0.20	0.40	0.00
CaO	0.00	0.01	0.01
Na_2O	0.14	0.19	0.46
K_2O	11.16	8.29	9.85
TOT.	98.37	93.51	96.84

82-132 (1) hydro (2),(3) metased

Sample 82-147

	(1)	(2)*	(3)
SiO_2	47.09	51.30	52.68
TiO_2	0.35	0.19	0.24
Al_2O_3	35.56	31.23	29.20
MgO	0.99	2.15	2.70
FeO	2.89	2.62	2.41
MnO	0.02	0.04	0.08
F	0.05	0.15	0.45
CaO	0.00	0.00	0.01
Na_2O	0.39	0.20	0.21
K_2O	7.69	8.48	9.27
TOT.	95.03	96.36	97.25

82-147 (1)-(3) metased

Sample 82-152

	(1)	(2)	(3)*	(4)
SiO_2	53.55	49.70	46.91	46.55
TiO_2	0.20	0.40	0.31	0.10
Al_2O_3	31.06	34.98	36.68	36.28
MgO	2.24	1.36	0.80	1.00
FeO	1.60	1.54	1.10	1.65
MnO	0.01	0.04	0.05	0.07
F	0.13	0.30	0.00	0.10
CaO	0.00	0.00	0.01	0.00
Na_2O	0.25	0.39	0.41	0.37
K_2O	8.63	9.35	9.39	8.46
TOT.	97.68	98.06	95.66	94.77

82-152 (1)-(4) metased

APPENDIX 4

ELECTRON MICROPROBE ANALYSES OF CARBONATES

Xsid represents siderite mole fraction

Xmag represents magnesite mole fraction

Xrho represent rhodochrosite mole fraction

Xcal represents calcite mole fraction

Sample	1164	1369		3DW 117	4DS 83		
	(1)	(1)	(2)	(1)	(1)	(2)	(3)
FeO	11.02	14.55	15.50	16.95	0.20	0.60	0.78
MgO	12.44	11.32	8.49	8.34	0.19	0.32	0.07
MnO	2.62	0.17	0.06	1.64	1.00	1.53	0.32
CaO	28.43	27.37	29.82	28.40	57.63	57.52	55.74
Tot.	54.55	53.41	53.87	55.33	59.02	59.97	56.91
Xsid	0.15	0.21	0.22	0.24	0.00	0.01	0.01
Xmag	0.31	0.29	0.22	0.21	0.00	0.01	0.00
Xrho	0.04	0.00	0.01	0.02	0.01	0.02	0.00
Xcal	0.50	0.51	0.55	0.52	0.98	0.96	0.98

Samples 1164, 1369, and 3DW 117 phyllic alteration
Sample 4DS 83 mineralization

Sample	81-15 494	81-32 39	81-42 92	81-55 19
	(1)	(1)	(1)	(1)
FeO	13.92	0.20	0.02	0.57
MgO	9.01	0.08	0.00	0.08
MnO	1.21	0.90	0.21	0.73
CaO	31.72	57.84	52.84	57.84
Tot.	55.86	59.02	53.07	59.22
Xsid	0.19	0.00	0.00	0.01
Xmag	0.22	0.00	0.00	0.00
Xrho	0.02	0.01	0.00	0.01
Xcal	0.57	0.98	1.00	0.98

Samples 81-15 494, and 81-42 92 mineralization
Samples 81-32 39, and 81-55 19 late potassic alteration

APPENDIX 5

FLUID INCLUSION DATA

H_2O-CO_2 Inclusions:

Groups are: 1 from late potassic alteration

2 from mineralized samples

3 from phyllic alteration

Types are: p primary

ps pseudosecondary

s secondary

Melt 1 is the final melting temperature of liquid CO_2

Homog. 1 is the homogenization temperature of CO_2

Melt 2 is the clathrate melting temperature

XCH4 is the calculated methane mole fraction

Dens. 1 is the density of the CO2 phase

Vol. % CO2 is the volume percentage of the CO_2 phase in the inclusion

Dens. 2 is the inclusion bulk density calculated by assuming 0 wt. % NaCl in the H_2O phase

Dens. 3 is the inclusion bulk density calculated by assuming 6 wt. % NaCl in the H_2O phase

Dens. 4 is the inclusion bulk density calculated by assuming 12 wt. % NaCl in the H_2O phase

XCO2 is the calculated CO_2 mole fraction in the inclusion

Homog. 2 is the H_2O-CO_2 homogenization temperature

Decrep. is the decrepitation temperature

Sample	Group	Type	Melt 1	Homog.1	Melt 2	XCH4	Dens.1	Vol.%CO2	Dens.2	Dens.3	Dens.4	XCO2	Homog.2	Decrep.
3DW 125	1	ps		+7.3				40						
3DW 125	1	ps		+3.1				30-40						
3DW 125	1	ps	-60.8	+0.5	+8.4	0.20	0.71	30	0.913	0.941	0.972	0.111		
3DW 125	1	ps	-56.9	+22.4		0.0	0.74	35	0.909	0.935	0.964	0.140		
81-60 203	1	ps		+14.0				20						
81-60 203	1	ps	-58.0	+24.5		0.03	0.65	40	0.860	0.884	0.910	0.151		
81-60 203	1	ps	-58.2	+22.7		0.03	0.71	50	0.855	0.875	0.897	0.225		
81-60 203	1	ps	-57.7	+25.2		0.03	0.65	50	0.825	0.845	0.867	0.210		
81-60 203	1	ps	-58.1	+24.8		0.03	0.65	40	0.860	0.884	0.910	0.151		
81-60 203	1	ps	-58.0	+23.5		0.03	0.70	30	0.910	0.938	0.969	0.109		
81-60 203	1	ps	-58.4	+26.4		0.04	0.60	20	0.920	0.952	0.987	0.058		
81-60 203	1	ps		+15.4				60						
81-60 203	1	ps	-58.4	+23.8		0.04	0.65	30	0.895	0.923	0.954	0.102		
81-60 203	1	ps	-58.2	+22.7		0.03	0.71	35	0.898	0.924	0.953	0.135		
81-60 203	1	ps	-60.1	+20.0		0.12	0.50	55	0.725	0.743	0.763	0.200		
81-60 203	1	ps	-58.0	+20.0		0.03	0.74	35	0.909	0.935	0.964	0.140		250
81-60 203	1	ps	-58.2	+23.2		0.03	0.70	35	0.895	0.921	0.950	0.134		250
81 60 203	1	ps	-58.7	+24.9		0.06	0.60	30	0.880	0.908	0.939	0.095		
4DS 141	1	ps	-62.1		+11.6			30						
4DS 141	1	ps		+7.0	+9.7			40						294
1498	2	ps	-57.5	+14.3	+10.7	0.02	0.80	20	0.960	0.992	1.03	0.076		
1498	2	ps	-57.7	+16.8		0.03	0.78	30	0.934	0.962	0.993	0.120		
1498	2	ps	-57.2	+13.5		0.01	0.83	40	0.932	0.956	0.982	0.185		300
1498	2	ps	-57.2	+20.2		0.01	0.77	60	0.862	0.878	0.896	0.321		300
1498	2	s	-59.5	+20.9	+8.3	0.10	0.59	50	0.795	0.815	0.837	0.194		
1498	2	s	-59.6	+19.3		0.10	0.60	35	0.860	0.886	0.915	0.117		
1498	2	s	-59.5	+17.4		0.10	0.65	50	0.825	0.845	0.867	0.210		
1498	2	ps	-59.0	+12.8		0.07	0.77	40	0.908	0.932	0.958	0.171	278.0	
1498	2	s	-60.3	+15.3		0.19	0.40	40	0.760	0.784	0.810	0.098		250
1498	2	s	-59.5	+15.4		0.11	0.55	60	0.730	0.746	0.764	0.253		267
1498	2	s	-59.9	+15.0	+5.0	0.17	0.50	50	0.750	0.770	0.792	0.170		
1498	2	s	-58.5	+15.3		0.05	0.77	40	0.908	0.932	0.958	0.174		
1503	2	ps	-58.1	+23.4		0.03	0.70	40	0.880	0.904	0.930	0.160		
1503	2	ps		+19.8				50						
1503	2	ps	-56.5	+22.7	+8.9	0.0	0.75	60	0.850	0.866	0.884	0.315		
4DS25	2	ps	-57.8	+17.0		0.03	0.77	40	0.908	0.932	0.958	0.174		
4DS25	2	ps	-57.9	+13.0		0.03	0.83	50	0.915	0.935	0.957	0.254		
4DS25	2	ps	-57.9	+15.5		0.03	0.78	50	0.890	0.910	0.932	0.242		
4DS25	2	ps	-56.8	+16.5	+7.0	0.0	0.81	50	0.905	0.925	0.947	0.249		
4DS25	2	ps	-57.6	+10.1		0.02	0.84	80	0.872	0.880	0.889	0.579		
4DS25	2	ps	-59.6	+7.4	+7.2	0.10	0.80	50	0.900	0.920	0.942	0.247		250
4DS25	2	ps		+5.0				50						290
4DS25	2	ps	-57.9	+20.6	+10.2	0.03	0.74	35	0.909	0.935	0.964	0.140		220
4DS25	2	ps		+17.2	+9.8			25						250
4DS25	2	ps		+15.0				30						
4DS25	2	ps	-60.7	+17.0		0.19	0.40	50	0.700	0.720	0.742	0.141		
4DS25	2	ps		+11.0				50						250
4DS25	2	ps		+15.6				35						250
4DS25	2	ps	-60.4	+15.8		0.17	0.50	30	0.850	0.878	0.909	0.081		260
4DS25	2	ps	-60.5	+16.5		0.17	0.50	20	0.900	0.932	0.967	0.049		276
4DS25	2	ps	-60.2	+17.4		0.14	0.52	20	0.904	0.936	0.971	0.051		210

Sample	Group	Type	Melt 1	Homog.1	Melt 2	XCH4	Dens.1	Vol.%CO2	Dens.2	Dens.3	Dens.4	XCO2	Homog.2	Decrep.
1502c	2	ps	-57.2	+25.4	+4.2	0.01	0.70	25	0.925	0.955	0.988	0.087		
1502c	2	ps		+25.2				30						
1502c	2	ps	-58.2	+21.0		0.03	0.73	40	0.892	0.916	0.942	0.166		275
1502c	2	ps	-58.2	+21.8		0.03	0.73	40	0.892	0.916	0.942	0.166		250
1389	2	ps	-58.9	+19.9	+7.5	0.07	0.65	65	0.773	0.787	0.802	0.331		
1389	2	ps	-58.3	+21.3	+6.6	0.03	0.73	30	0.919	0.947	0.978	0.114		
1389	2	ps	-58.7	+18.6		0.05	0.74	65	0.831	0.845	0.860	0.360		
1389	2	ps	-57.9	+20.3		0.03	0.74	65	0.831	0.845	0.860	0.360		
1389	2	ps		+25.5				30						
1389	2	ps	-58.0	+21.1		0.03	0.72	45	0.874	0.896	0.920	0.194		
1164	3	ps	-56.7	+27.6	+8.4	0.0	0.65	15	0.995	1.034	1.077	0.040		
1164	3	ps	-56.9	+27.0		0.0	0.67	30	0.901	0.929	0.960	0.105		
1164	3	ps	-56.4	+27.7		0.0	0.65	15	0.995	1.034	1.077	0.040		
1164	3	ps	-56.7	+25.6		0.0	0.71	20	0.942	0.974	1.009	0.068		
1164	3	ps						20					289.0	
1164	3	ps						20					335.0	
2DS34	3	ps		+29.2	+8.8			20						
2DS34	3	ps	-56.5	+23.3		0.0	0.75	30	0.925	0.953	0.984	0.116		280
2DS34	3	ps	-57.5	+26.0		0.02	0.65	20	0.930	0.962	0.997	0.062		270
2DS34	3	ps	-57.5	+15.8		0.02	0.80	30	0.940	0.968	0.999	0.123		279
2DS34	3	ps		+22.2				20						
2DS34	3	ps	-57.9	+20.5		0.03	0.74	25	0.935	0.965	0.998	0.092		
2DS34	3	ps	-56.4			0.0		30					267.0	
2DS34	3	ps	-57.0	+26.6		0.01	0.70	20	0.940	0.971	1.007	0.069		
2DS34	3	ps		+26.5				30					278.0	
2DS34	3	ps		+27.0				30						
2DS34	3	ps		+26.4				20						
2DS34	3	ps	-57.0	+25.2		0.01	0.70	20	0.940	0.972	1.007	0.067		250
2DS34	3	ps	-56.7	+27.9		0.0	0.65	15	0.948	0.982	1.019	0.045		260
2DS34	3	ps	-57.2	+22.0		0.01	0.75	30	0.993	1.031	1.074	0.094		240
2DS34	3	ps	-56.9	+25.2	+8.0	0.0	0.71	40	0.884	0.908	0.934	0.162		
2DS34	3	ps	-56.6	+23.0	+7.1	0.0	0.73	85	0.771	0.777	0.783	0.629		
2DS34	3	ps	-56.9	+25.3		0.0	0.71	50	0.855	0.875	0.897	0.225		
2DS34	3	ps	-56.7	+27.2	+9.0	0.0	0.67	40	0.868	0.892	0.918	0.155		
2DS34	3	ps	-56.7	+23.6		0.0	0.73	50	0.865	0.885	0.907	0.230		
2DS34	3	ps	-55.7	+22.0	+8.0	0.0	0.74	50	0.870	0.890	0.912	0.233		
2DS34	3	ps		+22.2				50						
2DS34	3	ps	-55.8	+23.9		0.0	0.73	60	0.838	0.854	0.872	0.310		
2DS34	3	ps	-56.3	+16.2		0.0	0.82	80	0.856	0.864	0.873	0.573		

H$_2$O Inclusions:

Melt is the ice melting temperature

Homog. is the H$_2$O homogenization temperature

Sample	Group	Origin	Melt	Homog.
4DS141	1	ps		216.4
4DS141	1	ps	-2.0	
4DS141	1	ps		206.4
4DS141	1	ps		258.8
4DS141	1	ps		272.2
4DS141	1	ps		223.3
4DS141	1	ps		219.5
4DS141	1	ps		193.5
4DS141	1	ps		183.9
3DW125	1	s		308.0
3DW125	1	ps		209.0
3DW125	1	ps		284.0
3DW125	1	ps		249.5
3DW125	1	ps		254.0
81-20 203	1	ps	-6.0	233.5
81-60 203	1	ps		212.0
81-60 203	1	ps		204.0
81-60.203	1	ps		201.5
81-60 203	1	ps		214.0
81-60 203	1	ps		190.0
81-60 203	1	ps	-10.6	200.0
81-60 203	1	ps		253.0
81-60 203	1	ps	-10.4	193.0
81-60 203	1	ps	-10.6	222.0
81-60 203	1	ps		257.0

Sample	Group	Origin	Melt	Homog.
1502c	2	s		209.9
1502c	2	s		204.8
1502c	2	s		210.2
1502c	2	s		264.0
1503	2	ps		274.7
1503	2	ps	-2.8	250.3
1503	2	ps	-3.0	257.3
1503	2	ps		276.0
1503	2	s		235.0
1503	2	s		229.8
1503	2	s		225.0
1503	2	s		265.0
4DS25	2	ps		294.5
1389	2	s	-5.2	229.0
1389	2	s	-5.2	235.4
1389	2	s		268.0
1389	2	ps		228.0
1389	2	ps		207.0
1389	2	ps	-4.2	188.0
3DW28	2	p	-1.7	330.0
3DW28	2	p	-1.8	366.8
3DW28	2	p	-1.6	369.1
3DW28	2	p	-1.3	276.3
3DW28	2	p	-1.6	
3DW28	2	p	-1.4	317.0